

Pharmaceutical Powder Technology:
Towards a science based understanding of
the behavior of powder systems

Inauguraldissertation

zur
Erlangung der Würde eines Doktors der Philosophie
vorgelegt der
Philosophisch-Naturwissenschaftlichen Fakultät
der Universität Basel

von

Michael Lanz
aus Rohrbach (BE)

Basel, 2006

Genehmigt von der Philosophisch-Naturwissenschaftlichen Fakultät
auf Antrag von

Professor Dr. H. Leuenberger
und
PD Dr. P. van Hoogevest

Basel, den 21. Juni 2005

Professor Dr. H.-J. Wirz
Dekan

Meinen Eltern

Danksagung / Acknowledgements

Die Doktorarbeit wurde an der Uni Basel am Institut für Pharmazeutische Technologie unter der Leitung von Prof. Dr. H. Leuenberger durchgeführt und grossteils vom Schweizerischen Nationalfonds (Beitrag Nr. 20-58941.99) unterstützt.

Meinem Betreuer Prof. Dr. H. Leuenberger danke ich herzlich für die Ermöglichung der Dissertation sowie für die wertvolle und wohlwollende Unterstützung, die er mir während der gesamten Arbeit entgegengebracht hat. Ihm verdanke ich auch das Vertrauen eigene Ideen konsequent zu verfolgen und umzusetzen.

Mein Dank geht auch an PD Dr. P van Hoogevest, der freundlicherweise das Korreferat der Arbeit übernommen hat.

Herrn P. Tschopp von der Firma Pharmatrans Sanaq AG danke ich für das Beschaffen von Cellets[®] und Sugar spheres[®]. Herrn D. Mathys vom Zentrum für Mikroskopie der Universität Basel (ZMB) danke ich für die Anfertigung der REM-Aufnahmen. Eva Völker möchte ich danken für ihre Untersuchungen über das Kompressionsverhalten von verschiedenen Substanzen während ihrer Diplomarbeit. I thank Prof. Dr. V. Kumar for providing me with UICEL and for the fruitful discussion during his stay at the University of Basel. Many thanks go to PD Dr. D. Giron (Novartis Pharma, Basel) and Dr. F. Thielmann (Surface Measurement Systems, London) for performing the x-ray and the IGC measurements, respectively.

Danken möchte ich auch Tanja Kuny für die Durchsicht des Manuskriptes sowie Frau Erb für ihre hilfreichen Tipps, die das Erstellen des Dokumentes erleichterten.

Meinen Kolleginnen und Kollegen vom Institut für Pharmazeutische Technologie danke ich für die angenehme Arbeitsatmosphäre. Insbesondere möchte ich Stefan Winzap danken, der mir als Freund während den vier Jahren zur Seite gestanden ist. Mit seiner stets tatkräftigen, unkomplizierten und für ihn selbstverständlichen Hilfeleistung, bewies er ein aussergewöhnliches und für mich vorbildliches wie auch unvergessenes Verständnis seiner Arbeit. Sonja Reutlinger danke ich für viele interessanten Gespräche und für die stets aufmunternden Worte. Susanne Reitbauer, Matthias Plitzko und Johannes von Orelli möchte ich danken für die angenehme Zusammenarbeit während der Praktikumsbetreuung und für die vielen Abwechslungen, die den Alltag bereicherten.

Aus tiefstem Herzen danke ich meinen Eltern, der ganze Familie und Lidia Gagno für die Unterstützung, die Aufmunterungen und die Liebe.

Table of contents

Table of contents.....	i
Abbreviations.....	iii
A. UICEL	1
1 Summary	2
2 Introduction	5
2.1 Relevance of polymorphism	5
2.2 Cellulose	6
2.3 Aims of the study	11
3 Materials and Methods.....	12
3.1 Preparation and manufacturing processes	12
3.2 Test for purity.....	13
3.3 Basic powder characteristics	14
3.4 Investigation of the structure.....	15
3.5 Determination of the contact angle and the surface free energy	18
3.6 Powder-water interactions	25
3.7 Behavior upon compression	27
3.8 Basic tablet characteristics	29
3.9 Tablet-water interactions	31
3.10 Dissolution rate measurements	34
3.11 Stability test of acetylsalicylic acid	36
4 Results and Discussion.....	38
4.1 Test for purity.....	38
4.2 Identification tests and structural investigations.....	39
4.3 Powder characterization	44
4.4 Moisture sorption	46
4.5 Compaction of the powder.....	51
4.6 UICEL – a superdisintegrant?.....	58
4.7 Drug release from tablets consisting of proquazone and disintegrant in different ratios.....	76
4.8 Stability of acetylsalicylic acid in combination with UICEL and Avicel PH102®	85
5 Conclusions and outlook.....	89
6 References	95
B. From art to science	107
1 Summary	108

Table of contents

2	Introduction	110
2.1	Aims of the study	110
3	Theory.....	111
3.1	Powder – the 4 th state of matter.....	111
3.2	Compression.....	112
3.3	Flow	115
3.4	Percolation theory.....	117
3.5	Dilution capacity.....	120
4	Materials and methods.....	122
4.1	Storage	122
4.2	Characterization of the substances.....	123
4.3	Compression study	123
4.4	Flow study.....	124
4.5	Dilution capacity study	125
5	Results and Discussion.....	127
5.1	Compression study	127
5.2	Flow study.....	132
5.3	Dilution capacity study	136
6	Conclusions and outlook.....	141
7	References	144
	Appendix	147
	Curriculum vitae	162

Abbreviations

ASA:	Acetylsalicylic Acid
BCS:	Biopharmaceutical Classification System
BET:	Equation derived by <u>B</u> runauer, <u>E</u> mmett and <u>T</u> eller
cps:	counts per second
DMSNT:	Diffraction Management System Software for Windows NT
DP:	Degree of Polymerization
DSC:	Differential Scanning Calorimetry
GAB:	Equation developed by <u>G</u> uggenheim, <u>A</u> ndersen and de <u>B</u> oer
HPLC:	High Pressure Liquid Chromatography
ICH:	International Conference on Harmonisation
IGC:	Inverse Gas Chromatography
IR:	Infrared Radiation
IUPAC:	International Union of Pure and Applied Chemistry
LOPD:	Leveling Off the Degree of Polymerization
MCC:	microcrystalline cellulose
n.d.:	not determined
NF:	National Formulary
no.:	number
PEG:	Polyethylen Glycol
RH:	Relative Humidity
rpm:	rounds per minute
SA:	Salicylic Acid
SEM:	Scanning Electron Microscope; in a statistical context: Standard Error of the Mean
UICEL:	<u>U</u> niversity of <u>I</u> owa <u>C</u> ellulose
USP:	United States Pharmacopeia

A. UICEL

A cellulose II based product and its interaction with water

1 Summary

Microcrystalline cellulose is one of the most useful filler for direct compression. Cellulose in general consists of an amorphous part and a crystalline part, which can exist in two polymorphic forms: cellulose I and cellulose II. UICEL (University of Iowa cellulose) is a cellulose II product and can be obtained by mercerization (chemical treatment with sodium hydroxide) from Avicel PH102[®], a microcrystalline cellulose, which contains the cellulose I polymorph. X-ray measurements of the two substances confirmed the different polymorphic forms and demonstrated a higher degree of crystallinity for Avicel PH102[®] (73%) than for UICEL (64%).

The aim of the study was a comprehensive investigation of UICEL and Avicel PH102[®] concerning relevant properties in pharmaceutical technology.

The moisture content of powder samples stored over different saturated salt solutions was measured gravimetrically. The resulting moisture sorption isotherms were analyzed according to the BET (Brunauer, Emmett and Teller) and GAB (Guggenheim, Andersen and de Boer) equation. The latter proved to be valid over a larger range of relative humidity and should therefore be favored in order to describe the moisture content of excipients in dependency of the relative humidity. The higher moisture content of UICEL compared to Avicel PH102[®] could not unambiguously be ascribed to the different polymorphic form of the crystalline part, since the higher amorphous fraction in UICEL results in a higher surface area, which is available for water molecules.

UICEL and Avicel PH102[®] were compressed with the Zwick[®] 1478 Universal Testing Instrument in a pressure range of 1 – 111 MPa. The compression characteristics of the two monosubstances were described according to the well-known Heckel and modified Heckel equation. Thereby, the modified Heckel equation turned out to be clearly superior compared to the Heckel equation. The fitting parameters K (Heckel equation) and C (modified Heckel equation) for both “in die” data and “out of die” data clearly indicated that UICEL is less ductile compared to Avicel PH102[®]. This difference is most likely caused by the different polymorphic form, because considering the higher moisture content and the higher amorphous fraction, a higher ductility would be expected for UICEL. After compression, UICEL has furthermore a significant greater tendency to recover elastically, especially when compressed at high pressures.

Tablets prepared of UICEL showed remarkable disintegration properties, which differed significantly from tablets consisting of Avicel PH102[®]: The disintegration time was shorter for

UICEL and almost independent of the relative density of the tablet. The force, which is responsible for the disintegration was measured using the Zwick® 1478 Universal Testing Instrument. The maximum force as well as the rate of force development was much higher for UICEL compared to Avicel PH102®.

Measuring the swelling capacity, water uptake, pore structure of tablets and surface free energy, the attention was consequently focused on the question, why UICEL is acting as a disintegrant. Thereby, it could be shown that the water uptake for tablets consisting of UICEL was less dependent on the relative density of the tablets compared to Avicel PH102®. Considering the extremely small swelling capacity of both UICEL and Avicel PH102® particles, an increase of the intraparticle volume could not provide a possible reason for the water uptake, which must therefore be explained by an increase of the interparticle volume within the tablet. The pore size of UICEL tablets measured by mercury porosimetry, was higher by a factor of 2-3 over the whole relative density range compared to Avicel PH102® tablets. The surface free energy was measured by water sorption and inverse gas chromatography (IGC). The results of both methods indicated that UICEL has a smaller surface free energy (polar and dispersive component) than Avicel PH102®.

Concerning UICEL, it was concluded that the small ductile behavior under pressure and the high elastic recovery result on the one hand in a higher pore size, which favors the fast water uptake (essential for disintegration) and on the other hand in a smaller binding surface area between two particles. The small binding surface area combined with a lower surface density of binding sites – suggested due to the lower surface free energy – effects a faster separation of the particles and thus a faster disintegration of the tablet. Additionally, the regeneration of the original shape of compressed UICEL particles upon water contact, is supposed to favor the disintegration process.

The feasibility of UICEL as disintegrant was examined. The dissolution profile of proquazone from tablets consisting of a binary mixture of proquazone and a disintegrant (sodium starch glycolate (Vivastar®), pregelatinized starch (Starch 1500®), microcrystalline cellulose (Avicel PH102®) and UICEL) was measured spectrophotometrically in a flow-through system. A new biexponential equation could excellently describe the release of proquazone. Related to the efficiency of drug release, the used disintegrants could be ranked in the order: Vivastar® > UICEL = Starch 1500® ≫ Avicel PH102®. Due to its good compactibility and flowability properties, UICEL is very well suitable as multipurpose excipient with the combined function as disintegrant and filler for direct compression. Vivastar® is very effective as disintegrant, but cannot be recommended as a filler. However, in order to use UICEL as disintegrant in more realistic multicomponent systems further investigations have to be performed.

Due to the higher moisture content of UICEL, the question raised whether incompatibility problems could occur when combined with moisture sensitive drugs. Thus, the decomposition of acetylsalicylic acid in a binary mixture with UICEL and Avicel PH102[®], respectively was investigated at various conditions (temperature, relative humidity) over various time periods. However, despite the higher moisture content, the decomposition of acetylsalicylic acid was for all selected storage conditions smaller in combination with UICEL instead of Avicel PH102[®]. It was concluded that differences in the surface properties and in the overall surface area of the two celluloses cause the difference in drug stability.



2 Introduction

2.1 Relevance of polymorphism

It is well known that about 50% of all drug substances (e.g. carbamazepine [1], spiperone [2], tamoxifen citrate [3], etc.) show polymorphism, which is the ability of a substance to exist in more than one crystalline form. Due to differences in physicochemical properties (solubility, wettability, melting point etc.) the polymorphic forms can have a different impact on the quality or performance of the drug product including bioavailability and stability (shelf life). The fact that a lot of attention should be paid to the polymorphism of drug substances can be illustrated by means of two examples: i) *In vivo* absorption studies showed that the polymorphic form of chloramphenicol palmitate has a significant effect on the bioavailability [4]. Therefore, the USP 24 limits the maximum allowed fraction of the unfavorable polymorphic form in the monograph of the oral suspension of chloramphenicol palmitate. ii) Norvir[®] (semi-solid capsules containing ritonavir as drug), which was introduced in 1996 had to be withdrawn two years later from the market and reformulated because the precipitation of a less soluble polymorphic form resulted in dissolution failures [5, 6]. These two examples emphasize the importance of the guideline developed by the International Conference on Harmonisation (ICH), which requires proper specifications by investigating the drug substances according to a decision tree [7, 8, 9].

It is an interesting fact that there is much less awareness about the potential of polymorphic forms of excipients compared to drug substances. However, the manufacturing process and thus the properties of the resulting product may depend heavily on the polymorphism of the excipients. This can be illustrated by a few examples: i) Cacao butter (theobroma oil) can exist in four polymorphic forms with different melting points. Thus, stable suppositories can only be produced by melting cacao butter at the lowest possible temperature (about 33°C) [10]. ii) Sorbitol can exist in different polymorphic forms. Because the most stable γ form is less sensitive to humidity and shows better compression properties compared to the other polymorphic forms, it is the most appropriate form as filler in tablets [11, 12]. iii) α -lactose monohydrate is reported to be suitable for wet granulation, whereas the anhydrous α and β forms are preferably used for direct compression [13, 14, 15]. iv) D-mannitol exists in three polymorphic forms (α , β , δ) [16] showing different properties concerning the compactibility and compressibility [17]. No polymorphic transition could be observed under pressure [18]. However, a moisture-induced polymorphic transition from δ to β can occur during a wet granulation process [19, 20]. v) The investigation of the polymorphism of cellulose and its influence on the tablet properties are part of this study. It can be concluded, that the

polymorphism of excipients deserves a high attention and should be investigated as a matter of routine in the same manner as the polymorphism of drug substances.

2.2 Cellulose

“Used the longest, known the least”: this statement applies extremely well to cellulose [21]. On the one hand, cellulose is the most abundant biopolymer and was used for thousand of years by mankind for instance as a material for housing and clothing. Cellulose is the main component of cell walls in higher plants including wheat straw, wood, cotton, flax, hemp, jute, ramie, etc. Furthermore, it is also present in bacteria, fungi and algae. Also in the future, cellulose will keep on playing an important role in our lives since it is renewable, biodegradable and biocompatible. On the other hand, the scientific characterization started not until 1830. Despite huge research efforts, the structure of cellulose has not yet been completely unraveled.

The structure of cellulose can be divided into three levels [22]. i) the molecular level, ii) the supramolecular level, which comprises the arrangement of the molecules and iii) the morphological level, *i.e.* the arrangement of the supramolecular elements. In the following section the first two levels will be presented in detail.

2.2.1 The molecular structure of cellulose

In the year 1838 cellulose was for the first time isolated from wood by the French botanist Anselme Payen [23]. It took almost another century till Freudenberg and Haworth could independently reveal the structure of cellulose on a molecular level [24, 25, 26]. Cellulose is an unbranched, linear syndiotactic (*e.g.* A-A'-A-A') homopolymer composed of D-anhydroglucopyranose (A) units, which are linked together by β -(1 \rightarrow 4)-glycosidic bonds. The dimer cellobiose (C) is the basic unit, thus cellulose can be considered as an isotactic polymer of cellobiose (C-C-C). n in the constitutional formula of cellulose (see figure 1) equals the degree of polymerization (DP) and stands for the total number of anhydroglucose units. Native cellulose has degrees of polymerization higher than 10'000 [27]. Isolated and processed celluloses have degrees of polymerization around 200 for microcrystalline cellulose and between 700 and 1000 for powdered cellulose [28, 29, 30].

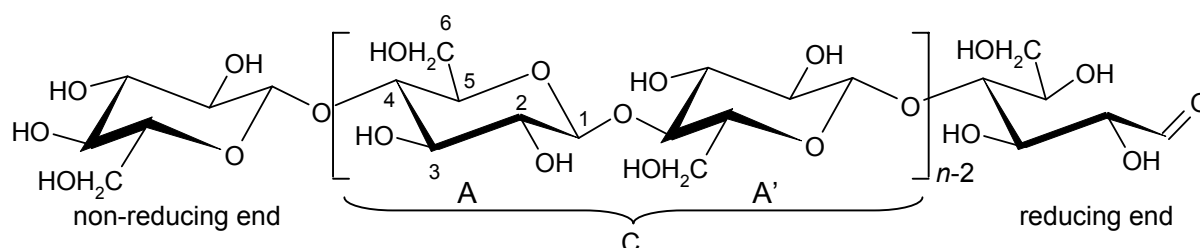


Figure 1: Molecular structure of cellulose. C: cellobiose; A, A': anhydroglucose unit.

2.2.2 The supramolecular structure of cellulose

Prior to the determination of the molecular structure of cellulose, Nägeli proposed that the cell walls consist of crystalline particles (micelles) embedded in an intermicellar substance (see figure 2 A) [31]. Measuring the viscosity of different polymer solutions Staudinger calculated a higher molecular weight for cellulose as expected on the basis of Nägeli's concept [32]. Based on these measurements, Staudinger dismissed the idea of isolated crystalline regions and suggested that polymers are continuous crystals, which are imperfect especially due to local distortions at the end of the molecules (see figure 2 B) [33].

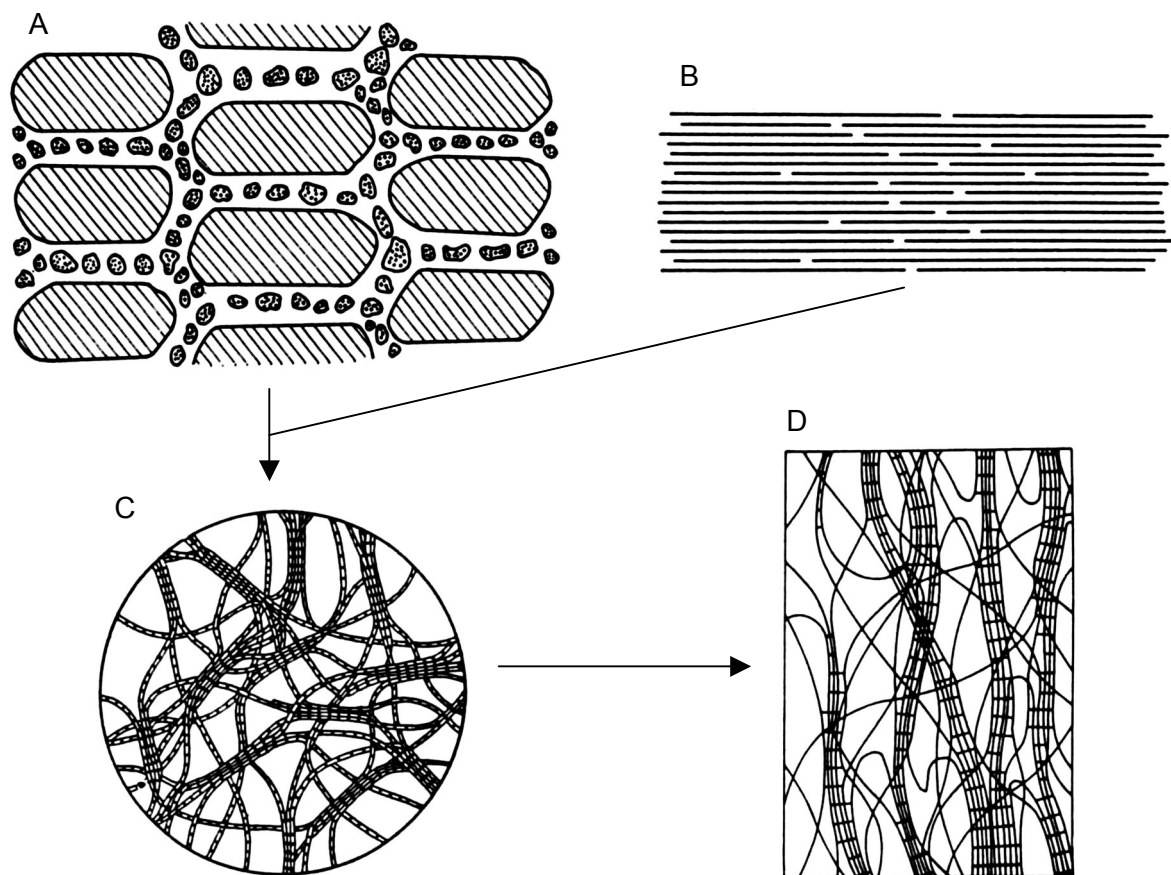


Figure 2: Development of the ideas of the supramolecular structure. A: micelle structure according to Nägeli, B: continuous structure of crystalline structure according to Staudinger, C: fringed-micelles, D: fringed-fibrils according to Hearle.

The fringed micelle-theory emerged from a combination of the two conflicting views. The structure can be divided into crystalline and non-crystalline regions. Like the brick-shaped micelles according to the theory of Nägeli, the crystalline regions are still discrete crystallites. However, a single molecule is much longer than a crystallite and passes therefore through both, crystalline and non-crystalline regions (see figure 2 C).

Hearle then further modified the fringed-micelle theory [34]. The crystalline regions are no longer considered as well-defined crystallites but as fringed fibrils, from which molecules diverge at different positions along its length (see figure 2 D). The fringed-fibril theory is still the generally accepted view, which is also consistent with photographs obtained by scanning electron microscopy (SEM) and x-ray measurements, which were indicating the presence of two phases (crystalline and non-crystalline regions).

The interlinked fibrillar network of fringed fibrils is referred to as microfibrils reaching an approximate length of a few micrometers. The concept of microfibrils has been established through the application of the electron microscopy [35]. The microfibril might be considered as basic level of the structural organization of cellulose. The question, whether there is an intermediate structural element called elementary fibril is still a controversial subject. However, the formation of macrofibrils by the aggregation of microfibrils seems to be beyond dispute.

2.2.3 Polymorphism of the crystalline regions in cellulose

Cellulose exists in four major crystal modifications, cellulose I, II, III and IV. The polymorphic forms can be interconverted according to figure 3 mostly by certain chemical and thermal treatments [36].

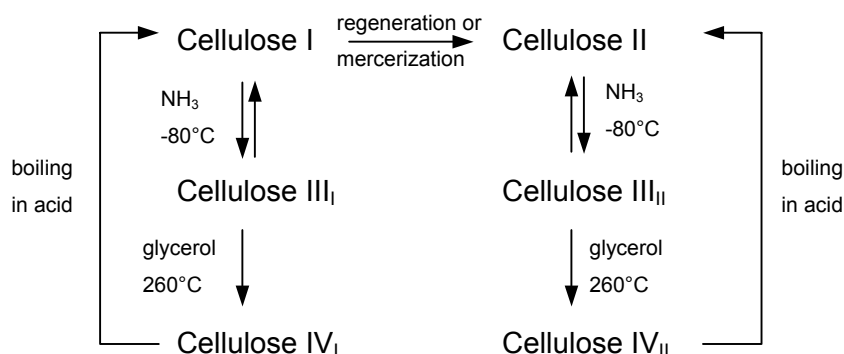


Figure 3: Interconversion of the polymorphs of cellulose.

Cellulose I and II are the most important forms and will therefore be discussed in more detail. Apart from few exceptions, native cellulose adopts the cellulose I lattice. 1984 Atalla *et al.* could demonstrate that cellulose I represents a mixture of cellulose I α and cellulose I β [37]. Both allomorphs were coexisting in different proportions, depending on the origin [38]. The celluloses produced by primitive organisms (bacteria, algae etc.) are said to be dominated by the I α phase whereas the cellulose of higher plants (wood, cotton, ramie etc.) consists mainly of the I β phase [39].

Although cellulose II was recently reported to be produced by the bacterium *Acetobacter xylinum* at low temperatures [40] and by the alga *Halicystis* [41], cellulose II is mainly

manufactured either by regeneration or by mercerization. Regeneration is performed by dissolving cellulose in an appropriate solvent followed by reprecipitation in water. Mercer developed the mercerization process already more than 150 years ago. It involves the swelling of cellulose I and the formation of Na-cellulose in concentrated aqueous NaOH followed by recrystallization of cellulose II upon washing. Thereby, the strength of the NaOH concentration turned out to be decisive. The lattice transition from cellulose I to cellulose II sets in above 10% of NaOH but is not completed below 15% of NaOH [42, 43]. Although doubted by some experts [44], most workers considered that the transition is irreversible and that cellulose II is thermodynamically the more favorable form compared to cellulose I [45, 46, 47].

The crystalline structures of cellulose I and II differ in two main characteristics: The unit cell dimension and the polarity of the chains.

In literature plenty of slightly different suggestions for the dimensions of the unit cell can be found (e.g. compare with values for cellulose I of Andress and of Meyer in table 1). However, the unit cell dimensions (see table 1) proposed by Meyer, Mark and Misch [48, 49] for cellulose I and by Andress [50] for cellulose II are still generally accepted. The two unit cells are depicted in figure 4.

Since the two ends of the cellulose molecules are not identical (reducing, non-reducing), a polarity can be assigned to the chains. If the reducing ends are all on the same side, then the arrangement is called parallel. If the reducing and non-reducing ends of the chains are arranged in an alternating way, then the packing is referred to as antiparallel. In the meantime the parallel arrangement of cellulose I is widely accepted [51, 52]. Concerning cellulose II the question about the polarity is still open for discussion. Despite the fact that most workers favor the antiparallel packing for cellulose II [46, 51, 53], some scientists still maintain the assumption of parallel chains [54, 55].

The differences in cell unit and chain polarity result in a totally different hydrogen bonding network. The knowledge about the formation of hydrogen bonds is essential in order to clarify the correlation between structure and physical properties. However, for a long time, the hydrogen bonding network could not have been determined experimentally because the resolution of x-ray diffraction goes not below 0.25 nm, which is not enough to detect the position of hydrogen atoms. Blackwell *et al.* assumed that cellulose II is tighter packed than cellulose I [47]. The different chain packing can also be expressed by the average bond length of hydrogen bonds, which are shorter for cellulose II (0.272 nm) than for cellulose I (0.280 nm). The same authors proposed that the intramolecular bonds are the same for the two cellulose polymorphs, however cellulose II is more strongly interbonded. Recently

molecular dynamics simulations revealed that cellulose I tends to form more intramolecular hydrogen bondings compared to cellulose II, while the formation of more intermolecular hydrogen bonds by cellulose II was confirmed [44].

Table 1: Unit cell dimensions of cellulose I and cellulose II.

polymorphic form	author	a [nm]	b (fibre axis) [nm]	c [nm]	β
cellulose I	Meyer, Mark, Misch	0.835	1.03	0.79	84°
cellulose I	Andress	0.823	1.03	0.784	84°
cellulose II	Andress	0.814	1.03	0.914	62°

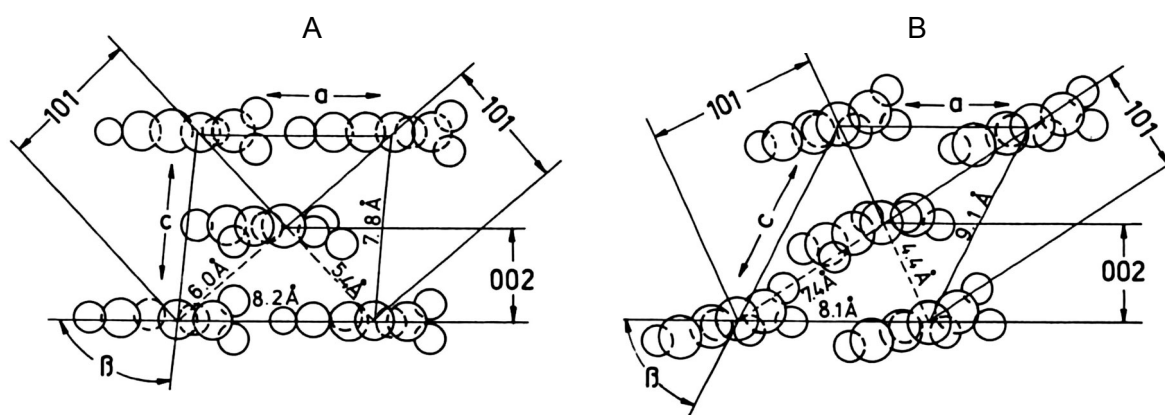


Figure 4: The unit cells of cellulose I (A) and cellulose II (B) in projection along the fibre axis b according to Andress [50, 56]. The notation relates to the old-fashioned and not modern convention in crystallography.

2.2.4 Preparation of the studied celluloses: UICEL and Avicel PH102[®]

Avicel PH102[®] is a so-called microcrystalline cellulose, which is prepared by depolymerizing alpha cellulose* with dilute hydrochloric acid to the point of leveling off the degree of polymerization (LOPD). According to Battista *et al.* the acid attacks mainly the amorphous regions, thus the final degree of polymerization (\triangleq LOPD) corresponds approximately to the degree of polymerization of macromolecules, which just consists of microcrystals [57, 58]. After purification and mechanical fragmentation of the cellulose in the aqueous slurry, the microcrystalline cellulose powder is obtained by spray drying.

UICEL (University of Iowa cellulose) was produced from Avicel PH102[®] at the University of Iowa by mercerization according to Kumar [59].

* Alpha cellulose is the portion of cellulose that does not dissolve in a 17.5% solution of sodium hydroxide at 20°C. Alpha cellulose should not be mistaken for cellulose I α .



2.3 Aims of the study

Remembering the amazing difference between the hardness of graphite and diamond, it is possible that various polymorphic forms of the same chemical compound show different properties on a macroscopic level. Analogous, different properties could also be expected for various polymorphs of cellulose. Kumar was the first who introduced a cellulose II product (UICEL) in pharmaceutical technology [60]. Although he already found a significant different disintegration behavior between tablets containing UICEL and Avicel PH102[®], very little is known about the characteristics of UICEL. Thus, the aim of the study includes the following issues:

- Characterization of powder properties of UICEL and Avicel PH102[®].
- Investigation of the compression behavior of UICEL and Avicel PH102[®].
- Clarification why UICEL is acting as a disintegrant.
- Testing the suitability of UICEL as disintegrant for the drug release from tablets.
- Stability study of acetylsalicylic acid in combination with UICEL or Avicel PH102[®].

3 Materials and Methods

Table 2 gives a short overview of the used substances, which include two types of microcrystalline celluloses (UICEL, Avicel PH102[®]), two well-known disintegrants (Starch 1500[®], Vivastar[®]) and two drugs (proquazone, acetylsalicylic acid).

Table 2: Overview of the used substances.

substance	trade name	distributor
Cellulose II based product ¹⁾	UICEL	University of Iowa
Cellulose I based MCC ^{1),2)}	Avicel PH102 [®]	FMC, Philadelphia, USA
Pregelatinized Starch	Starch 1500 [®]	Colorcon, Indianapolis, USA
Sodium Starch Glycolate	Vivastar [®]	JRS, Rosenberg, Germany
Proquazone	-	Sandoz Pharma AG, Basel, Switzerland
Acetylsalicylic acid pulvis	-	Hänseler, Herisau, Switzerland

¹⁾ fractionated by sieving (75-105 μm)

²⁾ MCC: microcrystalline cellulose

3.1 Preparation and manufacturing processes

3.1.1 Storage

Before processing or testing, the powders were stored for at least 14 days at 20-25°C and a relative humidity (RH) of about 45±10% (over a saturated solution of K₂CO₃) [61]. Possible exceptions to these conditions are emphasized in the corresponding methods. Temperature and RH were controlled with a hygrometer (HygroPalm 1 with Hygro Clip S, Rotronic AG, Bassersdorf, Switzerland).

The manufactured tablets were stored at the same conditions for 48 hours before testing.

3.1.2 Binary powder mixtures

After sieving, the components were mixed in a blender (Turbula[®] T2C, W. Bachofen AG, Basel Switzerland) for 5 minutes. The used ratios are mentioned in the corresponding instructions of the methods.

3.1.3 Powder compaction

The round flat tablets were manufactured using the Zwick[®] 1478 Universal Testing Instrument (Zwick[®] GmbH, Ulm, Germany). The compression and the decompression took place with a speed of 10 mm/min. The ejection speed was 50 mm/min. Before each compression cycle, the punches and the die wall were lubricated with magnesium stearate. The excess of the lubricant was removed with compressed air. The height of the tablets was

measured “in die” at highest pressure with the Zwick® 1478 Universal Testing Instrument (Zwick® GmbH, Ulm, Germany) and 48 h after compaction with a thickness gage (Type 532 G, Compac, Geneva, Switzerland). The self-deformation of the machine was taken into account with a correction curve (polynomial of fifth degree) receiving from a blank compression.

The weight and the diameter of the tablets as well as the used compression forces depended on the experiment and are mentioned in the corresponding methods.

3.2 Test for purity

3.2.1 Conductivity

The conductivity was measured according to the official monograph of microcrystalline cellulose in the USP 24-NF 19 using a conductivity meter (Metrohm 660 Conductometer, Herisau, Switzerland). The calibration was performed using a 0.01N KCl-solution instead of a commercially available conductivity calibration solution as required by the USP 24-NF 19. KCl puriss. was dried for 12 h at 150°C, cooled down in a desiccator over phosphorus pentoxide (P₂O₅) and then dissolved in distilled water.

3.2.2 pH-measurement

The pH was measured according to the monograph of microcrystalline cellulose in the USP 24-NF 19 with a pH-meter (744 pH-Meter, Metrohm, Herisau, Switzerland) equipped with a pH glass electrode.

3.2.3 Water-soluble substances

The determination of the water-soluble substances was accomplished according to the monograph of microcrystalline cellulose in the USP 24-NF 19.

3.2.4 Determination of ethanol

10 g of each substance were suspended in 30 ml of deionized water. The suspension was mechanically stirred for 30 minutes in a stoppered Erlenmeyer flask and then centrifuged (Sigma 302 K, Osterode am Harz, Deutschland) for 15 minutes at 4500 rpm (*i.e.* 3500 times gravity). In the supernatant liquid the ethanol concentration was determined using the enzymatic UV-test kit (no.: 10 176 290 035) of R-Biopharm (Darmstadt, Deutschland) with a detection limit of 0.5 mg/l sample solution.

3.3 Basic powder characteristics

3.3.1 True density

The true density was measured with the gas displacement pycnometer AccuPyc 1330 (Micromeritics Instrument Corporation, Norcross, USA) with a nominal cell volume of 10 ml. Helium was used as gas. Before and after each series of measurement a zero-point check was performed. If this measured volume was beyond ± 0.05 ml, the pycnometer was calibrated using two steel balls as calibration standard with known and certificated volumes. In order to get results with good accuracy, the amount of the sample was chosen so that the measured volume was at least 10% of the nominal cell volume.

3.3.2 Bulk and tapped density

The bulk and tapped density were determined using an appropriate apparatus (Type STAV 2003, Engelsmann AG, Ludwigshafen, Germany). The test conditions according to USP 24-NF 19 were modified in respect of the used amount of the sample. The weight of the tested powder was reduced from 100 g to 10.0 g for UICEL and from 100 g to 7.0 g for Avicel PH102[®], respectively. Correspondingly the volume of the used cylinder was also reduced to 25 ml (readable to 0.25 ml). The volumes at the beginning (unsettled or poured volume V_0) and after tapping 500 (V_{500}) and 1250 (V_{1250}) times were noted. If the difference between the last two volumes ($V_{500} - V_{1250}$) was higher than 2% the test material was tapped additional 1250 times. The bulk density is calculated with the volume V_0 , the tapped density with the volume at the end of the experiment. The relative bulk density ρ_{rbulk} and the relative tapped density $\rho_{rtapped}$ were then calculated as the ratio of the bulk density to the true density and as the ratio of the tapped density to the true density, respectively.

The Hausner ratio H [62] and the Carr's Index CI [63, 64] were determined according to equation (1) and equation (2), respectively.

$$H = \frac{\rho_{tapped}}{\rho_{bulk}} \quad \text{equation (1)}$$

$$CI = \frac{(\rho_{tapped} - \rho_{bulk})}{\rho_{tapped}} \cdot 100 \quad \text{equation (2)}$$

where: H : Hausner ratio

ρ_{bulk} : bulk density [g/cm^3]

ρ_{tapped} : tapped density [g/cm^3]

CI : Carr's index [%]

3.3.3 Particle size measurement

The particle size distribution was measured using a laser scattering based particle sizer (MasterSizer X Long Bed, Malvern Instruments, Worcestershire, UK) with a 300 mm range lens. The samples were prepared in two ways: i) dry measurement: A sample preparation unit (MSX64 - Manual Dry Powder Feeder, Malvern Instruments, Worcestershire, UK) introduced an adequate amount of the powder (approximately 1 g) with a dispersion air pressure of 3 bars into the air cell (sample cell), which has an active beam length of 10 mm. This procedure was used for UICEL, Avicel PH102[®] and for acetylsalicylic acid. ii) wet measurement: The powder was dispersed in 0.1N HCl, which was saturated prior to the experiment with the substance itself. MSX1 dispersion unit (MSX1 – Small Volume Sample Preparation Unit, Malvern Instruments, Worcestershire, UK) pumped the dispersion through the circulating flow-through system with a sample cell of 2.4 mm active beam length. This method was applied for proquazone.

The software Mastersizer X version 2.19 (Malvern Instruments, Worcestershire, UK) controlled the measurement and used the data collected to calculate the particle size distribution using the Fraunhofer scattering theory, which requires no assumptions of the particles' optical properties.

3.4 Investigation of the structure

3.4.1 Chemical identity test

According to the identification test A of the USP 24-NF 19 10 mg of the sample were dispersed in 2 ml of iodinated zinc chloride solution. The iodinated zinc chloride solution was prepared by dissolving 20 g of zinc chloride and 6.5 g of potassium iodide in 10.5 ml of water. 0.5 g of iodine was added and shaken for 15 minutes.

3.4.2 X-ray analysis of cellulose samples

X-ray diffraction analysis of the sample was performed by Dr. D. Giron at Novartis Pharma Basel using a Scintag[®] XDS 2000 diffractometer (Scintag Inc., Cupertino, USA) with Cu-K α radiation (45 kV, 40 mA) from 2 to 40° 2 θ at a step size of 0.020° and a scan rate of 0.5°/min. Data was collected by the Diffraction Management System Software for Windows NT (DMSNT version 1.32, crystallinity version 1.0, Scintag Inc., Cupertino, USA), which was then used to identify the substance.

3.4.3 Degree of crystallinity, crystallinity index (*Crl*)

The degree of crystallinity of the cellulose samples was calculated by three methods. The first two are based on the evaluation of x-ray data and are visualized simplified in figure 5.

The first method is based on the integration of the scattered intensity. The crystallinity index *Crl* is defined as the ratio of the crystalline area to the total area under the curve (amorphous and crystalline). The software (DMSNT version 1.32, crystallinity version 1.0, Scintag Inc., Cupertino, USA) performed the calculation.

The second method uses the height of the scattered intensity for the calculation of the crystallinity index [65, 66, 67]. Equation (3) was used for Avicel PH102[®] and equation (4) for UICEL.

$$Crl = \frac{(I_{(002)} - I_{18^\circ})}{I_{(002)}} \cdot 100 \quad \text{equation (3)}$$

$$Crl = \frac{(I_{(10\bar{1})} - I_{16^\circ})}{I_{(10\bar{1})}} \cdot 100 \quad \text{equation (4)}$$

where: *Crl*: Crystallinity index (Degree of crystallinity) [%]

$I_{2\theta}$: scattered intensity at a angle of incidence θ

$I_{(002)}$: maximum intensity of the (002) lattice plane for cellulose I

$I_{(10\bar{1})}$: maximum intensity of the $(10\bar{1})$ lattice plane for cellulose II

The calculations were performed evaluating the diffraction diagrams, which were obtained according to the method described on page 15.

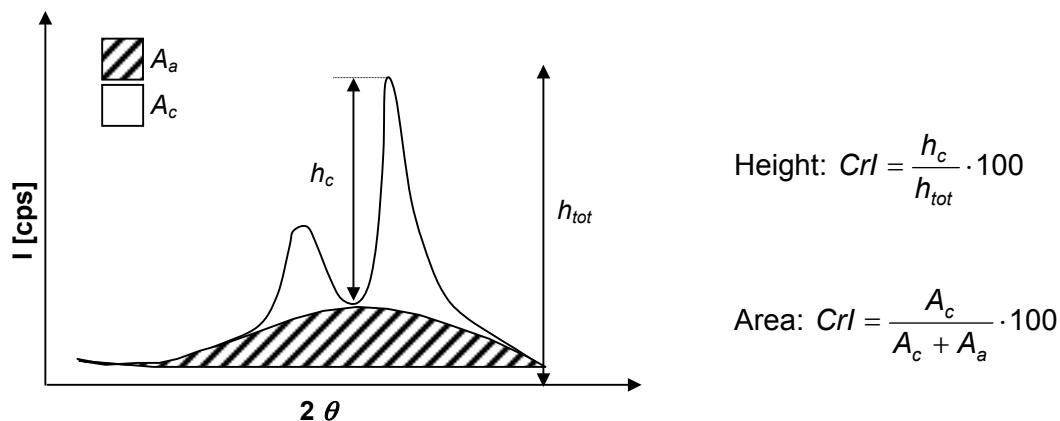


Figure 5: Visualization of the calculation method of the crystallinity Index *Crl*. (*A*: Area; *h*: height; *c*: crystalline; *a*: amorphous)

The third method is based on the measurement of the true density. The degree of crystallinity (weight fraction) is given by the equation (5) according to Kilian [68].

$$Crl = \frac{\rho_{tc}}{\rho_t} \cdot \left(\frac{\rho_t - \rho_{ta}}{\rho_{tc} - \rho_{ta}} \right) \cdot 100 \quad \text{equation (5)}$$

where: *Crl*: crystallinity index (weight fraction) of the sample [%]

ρ_t : true density of the sample [g/cm³]

ρ_{tc} : crystalline true density [g/cm³]

ρ_{ta} : amorphous true density [g/cm³]

The appliance of this formula requires the knowledge of the true density of the crystalline (100% crystalline) and of the amorphous (0% crystalline) form. Within the scope of this study values from the literature were used (see table 3). The values for the true density of the samples were taken from the results mentioned in the chapter “powder characterization” (page 45).

Table 3: Values for the true density found in literature (bold values were used).

material	true density [g/cm ³]	literature
Cellulose I (crystalline 100%)	1.592	[69]
	1.50	[70]
Cellulose II (crystalline 100%)	1.583	[69]
Cellulose (amorphous 100%)	1.482	[70, 71]
	1.50	[72]
	1.455	

3.4.4 Determination of the crystallite size

The crystallite size was determined according to the well-known Scherrer equation [73] (see equation (6)).

$$D = \frac{K \cdot \lambda}{\cos \theta \cdot FWHM} \quad \text{equation (6)}$$

where: *D*: crystallite size vertically to corresponding lattice plane [nm]

K: form factor (0.89 – 1.39) here *K* = 1

λ : wave length of Cu-K α radiation [nm] (λ = 0.1542 nm)

θ : angle of incidence [rad]

FWHM: Full width at half maximum peak intensity [rad]

The peak width (*FWHM*) was obtained by analyzing the Gaussian distribution used for the separation and least square fitting of the “crystalline” peaks (PeakFit Version 4.12, SeaSolve Software, Incorporation, Richmond, USA). In order to get the diffraction pattern of the crystalline phase, the global background scattering (including “amorphous” peaks or “haloes” and diffuse scattering due to thermal disorder of the crystalline phase) obtained by the

software (DMSNT version 1.32, crystallinity version 1.0, Scintag Inc., Cupertino, USA) was subtracted from the total measured scattering.

3.4.5 Scanning electron microscopy (SEM)

The upper surfaces of tablets compressed to a relative density of 0.8 as well as the powder of each substance were examined in a scanning electron microscope (Philips XL30 ESEM, Philips, Eindhoven, the Netherlands). The samples were mounted with carbon adhesive on aluminum stups, sputtered with 20 nm of gold (MED 020 Modular Coating Unit, BAL-TEC, Balzers, Principality of Liechtenstein) and photographed at an acceleration voltage between 3 and 5 kV.

3.5 Determination of the contact angle and the surface free energy

The contact angle and the surface free energy were measured by different methods and analyzed by various evaluation procedures.

3.5.1 Contact angle: sessile drop method

100 ± 1 mg tablets with a diameter of 11 mm were produced applying a compression force of 80 kN. The procedure of putting a drop of water (5 µl) carefully onto the upper surface of the tablet was filmed with 25 frames per second. The digital video camera recorder (Sony DCR-TRV11E, Sony corporation, Tokyo, Japan) was installed on the same height like the upper surface of the tablet, thus on the frame the surface of the tablet appears as a line (x-axis). The contact angle of the drop on the first frame (after 40 ms) was determined using three different evaluation procedures.

a) Height and length method

The first calculation was performed according to equation (7) using the height and length of the drop measured with Corel Photo-paint® (Corel Corporation, Ottawa, Canada). The derivation of the equation was accomplished on the assumption that the drop on the picture has the shape of a circle segment (appendix A).

$$\theta = \pi - 2 \arctan\left(\frac{l}{2h}\right) \quad \text{equation (7)}$$

where: θ contact angle

l : "length of the segment" [mm] (compare with appendix A)

h : "height of the segment" [mm] (compare with appendix A)

b) Ellipse fitting method

The second determination of the contact angle is based on the hypothesis that the shape of the drop is an ellipse segment. The contour coordinates of the drop were first determined

using the software ScionImage Beta 4.0.2 (Scion Corporation, Frederick, USA) and then fitted with the ellipse equation (compare with appendix B). The calculation of the contact angle was performed using equation (8).

$$\theta = \arctan\left(\frac{c^2}{m}\right) \quad \text{equation (8)}$$

where: θ : contact angle

$c = b/a$: b : semiminor axis of the ellipse [mm]; a : semimajor axis of the ellipse [mm]

m : parameter that determines the segment (compare appendix B)

c) Linear regression of secant angles

As mentioned above, the projected surface of the tablet was considered as the x-axis. On the picture the origin was defined as the contact point of the drop surface with the tablet. The angle φ between the x-axis and a secant through the origin and a point P on the drop profile was considered as a function of the x-coordinate of the point P . If point P moves towards the origin then the corresponding angle φ is increasing. In the case where point P equals the origin the secant becomes a tangent and the angle φ becomes the contact angle θ . Thus, the contact angle results by the linear extrapolation of the angles of small corresponding x-values back to $x = 0$. The procedure is visualized in figure 6.

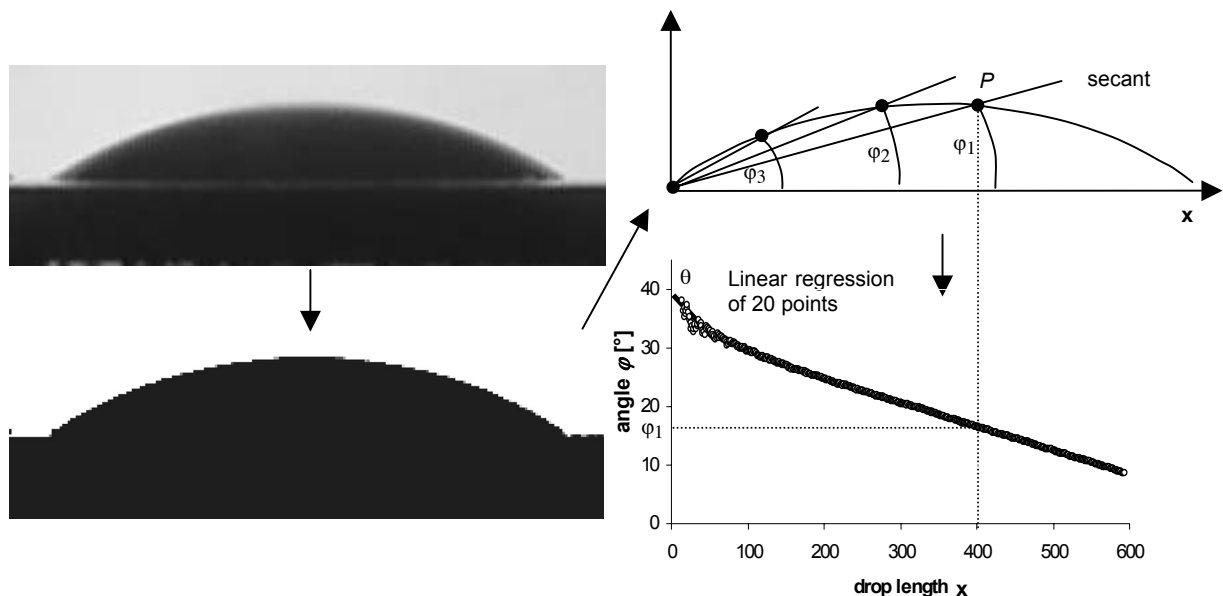


Figure 6: Contact angle determination from linear regression of secant angles φ . The unit of the drop length is arbitrary.

3.5.2 Contact angle: sorption method

The contact angle of the substances was also measured by means of the sorption method, using a tensiometer (Tensiometer K100, Krüss GmbH, Hamburg, Germany) (see figure 7) in combination with the Krüss Laboratory Desktop software (Version 3.0.1.2509, Krüss GmbH, Hamburg, Germany). The powder was dried for 14 days over phosphorus pentoxide (P₂O₅, 0% RH) and filled (Avicel PH102[®]: 1 g; UICEL: 1.3 g) into a little glass cylinder (9 mm diameter) with a porous glass base (no. P2), which was covered by a filter paper (593, Schleicher and Schuell GmbH, Dassel, Germany). The material was manually tapped always to the same volume (Avicel PH102[®]: 4.4 ml; UICEL: 4.6 ml).

The cylinder was then brought automatically in contact with the test liquid (surface detection: 0.02 g). A microbalance, which was connected to the cylinder, measured the weight increase due to liquid penetration into the powder material as a function of time. The liquid sorption of the glass frit and the filter was taken into account.

The calculation of the contact angle was performed according to the modified Washburn equation (equation (9)), which is based on Poiseuille's law and the capillary pressure (compare with appendix C, [74]).

$$\frac{m^2}{t} = \frac{c \cdot \rho^2 \cdot \gamma_L \cdot \cos \theta}{\eta} \quad \text{equation (9)}$$

where: m : mass of adsorbed liquid [g]
 t : time [s]
 ρ : density of the liquid [g/cm³]
 γ_L : surface tension of the liquid [mJ/m²]
 θ : contact angle
 η : viscosity of the liquid [mPa·s]

For the parameter c we can write equation (10):

$$c = \frac{1}{2} \pi^2 r^5 \cdot n^2 \quad \text{equation (10)}$$

where: r : mean radius of capillaries [mm]
 n : number of capillaries

The factor c depends on the packing density and the particle size. It has to be determined prior to the experiment with a liquid (e.g. *n*-hexane) that completely wets the sample ($\theta = 0$). Measuring m^2/t and knowing the values for the other parameters concerning the liquids (see table 4), allow to calculate the contact angles for these liquids.



Table 4: Characteristic parameters of the test liquids.

liquid	density, ρ	viscosity, η	surface tension, γ_L	dispersive component, γ_L^d	polar component, γ_L^p
	[g/cm ³]	[mPa·s]	[mJ/m ²]	[mJ/m ²]	[mJ/m ²]
Water	0.998	1.002	72.8	21.8	51.0
<i>n</i> -Hexane	0.661	0.326	18.4	18.4	0.0
Diiodomethane	3.325	2.762	50.8	50.8	0.0
Formamide	1.133	3.607	58.0	39.0	19.0
Ethylene glycol	1.110	21.810	48.0	29.0	19.0

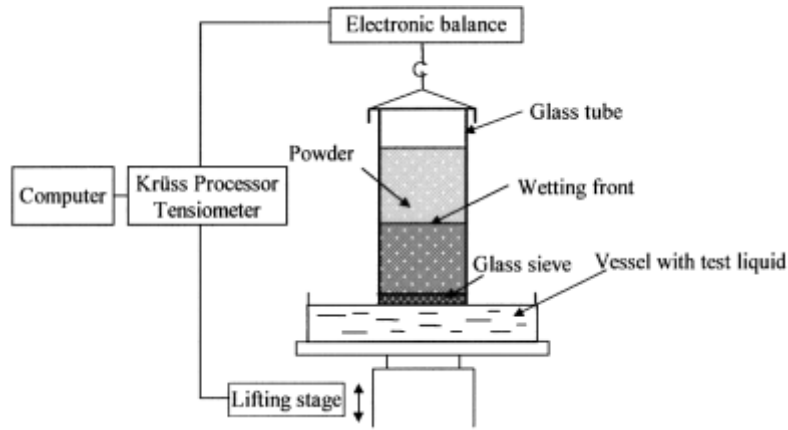


Figure 7: Experimental setup for the determination of the contact angle [75].

3.5.3 Surface free energy: two component-model according to Owens/Wendt

Owens and Wendt [76] combined the equations of Young (equation (11)) [77, 78] and Good (equation (12)) [79, 80] to equation (13):

$$\gamma_S = \gamma_{SL} + \gamma_L \cdot \cos \theta \quad \text{equation (11)}$$

where: γ_S : overall surface energy of the solid [mJ/m²]
 γ_{SL} : interfacial surface tension between the solid and the liquid [mJ/m²]
 γ_L : surface tension of the liquid [mJ/m²]
 θ : contact angle

$$\gamma_{SL} = \gamma_S + \gamma_L - 2\left(\sqrt{\gamma_L^d \cdot \gamma_S^d} + \sqrt{\gamma_L^p \cdot \gamma_S^p}\right) \quad \text{equation (12)}$$

where: γ_L^d : dispersive component of the surface tension of the liquid [mJ/m²]
 γ_S^d : dispersive component of the surface energy of the solid [mJ/m²]
 γ_L^p : polar component of the surface tension of the liquid [mJ/m²]
 γ_S^p : polar component of the surface energy of the solid [mJ/m²]

$$\underbrace{\frac{\gamma_L (\cos \theta + 1)}{2\sqrt{\gamma_L^d}}}_y = \underbrace{\sqrt{\gamma_S^p}}_m \cdot \underbrace{\sqrt{\frac{\gamma_L^p}{\gamma_L^d}}}_x + \underbrace{\sqrt{\gamma_S^d}}_b \quad \text{equation (13)}$$

The y-values were plotted against the x-values of various liquids with known values for the contact angle (determined by the sorption method, see page 20), surface tension and its components (see table 4). The polar and dispersive components of the solid were then calculated from the slope and the intercept of the linear regression curve. The total surface energy of the solid γ_S equals the sum of the dispersive and polar component [81, 82].

3.5.4 Surface free energy: inverse gas chromatography (IGC)

The surface properties of the two celluloses were investigated by inverse gas chromatography (IGC) by Dr. F. Thielmann (Surface Measurement Systems, London) using a commercial inverse gas chromatograph (SMS *iGC* 2000, Surface Measurement Systems, London, England) equipped with a flame ionization detector (FID) (see figure 8). The stationary phase (substrate, adsorbent) was obtained by packing the material of interest into a silanized glass column. In order to fix the powder, silanized glass wool was put on both sides of the column. The stationary phase was investigated by injecting gases or vapors of pure and known liquids (probe, adsorbate), which were carried through the column by helium. Table 5 presents the relevant characteristics of the substances used as probes.

Table 5: Characteristic parameters of the probe molecules used for IGC [83, 84, 85].

probe	surface area, a	dispersive surface free energy of the probe γ_L^D	DN	AN^*
	10^{-19} [m ²]	[mJ/m ²]	[kcal/mol]	[kcal/mol]
Ethyl acetate	3.3	19.6	17.1	1.5
Acetone	3.4	16.5	17.0	2.5
Ethanol	3.5	21.1	20.0	10.3
Acetonitrile	2.1	27.5	14.1	4.7
Heptane	5.7	20.3	-	-
Octane	6.3	21.3	-	-
Nonane	6.9	22.7	-	-
Decane	7.5	23.4	-	-

The measured retention time t_r for the probes was used to calculate the total retention volume V_T . V_T is then corrected to the net retention volume V_N by subtracting the column void space, which equals the retention volume of a non-adsorbing probe (methane) [86].

The detailed chromatographic conditions for the IGC measurement can be inferred from table 6. The measurement was fully automated and controlled by the software SMS *iGC* Controller v1.8).

Table 6: Chromatographic conditions for the IGC measurements.

settings	
column	glass column; 30 cm long, 3 mm inner diameter
amount of sample	about 1.5 g
inert carrier gas	Helium
flow rate	10 ml/min
column temperature	30°C
injection temperature	30°C
detection temperature	250°C
relative humidity	0%
injection volume	250 μ l
marker	Methane

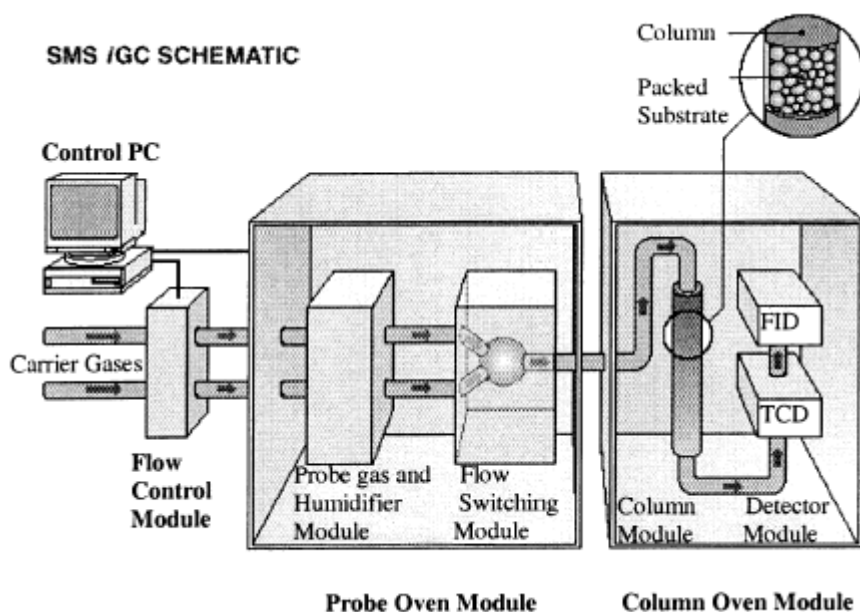


Figure 8: Experimental setup of the IGC measurement.

The free energy of desorption can be divided into a dispersion (London interactions) and specific (acid-base interactions) component (equation (14)).

$$\Delta G_D = \Delta G_D^D + \Delta G_D^{SP} \quad \text{equation (14)}$$

where: ΔG_D : total free energy of desorption [J/mol]

ΔG_D^D : dispersive component of the free energy of desorption [J/mol]

ΔG_D^{SP} : specific component of the free energy of desorption [J/mol]

As the interactions of *n*-alkanes with any substrate are restricted to dispersive Van der Waals forces, the overall free energy equals the dispersive component. Thus, a series of *n*-alkanes is appropriate to determine the dispersive component of the surface energy of the substrate according to equation (15) [87].

$$\Delta G_D = \underbrace{RT \ln(V_N)}_y = \underbrace{2N_A \cdot a \cdot (\gamma_L^D)^{1/2}}_x \cdot (\gamma_S^D)^{1/2} + C \quad \text{equation (15)}$$

where: ΔG_D : total free energy of desorption [J/mol]

R : universal gas constant: 8.3145 J/(mol·K)

T : absolute temperature [K]

V_N : net retention volume [ml]

N_A : Avogadro's constant ($6.023 \cdot 10^{23}$ molecules/mol)

a : interaction surface area of the probe molecule [m²]

γ_L^D : dispersive component of surface free energy of the probe (adsorbate) [J/m²]

γ_S^D : dispersive component of surface free energy of the substrate (adsorbent) [J/m²]

C : constant [J/mol]

When plotting y versus x of equation (15), the slope of the resulting line equals the square root of the dispersive component of surface free energy of the stationary phase, $(\gamma_S^D)^{1/2}$. Polar (acid/base) probes are characterized not only by dispersive interactions but also by specific interactions, which are based on the acid-base properties of the probe molecule. The base property of the probe can be expressed by the electron donor number DN , whereas the acid property is expressed by the electron acceptor number AN , which was modified by Riddle and Fowkes to give AN^* [83]. The net retention volume V_N of a polar probe is increased compared to a corresponding reference *n*-alkane. ΔG_D^{SP} is defined according to equation (16) and visualized in figure 9.

$$\Delta G_D^{SP} = RT \ln \left(\frac{V_N}{V_N^{ref}} \right) \quad \text{equation (16)}$$

where: ΔG_D^{SP} : specific component of the free energy desorption [J/mol]

R : universal gas constant: 8.3145 J/(mol·K)

T : absolute temperature [K]

V_N : net retention volume of the polar probe [ml]

V_N^{ref} : net retention volume of a corresponding reference *n*-alkane [ml]

Using the concept of Gutmann [85], which was then extended by Saint Flour *et al.* [88], the acid and base properties of the substrate can be characterized by K_A and K_D , respectively.

Plotting $\Delta G_D^{SP} / AN^*$ versus DN / AN^* of several probe molecules provides a regression line with slope K_A and intercept K_D . Strictly speaking, equation (17) is only valid for ΔH_D^{SP} and not

for ΔG_D^{SP} . In order to get the enthalpy it would be necessary to measure ΔG_D^{SP} at several temperatures ($\Delta G = \Delta H + \Delta S \cdot T$). Since the error of the measurement is in the same order as neglecting the entropic effect, it is common to use ΔG_D^{SP} instead of ΔH_D^{SP} [89, 90, 91]. However, it has to be kept in mind that the values for K_A and K_D are not exactly the same whether the calculation is based on ΔH or ΔG .

$$\Delta G_D^{SP} \approx K_A \cdot DN + K_D \cdot AN^* \quad \text{equation (17)}$$

where: ΔG_D^{SP} : specific component of the free energy of desorption [kcal/mol]

K_A : acceptor parameter of the substrate

K_D : donor parameter of the substrate

DN : electron donor number of the probe (base property of the probe) [kcal/mol]

AN^* : electron acceptor number of the probe (acid property of the probe) [kcal/mol]

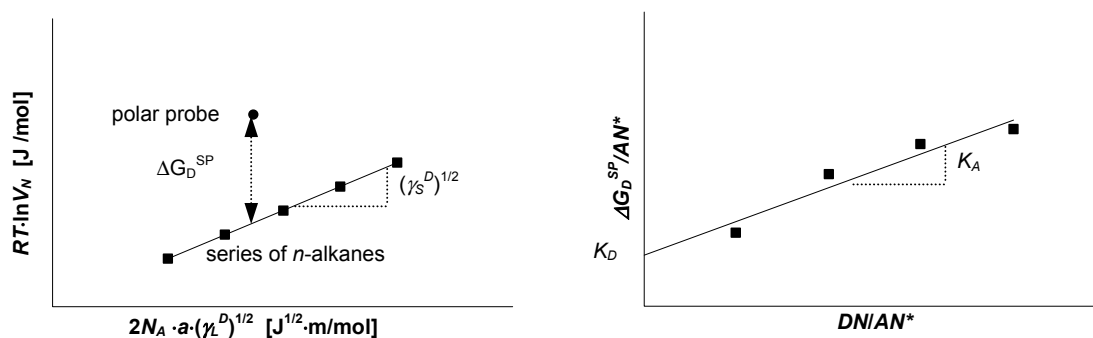


Figure 9: Visualization of the evaluation of IGC measurements.

3.6 Powder-water interactions

3.6.1 Moisture sorption

The moisture content was measured gravimetrically. Powder samples (approximately 1 g) were dried over phosphorus pentoxide (P_2O_5 , 0% RH) for 14 days and weighed (m_d). The samples were then stored at 20-25°C over saturated salt solutions of lithium chloride monohydrate ($LiCl \cdot H_2O$, 11.6% RH), potassium acetate (CH_3COOK , 22.4% RH), calcium chloride hexahydrate ($CaCl_2 \cdot 6H_2O$, 28.8% RH), magnesium chloride hexahydrate ($MgCl_2 \cdot 6H_2O$, 32.8% RH), potassium carbonate (K_2CO_3 , 44.0% RH), magnesium nitrate hexahydrate ($Mg(NO_3)_2 \cdot 6H_2O$, 53.4% RH) and sodium chloride ($NaCl$, 75.5% RH). After 14 days the samples were reweighed (m_w). The difference between m_w and m_d was considered as the moisture content m of the adsorption process (water gain). For the determination of the moisture content during the desorption process (water loss), the

samples were first stored for 14 days over pure water (H₂O, 100% RH) and then over the saturated solution of the same salts mentioned above [61, 92].

The RH was controlled with a hygrometer (HygroPalm 1 with Hygro Clip S, Rotronic AG, Bassersdorf, Switzerland).

The resulting adsorption curve was fitted according to the BET equation (equation (18)) derived by Brunauer, Emmett and Teller [93] and the modified and extended GAB equation (equation (19)) developed by Guggenheim, Andersen and de Boer [94, 95, 96]. The fitting ranges for the BET and GAB equation were $0 < p/p_0 < 0.5$ and $0 < p/p_0 < 1$, respectively.

$$m = \frac{c_{BET} \cdot m_m \cdot \frac{p}{p_0}}{\left(1 - \frac{p}{p_0} + c_{BET} \frac{p}{p_0}\right) \left(1 - \frac{p}{p_0}\right)} \quad \text{equation (18)}$$

$$m = \frac{c_{GAB} \cdot m_m \cdot k \frac{p}{p_0}}{\left(1 - k \frac{p}{p_0} + c_{GAB} k \frac{p}{p_0}\right) \cdot \left(1 - k \frac{p}{p_0}\right)} \quad \text{equation (19)}$$

where: m : weight of adsorbate (here: water) per 1 g of adsorbent (here: water) [g/g]

m_m : monolayer capacity or weight of the adsorbate when the surface of 1 g of adsorbent is covered by a monolayer [g/g]

p/p_0 : equilibrium (partial) relative pressure of the adsorbate (water activity)

p : (partial) vapor pressure

p_0 : vapor pressure at saturation

$$c_{BET} = E \cdot e^{(H_1 - H_L)/RT} \quad \text{equation (20)}$$

$$c_{GAB} = D \cdot e^{(H_1 - H_m)/RT} \quad \text{equation (21)}$$

$$k = B \cdot e^{(H_L - H_m)/RT} \quad \text{equation (22)}$$

with: c_{BET} , c_{GAB} : "energy" constant

E , B , D : constants

H_1 : heat of sorption of adsorbate in first layer [J/mol]

H_m : heat of sorption of adsorbate in intermediate state [J/mol]

H_L : heat of liquefaction [J/mol]

R : universal gas constant: 8.3145 J/(mol·K)

T : absolute temperature [K]

k : constant

The fitting procedure concerning equation (18) and equation (19) was performed using Systat for Windows Version 10.0 (SPSS Incorporation, Chicago, USA). A non-linear regression model was applied with the principle of least squares as loss function.

The surface area was then calculated according to equation (23).



$$A_{H_2O} = \frac{m_m}{M} \cdot N_A \cdot a_{H_2O} \quad \text{equation (23)}$$

where: A_{H_2O} : specific surface area [m^2/g]

m_m : monolayer capacity

M : molecular weight [g/mol] (water: 18.0 g/mol)

N_A : Avogadro's constant ($6.023 \cdot 10^{23}$ molecules/mol)

a_{H_2O} : cross-sectional area of one molecule: $12.5 \cdot 10^{-20} m^2$ [84]

3.6.2 Water retention capacity

30 ml of a 5% (w/w) dispersion of the substance (except for Vivastar[®]: 1% (w/w)) in deionized water was stirred for 24 h at room temperature. Next, the dispersion was centrifuged (Sigma 302 K, Osterode am Harz, Deutschland) at 4500 rpm (*i.e.* 3500 times gravity) for 30 minutes. The supernatant was decanted. The sediment was weighed (m_w), dried till constant weight at 75°C and reweighed (m_d). The water retention capacity was defined as the ratio of m_w to m_d [97, 98].

3.6.3 Swelling capacity

The bulk volume (V_d) of 5 g of each substance (except for Vivastar[®]: 1 g) was read in a 100 ml ground-glass stoppered cylinder. After the material had been mixed by gentle shaking in 80 ml of deionized water the dispersion was adjusted to 100 ml. The volume of the sediment (V_w) was noted after 24 h. The swelling capacity was defined as the ratio of V_w to V_d [97, 99].

3.7 Behavior upon compression

3.7.1 Compression behavior analysis

In order to describe the compression characteristics of UICEL and Avicel PH102[®] the compression data were fitted according to the Heckel equation (equation (24)) [100] and the modified Heckel equation (equation (25)) [101].

$$\ln\left(\frac{1}{1-\rho_r}\right) = K \cdot \sigma + A \quad \text{equation (24)}$$

$$\sigma = \frac{1}{C} \left[\rho_{rc} - \rho_r - (1 - \rho_{rc}) \ln\left(\frac{1 - \rho_r}{1 - \rho_{rc}}\right) \right] \quad \text{equation (25)}$$

where: ρ_r : relative density ($\rho_r = 1 - \varepsilon$ with ε : porosity) of the tablet

σ : compression pressure [MPa]

K : constant [MPa^{-1}]

A : constant

ρ_{rc} : relative critical density

C : constant [MPa^{-1}]

The fitting was performed with Systat for Windows Version 10.0 (SPSS Incorporation, Chicago, USA) using a non-linear regression with the principle of least squares as loss function.

ρ_t was calculated according to equation (26).

$$\rho_r = \frac{\rho_a}{\rho_t} = \frac{m}{\rho_t \cdot V_a} = \frac{m}{\rho_t \cdot h \cdot r^2 \cdot \pi} \quad \text{equation (26)}$$

where: ρ_a : apparent density [g/cm³]
 ρ_t : true density [g/cm³]
 m : weight of the tablet [g]
 V_a : apparent volume of the tablet [cm³]
 h : thickness of the tablet [cm]
 r : radius of the tablet [cm]

The parameters K and A of equation (24) and C and ρ_{rc} of equation (25) were used to characterize the compression behavior of the material. The Heckel parameters can be used to derive further characteristic parameters. According to equation (27) the constant K is inversely proportional to the mean yield pressure σ_y [102].

$$\sigma_y = \frac{1}{K} \quad \text{equation (27)}$$

where: K : Heckel parameter [MPa⁻¹]
 σ_y : mean yield pressure [MPa]

According to equation (28) the constant A can be used to calculate ρ_{rB} , which can be considered as a measure for the initial rearrangement of the particles [103]. For practical reasons ρ_{r0} was not related to the initial die filling (according to the original equation [100]) but defined as the relative density at the smallest compression pressure.

$$\rho_{rB} = \underbrace{1 - e^{-A}}_{\rho_{rA}} - \rho_{r0} \quad \text{equation (28)}$$

where: ρ_{rB} : relative density: measure for the curvature in the Heckel plot
 A : Heckel constant
 ρ_{r0} : relative density of the initial packing (compression pressure: 1.06 MPa)

The analysis was performed with „in die“ data as well as with „out of die“ data. In the case of the „in die“ analysis the thickness h in equation (26) was monitored with the Zwick® 1478 Universal Testing Instrument (Zwick® GmbH, Ulm, Germany) under maximum pressure. For the “out of die” analysis the thickness h was measured 48 hours after manufacturing with a thickness gage (Type 532 G, Compac, Geneva, Switzerland).

400 ± 1 mg tablets with a diameter of 11 mm were produced in a compression pressure range of 1.06-111.6 MPa.



3.7.2 Relaxation study of tablets

The elastic recovery (ER) according to equation (29) was chosen to express the relaxation behavior of the substances under pressure [104].

$$ER = \frac{h_0 - h_p}{h_p} \cdot 100 \quad \text{equation (29)}$$

where: ER : elastic recovery [%]

h_0 : thickness of the tablet “out of die” [mm]

h_p : thickness of the tablet “in die” [mm]

h_0 was measured using a thickness gage (Type 532 G, Compac, Geneva, Switzerland) 48 hours after manufacturing (zero-pressure, “out of die”). h_p was determined with the Zwick® 1478 Universal Testing Instrument (Zwick® GmbH, Ulm, Germany) under maximum pressure (at-pressure, “in die”).

400 ± 1 mg tablets with a diameter of 11 mm were produced in a compression pressure range of 1.05-105.2 MPa.

3.7.3 Determination of the extent of fragmentation during compression

Tablets, compressed to a relative density of 0.8, were suspended for 10 minutes in distilled water. The particle size of the dried substance was then measured as described in the section “particle size measurement” (see page 15). In order to determine the particle size reduction due to compression, uncompressed powder was subjected to the same procedure like the tablets. The difference in particle size between the compressed and the uncompressed powder was considered as a measure for the degree of fragmentation.

3.8 Basic tablet characteristics

3.8.1 Radial tensile strength measurement

The crushing force F (maximal force, which is used to crush a tablet) was measured using the Zwick® 1478 Universal Testing Instrument (Zwick® GmbH, Ulm, Germany). The preforce was set to 0.3 N and the testing speed to 10 mm/min.

The radial tensile strength σ_t was calculated according to equation (30) [105].

$$\sigma_t = \frac{2F}{\pi \cdot D \cdot h} \quad \text{equation (30)}$$

where: σ_t : radial tensile strength [MPa]

D : tablet diameter [mm]

h : thickness of the tablet [mm]

F : crushing force [N]

The data for the radial tensile strength σ_t versus the product of the relative density ρ_r and the compression pressure σ was fitted according to the equation of Leuenberger [106] (equation (31)). For this test 400 ± 1 mg tablets with a diameter of 11 mm were produced in a compression pressure range of 1.06-315.7 MPa. The fitting was performed with Systat for Windows Version 10.0 (SPSS Incorporation, Chicago, USA) using a non-linear regression with the principle of least squares as loss function.

$$\sigma_t = \sigma_{t\max} \cdot \left(1 - e^{-\gamma_t \cdot \sigma \cdot \rho_r}\right) \quad \text{equation (31)}$$

where: σ_t : radial tensile strength [MPa]
 γ_t : compression susceptibility [MPa⁻¹]
 ρ_r : relative density
 σ : compression pressure [MPa]

3.8.2 Mercury porosimetry

The pore size analysis was performed using a low-pressure and a high-pressure mercury porosimeter (PoreSizer 9320, Micromeritics Instrument Corporation, Norcross, USA).

Powders as well as tablets (400 ± 1 mg, 11 mm diameter, pressure range: 10.5 – 158 MPa) were measured. The sample cells (no. 920-61713 for tablets; no. 920-61710 for powders) were filled with mercury in an evacuated state (50 mm Hg equivalent to 6.7 kPa). The low-pressure analysis was performed manually in the pressure range 35 kPa - 150 kPa (*i.e.* 5 - 20 psia). The high-pressure analysis was run automatically from 150 kPa - 207 MPa (*i.e.* 20 psia - 30 kpsia) with an equilibration time of 10 s after each pressure. The whole pressure range corresponded to pore diameters ranging from 360 μm to 6 nm according to equation (32). The instrument provided the cumulative intrusion volume V at the corresponding pressure p . The associated pore diameter d and the pore surface area A_{Hg} were calculated according to equation (32) and equation (33), respectively. The pore size distribution was depicted by plotting the derivative of the cumulative logarithmic curve ($dV/d(\log d)$) versus the $\log d$. The peak diameters of those curves were considered as characteristic pore diameters. Equation (34) was used for the calculation of the derivative $dV/d(\log d)$ of the cumulative logarithmic curve [107].

$$d = - \frac{4\gamma_{Hg} \cdot \cos \theta_{Hg}}{p} \quad \text{equation (32)}$$

$$A_{Hg} = - \frac{\sum_{i=1}^{\max} p_i \cdot \Delta V_i}{\gamma_{Hg} \cdot \cos \theta_{Hg} \cdot m} \quad \text{equation (33)}$$

$$\frac{dV}{d(\log d)} \approx \frac{\Delta V}{\Delta p} \cdot p \quad \text{equation (34)}$$

where: d : pore diameter [μm]
 γ_{Hg} : surface tension of mercury (485 mN/m)
 θ_{Hg} : contact angle of mercury (130°)
 p : pressure [kPa]
 A_{Hg} : specific pore surface area [m^2/g]
 i : index for the pressure interval
 ΔV : incremental intrusion volume [ml]
 m : weight of the sample [g]

3.9 Tablet-water interactions

3.9.1 Disintegration

The disintegration time was measured with a disintegration apparatus (Sotax DT3, Sotax AG, Basel, Switzerland) in deionized water ($37 \pm 1^\circ\text{C}$) using disks according to the Ph. Eur. 4.

The disintegration of tablets containing proquazone was measured at the same conditions as mentioned above, but in 800 ml of 0.1N HCl instead of deionized water.

3.9.2 Visualization of the disintegration

100 ± 1 mg tablets (Avicel PH102[®] and UICEL) with a diameter of 11 mm were produced applying a compression force of 80 kN. The lubrication of the punches was omitted for these tablets.

The reaction of the tablet after putting 5 μl of water carefully on the upper surface of the tablet was registered with a digital video camera recorder (Sony DCR-TRV11E, Sony corporation, Tokyo, Japan).

3.9.3 On-line monitoring of the particle size during disintegration

The particle size during the disintegration of tablets was monitored on-line with the laser scattering based particle sizer (MasterSizer X Long Bed, Malvern Instruments, Worcestershire, UK) equipped with the MSX1 dispersion unit (MSX1 – Small Volume Sample Preparation Unit, Malvern Instruments, Worcestershire, UK) and a 1000 mm range lens. Deionized water (120 ml) was used as dispersant. The speed of the stirrer was always kept constant.

400 ± 1 mg tablets with a diameter of 11 mm and a relative density of 0.8 were produced and introduced to the closed flow-through system with a sample cell of 2.4 mm active beam length. The particle size was measured at various time intervals during 30 minutes.

The software (Mastersizer X version 2.19, Malvern Instruments, Worcestershire, UK) was used for the data acquisition and the calculation of the particle size distribution using the Fraunhofer scattering theory.

3.9.4 Water uptake

The determination of water uptake of tablets was performed using a modified Enslin-apparatus [108]. The apparatus is depicted in figure 10 and is described in detail by Ferrari *et al.* [109], Luginbühl [110] and Schmid [111].

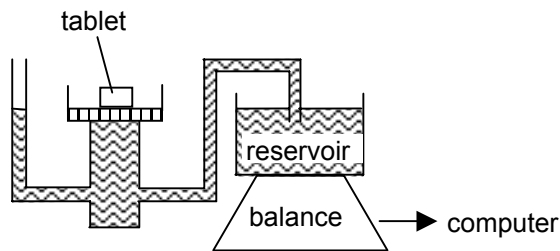


Figure 10: Experimental setup for the water uptake.

The reservoir was covered with Tesa-Film to prevent evaporation. The tablet was put on a filter paper (597, Schleicher & Schuell, GmbH, Dassel, Germany) covering the sintered glass filter (no. P0). The water, which is soaked into the tablet, was supplied by the reservoir via the communicating-vessel system. The decreased mass in the reservoir was registered by the balance (AT 460 Delta Range[®], Mettler-Toledo AG, Greifensee, Switzerland), which was connected to a computer. The experiment was performed during 10 minutes. BalanceLink[®] V3.01 Software was used for data acquisition (Mettler-Toledo AG, Greifensee, Switzerland).

The process of water uptake was characterized by the maximum water uptake m_{max} (amount of water taken up at the end of the experiment) and the time $t_{60\%}$, which it took for the tablet to take up 60% of the maximum water uptake. Additionally the rate of the water uptake was analyzed by the Washburn equation. For these purposes the Washburn equation (equation (9)) can be simplified (see equation (35)). Plotting the square of the water uptake versus the time, the slope of the regression line in the linear region was defined as water penetration index k_w .

$$k_w = \frac{m^2}{t} \quad \text{equation (35)}$$

where: k_w : water penetration index [g^2/s]
 m : mass of absorbed liquid [g]
 t : time [s]



3.9.5 Determination of the swelling force

The swelling force was measured with the apparatus shown in figure 11.

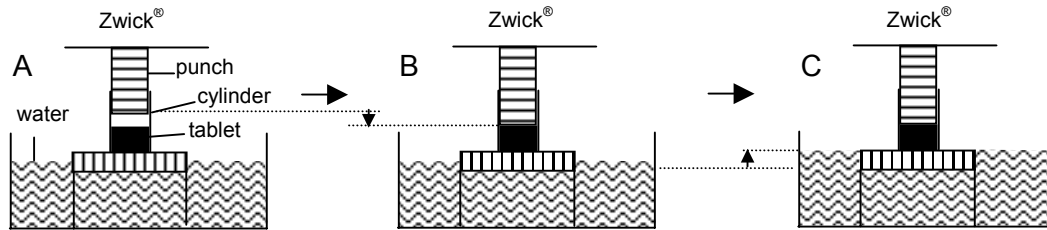


Figure 11: Experimental setup for measuring the swelling force.

The starting position is described in picture A of figure 11. A tablet was placed on a glass frit (no. P0). A glass tube (inner radius equals radius of the tablet) was put over the tablet on the glass frit, in order to avoid radial deformation of the tablet during water uptake. The force measurement was conducted with the Zwick® 1478 Universal Testing Instrument (Zwick® GmbH, Ulm, Germany) *via* a punch having the same radius like the tablet.

In a second step (compare with picture B in figure 11) the punch was brought in contact with the tablet (preforce = 0.05 N), where it held the position. During the last step, the water level of the reservoir was increased until the level reached the lower surface of the tablet. At this time the recording of the force caused by the swelling of the tablet started (compare with picture C in figure 11). The resulting profiles (force versus time) were fitted according to the Weibull function (see equation (36)) [112, 113, 114] and described by means of the maximum developed force F_{max} , the time τ_d needed to reach 63.2% of the maximum disintegrating force and the lag time t_0 . The derivative (“input” value) of the fitted curve at the time $t = t_0 + \tau_d$ is calculated according to equation (37).

$$F = F_{max} \left(1 - e^{-\left(\frac{t-t_0}{\tau_d}\right)^b} \right) \quad \text{equation (36)}$$

$$input = \frac{F_{max}}{\tau_d} \cdot b \cdot e^{-1} \quad \text{equation (37)}$$

where: F : recorded force [N]

F_{max} : maximum developed force [N]

t : time [s]

t_0 : lag time [s]

τ_d : time needed to reach 63.2% of the maximum disintegrating force [s]

b : shape factor

input: force development rate at time $t = t_0 + \tau_d$ [N/s]

e : Euler’s number, base of the natural logarithm (2.718...)

3.10 Dissolution rate measurements

150 ± 1 mg tablets consisting of proquazone and a disintegrant (UICEL, Avicel PH102[®], Vivastar[®] and Starch 1500[®]) were manufactured in different ratios (see table 7). The tablets – with a diameter of 7 mm – were compressed to a relative density of 0.88 (“out of die”).

Table 7: Composition of the tablets. UICEL, Avicel PH102[®], Starch 1500[®] and Vivastar[®] were used as disintegrants.

ingredient	composition [% (w/w)]						
Proquazone	100	95	90	80	70	60	50
disintegrant	-	5	10	20	30	40	50
UICEL		✓	✓	✓	✓	✓	✓
Avicel PH102 [®]		✓					✓
Starch 1500 [®]		✓					✓
Vivastar [®]		✓					✓

The dissolution was performed with a dissolution apparatus (Sotax AT7, Sotax AG, Basel, Switzerland) equipped with paddles. The speed of the paddles was set to a constant speed of 100 rpm. The dissolution medium was 0.1 N HCl (1000 ml, 37±1°C). The concentration of proquazone was quantified with a spectrophotometer DU[®]-37 (Beckman Coulter, Inc. Fullerton, USA) in a flow-through cell (flow rate: 3 mm/min) until the drug was totally released but for max. 90 minutes. First the quantification was carried out at a wavelength of 392 nm (λ_{max}), after reaching the absorption of 0.8 the wavelength was changed to 429 nm.

Continuously fresh 0.1 N HCl was added to the open system. Little differences in the speed of adding and removing of the dissolution medium were mathematically taken into account. Sink conditions (drug concentration in medium < 10% of the solubility [115, 116]) were maintained throughout the entire experiment.

3.10.1 Determination of the solubility (concentration of a saturated solution)

A saturated solution was prepared by adding an excess of proquazone to 0.1N HCl. The concentration of proquazone in 0.1N HCl at 37°C was measured over several days until the concentration remained unchanged.

3.10.2 Evaluation of the dissolution measurements

On the one hand the dissolution profiles were characterized with the empirical parameter $t_{50\%}$, which represents the time it takes until 50% of the total amount of proquazone are dissolved. On the other hand the data were fitted according to equation (38), which is deduced extensively in appendix D.



$$m(t) = J \cdot A_0 \frac{k_1}{k_1 - k_2} \left(\frac{1}{k_2} (1 - e^{-k_2 t}) - \frac{1}{k_1} (1 - e^{-k_1 t}) \right) \quad \text{equation (38)}$$

where: $m(t)$: dissolved amount of proquazone at time t [mg]
 k_1 : rate of area increase due to disintegration [min^{-1}]
 k_2 : rate of area decrease due to dissolution [min^{-1}]
 J : flux, which is determined prior to fitting [$\text{mg}/\text{min}/\text{cm}^2$]
 A_0 : maximum possible surface area during drug release [cm^2]

3.10.3 Calculation of the maximum possible volume-specific surface area A_{v0}

The volume-specific surface area A_{v0} is the surface area A_0 per unit volume of proquazone and can be calculated according to equation (39).

$$A_{v0} = \frac{A_0 \cdot \rho_t}{m_0} \quad \text{equation (39)}$$

where: A_{v0} : maximum possible volume-specific surface area [cm^2/cm^3]
 ρ_t : true density of proquazone [g/cm^3]
 m_0 : weight of proquazone at $t = 0$ (dose strength) [g]

3.10.4 Calculation of the maximum volume-specific surface area A_{vmax}

The maximum volume-specific surface area A_{vmax} was calculated analogous to the volume-specific surface area A_{v0} according to equation (40).

$$A_{vmax} = \frac{A_{max} \cdot \rho_t}{m(t_{max})} = A_0 \frac{k_1}{k_1 - k_2} (e^{-k_2 t_{max}} - e^{-k_1 t_{max}}) \cdot \frac{\rho_t}{m(t_{max})} \quad \text{equation (40)}$$

where: A_{vmax} : maximum volume-specific surface area [cm^2/cm^3]
 A_{max} : maximum surface area during drug release [cm^2]
 ρ_t : true density of proquazone [g/cm^3]
 $m(t_{max})$: weight of undissolved proquazone at time t_{max} [g]
with: $t_{max} = \ln(k_1/k_2)/(k_1 - k_2)$
 k_1 : rate of area increase due to disintegration [min^{-1}]
 k_2 : rate of area decrease due to dissolution [min^{-1}]
 A_0 : maximum possible surface area during drug release [cm^2]

3.10.5 Determination of the flux J

Flux J was deduced from the dissolution profile of a proquazone tablet without any excipient. Since the tablet is not disintegrating, the decisive surface area for dissolution at the very beginning of the dissolution experiment equals the surface area of the tablet and may be assumed to be constant. Thus, flux J resulted from a linear fit of the dissolution data at $t < 60$ min according to equation (41).

$$m(t) = J \cdot A \cdot t \quad \text{equation (41)}$$

where: $m(t)$: dissolved amount of proquazone [mg]

A : surface area of the tablet [cm^2]

($A = 2\pi(r^2 + r \cdot h)$ with r : radius of tablet, h : height of tablet)

t : time ($0 < t < 60$ min) [min]

J : flux [$\text{mg}/\text{min}/\text{cm}^2$]

3.11 Stability test of acetylsalicylic acid

Binary powder mixtures consisting of acetylsalicylic acid and cellulose (Avicel PH102[®], UICEL) were prepared in different ratios (see table 8). One half of the powder mixture was used for the compression of 400 ± 1 mg tablets with a diameter of 11 mm and a relative density of 0.8. The other half of the powder mixture as well as the compressed tablets were stored at different conditions over different time periods (see table 9).

Table 8: Composition [% (w/w)] of the binary mixtures.

ingredient	mixture 1	mixture 2	mixture 3
acetylsalicylic acid	100	50	10
cellulose	-	50	90

Table 9: Storage conditions (P: powder; C: compact).

condition	time [day]			
	0	7	29	62
45% RH, 25°C	P; C	P; C	P; C	P; C
45% RH; 70°C	P; C	P; C	-	-
75% RH; 25°C	P; C	-	-	P; C

(45% RH: storage over K_2CO_3 ; 75% RH: storage over NaCl)

An accurately weighed quantity of the powder mixtures or of the finely powdered tablets equivalent to about 40 mg of acetylsalicylic acid was suspended in 25.0 ml of acetonitrile. After shaking for 15 minutes the samples were centrifugated (Centrifuge 5415 C, Eppendorf AG, Hamburg, Germany) for 5 minutes at 14'000 rpm (*i.e.* 15'800 times gravity). Acetylsalicylic acid and salicylic acid were separated and quantified by HPLC (flow rate: 0.25 ml/min; injection volume: 2 μl ; wavelength: 280 nm) with an external standard. The determination of salicylic acid was used to quantify the degradation of acetylsalicylic acid. The instrument (Hewlett Packard series 1050, Hewlett Packard, Waldbronn, Germany) was equipped with a Spherisorb 80-5 ODS2 column (2 mm x 125 mm) (Macherey-Nagel AG, Düren, Germany).

The mobile phase was a mixture of 15% (v/v) acetonitrile and 85% (v/v) sodium dihydrogen phosphate buffer (10 mmol). The solution was adjusted to a pH of 2.0 with phosphoric acid (85%).

The decomposition of acetylsalicylic acid at ambient conditions (45% RH, 25°C) was characterized by the degradation rate constant k_0 , assuming a pseudo zero-order hydrolysis.

4 Results and Discussion

4.1 Test for purity

The purity of UICEL and Avicel PH102[®] was just investigated in respect of the solvents used during the preparation of UICEL from Avicel PH102[®]. The measurements of the conductivity and of the pH-value were performed in order to detect possible residue of sodium hydroxide. The ethanol test should detect impurity caused by ethanol, which was added during manufacturing for the precipitation of UICEL. The results of the corresponding purity tests can be inferred from the table 10.

Table 10: Results of the purity tests (with the Standard Error of the Mean (SEM); (n=3)).

substance	pH-value (**)	conductivity (**) [μ S/cm]	concentration of ethanol (*) [mg/kg substance]	Water-soluble substances (*) [%]
UICEL	7.09 (0.02)	29.4 (0.1)	7.7 (0.8)	0.07 (0.01)
Avicel PH102 [®]	6.54 (0.05)	49.5 (1.9)	3.9 (0.5)	0.15 (0.02)
water	6.92 (0.03)	1.2 (0.1)	-	-

(*): significant difference ($p < 0.05$) between UICEL and Avicel PH102[®]

(**): highly significant difference ($p < 0.005$) between UICEL and Avicel PH102[®]

Although the pH-values for the two substances differed, both can be considered as neutral. Despite the same test conditions, the requirements concerning the acceptable pH-value are stricter according to the USP 24-NF 19 (pH: 5 - 7) compared to the Ph. Eur. 4 (pH: 5 – 7.5). Thus, UICEL and Avicel PH102[®] are both conforming to the Ph. Eur. 4 while the pH value of UICEL is marginally higher than the upper limit of the USP 24-NF 19.

The measured pH-value is meaningful only if the ions, which are determining the pH-value leave the substance and go into solution. Carstensen *et al.* showed that the pH-value near the particle (microscopic or microenvironmental pH-value) parallels but does not equal the pH-value of the surrounding aqueous medium [117]. The compression of a mixture consisting of the substance and a pH-indicator could be a possible approach how the microenvironmental pH-values could be detected. By this procedure a deep contact between the indicator and the sample substance could be assured.

According to the USP 24-NF 19 the conductivity of the sample solution may not exceed the conductivity of the water by more than 75 μ S/cm. The solution of Avicel PH102[®] showed a significant higher value for conductivity than UICEL ($p < 0.005$). Nevertheless, both substances meet the requirement of the USP 24-NF 19. Considering the results of the

conductivity and the pH-measurements the inference may be drawn that the presence of sodium hydroxide is highly improbable.

Concerning the determination of ethanol, it has to be pointed out, that the test is based on the assumption that ethanol is extracted from the substances. Even though the concentration of ethanol is very low for both substances, the presence cannot be completely excluded. However, the test is very sensitive. Thus, the result or at least a part of the determined ethanol may be explained by the detection of traces of ethanol in the air.

Both substances contain less than 0.24% water-soluble substances and meet therefore the requirements of the USP 24-NF 19. Since UICEL is washed several times during the preparation procedure, it is not surprising that the amount of water-soluble substances is smaller compared to Avicel PH102[®]. Apart from impurities caused by the preparation procedure, some sugar components of hemicellulose such as xylose (predominant in hardwoods) and mannose (predominant in softwoods) are possible water-soluble substances [118]. But also lignin could be a possible origin of these substances [119]. As the sample preparation for the conductivity test is performed very similar to that for the quantification of water-soluble substances we can conclude that at least a part of the water-soluble substances has to be ionized.

4.2 Identification tests and structural investigations

Adding iodinated zinc chloride solution, both UICEL and Avicel PH102[®] took on a violet-blue color. According to this test, both substances meet the requirements for MCC of the USP 24-NF 19. Instead of two other identification tests, which are regulated by the USP, the x-ray diffraction patterns (see figure 12) of each substance were measured. The peaks of intensity result from crystallographic planes, which are labeled according to the Miller crystallographic indices.

The two substances show significantly different patterns. According to the database included in the software, the diffractogram of Avicel PH102[®] corresponds to cellulose whereas the pattern of UICEL couldn't be recognized by the computer. The 2θ -values for the peak maxima are in quite good agreement with values from literature [120]. Thus, the cellulose I lattice of Avicel PH102[®] and the cellulose II lattice of UICEL could be affirmed (compare with table 11 and table 12). The double peak caused by the $(10\bar{1})$ and (002) lattice plane is very characteristic for cellulose II. The d -spacings for Avicel PH102[®] and UICEL in table 11 and table 12 are calculated from the corresponding angles of incidence θ according to Bragg's law (see equation (42)) with $n = 1$ and a wavelength of Cu-K α radiation $\lambda = 0.1542$ nm. For cellulose I the d -spacings enable us, according to equation (43), to determine whether the $I\alpha$ or the $I\beta$ type is the dominating allomorph [121, 122].

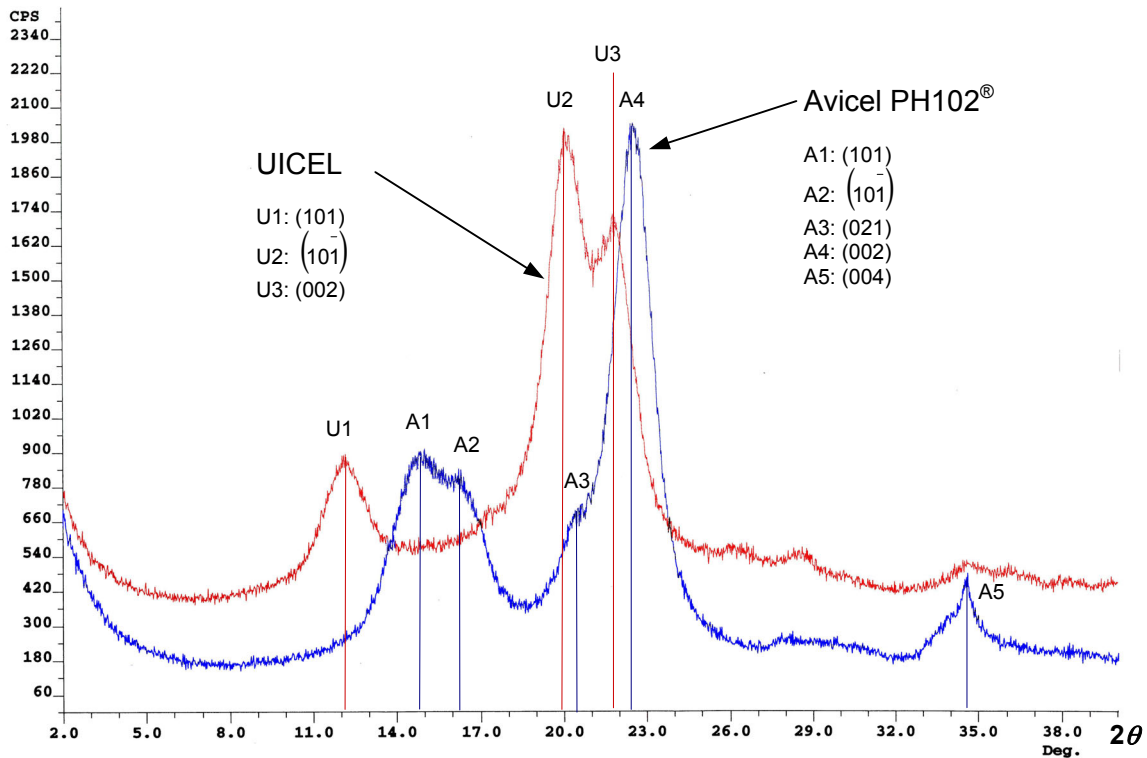


Figure 12: Powder x-ray diffractograms of Avicel PH102[®] and UICEL.

$$n \cdot \lambda = 2d \cdot \sin(\theta) \tag{equation (42)}$$

where: n : integer 1,2,3,... (here: $n = 1$)
 λ : wavelength of Cu-K α radiation [nm] ($\lambda = 0.1542$ nm)
 d : lattice spacing [nm]
 θ : angle of incidence [rad]

$$Z = 1693d_{101} - 902d_{10\bar{1}} - 549 \tag{equation (43)}$$

where: Z : discriminating value: $Z > 0$: I α rich; $Z < 0$: I β rich
 d_{101} : d -spacing of (101)
 $d_{10\bar{1}}$: d -spacing of (10 $\bar{1}$)

Using equation (43) the Z -value for Avicel PH102[®] equals -30.8 indicating that Avicel PH102[®] is dominated by the I β -allomorph. This result is not surprising because Avicel PH102[®] is manufactured as mentioned in the introduction (see pages 8, 10) from purified plant fibers, consisting mainly of the I β phase.

Table 11: Overview of 2θ -values for the peak maxima and crystallite size D of Avicel PH102[®] (n=1).

Avicel PH102 [®]					
Plane*	Plane**	measured 2θ (Lit.*)	d -spacing [nm]	FWHM [rad]	$D \perp$ to plane [nm] (Lit.*)
(101)	$l\alpha$ (100), $l\beta$ ($\bar{1}\bar{1}0$)	14.84 (14.7)	0.597	0.0352	4.4 (4.9)
($10\bar{1}$)	$l\alpha$ (010), β (110)	16.24 (16.8)	0.546	0.0311	5.0 (4.0)
(021)	$l\alpha$ ($\bar{1}\bar{1}2$), $l\beta$ (012)	20.41 (20.5)	0.435	0.0246	6.4
(002)	$l\alpha$ (110), $l\beta$ (200)	22.38 (22.7)	0.397	0.0299	5.3 (7.1)
(004)	$l\alpha$ ($\bar{1}\bar{1}4$), $l\beta$ (004)	34.54 (34.6)	0.260	0.0124	13.0 (12.5)

* according to [120]

** according to [123]

Table 12: Overview of 2θ -values for the peak maxima and crystallite size D of UICEL (n=1).

UICEL				
Plane*	measured 2θ (Lit.*)	d -spacing [nm]	FWHM [rad]	$D \perp$ to plane [nm] (Lit.*)
(101)	12.14 (12.3)	0.729	0.0274	5.7 (4.5)
($10\bar{1}$)	19.86 (20.0)	0.447	0.0331	4.7 (4.5)
(002)	21.73 (21.8)	0.409	0.0258	6.1 (5.1)

* according to [120]

The separation of the crystalline peaks in order to calculate the crystallite size is illustrated in figure 13 and figure 14 for UICEL and Avicel PH102[®], respectively.

The crystallite sizes D (see table 11 and table 12) calculated for the lattice planes (101), ($10\bar{1}$), (002) and (021) for Avicel PH102[®] represent the crystallite width. The values are different for each plane because D is the projection of the crystallite width perpendicular to the plane. The value deduced from the reflection profile caused by the (004) lattice plane is referred to the length of the crystallite.

Beside the fact, that the broadening due to instrumental influences was neglected (maximal error of 10% [124]), the small differences between the measured values and those found in literature can also be attributed to different method of manipulation and evaluation of the data. Some authors preferred to use the total scattering for calculation of the crystallite size instead of the "crystalline" scattering [120]. The peak separation was performed applying Gaussian-functions. Fink *et al.* [124] favored the use of Pearson-VII-functions in order to separate overlapping reflections. Nevertheless, the obtained values for the crystallite size are in the same order of magnitude compared to those found in literature and are therefore considered as feasible.

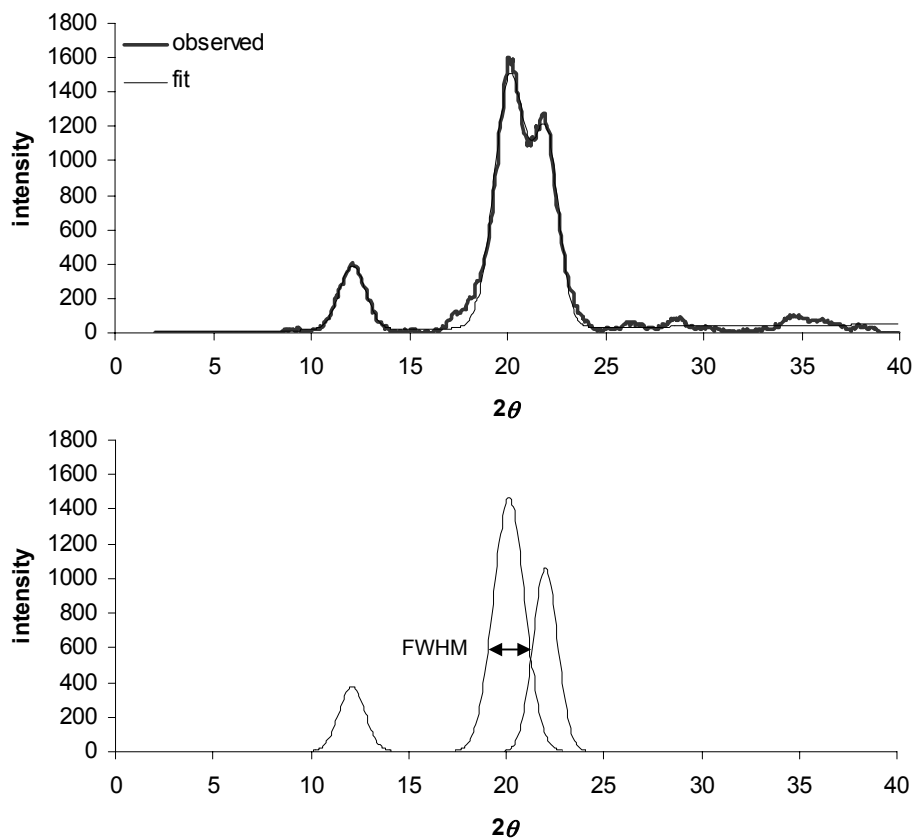


Figure 13: Separation and fitting of the “crystalline” peaks of UICEL using Gaussians functions (r^2 : 0.991).

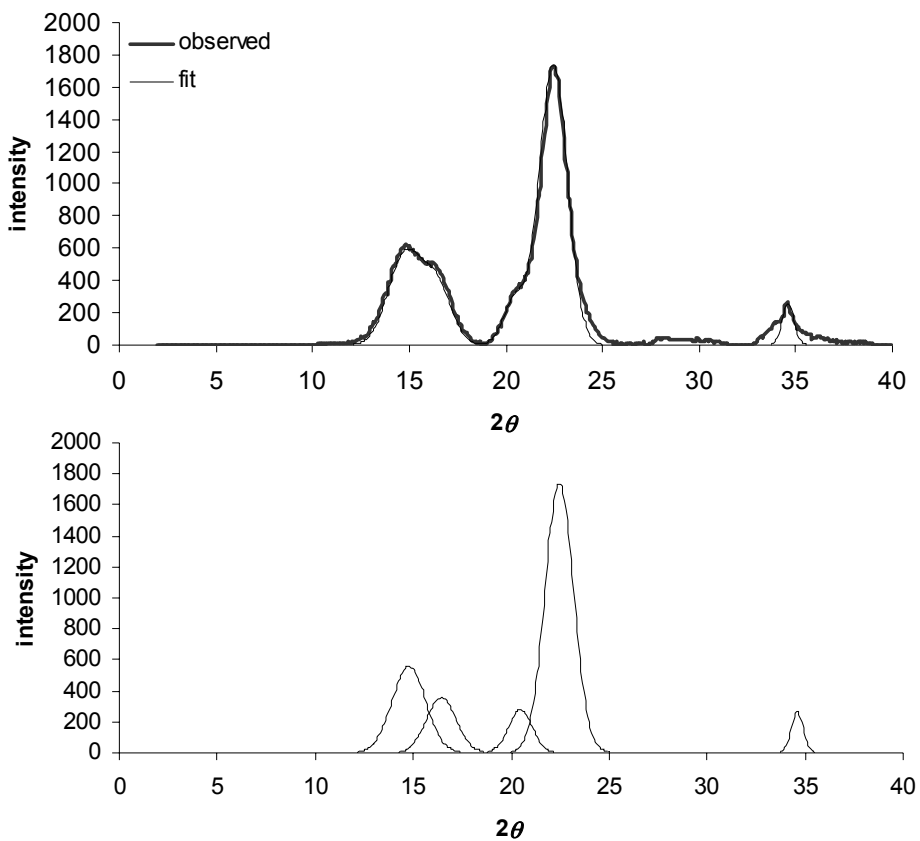


Figure 14: Separation and fitting of the “crystalline” peaks of Avicel PH102[®] using Gaussians functions (r^2 : 0.987).

For UICEL no diffraction peak can be assigned to the (004) plane, thus the length of the crystallite cannot be determined. A comparison between the values for UICEL and Avicel PH102[®] shows that there is no remarkable difference in the crystallite size at least for the comparable lattice planes. However, this result does not imply that the crystallite dimension during the transition from cellulose I to cellulose II persists [124].

The results for the determination of the degree of crystallinity are listed in table 13.

Table 13: Degree of crystallinity calculated by different methods.

Substance	degree of crystallinity [%]		
	X-ray; area	X-ray; height	True density
Avicel PH102 [®]	73	82	85
UICEL	64	71	57

With all three calculation methods the crystallinity index was higher for Avicel PH102[®] compared to UICEL. The difference of crystallinity between both substances was around 10% for the two methods based on the x-ray measurement and almost 30% for the method based on the true density.

Concerning the x-ray measurement, Jayme and Knolle compared the „area“ and „height“ evaluation and concluded that the first is superior to the latter [125]. Ruland [126] and Vonk [127] developed a more elaborate, mathematical based method to determine the crystalline fraction. Their approach even considered the fact that the scattered intensity of the crystalline region can also appear in the background due to thermal vibration and lattice imperfection. The intensity separation between the crystalline peaks and the amorphous background remained tricky. Other authors [128] suggested the use of some probability functions like the Gaussian distribution in order to characterize the contribution of the amorphous part to the measured intensity.

The calculation of the crystallinity by means of the true density is based on the fact that the true density is principally correlated with the packing arrangement of the molecules (dimensions of the unit cell) in a crystalline material. The difficulty of this evaluation method lies in the selection of reference values for the density of the totally amorphous and totally crystalline substance. The densities of the crystalline material originate from theoretical calculation based on the unit-cell dimensions. The density of the completely amorphous cellulose was determined experimentally. The values found in the literature lie within a broad range as can be seen in table 3. Most of the density values found in literature for the totally amorphous cellulose were derived from the density gradient method and not from the gas displacement method, which we used for the measurement of the sample density.

In literature we find further methods to determine the degree of crystallinity. The absorption of infrared radiation (IR) by a macromolecule is not only dependent on the intramolecular environment but is also affected by the interaction with surrounding molecules. Thus, it is possible to assign certain bands to the crystalline others to the amorphous phase. Because it is possible that the absorption is not only influenced by the degree of crystallinity but also by the polymorphic form of the cellulose, the choice of the bands for the calculation of the degree of crystallinity can be delicate [129, 130].

Even if the results differ from one method to the other, Avicel PH102[®] is considered to have a higher crystallinity than UICEL.

The values calculated from the x-ray measurements (especially the “area” evaluation) should be considered as the most reliable, not because the x-ray has an absolute accuracy but because it is the best established method.

Depending on the settings of the test parameters the measurement of a x-ray diffraction diagram takes between 30 and 75 minutes. Therefore x-ray diffraction can be applied routinely (routine analysis) and should be considered as state of the art because it is a powerful tool: it allows not only the identification of polymorphic forms but also the determination of the degree of crystallinity. Additionally x-ray measurements provide information of the purity or give at least an indication for the presence of mixtures of substances or polymorphic forms.

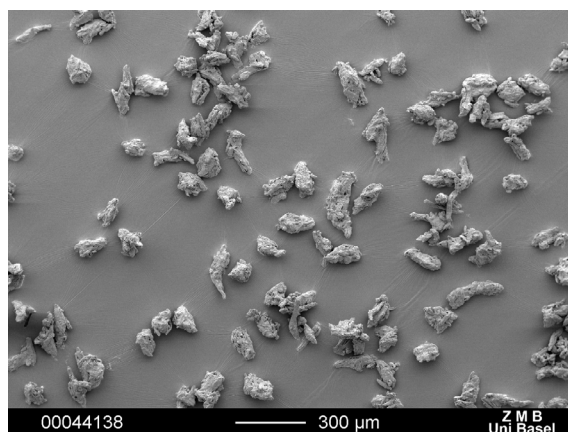
4.3 Powder characterization

The powder characteristics of UICEL and Avicel PH102[®] including values for the particle size, several densities (true, bulk and tapped) and the derived Hausner ratio and Carr index (compressibility index) are summarized in table 14.

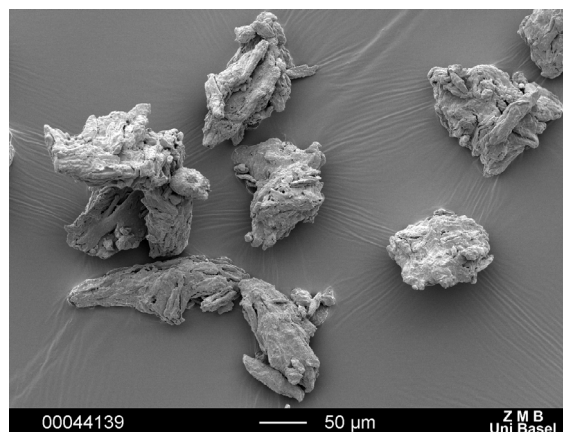
The particle size of both substances is very similar. This can be visually confirmed by the SEM photographs (see figure 15). The median, mean and mode value for UICEL as well as for Avicel PH102[®] are very close together indicating a normal distribution. The similarity in the particle size is not surprising because both materials represent the sieve fraction 75-105 μm . By using a sieve fraction, the possibility of a significant influence of the particle size on different properties should be avoided. The fact that the particle size for UICEL in table 14 is higher than the upper mesh size used for achieving the sieve fraction demonstrates impressively that the result of particle size measurement differs from one method to the other.

Table 14: Powder characteristics of UICEL and Avicel PH102[®] (with the Standard Error of the Mean (SEM)).

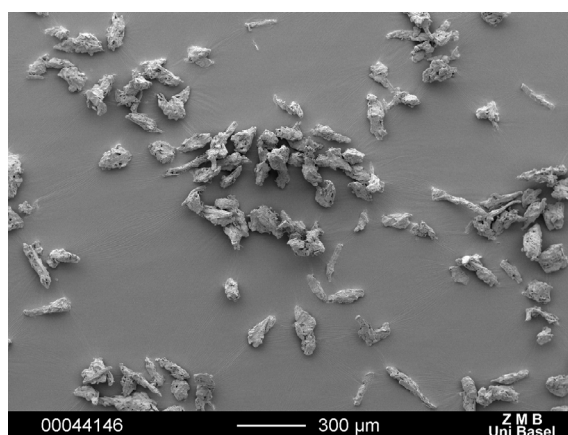
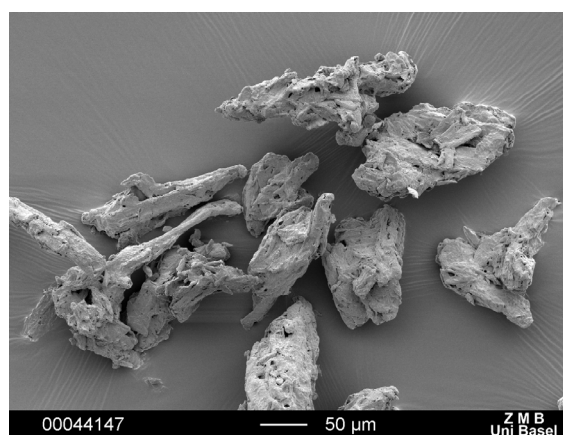
	UICEL	Avicel PH102 [®]
Particle size		
mean [μm] (n=3)	111.7 (0.09)	102.9 (0.19)
median [μm] (n=3)	107.0 (0.06)	97.1 (0.12)
mode [μm] (n=3)	106.3 (0.20)	100.7 (0.13)
Densities		
true density, ρ_t [g/cm^3] (n=4)	1.538 (0.0007)	1.575 (0.0004)
bulk density, ρ_{bulk} [g/cm^3] (n=3)	0.435 (0.012)	0.302 (0.010)
rel. bulk density, ρ_{rbulk}	0.283 (0.008)	0.192 (0.006)
tapped density, ρ_{tapped} [g/cm^3] (n=3)	0.513 (0.008)	0.384 (0.007)
rel. tapped density, ρ_{rtapped}	0.333 (0.005)	0.244 (0.004)
Hausner ratio (n=3)	1.18 (0.04)	1.27 (0.05)
Carr's index (n=3)	15.2 (2.7)	21.3 (3.0)



UICEL (magnification: 50x)



UICEL (magnification: 200x)

Avicel PH102[®] (magnification: 50x)Avicel PH102[®] (magnification: 200x)Figure 15: SEM photographs of UICEL and Avicel PH102[®] (prepared by the center of microscopy of the University of Basel (ZMB)).

The Hausner ratio and Carr's index can be used as an index for the flowability of a powder, because the densification occurring during the tapped density measurement is influenced by

the same interparticulate interactions which are affecting the flow of the powder. Wells [131] classified the flowability by means of the Hausner ratio in the following manner: $1 < H < 1.2$: good; $1.5 < H$: poor. According to Carr [63] a value between 5 and 10, 11 and 15, 16 and 20, 21 and 25, 26 and 31 indicates excellent, good, fair, passable and poor flow properties, respectively.

The Carr index and the Hausner ratio attest a good flowability for UICEL. Avicel PH102[®] on the contrary possesses fair to poor flow properties. This result can be explained by the fact that – considering the SEM photographs (see figure 15) – the fraction of needle-shaped fibers seems to be slightly higher for Avicel PH102[®] than for UICEL. Needle-shaped fibers are well-known to hamper the flow by the entanglement between particles.

As the bulk density is very sensitive to the sample preparation and especially to the filling of the cylinder, it is difficult to compare the derived Hausner ratio (and the Carr index) with corresponding values from literature. Despite this disadvantage, the relative comparison of the Hausner ratio (and the Carr index) between UICEL and Avicel PH102[®] shows that UICEL has the better flowability than Avicel PH102[®]. Published data of flow rate measurements through a funnel support the conclusion of the better flow properties of UICEL compared with Avicel PH102[®] [59].

The significant lower true density for UICEL compared to Avicel PH102[®] is not only due to the lower degree of crystallinity of UICEL (see table 13) but also to the different values of the true density of the two polymorphic forms. Different polymorphic forms can also show different preferred crystal habits. The polymorphic form is a function of thermodynamics whereas the crystal habit describes the shape and is linked to the kinetics of growth. Thus, it has to be considered, that the same polymorphic form could even grow in different crystal habits. However, since the two materials are both semicrystalline (consisting of an amorphous and crystalline part), no possible difference in the crystal habit can be seen in the SEM pictures (see figure 15).

4.4 Moisture sorption

The water sorption isotherms for UICEL and Avicel PH102[®] are depicted in figure 16. The moisture content of UICEL compared to Avicel PH102[®] is higher over the whole relative humidity range. However, according to the classification system of Callahan *et al.*, both celluloses can be referred to as slightly hygroscopic [132]. Both materials show the classic profile of a Type IV isotherm, with a broad hysteresis between the adsorption and the desorption curve.

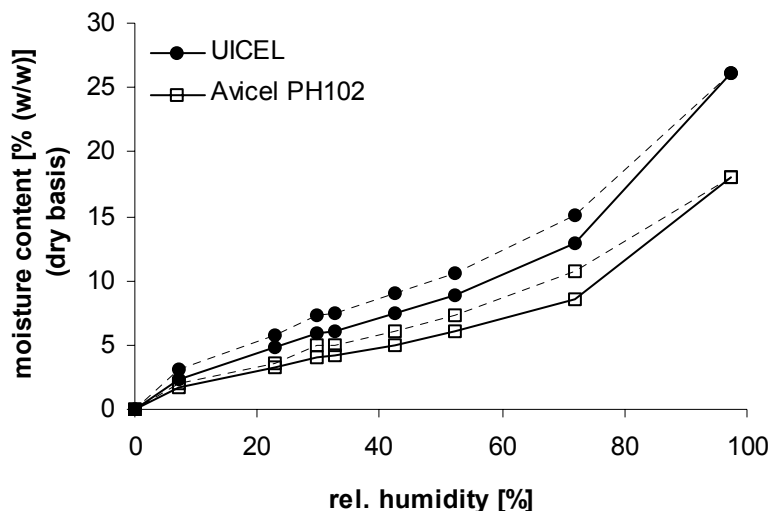


Figure 16: Water sorption isotherm for UICEL and Avicel PH102[®] (— adsorption; - - - desorption) (n=3).

At least for lower relative humidities, there is some evidence that the difference between the adsorption and desorption curve is broader for UICEL than for Avicel PH102[®]. This observation is in agreement with the results of Mihranyan *et al.* [133] who found that the level of hysteresis is smaller for a material with a high crystallinity index. Possible reasons for the moisture sorption hysteresis are manifold:

Frequently the hysteresis is explained by capillary condensation [134]. Differences in the advancing and receding contact angles are also mentioned as a reason for the loop. Last but not least it is possible that the swelling of the polymer uncovers new polar sites, which can interact with water molecules [92].

The moisture content of UICEL and Avicel PH102[®] at a relative humidity of 42%, corresponding approximately to a mean relative room humidity, is 7.5% and 5.0%, respectively. The loss on drying for microcrystalline cellulose according to USP 24-NF 19 may not exceed 7.0%. Even if the Pharmacopeia does not require the storage of the samples under well-defined conditions prior to the test “loss on drying”, it can be stated that the measured moisture content of 7.5% is rather high. Thus, a negative impact of the high water content of UICEL on the stability of moisture sensitive drugs cannot be excluded, if the two substances are mixed together.

The fitting of the adsorption curve of UICEL and Avicel PH102[®] is illustrated in figure 17 according to the BET equation and in figure 18 according to the GAB equation. The corresponding values for the fitted parameters are listed in table 15.

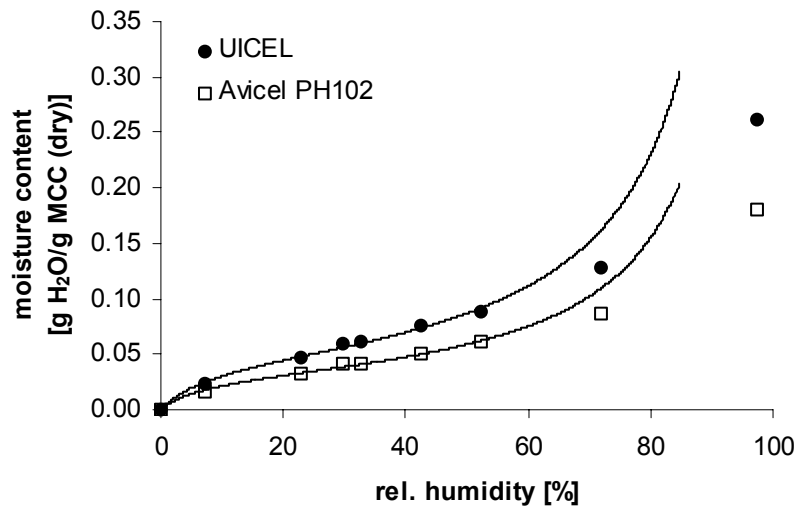


Figure 17: Fitting of the adsorption curves of UICEL and Avicel PH102[®] according to the BET equation.

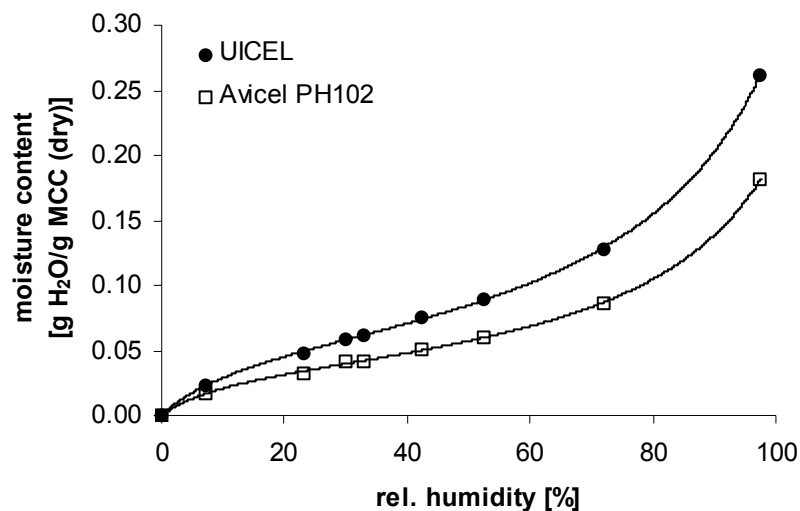


Figure 18: Fitting of the adsorption curves of UICEL and Avicel PH102[®] according to the GAB equation.

The GAB model is a refinement of the BET model. As the BET model distinguishes between a first tightly bound layer and multilayers having the properties of bulk free water, the GAB model takes into account an additional layer between the first layer and the bulk water. The GAB model is based on the BET model, thus the monolayer capacity m_m has in both equations the same physical meaning. Nevertheless, a comparison shows that the GAB monolayer capacity m_m is higher than the corresponding BET value. The GAB “energy constant” c_{GAB} is slightly lower but comparable to the BET constant c_{BET} .

A thorough comparison between the BET and the GAB equation came to the conclusion, that the GAB equation provides the more general information [135]. From a mathematical point of view it is not surprising that the introduction of a third parameter leads to a better correlation coefficient and a broader range of validity. However, the work of Timmermann showed that the application of the GAB model is justified and certainly more than just a fitting exercise [135]. Although the GAB equation is successfully applied in food technology [136, 137, 138]

and although the food industry considers the GAB equation as the fundamental equation for the characterization of the water sorption by food materials, the BET equation has still the approval of the International Union of Pure and Applied Chemistry (IUPAC) [139].

Table 15: Fitted parameters of the water sorption isotherm according to BET and GAB equation for UICEL and Avicel PH102[®] (with the Standard Error of the Mean (SEM); (n=3)).

substances	model	Range	m_m [g/g]	c_{BET}, c_{GAB}	k	r^2
UICEL	BET	$0 < p/p_0 < 0.5$	0.0469 (0.0012)	12.4 (2.2)	-	0.996
	GAB	$0 < p/p_0 < 1$	0.0589 (0.0008)	9.4 (0.5)	0.801 (0.003)	1.000
Avicel PH102 [®]	BET	$0 < p/p_0 < 0.5$	0.0315 (0.0008)	14.2 (2.7)	-	0.996
	GAB	$0 < p/p_0 < 1$	0.0384 (0.0007)	11.1 (1.0)	0.813 (0.004)	1.000

The power and significance of the GAB model could be demonstrated comparing derived values for $(H_1 - H_L)$ and $(H_m - H_L)$ according to equation (21) and equation (22) with calorimetric data. Unfortunately the values for the constants D and B are unknown. Being aware of a risky simplification the values for D and B can be assumed to be 1. The resulting values for $(H_1 - H_L)$ and $(H_m - H_L)$ are listed in table 16, indicating that Avicel PH102[®] and UICEL have approximately the same affinity to water. According to Differential Scanning Calorimetry (DSC) measurements the value of $(H_1 - H_L)$ is about 20 kJ/mol showing that B and D are smaller than unity [140]. Since the enthalpy of a hydrogen bond is also around 20 kJ/mol the adsorbed water up to the value of the monolayer capacity m_m is in a tightly bound state. The intermediate water is believed to exist up to three times the value of m_m [141].

Table 16: Derived parameters for UICEL and Avicel PH102[®] based on the fitted parameters according to the GAB equation.

substance	model	$(H_1 - H_L)$ [kJ/mol]	$(H_m - H_L)$ [kJ/mol]	Crl (x-ray, area)* [%]	m_{mcorr} (BET) [g/g]	m_{mcorr} (GAB) [g/g]
UICEL	GAB	6.10	0.55	64	0.130	0.163
Avicel PH102 [®]	GAB	6.48	0.51	73	0.117	0.142

* compare with table 13

According to equation (23) the surface area covered by water molecules can be calculated. The corresponding values are listed in table 17 together with the specific surface area determined by mercury porosimetry. Also values from the literature derived by nitrogen adsorption can be found in table 17.

Table 17: Specific surface area of cellulose samples determined by several methods (with the Standard Error of the Mean (SEM); (n=3)).

substance	A_{H_2O} (BET) [m ² /g]	A_{H_2O} (GAB) [m ² /g]	A_{Hg} [m ² /g]	A_{N_2} (Lit.*) [m ² /g]
UICEL	196 (5.1)	246 (3.3)	0.540 (0.001)	-
Avicel PH102 [®]	132 (3.4)	161 (3.1)	1.360 (0.006)	1.3

* according to [142]

The specific pore surface areas determined by mercury porosimetry were acquired exerting a maximal pressure of 12 MPa (corresponding to a pore diameter of 0.1 μm), because at higher pressures the values of the intrusion volumes were adulterated by the self-compression of the microcrystalline celluloses. The obtained value for Avicel PH102[®] is in perfect agreement with the value found in literature determined by BET-nitrogen experiment [142]. Marshall *et al.* [143] also measured the surface area. Their value, obtained by the BET-nitrogen technique, was too high (10.0 m²/g) for Avicel PH102[®] and therefore considered as wrong [142, 144]. However, using the mercury porosimetry Marshall *et al.* found a value of 1.26 m²/g for Avicel PH102[®]. Thus, the values obtained within this study may be considered as reliable. Furthermore, since the value for the surface area obtained by BET-nitrogen experiment are so close to the value derived from mercury porosimetry, it can be concluded that there are no smaller pores than 0.1 μm at least concerning Avicel PH102[®]. The specific areas determined by water adsorption for UICEL as well as for Avicel PH102[®] are extremely high. Considering that the values obtained by mercury porosimetry reflect the specific surface area, it is evident that the adsorption of water vapor cannot be safely used for the determination of the surface area.

The huge discrepancy between the “water” and “nitrogen” (and “mercury”) areas has to be attributed to the water penetration into the amorphous part of the cellulose [142]. This assumption can be verified by correcting or normalizing the monolayer capacity m_m with the non-crystalline fraction. The corrected values m_{mcorr} (see table 16) for UICEL and Avicel PH102[®] are coming closer (difference in percent is decreasing). This fact certainly supports the theory that the water is mainly adsorbed in the amorphous part of the material. The remaining difference between the corrected monolayer capacities m_{mcorr} for UICEL and Avicel PH102[®] could be an indication for different specific surface areas of the crystallites or different binding capacities of the crystalline parts for water molecules. However, beside the fact that different specific surface areas of the crystallites could not be supported by the determination of the crystallite size by x-ray (compare with table 11 and table 12) any further conclusions may be considered as speculations facing the uncertainty of the exact degree of crystallinity.

By the way, the suggested penetration of water into the amorphous part is consistent with the swelling as a possible reason for the observed hysteresis in the water sorption isotherm. To achieve a deeper insight into the different thermodynamic states of the involved water, thermogravimetric measurements would certainly be helpful.

4.5 Compaction of the powder

4.5.1 Elastic recovery

The elastic recovery ER is accepted as a good measure for the elastic deformation undergone by the compact during compression. Compared with other excipients Avicel PH102[®] showed already high values for the elastic recovery ER [28]. However, UICEL was characterized by even higher values, which were almost double as high as those of Avicel PH102[®] at high pressures (see figure 19). The elastic recovery ER of the two substances differed significantly ($p < 0.05$) above a compression pressure of 10.6 MPa. Thus, the greater tendency of UICEL to recover elastically has to be pointed out.

In the case of Avicel PH102[®], there was a slight decrease of the elastic recovery after a maximum value at a compression pressure of about 16 MPa. Krycer *et al.* [145] ascribed the decrease of the elastic recovery to an increase of interparticulate bonding (especially hydrogen bonds). Performing the measurement of the elastic recovery it could be observed that the decrease was more pronounced measuring the height of the tablets a few hours after manufacturing. By and by the values of the elastic recovery ER at higher compression pressures were then increasing. Thus, it can be concluded that the relaxation rate is depending on the corresponding relative density. Furthermore the still slight decrease of ER for Avicel PH102[®] indicates that the reorganization of the material was not totally completed after two days [146].

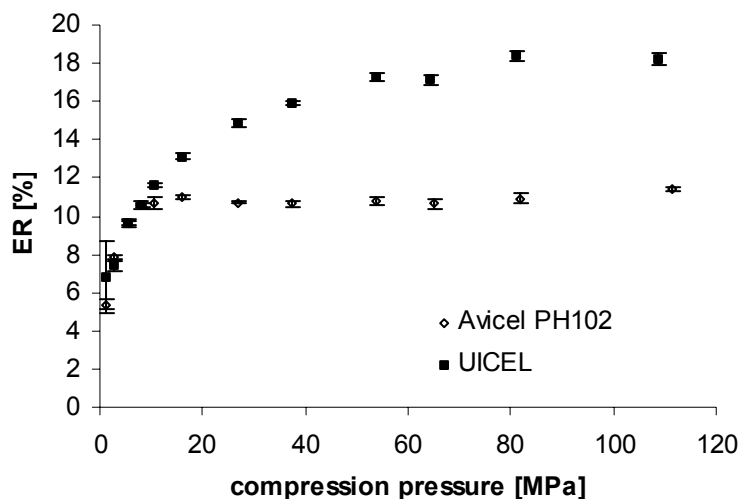


Figure 19: Profiles of the elastic recovery ER for Avicel PH102[®] and UICEL. Error bars: ± 1 SEM ($n=6$).

4.5.2 Heckel and modified Heckel analysis

In the contrary to the Heckel equation, the modified Heckel equation takes into consideration that the pressure susceptibility is depending on the relative density. The modified Heckel equation is therefore especially suitable for the low-pressure range. In order to enable a fair comparison between the Heckel equation and the modified Heckel equation both models were applied over the whole compression pressure range. The results in table 18 show that the goodness of fit is always better for the modified Heckel equation independent whether the analyzed data was generated by “in die” or “out of die” measurements. The corresponding fitting is visualized in figure 20 concerning the Heckel equation and in figure 21 concerning the modified Heckel equation.

Table 18: Comparison of the Heckel and modified Heckel equation for the characterization of the compression behavior of UICEL and Avicel PH102[®] (fitting range: 1-111.6 MPa) (with the Standard Error of the Mean (SEM); (n=6)).

substance		Heckel equation			modified Heckel equation		
		<i>K</i> [10 ⁻³ ·MPa ⁻¹]	<i>A</i>	<i>r</i> ²	<i>C</i> [10 ⁻³ ·MPa ⁻¹]	<i>ρ_{rc}</i>	<i>r</i> ²
UICEL	“in die”	16.1 (0.4)	0.513 (0.017)	0.995	9.01 (0.58)	0.144 (0.026)	0.995
	“out of die”	10.9 (0.4)	0.485 (0.019)	0.987	4.35 (0.16)	0.213 (0.011)	0.998
Avicel PH102 [®]	“in die”	18.7 (0.9)	0.431 (0.042)	0.980	10.66 (0.11)	0.113 (0.005)	1.000
	“out of die”	15.0 (0.9)	0.402 (0.042)	0.968	6.96 (0.27)	0.153 (0.015)	0.999

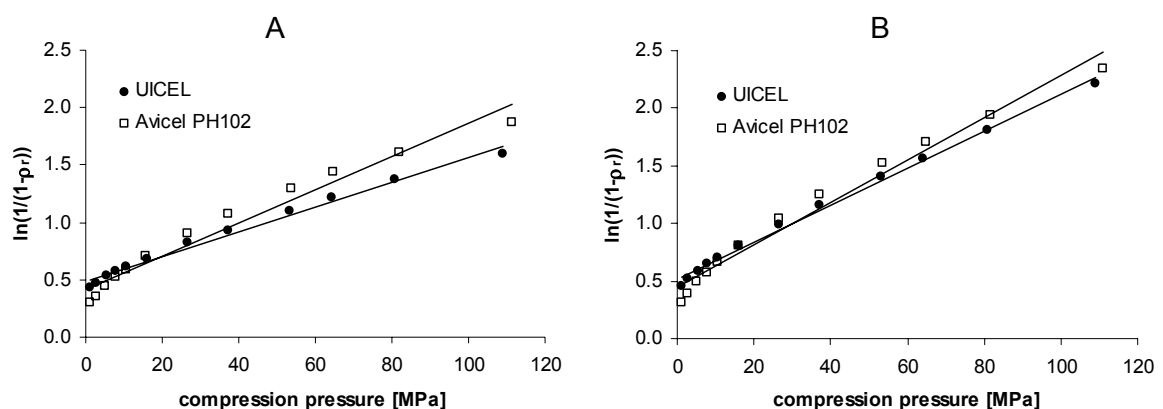


Figure 20: Heckel plots for UICEL and Avicel PH102[®] based on “out of die” (A) and “in die” data (B).

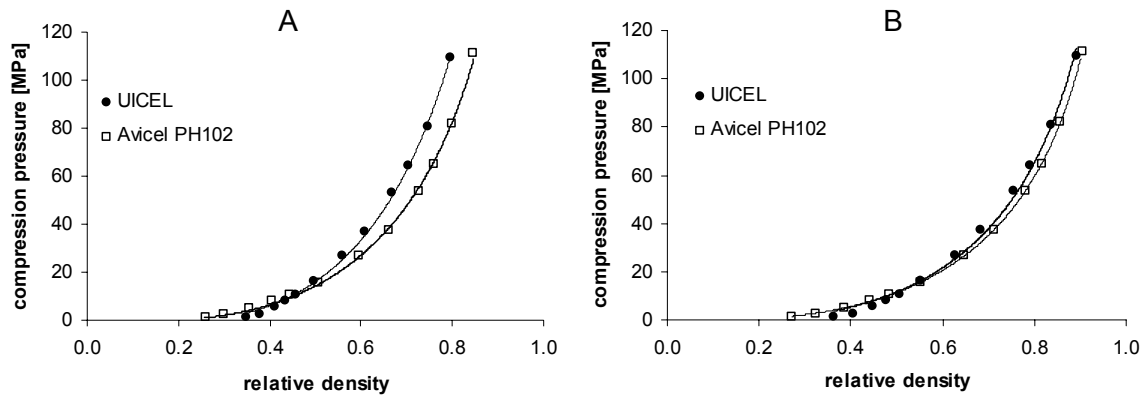


Figure 21: Modified Heckel plots for UICEL and Avicel PH102[®] based on “out of die” (A) and “in die” data (B).

Table 19: Heckel parameters for the compression of UICEL and Avicel PH102[®] in the linear range of the Heckel plot (15.8-111.6 MPa) (with the Standard Error of the Mean (SEM); (n=6)).

substance		K [$10^{-3} \cdot \text{MPa}^{-1}$]	A	r^2	σ_y [MPa]	ρ_{r0}	ρ_{ra}	ρ_{rB}
UICEL	“in die”	14.9 (0.1)	0.598 (0.009)	1.000	67.1 (0.5)	0.364 (0.0003)	0.450 (0.005)	0.086 (0.005)
	“out of die”	9.4 (0.4)	0.590 (0.024)	0.995	106.2 (4.5)	0.349 (0.0004)	0.446 (0.013)	0.097 (0.005)
Avicel PH102 [®]	“in die”	15.4 (0.5)	0.672 (0.035)	0.996	65.1 (2.1)	0.271 (0.0003)	0.489 (0.018)	0.218 (0.018)
	“out of die”	11.5 (0.7)	0.647 (0.044)	0.988	86.8 (5.3)	0.258 (0.0001)	0.476 (0.023)	0.218 (0.023)

The Heckel analysis is usually performed just in the linear range of the Heckel plot.

Therefore the Heckel parameters mentioned in the following considerations refer to the values listed in table 19, which are based on the evaluation of the linear range only.

The parameters involved in both equations can be assigned to a physical meaning:

i) ρ_{rc} , and ρ_{rB}

When the relative density of the material during compression is reaching the critical relative density ρ_{rc} , the substance shows for the first time a mechanical resistance. Thus, the critical relative density represents the relative density where the force, which is transmitted by the contact points in the powder, is percolating.

Even though the modified Heckel equation is superior compared to the Heckel equation, the pressure within the range of small relative densities is slightly too highly predicted by the modified Heckel equation (see figure 21). In the consequence a too small critical relative density results, which is smaller than the relative bulk density. Nevertheless, since the values for the critical relative densities concerning UICEL are always higher compared to those for

Avicel PH102[®], the conclusion can be drawn that Avicel PH102[®] forms rigid compacts at smaller relative densities compared to UICEL.

In the Heckel plots a curvature at small compression pressures can be observed. This was generally related to fragmentation and rearrangement of the powder particles [147]. ρ_{rB} is deduced from the relative density of the initial packing ρ_{r0} and the Heckel constant A . ρ_{rB} can be used as a measure for the extent of fragmentation and rearrangement [148]. Here, fragmentation does not seem to play a decisive role since the mean particle size of the substance after the compression was just slightly smaller than before the compression (see table 20). Thus, it can be concluded that the particle rearrangement is principally responsible for the curvature in the Heckel plot. The values for ρ_{rB} are always higher for Avicel PH102[®] than for UICEL. The great extent of particle movement in the case of Avicel PH102[®] could be caused by rough or irregularly shaped particles. The evaluation of the SEM pictures of Avicel PH102[®] (see figure 15) supports this assumption by the impression of a higher fraction of needle-shaped particles.

Table 20: Mean particle size of compressed and uncompressed powder (with the Standard Error of the Mean (SEM); (n=3)).

substances	mean particle size	
	uncompressed [μm]	compressed ($\rho_r = 0.8$) [μm]
UICEL	103.8 (0.59)	92.7 (1.47)
Avicel PH102 [®]	94.3 (0.89)	80.4 (0.42)

ii) C and K (σ_y)

The Heckel parameter K (and the deduced mean yield pressure σ_y) as well as the analogous parameter C of the modified Heckel equation can be used in order to quantify the extent of plastic flow occurring during the compression. The values for K and C are always higher for Avicel PH102[®] than for UICEL irrespective of the used data (“in die” or “out of die”). This fact demonstrates the outstanding property of Avicel PH102[®] to deform plastically under pressure. The difference between both substances concerning the K and C values is significant (K : $p < 0.05$; C : $p \ll 0.001$) for the “out of die” data. Considering the “in die” data, the two substances differ not that much in the K and C values compared to the “out of die” data. This can be explained by a higher extent of elastic recovery after compression for UICEL. The difference in the K values between “in die” and “out of die” data, which can also serve as a measure for the elastic recovery [149, 150, 151], is higher for UICEL ($5.5 \cdot 10^{-3} \text{ MPa}^{-1}$) than for Avicel PH102[®] ($3.9 \cdot 10^{-3} \text{ MPa}^{-1}$) and thus in perfect agreement with the findings on page 51 concerning the elastic recovery. The different capability of both substances to deform plastically can also be illustrated by SEM pictures made of the upper



surface of tablets ($\rho_r = 0.8$) (see figure 22). In the case of UICEL the original shape of the particles can still be recognized whereas the initial boundaries of the Avicel PH102[®] particles are no longer existent due to plastic deformation.

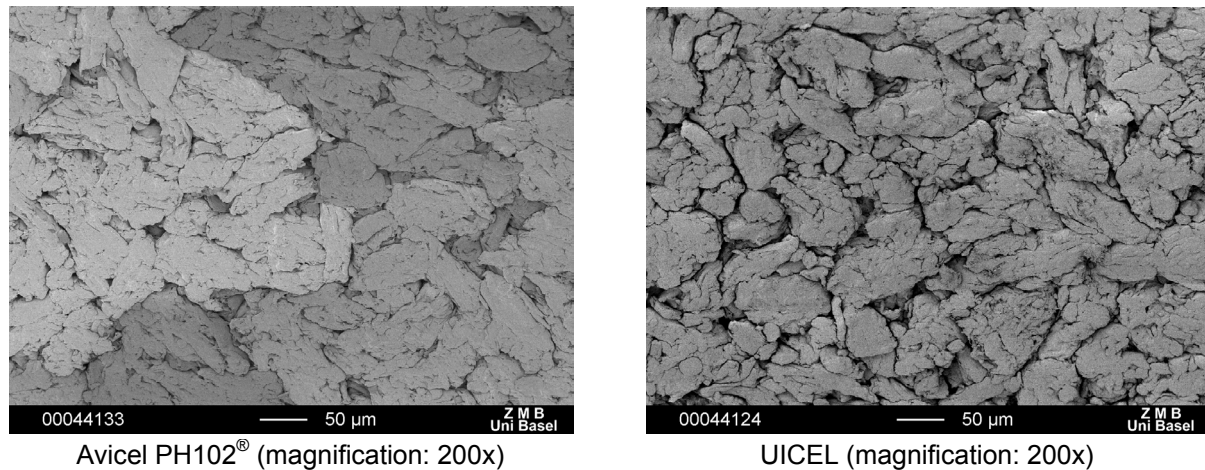


Figure 22: SEM photographs of the upper surfaces of tablets made of UICEL and Avicel PH102[®] at a relative density of 0.8 (prepared by the center of microscopy of the University of Basel (ZMB)).

In literature the values of the mean yield pressure σ_y for microcrystalline cellulose samples are ranging from 30 to 104 MPa [28]. Beside the fact that different qualities of microcrystalline cellulose were investigated, the moisture content could also provide a possible cause for this broad range. Water is acting like a plasticizer by disrupting hydrogen bonds and by cross-linking the hydroxyl groups on the cellulose chains [152]. In consequence, an increase of the moisture content of a substance will result in a decrease of the mean yield pressure σ_y (increase of the K value). Although UICEL has the higher moisture content, it is characterized by a higher mean yield pressure compared to Avicel PH102[®]. Thus, the difference in the mean yield pressures cannot be related to the moisture content.

Suzuki *et al.* [153] pointed out that the mean yield pressure was lowered as the degree of crystallinity is decreasing. So, considering the lower degree of crystallinity for UICEL compared to Avicel PH102[®], UICEL would be expected to show the smaller value for the mean yield pressure, which is not the case. Thus, the reason for the discrepancy in the mean yield pressures can neither be explained by differences in the moisture content nor by differences in the degree of crystallinity. Quite the contrary, despite the lower moisture content and despite the higher degree of crystallinity, Avicel PH102[®] deforms much better under pressure than UICEL.

Fell *et al.* [154] pointed out the influence of the particle size on the derived Heckel parameters such as the mean yield pressure. Since in this case the particle size distribution is very similar for both substances the particle size is not a possible reason for the different

mean yield pressures. The different polymorphic forms are therefore supposed to cause the different behavior of the two substances under pressure.

4.5.3 Crushing strength

The compactibility, *i.e.* the ability of the substance to form coherent tablets under pressure, can be assessed by the radial tensile strength σ_t . The tensile strength versus the relative density is depicted in figure 23 together with the fitting according to the equation of Leuenberger (equation (31)). The SEM values for the tensile strength measurement are so small (0.1 – 1.6%), that the plotting of the error bars in figure 23 is omitted for a better readability. The fitting parameters are listed in table 21.

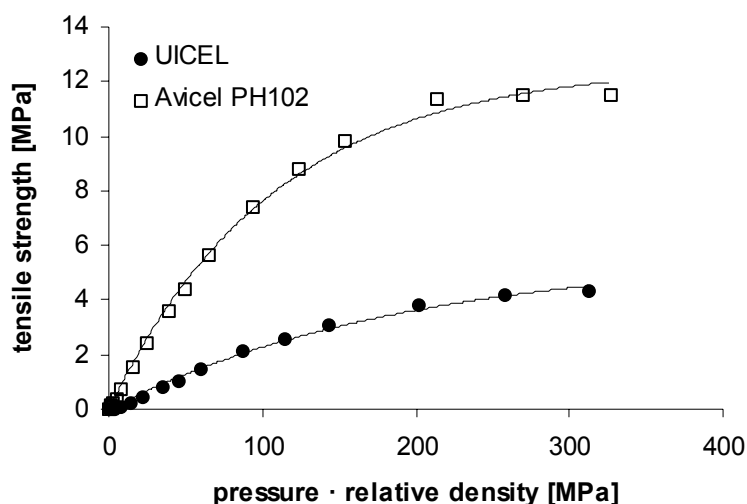


Figure 23: Diagram of the tensile strength according to equation (31).

Table 21: Fitting parameters for the tensile strength according to equation (31) (with the Standard Error of the Mean (SEM); (n=3)).

substances	σ_{tmax} [MPa]	γ_t [$10^{-3} \cdot \text{MPa}^{-1}$]	r^2
UICEL	5.7 (0.3)	5.14 (0.51)	0.994
Avicel PH102 [®]	12.6 (0.2)	9.29 (0.40)	0.997

The maximum radial tensile strength σ_{tmax} of Avicel PH102[®] demonstrates the extraordinary ability of Avicel PH102[®] to form rigid compacts. In comparison with other excipients (PEG: 3.3 MPa, lactose: 1.0 MPa, Starch 1500[®]: 5.3 MPa [155]) the value of UICEL is still adequate. Thus, UICEL can ensure mechanically resistant compacts even though the maximum radial tensile strength is just half as high as the value for Avicel PH102[®].

The compression susceptibility γ_t is a material specific constant describing the compressibility. The higher the value is, the sooner the plateau of the tensile strength will be achieved by increasing the compression pressure. Since both, the Heckel constant K and the compression susceptibility γ_t , describe the compressibility it is not astonishing that the values are in the same order of magnitude. The observed differences can be explained by different experimental determinations. However, as the tendency is the same, the values of the compression susceptibility for UICEL and Avicel PH102[®] support the findings of the Heckel analysis that Avicel PH102[®] has a more pronounced plastic behavior compared to UICEL.

4.5.4 Bonding surface area

The dominating bonding mechanism and the bonding surface area are regarded as primary factors influencing the compactibility of substances. Due to experimental problems both factors are hardly accessible. Concerning the bonding mechanism it is easily conceivable that the maximum possible hydrogen bonding density between two particles could be dependent on the polymorphic form. Furthermore, the higher fraction of needle-shaped particles for Avicel PH102[®] compared to UICEL could favor the formation of shape-related bonding due to the mechanical interlocking.

The bonding surface area is defined as the effective surface area taking part in the interparticulate attraction [156]. Since a pronounced fragmentation during compression can be excluded for both materials (see page 54) the following relationship (equation (44)) can be postulated:

$$A_T = A_p - A_b \quad \text{equation (44)}$$

where: A_T : surface area of the compressed particles in the tablet ("tablet surface area") [m²/g]

A_p : surface area of the particles [m²/g]

A_b : bonding surface area [m²/g]

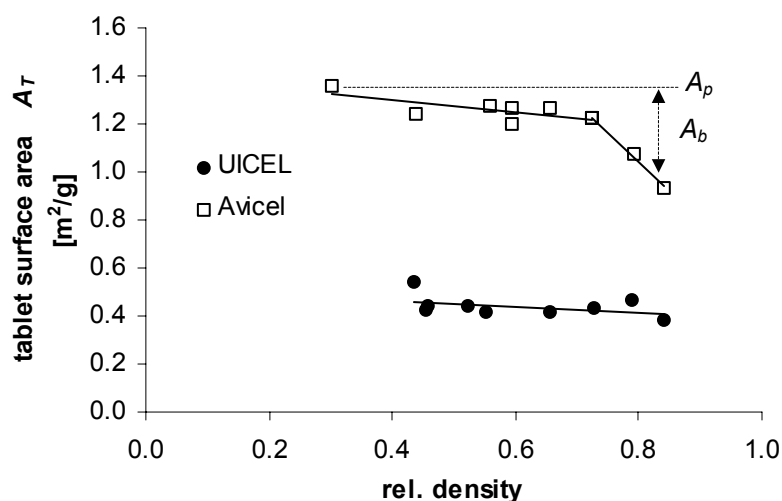


Figure 24: Diagram of the tablet surface area A_T versus the relative density for UICEL and Avicel PH102[®]. A_p : particle surface area; A_b : bonding surface area according to equation (44).

The tablet surface area A_T is plotted in figure 24 versus the relative density for UICEL and Avicel PH102[®]. Even if the precision of the method for the determination of the tablet surface area is not that good, it can be stated that the decrease of the tablet surface area is smaller for UICEL than for Avicel PH102[®]. Thus, according to equation (44) the bonding surface area A_b is higher for Avicel PH102[®] compared to UICEL. The sharp bend in the case of Avicel PH102[®] may be attributed to an increase in the plastic deformation. For UICEL no sharp bend could be observed. The higher mean yield pressure and the pronounced elastic recovery, which is counteracting the formation of the bonding surface area [157] can explain the smaller bonding surface area for UICEL in comparison with Avicel PH102[®].

The fact that the tablet surface area A_T is not increasing at higher relative densities justifies the assumption that the particles were not fragmenting under pressure.

Equation (44) is only a rough estimation of the bonding surface area, because it is strictly valid just for non-porous particles [156] and it does not take into account the increase of the tablet surface area due to plastic deformation.

The determination of the tablet surface area was performed using mercury porosimetry. For experimental reasons (see page 50) it was just possible to measure interparticle pores down to a diameter of 100 nm. Since a hydrogen bond is much shorter (about 3 nm) the effective bonding surface is surely overestimated by the bonding surface depicted in figure 24. Similar to the determination of the tablet surface area by a gas adsorption method, the area used for bonding between particles is just a part of the “non-available” surface area [158].

But nevertheless, it is widely accepted that plastic deformation and the elastic recovery is of enormous importance for the effective bonding area [156]. Thus, the two properties, plastic deformation and elastic recovery, let assume a higher bonding surface area for Avicel PH102[®] compared to UICEL.

4.6 UICEL – a superdisintegrant?

In the following chapter we are focusing our attention on the disintegration properties of tablets prepared of UICEL and Avicel PH102[®]. The disintegration time in respect of the relative density of the tablets is depicted in figure 25. The plot of the disintegration time versus the relative density of Avicel PH102[®] tablets is characterized by a steady increase with a steep increase at high relative densities. This does not apply to UICEL tablets. The disintegration time of UICEL tablets is very small over the whole relative density range and hardly dependent on the relative density. It could be argued that it would make more sense to relate the disintegration time to the compactibility than to the relative density, which just represents the state of compression. In order to compare the results of the disintegration test with a compactibility property of the substances, the disintegration time is plotted versus the

radial tensile strength in figure 26. After a first linear section, which shows a close correlation between disintegration time and radial tensile strength, an upswing can be observed in the case of Avicel PH102[®]. Two possible reasons could explain this phenomenon. i) Different bonding types are affecting the radial tensile strength and the disintegration test, *i.e.* the radial tensile strength is determined by the weakest links in the structure whereas for the disintegration test the bonds of any strength have to be overcome. It could be supposed that this difference comes more into account at higher pressures. ii) The disintegration time includes not only the time for the disintegration itself (weakening of the interparticulate bonding, annihilation of hydrogen bonds) but also the time it takes for the water to penetrate into the tablet. Thus, the sharp increase of the disintegration time above a relative density of about 0.85 can be explained by the assumption that the pores, which are favoring the penetration of the water are no longer percolating. The measured “disintegration time” is therefore overestimating the time which is required to loosen the interparticulate bonds.

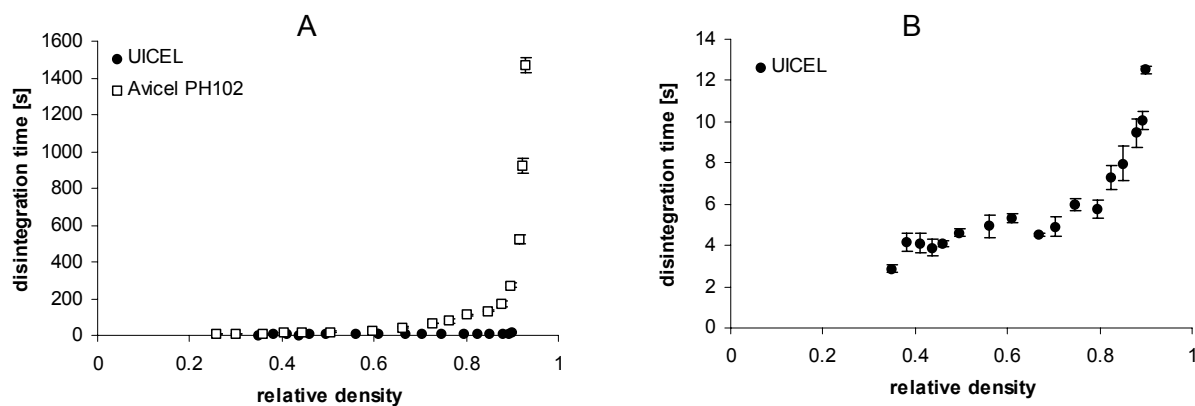


Figure 25: Diagrams of the disintegration time versus the relative density. A: results for UICEL together with Avicel PH102[®]. B: results only of UICEL with a rescaled y-axis. Error bars: ± 1 SEM (n=3).

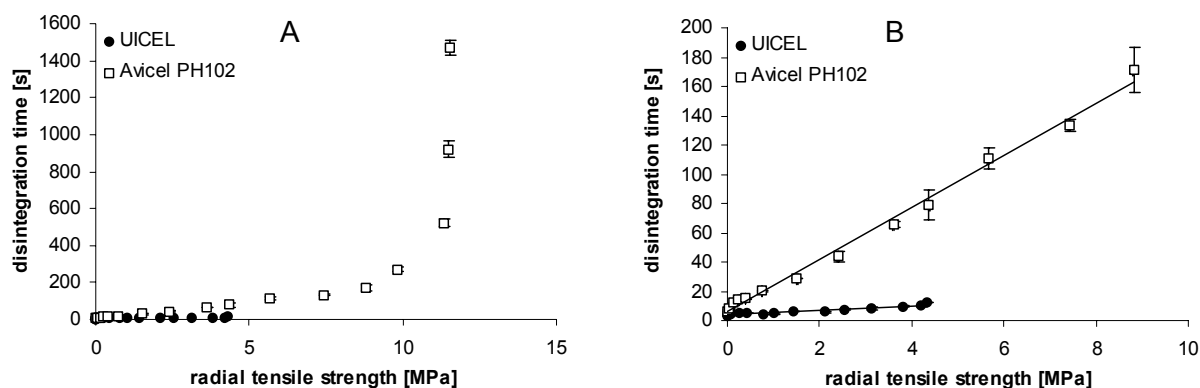


Figure 26: Diagrams of the disintegration time versus the radial tensile strength. A: results for UICEL and Avicel PH102[®]. B: section of A with rescaled x-axis and y-axis. Error bars: ± 1 SEM (n=3).

In the case of UICEL, the slope of the correlation curve is small (figure 26 B). This circumstance is really surprising, as we would expect a correlation between the interparticulate bonding strength and the disintegration time. Regarding figure 26 it can be concluded that the bonding area, which is closely correlated with the tensile strength [156] is much more relevant for the disintegration of Avicel PH102[®] tablets than of UICEL tablets. Thus, for UICEL a disintegration mechanism can be proposed where the disintegration time is not expected to depend on the bonding area like in the case of annihilation of interparticulate hydrogen bonds. The higher elastic recovery of UICEL supports the assumption that the elastic energy, which is stored in UICEL tablets (similar to compressed springs), is completely released upon coming in contact with water. As soon as the penetrating water slightly weakens the forces (interparticulate hydrogen bonds, water bridges), which hold the particles together, the particles regain their original shape. The associated expansion of the particles could initiate the disintegration of the tablet or at least could contribute to the whole disintegration process. The relevance of the regeneration of the original shape on the disintegration process was already shown for compressed starch grains [159].

Figure 26 also reflects the findings of chapter 4.5.3 (page 56). At high compression pressures it is possible to obtain much higher values of the radial tensile strength for Avicel PH102[®] tablets than for UICEL tablets. But nevertheless UICEL is capable to form rigid tablets with an adequate mechanical resistance.

The on-line monitoring (see figure 27) of the disintegration process of UICEL and Avicel PH102[®] tablets ($\rho_r = 0.8$) could confirm the impressive discrepancy of the disintegration properties between the two substances. The disintegration of UICEL tablets happened so fast that the main decrease of the particle size could even not be detected because for technical reasons it was not possible to measure before 30 s after starting the measurement. Unlike UICEL tablets, the disintegration of Avicel PH102[®] tablets took several minutes.

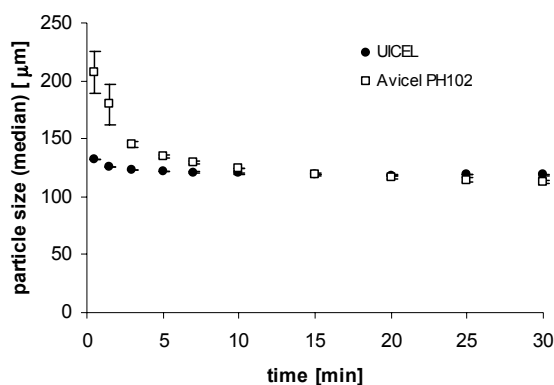


Figure 27: On-line monitoring of the disintegration of UICEL and Avicel PH102[®] tablets ($\rho_r = 0.8$). Error bars: ± 1 SEM (n=3).



The effect that water exerts on tablets prepared of UICEL and Avicel PH102[®] can also be visualized by putting a drop of water onto the upper surface of the tablet (see figure 28 and figure 29). In the case of Avicel PH102[®] the drop stays stable apart from a small spreading of the drop. UICEL tablets react totally different: Coming into contact with the tablet, the water is penetrating into the tablet. Approximately 3 seconds after applying the drop onto the tablet, the surface starts bursting and the material is disintegrating very rapidly into the primary particles. Upon the contact with water, a force is obviously developed in the UICEL tablet, which is able to rupture the surface.

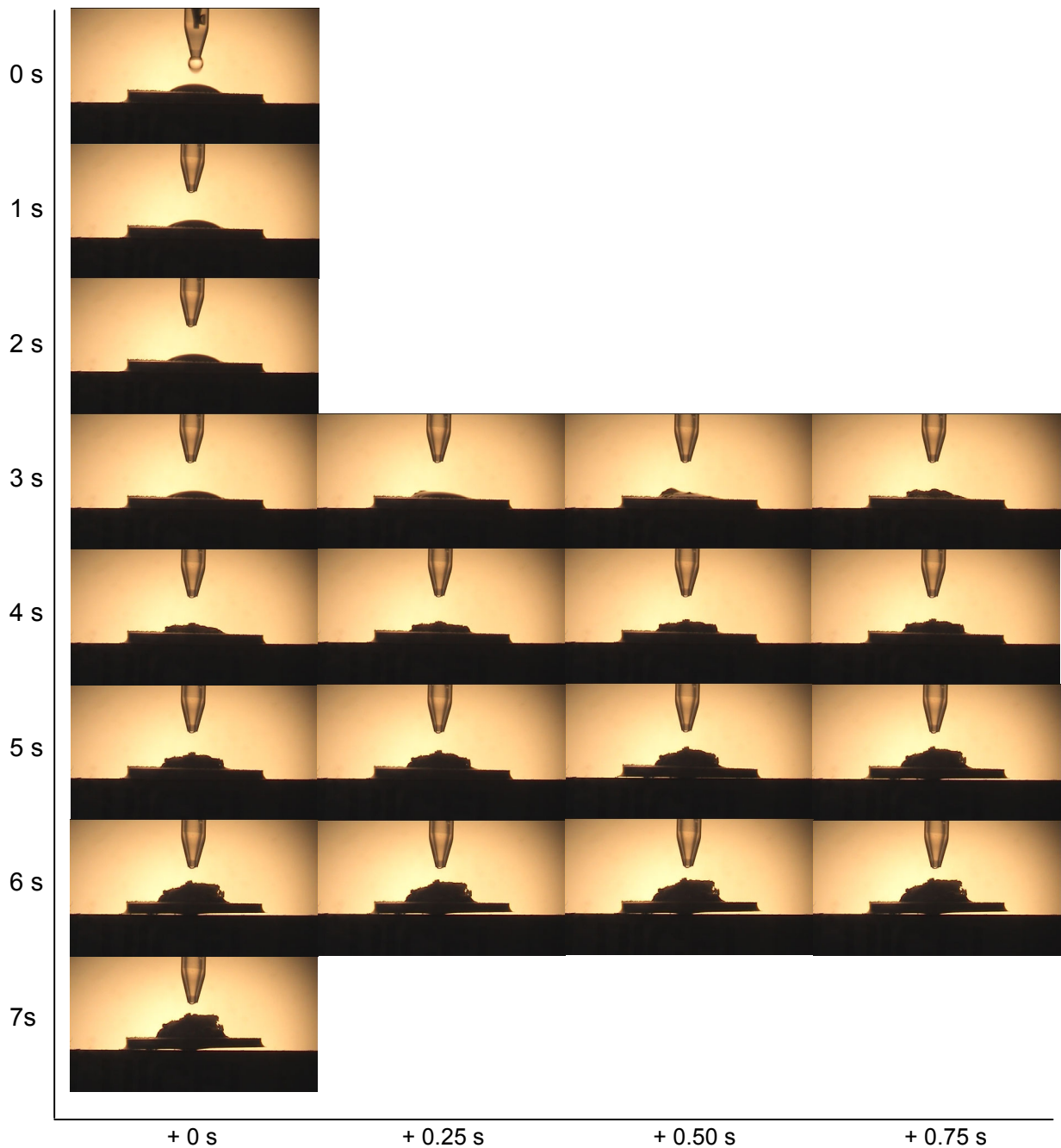


Figure 28: Picture sequence for the visualization of the disintegration of UICEL tablets.

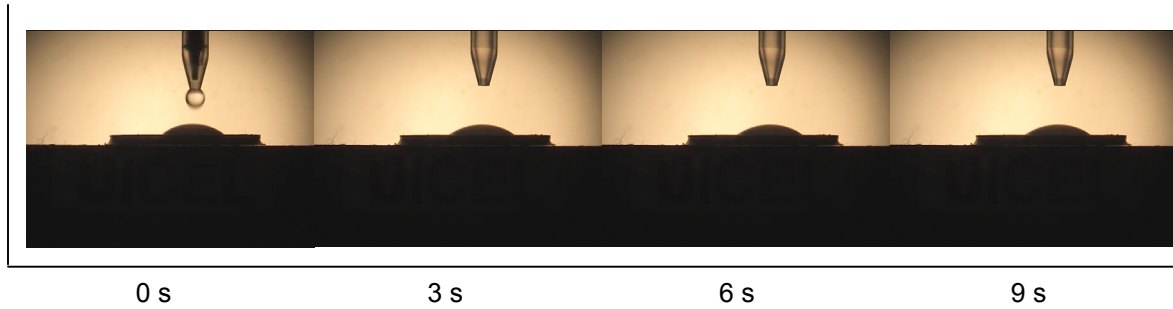


Figure 29: Picture sequence for the visualization of the interaction between water and Avicel PH102[®].

The developed force can be measured at isochoric conditions (allowing no volume expansion to the tablet) by bringing the lower surface of the tablet in permanent contact with water. The results for tablet made of UICEL and Avicel PH102[®] at a relative density of 0.8 are shown in figure 30.

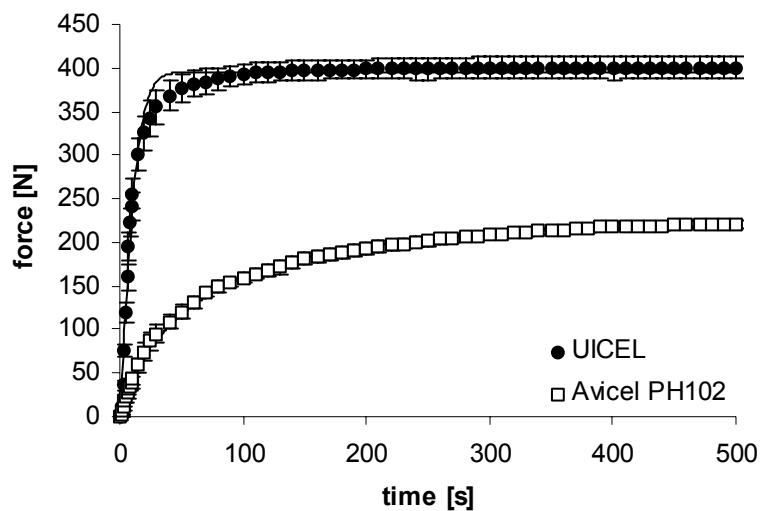


Figure 30: Force development within a tablet made of UICEL and Avicel PH102[®] at a relative density of 0.8. Error bars: ± 1 SEM ($n=3$).

The measured force is the resulting force of cohesive forces, which hold the particles together and the disintegrating forces, which tear the particles apart. The maximum developed force is much higher in UICEL tablets than in Avicel PH102[®] tablets. Although the maximum disintegration force expresses the ability of the disintegrant to disaggregate the tablet, Colombo *et al.* [112] showed in their work that the time τ_d (time needed to reach 63.2% of the maximum disintegration force according to the Weibull equation) can also be decisive for the disintegration time. To characterize the whole disintegrating force development they introduced the “*input*” value, which is combining the maximum force and the time τ_d . The “*input*” value, also referred to as force development rate, equals the



derivative of the Weibull equation at the time $t = t_0 + \tau_d$. The values for the time τ_d and the “input” value are listed in table 22. Concerning UICEL the higher value for the maximum force combined with a lower value for the time τ_d lead to a higher value for the “input” value compared to Avicel PH102[®]. This difference in the “input” values between both substances confirms the already stated different disintegration properties. The disintegrating force starts developing immediately after the tablet has coming into contact with water. Thus, UICEL and Avicel PH102[®] showed no lag time ($t_0 = 0$).

Table 22: Fitting parameters for the disintegrating force according to the Weibull equation (equation (36)) (with the Standard Error of the Mean (SEM); (n=3)).

substance	F_{max} [N]	τ_d [s]	b	t_0 [s]	“input” [N/s]	r^2
UICEL	395.6 (1.9)	10.8 (0.3)	1.24 (0.06)	0	16.68 (1.01)	0.987
Avicel PH102 [®]	222.4 (1.2)	74.0 (1.6)	0.75 (0.01)	0	0.83 (0.02)	0.998

As the force generation is the result of any possible disintegration mechanism, the force measurement does not allow any conclusions about the cause of the force development. However, assuming that the particles represent small springs, equation (45) and equation (46) can be postulated to hold for one particle.

$$F_i = k \cdot x \quad \text{equation (45)}$$

$$E_i = \frac{1}{2} k \cdot x^2 \quad \text{equation (46)}$$

where: F_i : force exerted by one particle [N]
 k : spring constant [N/m]
 x : displacement of the spring [m]
 E_i : potential elastic energy stored within a compressed particle [J]

Equation (45) is the commonly encountered form of Hooke’s law. The resulting force F within a tablet equals the sum of all “microscopic” forces F_i (see equation (47)). The overall potential energy E , which is stored within a tablet, can be expressed in an analogous manner as the sum of E_i according to equation (48).

$$F = \sum_{i=1}^N F_i = N \cdot k \cdot x \quad \text{equation (47)}$$

$$E = \sum_{i=1}^N E_i = N \cdot \frac{1}{2} k \cdot x^2 \quad \text{equation (48)}$$

where: F : resulting force [N]
 N : number of springs (particles)
 E : potential elastic energy stored in a tablet [J]

Due to the fact, that both materials (UICEL and Avicel PH102[®]) exhibit a similar density and a similar particle size we can furthermore assume that the number of particles within a tablet consisting of UICEL is about the same as for a tablet made of Avicel PH102[®]. In a first approximation, the strain x for UICEL and Avicel PH102[®] can be considered to be equal since both materials were compressed to the same relative density. Thus, the ratio of the forces, which are exerted by UICEL and Avicel PH102[®] tablets during disintegration, equals the ratio of the spring constants and the ratio of the stored energies of the two materials (see equation (49)).

$$\frac{F_{UICEL}}{F_{Avicel}} = \frac{k_{UICEL}}{k_{Avicel}} = \frac{E_{UICEL}}{E_{Avicel}} \quad \text{equation (49)}$$

On the basis of these considerations and the maximum disintegration forces according to table 22 we can conclude that the elastic energy stored in UICEL tablets is higher by a factor of about 1.8 compared to Avicel PH102[®] tablets.

The availability of water is definitely an essential and indispensable requirement (*conditio sine qua non*) for the disintegration of compacts. However, looking at a sponge or at sintered glass, even though the water will penetrate very rapidly into these materials they will never disintegrate. Thus, the presence of water is not a sufficient but nevertheless a necessary condition for the disintegration process. In a first step it is surely worth investigating the water uptake of UICEL and Avicel PH102[®] tablets using a modified Enslin apparatus.

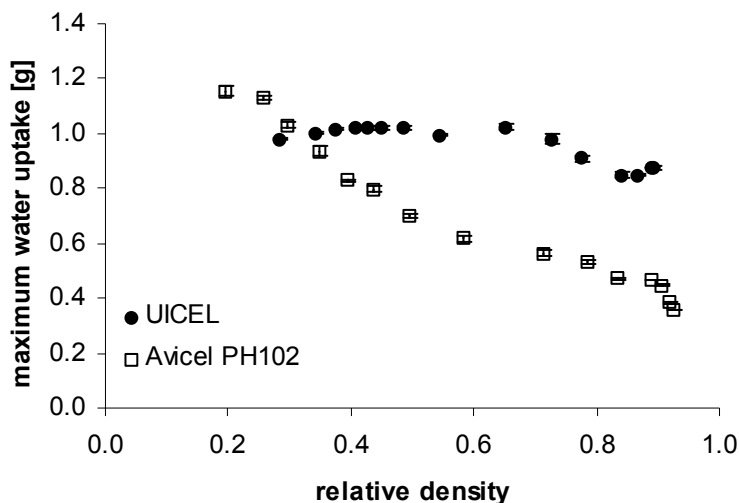


Figure 31: Diagram of the maximum water uptake versus the relative density for UICEL and Avicel PH102[®]. Error bars: ± 1 SEM (n=4).

The total water uptake of compacts with different relative densities is depicted in figure 31 for UICEL and Avicel PH102[®]. The two celluloses behave totally different: Considering UICEL, the maximum water uptake m_{max} is nearly independent of the relative density. Thus, the



packing density at the end of the water uptake is almost the same over the whole relative density range, *i.e.* a strongly compressed tablet has almost the same final volume like the bulk material. Consequently, it can be concluded that no interparticle bonding exists at the end of the water uptake for UICEL compacts. Whereas in the case of Avicel PH102[®] tablets, the maximum water uptake m_{max} is decreasing with an increase in relative density. The Avicel PH102[®] tablets are therefore not disaggregated to the same extent like the UICEL tablets at the end of the measurement.

In order to get a deeper insight into the mechanism of the disintegration process, the swelling capacity and the water retention of the bulk materials were determined for UICEL, Avicel PH102[®] and two well-established disintegrants Starch 1500[®] and Vivastar[®]. The results listed in table 23 allow the following conclusions: i) The swelling of the particles can be considered as main disintegration mechanism for Vivastar[®] and maybe Starch 1500[®] but certainly not for UICEL and Avicel PH102[®]. ii) The differences in the swelling capacity and water retention between Avicel PH102[®] and UICEL are not significant ($p = 0.05$) and cannot provide an explanation for the astonishing differences in the disintegration properties.

Coming back to the water uptake of the compacts, it can be supposed that the water, which is absorbed during water uptake by the UICEL and Avicel PH102[®] compacts is penetrating into the pore volume and is increasing the interparticle and not the intraparticle volume. Thus, the swelling of the particles and the swelling of the tablet must not be confused. As bulk materials, both substances behave very similar. The difference between both substances concerning the water uptake is increasing as the relative density of the compacts is increasing. Thus, the difference in the water uptake is closely related to the differences in the structure of the tablets and therefore to the compression properties of the substances.

Table 23: Swelling capacity and water retention of UICEL, Avicel PH102[®] and two disintegrants (with the Standard Error of the Mean (SEM); (n=3)).

substance	swelling capacity	water retention
UICEL	1.36 (0.05)	3.42 (0.17)
Avicel PH102 [®]	1.31 (0.02)	3.87 (0.45)
Starch 1500 [®]	4.54 (0.04)	5.19 (0.19)
Vivastar [®]	24.08 (0.14)	41.76 (0.87)

Water uptake is a kinetic driven process. Thus, analogous to the force development profile (see page 62) it is not sufficient to characterize the water uptake just by the maximum amount of water m_{max} taken up by the compact. The time dependency of the process can be taken into account by the determination of the expression $t_{60\%}$, defined as the time, which it takes for the compact to take up 60% of the total amount of water. At low relative densities

the $t_{60\%}$ values for the two substances are very similar, whereas at higher relative densities the values start to diverge (see figure 32). Above a relative density of 0.84 ($\rho_r > 0.84$) the $t_{60\%}$ values for Avicel PH102[®] sharply increase. As the plot of the disintegration time versus the relative density (see figure 25) shows a similar remarkable increase at high relative densities, the suggestion mentioned above that the water uptake is a decisive parameter at high relative densities for the disintegration time of Avicel PH102[®] tablets can be confirmed. In the case of Avicel PH102[®] tablets, the rate of water uptake is strongly affected by the percolation threshold of the pores. However, considering the $t_{60\%}$ values of UICEL in figure 32 no percolation threshold of the pores can be observed. There are two possible reasons: i) Due to the high elastic recovery, the critical porosity cannot be obtained. ii) The fast disintegration causes a pore widening, so that the original pore volume is no longer relevant.

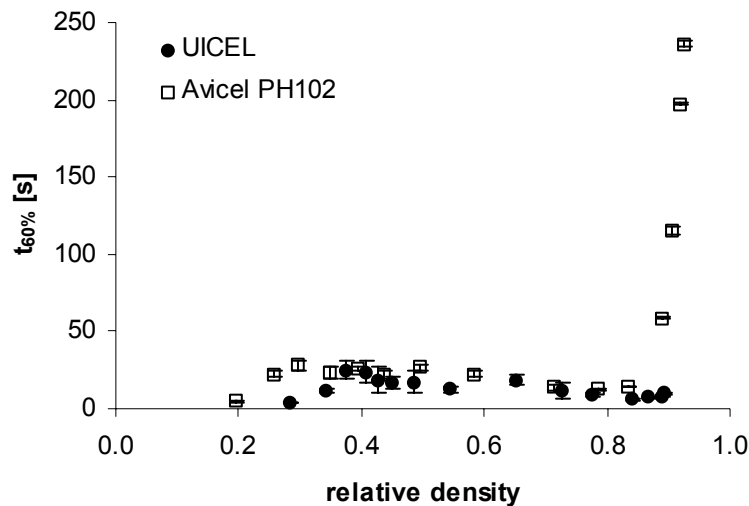


Figure 32: $t_{60\%}$ (time till 60% of the maximum water uptake are absorbed) versus the relative density for UICEL and Avicel PH102[®]. Error bars: ± 1 SEM (n=4).

Beside the evaluation of empirical parameters like m_{max} and $t_{60\%}$ it is also possible to explain the water uptake by more meaningful function-based parameters. The most frequently used equations for describing water uptake profiles are the Weibull equation (see also equation (29)) [114], the Hill equation and the Washburn equation. The Hill equation is appropriate to describe complicated water uptake profiles (e.g. biphasic uptake) [160]. Nevertheless the Hill equation, like the Weibull equation, was not used in this work due to the lack of physical background. The applied Washburn equation in the contrary is based on a physical model. However, the applicability of the Washburn equation on the water uptake of compacts is limited by several factors [161], whereas the increase of the pore radius (widening of the pores) during the water uptake seems to be the most important [162]. This circumstance was tried to take into account by analyzing just the initial part of the water uptake profile where a change in the pore radius is not yet expected.



The water penetration index k_w determined as the slope of the regression line in the linear section when plotting m^2 versus t is depicted in figure 33 in relation to the relative density. The correlation coefficients were in the range of 0.987-0.999 for both celluloses. In the case of Avicel PH102[®] the water penetration index k_w , which can be considered as a measure for the rate of the water uptake is decreasing almost continuously. At very high relative densities the water penetration index k_w for Avicel PH102[®] is very low (consistent with the high values for $t_{60\%}$), reflecting the percolation threshold of the pores. For UICEL the situation in the relative density range of 0.4-0.7 is rather confusing. Unlike Avicel PH102[®] there is no clear tendency visible for UICEL. The fluctuations of the water penetration index k_w can be ascribed to the observation that UICEL compacts in the corresponding relative density range were arching shortly after coming in contact with water. Thus, the lower and varying contact area, restricted to the edge of the tablet surface, influenced the rate of water uptake. The variations of k_w in the case of UICEL can additionally be explained by the arbitrary selection of the evaluated points and the fact, that the number of points was lower for UICEL compared to Avicel PH102[®], due to the faster water uptake. Nevertheless, even though the dots are apparently scattered randomly in the diagram, the water penetration index k_w is higher within the whole relative density range for UICEL compared to Avicel PH102[®].

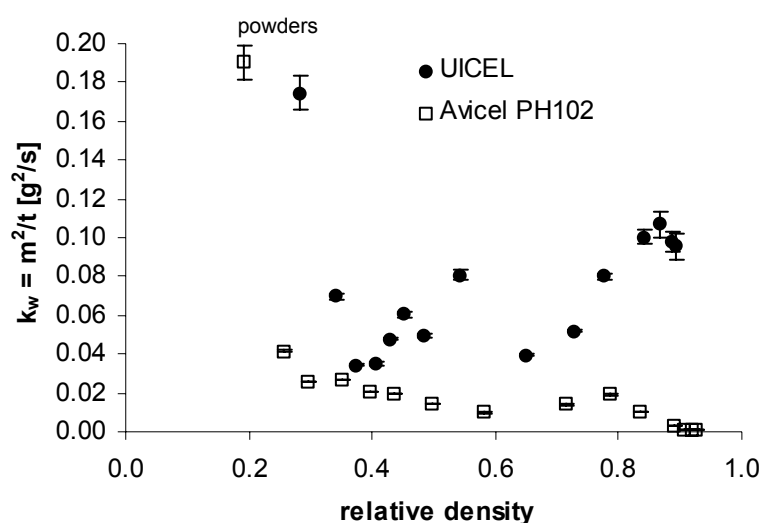


Figure 33: Diagram of the water penetration index k_w (based on the Washburn equation) versus the relative density for UICEL and Avicel PH102[®]. Error bars: ± 1 SEM (n=4).

The formation of arches in the case of UICEL tablets may raise the question if the assumption of a constant pore radius is justified even at the very beginning of the water uptake. Even though the Washburn equation is an oversimplification and even though its use is doubtful and questionable for compacts, it is at least suitable for the estimation of the influence of the involved parameters on the water uptake. Combining equation (9) and equation (10) the Washburn is recapitulated in equation (50).

$$\frac{m^2}{t} = \frac{\pi^2 \cdot n^2 \cdot r^5}{2} \frac{\rho^2 \cdot \gamma_L \cdot \cos \theta}{\eta} = k_w \quad \text{equation (50)}$$

where: m : mass of adsorbed liquid [g]
 t : time [s]
 n : number of capillaries
 r : mean radius of capillaries [mm]
 ρ : density of the liquid [g/cm³]
 γ_L : surface tension of the liquid [mN/m]
 θ : contact angle
 η : viscosity of the liquid [mPa·s]
 k_w : water penetration index [g²/s]

In order to explain the differences in the water uptake between both substances the parameters involved in the Washburn equation (equation (50)) will be checked out. Thus, it should be possible to assign the differences in the water uptake to one or several crucial parameters.

a) Density ρ , surface tension γ_L and viscosity η of the liquid

The liquid properties are considered to stay constant during the whole experiment. The parameters are supposed to be the same for both celluloses. A possible effect of the water-soluble substances – which were found in different amounts in the two substances – especially on the surface tension γ_L and the viscosity η were neglected.

b) Pore diameter ($d = 2 \cdot r$) of the capillaries

Since the mean pore radius appears in the 5th power in the extended Washburn equation (equation (50)), already small differences may have great impact on the water uptake.

To give an impression of the pore size distribution, the derivative of the logarithmic cumulative pore size distribution of UICEL and Avicel PH102[®] as powders and as compacts ($\rho_r = 0.8$) are depicted in figure 34. It has to be kept in mind that the curves in the figures do not equal volume pore size distributions. However, the chosen plot has the advantage that the area under the peak equals the pore volume of the corresponding pore fraction. The powders are characterized by interparticle pores with diameters between 10 and 100 μm and intraparticle pores, which are assumed to be around 1 μm [163]. The obviously higher intraparticle pore volume for Avicel PH102[®] as a powder explains the higher surface area of Avicel PH102[®] compared to UICEL (compare A_{Hg} in table 17).

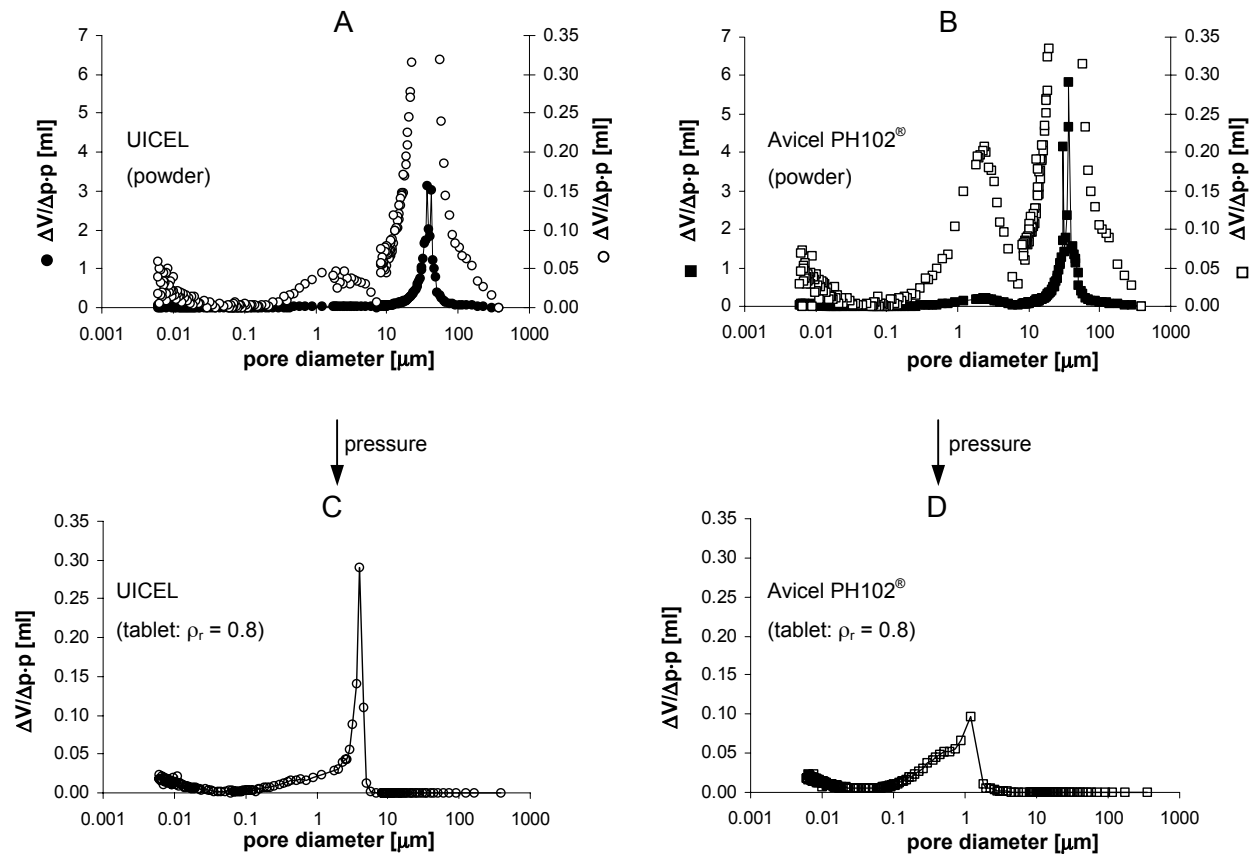


Figure 34: Derivative of the logarithmic cumulative pore size distribution of UICEL (A: powder; C: compact) and Avicel PH102[®] (B: powder; D: compact). The results for the powders are depicted with two different scaled y-axis.

Figure 34 illustrates impressively the effects of powder compression on porosity and pore size. The compression of the powder has two main effects, which can be elucidated by the means of figure 34: i) With increasing compression pressure the peaks (pores between the particles) are shifted towards a smaller pore diameter. In the case of Avicel PH102[®] tablet, the diameter of the interparticle pores have already the dimension of intraparticle pores. ii) The smaller areas under the curves for tablets indicate smaller overall pore volumes compared with powders, which is quite conceivable as the porosity is decreasing.

Comparing both substances it has to be pointed out, that the peak shift is more pronounced for Avicel PH102[®] than for UICEL. In order to illustrate the different pore size between both substances, the peak values of all investigated tablets are plotted in figure 35 versus the relative density. The pore size over the whole relative density range is higher for UICEL than for Avicel PH102[®]. The difference in the pore structure between the tablets of both substances is also visible in the SEM photographs of the upper surface of compacts at a relative density of 0.8 (see figure 22).

This example demonstrates quite impressively that the pore size is not defined by the porosity. Compacts with the same porosity do not show the same pore size distribution of necessity.

As soon as the disaggregation starts after the tablet has been coming in contact with water the pores are widening very rapidly. The increase in the pore size applies to both substances but in a higher degree to UICEL than to Avicel PH102[®] (see figure 31). Although the pore structure will change shortly after the beginning of the water uptake, the original pore size is influencing the initial phase of water penetration. Thus, the bigger pores for UICEL tablets favor the faster water uptake at the very beginning compared with Avicel PH102[®] tablets.

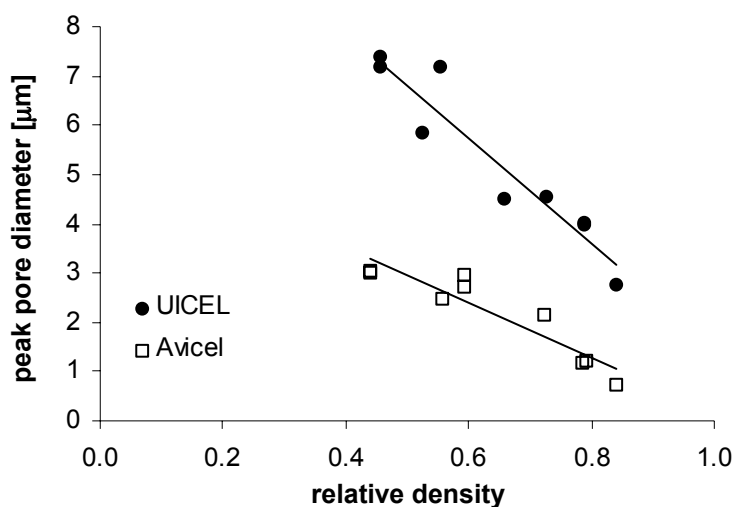


Figure 35: Diagram of the peak pore size versus the relative density for tablets made of UICEL and Avicel PH102[®].

c) Surface energetics

The results of the contact angle measurements are all summarized in table 24. With the exception of the ellipse fitting method, all other evaluation methods provide smaller contact angles for Avicel PH102[®] than for UICEL. However, the difference between both substances is only significant ($p < 0.05$) for the values obtained by the sorption measurement.

Concerning the evaluation method the values for the contact angle can be ranked for both substances in the following manner: sorption method < height and length method < ellipse fitting method < linear regression of secant angle.

Concerning the sessile drop measurements, the values for the contact angles are in the same order of magnitude for all evaluation methods. Nevertheless, the deviation of the constant c (ratio of the semiminor to the semimajor axis of the ellipse) from unity clearly indicates, that the shape of the droplet is better characterized by an ellipse than by a circle. However, since the cross sectional area of the drop is neither a circle nor an ellipse [164], the linear regression of secant angles certainly provides the most reliable values for the contact



angle because this method is not based on any assumption concerning the shape of the drop.

Table 24: Summary of the contact angle measurements (with the Standard Error of the Mean (SEM)).

Evaluation method	parameter	UICEL	Avicel PH102 [®]
height and length method (n=6)	contact angle, θ	36.9° (1.0)	35.3° (1.2)
ellipse fitting method (n=6)	contact angle, θ	38.2° (1.5)	40.0° (2.4)
	constant c	0.568 (0.046)	0.566 (0.040)
linear regression of secant angles (n=6)	contact angle, θ	42.4° (1.3)	40.8° (2.7)
sorption method (*) (n=3)	contact angle, θ	33.1° (3.3)	19.0° (2.8)

* significant difference ($p < 0.05$) between UICEL and Avicel PH102[®]

The values determined by the sorption method are markedly lower compared to those of the sessile drop method. This is quite in contrast to the findings of many other workers, who found that contact angles determined by liquid penetration experiment are higher compared to results obtained by sessile drop method [165, 166].

Possible reasons for the discrepancy between both methods can be associated with the measurements, which are both fraught with problems [167].

In the case of the sessile drop method, the contact angle is dependent on the roughness of the surface [168, 169] and the porosity of the tablet. In order to prevent penetration of the drop into the compact, the tablet is usually pre-saturated with water before the experiment. This procedure could not be performed because of the fast disintegration of UICEL. Thus, measuring the contact angle as fast as possible after placing the drop onto the compact ($t = 40$ ms), leaves the question open whether an equilibrium contact angle could have been measured.

Beside the problem to fill the powder homogeneously into the glass cylinder and the problem to find a perfectly wetting liquid [170], the sorption method is basically criticized for theoretical reasons. The Washburn equation neglects gravity and abstracts the complex porous system by a bundle of cylindrical capillaries [171]. Thus, the simplistic model is not a close approximation to reality.

The fact that the difference between both methods is much higher for Avicel PH102[®] than for UICEL could be an indication, that the difference is not related to the method but to the substance:

i) The contact angle determined by the sessile drop method is certainly depending on the process of compression. On one hand Buckton *et al.* [168] observed a decrease in the

contact angle with increasing compression pressure. They justified this phenomenon by heterogeneities in the uncompressed state. Kiesvaara *et al.* [172] reported on the other hand, that depending on the substance the contact angle could rise, fall or remain unchanged upon compression.

ii) Prior to the experiments, the samples were not stored at the same relative humidity (sorption measurement at 0% RH and sessile drop measurement at 40% RH). Several workers [89, 173] found that the dispersive surface free energy decreases (equivalent to a increase in the contact angle) with an increase in relative humidity. Since crystalline cellulose is considered to be most sensitive [89], it is conceivable, that the dispersive surface free energy of Avicel PH102® is more susceptible to changes in relative humidity.

The determination of the surface energy and its components according to the two component-model developed by Owens and Wendt is visualized in figure 36. Table 25 shows the corresponding values. The contact angles, which are required for the calculation according to the two component-model were measured by sorption experiments. Compared to other substances (e.g. lactose: 26.1 mJ/m²; HPMC: 7.5 mJ/m² [174]) the polar components for both celluloses are rather high. The fact that almost one half of the overall surface energy can be ascribed to the polar component may be explained by the plenty of hydroxyl groups, which render the molecules so hydrophilic. Even though all surface energy values listed in table 25 were higher for Avicel PH102® compared to UICEL the differences were statistically not significant ($p = 0.05$) due to the high standard deviations. The bad precision of the method can be explained by the difficult and hardly reproducible sample preparation and the problems mentioned above (page 71).

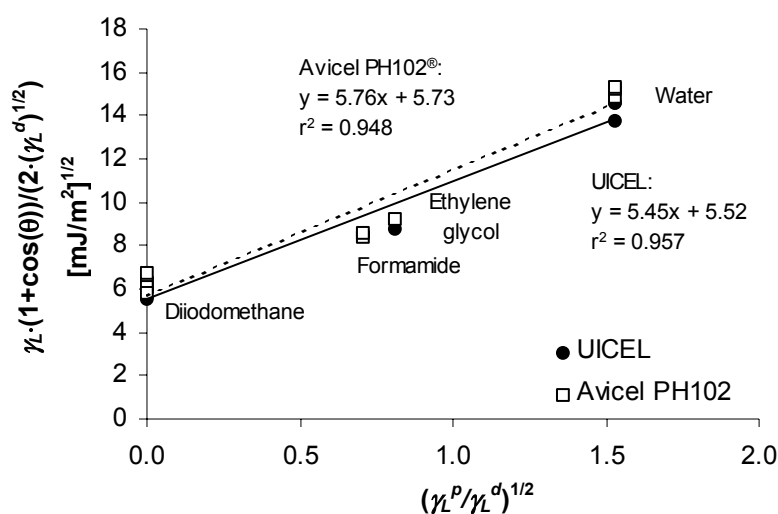


Figure 36: Evaluation of the surface properties of UICEL (—) and Avicel PH102® (- -) based on the two component-model according to Owens/Wendt Theory. The contact angle θ was determined by the sorption method.



Table 25: Surface properties of Avicel PH102[®] and UICEL obtained by the sorption method (with the Standard Error of the Mean (SEM); (n=3)).

substance	overall surface energy, γ_S [mJ/m ²]	dispersive component, γ_S^d [mJ/m ²]	polar component, γ_S^p [mJ/m ²]
UICEL	60.2 (6.7)	30.5 (4.7)	29.7 (4.7)
Avicel PH102 [®]	66.0 (7.5)	32.9 (5.1)	33.2 (5.5)

The evaluation of the IGC measurements is depicted in figure 37. The values for the dispersive free energy of desorption ΔG_D^D and the specific free energy of desorption ΔG_D^{SP} for all used probes (see table 26 and table 27) were used to calculate the dispersive surface free energy γ_S^D and the acceptor parameter K_A and donor parameter K_D (see table 28).

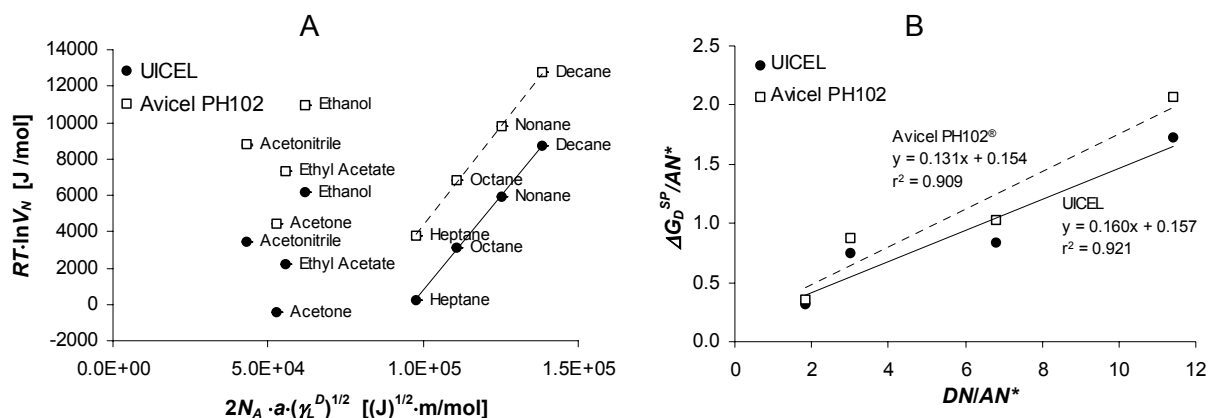


Figure 37: Surface energy plots for UICEL (—) and Avicel PH102[®] (- -) obtained by IGC measurements.

Table 26: Dispersive free energy of desorption for Avicel PH102[®] and UICEL (with the Standard Error of the Mean (SEM); (n=4)).

probe	dispersive free energy of desorption, ΔG_D^D [kJ/mol]	
	UICEL	Avicel PH102 [®]
Heptane	0.27 (0.06)	3.81 (0.09)
Octane	3.13 (0.04)	6.83 (0.06)
Nonane	5.94 (0.05)	9.78 (0.08)
Decane	8.75 (0.06)	12.73 (0.10)

Table 27: Specific free energy of desorption for Avicel PH102[®] and UICEL (with the Standard Error of the Mean (SEM); (n=4)).

probe	specific free energy of desorption, ΔG_D^{SP} [kJ/mol]	
	UICEL	Avicel PH102 [®]
Ethyl acetate	10.85 (0.03)	13.00 (0.13)
Acetone	8.83 (0.11)	10.70 (0.14)
Ethanol	13.52 (0.40)	15.21 (0.21)
Acetonitrile	14.8 (0.69)	17.18 (0.29)

Table 28: Surface properties of Avicel PH102[®] and UICEL obtained by IGC measurements (with the Standard Error of the Mean (SEM); (n=4)).

substances	dispersive surface free energy, γ_S^D (*) [mJ/m ²]	K_A (**)	K_D
UICEL	44.3 (0.1)	0.131 (0.002)	0.154 (0.026)
Avicel PH102 [®]	49.1 (0.3)	0.156 (0.001)	0.165 (0.014)

(*): highly significant ($p \ll 0.001$)

(**): highly significant ($p < 0.005$)

The K_A and K_D parameters express the polar surface properties of the material, similar to the polar surface energy obtained by the sorption method. However, it should be pointed out that they can only be considered as indicative parameters describing the acid-base strength of the material. As the calculation of the two parameters is not consistently performed in literature (AN instead of AN* or ΔH_D^{SP} instead of ΔG_D^{SP}), it is difficult to compare the results with published data. Nevertheless, considering the calculated values for K_A and K_D the inference may be drawn, that both celluloses show amphoteric properties. Considering the molecular structure of cellulose this result is not surprising. The hydrogen atoms in the hydroxyl groups act as electron acceptors (characterized by K_A) and the oxygen atoms in the hydroxyl groups and in the glycoside links act as electron donor (characterized by K_D). The K_A value of Avicel PH102[®] is - in contrast to the K_D value - significantly higher ($p < 0.005$) compared to UICEL. Grimsey *et al.* showed for two optical forms of mannitol that the probe/surface interaction (expressed by K_A) closely correlates with the concentration of acidic sites on the surface [175]. Thus, the difference in the K_A values between Avicel PH102[®] and UICEL can be explained by a higher concentration of polar sites on the surface of Avicel PH102[®]. The discrepancy in the surface density of acidic sites could be caused by differences in the degree of crystallinity but also the difference in the polymorphic form could provide a possible explanation analogous to the investigation of the above-mentioned mannitol. The goodness of fit (correlation coefficients) of the regression line used to determine K_A and K_B is very low (see figure 37 B). The detector response for acid/base



probes deviates from the expected Gaussian elution curve (see figure 38). Unlike the *n*-alkane probes, the chromatograms of the acid/base probes show a distinct peak tailing, which is related to bulk diffusion (absorption into the sample) [91] and/or to non-equilibrium adsorption [176]. However, the bad correlation (see figure 37 B) can be explained by the fact that the obtained data for the acid/base probes do not mirror the true process of sorption and desorption.

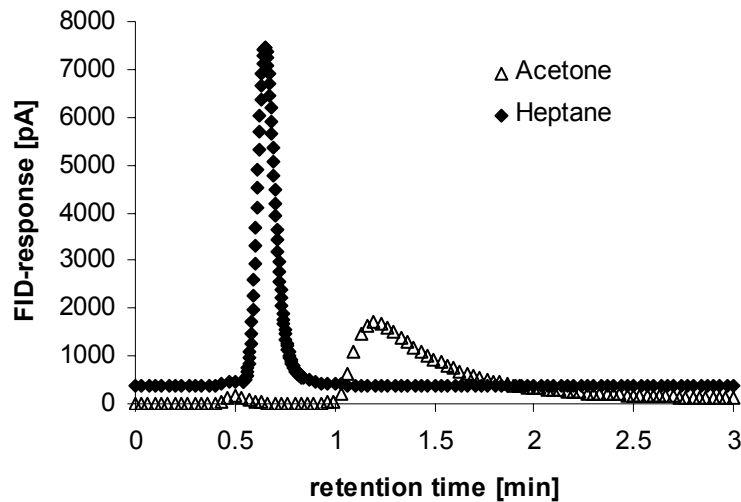


Figure 38: Detector response for the injection of acetone (asymmetrical peak) and heptane (symmetrical peak) into UICEL sample.

The values found in literature for the dispersive surface energy γ_S^D of cellulose samples vary from 27 to 52 mJ/m² depending on the origin (cotton, kenaf, wood), texture (microfibrinous, microcrystalline), pretreatment (washed, nonwashed) and the temperature [86, 173]. Since IGC represents a very sensitive technique, which is even appropriate to detect batch-to-batch variations in the surface properties [177], the big variability found for cellulose is not astonishing.

Belgacem *et al.* [178] ascribed the difference in dispersive properties between starch ($\gamma_S^D = 27.4$ mJ/m²) and microcrystalline cellulose ($\gamma_S^D = 40.3$ mJ/m²) to the different degree of crystallinity (see the empirical equation (51)). Therefore, the significant ($p < 0.001$) lower dispersive surface free energy for UICEL may be caused by the higher amorphous character compared to Avicel PH102®.

$$\log \gamma_S^D - \log \gamma_{S,a}^D = \frac{1}{3} Crl_s \cdot Crl_{max} \quad \text{equation (51)}$$

where: γ_S^D : dispersive surface free energy of the (semicrystalline) sample [mJ/m²]

$\gamma_{S,a}^D$: dispersive surface free energy of the totally amorphous substance [mJ/m²]

Crl_s : degree of crystallinity on the surface

Crl_{max} : maximum degree of crystallinity in the bulk

As both methods attribute the higher surface energies to Avicel PH102[®] and not to UICEL, the results of the IGC and the sorption measurements can be considered as consistent. However, the IGC measurements revealed to be more discriminating compared to the sorption method.

Comparing the values for the dispersive surface free energy of both methods, it is obvious that the IGC method provided higher values. Since the probe molecules were injected at infinite dilution (1-3% surface coverage by the probe molecules [179]), they are supposed to interact preferentially with the high-energy sites in contrast to the sorption method where the liquids were interacting with all possible sites.

Thus, the possible effects of the parameters involved in the water uptake according to the Washburn equation can be summarized as follows:

The pore radius is raised to the 5th power in the Washburn equation. Therefore the increased pore size of UICEL tablets compared to Avicel PH102[®] tablet will outweigh the opposed effect that the slightly lower surface free energy could exert on the rate of water uptake.

The pore radius is of particular importance and could be identified as the most important and dominating parameter determining the water uptake.

4.7 Drug release from tablets consisting of proquazone and disintegrant in different ratios.

In this chapter the applicability of UICEL as a disintegrant is investigated. For this purpose binary mixtures consisting of UICEL and proquazone as drug were compressed at different ratios to tablets with the constant relative density of 0.8. The compacts were tested for tensile strength and disintegration time. The main concern was the determination of the drug release. For comparative reasons, UICEL was replaced by Avicel PH102[®] and two well-known disintegrants (Vivastar[®], Starch 1500[®]) for comparison.

Table 29: Overview of some properties of proquazone (with the Standard Error of the Mean (SEM)).

property	value for proquazone
true density, ρ_t [g/cm ³] (n=3)	1.2556 (0.0002)
mean particle size [μm] (n=3)	19.75 (1.39)
volume-specific surface area*, A_v [m ² /cm ³] (n=3)	0.392 (0.014)
solubility**, c_s [g/100 ml] (n=3)	0.1423 (0.0003)
flux, J [mg/cm ² /min] (n=4)	0.1018 (0.0013)
contact angle***, θ (n=6)	81.8° (2.4°)

* determined by laser diffractometer ($A_v = 6/d_{median}$).

** measured at pH 1.0 (0.1N HCl).

*** evaluated according to the height and length method of the sessile drop measurement.



The properties of proquazone are listed in table 29. Concerning the volume-specific surface area, it has to be pointed out, that the determination by a laser diffractometer is based on the assumption of spherical shaped particles and does not take into account the roughness of the particles.

A solubility of 0.1423 g/100 ml means that 703 parts of solvent (0.1N HCl) are required to solve 1 part of proquazone. Thus, according to the USP proquazone can be described as slightly soluble at a pH of 1.0.

Concerning the solubility, the biopharmaceutical classification system (BCS) divides the substances in classes with high and low solubility depending whether the highest dose strength of the drug can be dissolved in 250 ml of aqueous media over the pH range 1.0-7.5 or not [180]. Since the highest dose strength is about 300 mg [181], proquazone meets the requirements for a highly soluble drug at the pH 1.0. Yu *et al.* suggested the intrinsic dissolution rate as criterion for the BCS instead of the dose related requirement [182]. According to this alternative approach, which sets the class boundary at 0.1 mg/min/cm², proquazone can still be considered as highly soluble. However, the requirements have to be fulfilled over the pH range of 1.0-7.5. Since proquazone is a weak base with a pKa of 1.1 it is conceivable that the solubility will decrease at higher pH values. This assumption is supported by the work of Hugentobler [183], who found a solubility value for proquazone of 1:10'000 in water. Since von Orelli *et al.* predicted a high permeability, it is justified to assign proquazone to the BCS class II, which is characterized by a high permeability and a low solubility [184].

Since the contact angles determined by liquid penetration are commonly higher compared to those measured by the sessile drop method [165], the contact angle of proquazone is in good agreement with the result of von Orelli *et al.* who noticed a contact angle higher than 90° [184]. However, coming in contact with water or 0.1N HCl, proquazone will dissolve and decrease the surface tension of the surrounding medium. The dissolution of proquazone in 0.1N HCl decreases the surface tension from 72.3 mN/m for water to 54.6 mN/m for the saturated solution of proquazone. Thus, the wettability could be increased as soon as proquazone is dissolved.

The results for the disintegration and tensile strength measurements are tabulated in table 30 and visualized in figure 39 and figure 40. For a better readability, the points in the figures are connected by straight lines knowing that the parameters will not behave linearly between the points.

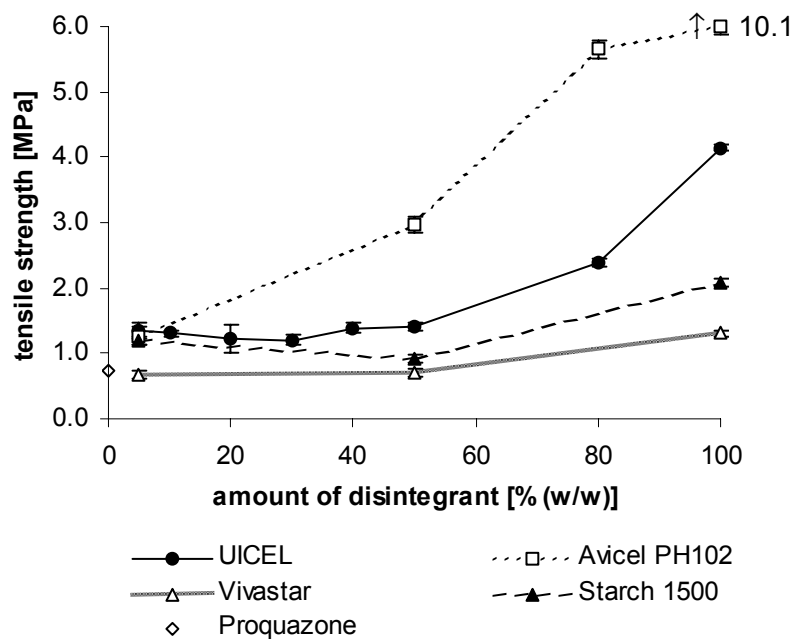


Figure 39: Tensile strength of tablets ($\rho_r = 0.88$) consisting of a binary mixture of proquazone and excipient versus the amount of excipient. Error bars: ± 1 SEM (n=4).

Concerning the influence on the tensile strength, the substances can be ranked in the following descending order: Avicel PH102[®] > UICEL > Starch 1500[®] > Vivastar[®].

Considering the effect of the amount of disintegrant on the tensile strength, the substances can be divided into two groups. Avicel PH102[®] increases the tensile strength of the tablets already in small amounts, whereas the other disintegrants effect the tensile strength just above an amount of 50% (compare figure 39).

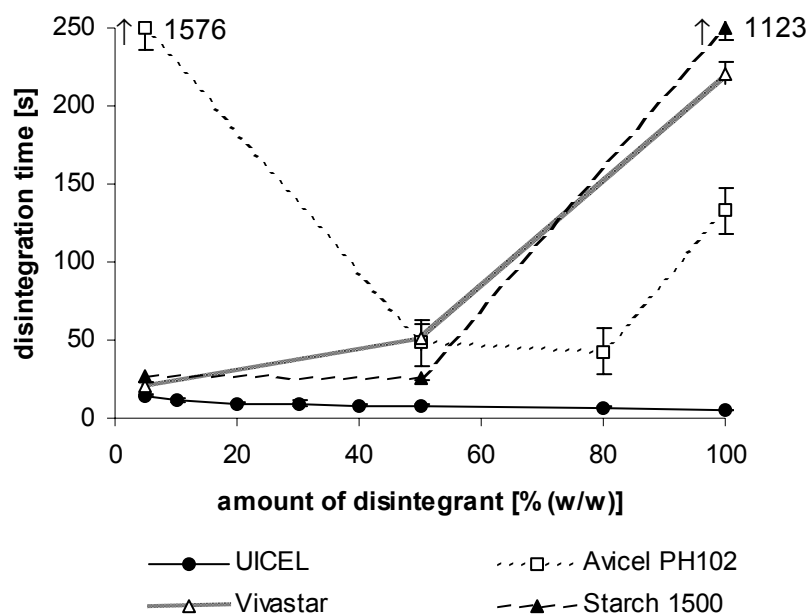


Figure 40: Disintegration time of tablets ($\rho_r = 0.88$) consisting of a binary mixture of proquazone and disintegrant in various amounts. Error bars: ± 1 SEM (n=4).



Table 30: Empirical parameters for tablets ($\rho_r = 0.88$) consisting of proquazone and excipient (with the Standard Error of the Mean (SEM); (n=4)).

excipient	tensile strength, σ_t [MPa]	disintegration time, t_d [s]	$t_{50\%}$ -value [min]
UICEL			
5%	1.35 (0.02)	14.5 (0.3)	11.9 (0.5)
10%	1.30 (0.11)	11.8 (0.6)	7.1 (0.1)
20%	1.23 (0.00)	9.5 (0.3)	3.7 (0.1)
30%	1.21 (0.04)	9.5 (0.8)	2.4 (0.2)
40%	1.39 (0.03)	8.0 (0.3)	1.6 (0.2)
50%	1.41 (0.03)	8.3 (0.3)	1.2 (0.0)
80%	2.38 (0.02)	6.6 (0.4)	n.d.
100%	4.14 (0.06)	5.5 (0.1)	
Avicel PH102[®]			
5%	1.27 (0.03)	15770 (300)	544.2 (8.7)
50%	2.97 (0.07)	48.3 (7.4)	23.8 (0.7)
80%	5.66 (0.06)	42.9 (1.5)	n.d.
100%	10.07 (0.06)	133.0 (9.4)	
Vivastar[®]			
5%	0.67 (0.03)	21.0 (1.1)	4.2 (0.0)
50%	0.70 (0.03)	51.5 (4.2)	1.1 (0.0)
100%	1.31 (0.05)	221.0 (3.3)	
Starch 1500[®]			
5%	1.20 (0.03)	26.5 (1.7)	13.6 (0.1)
50%	0.93 (0.02)	25.2 (0.4)	1.5 (0.0)
100%	2.09 (0.05)	1123 (4)	
Proquazone			
100%	0.74 (0.06)	39600 (60)	673.9 (18.5)

Regarding the disintegration time, the disintegrants can be classified into three groups:

- i) UICEL: Within the investigated range of mass fraction, the disintegration time of tablets consisting of UICEL is very short and mostly independent of the used amount.
- ii) Vivastar[®] and Starch 1500[®]: Vivastar[®] and Starch 1500[®] cause a significant increase in the disintegration time at a mass fraction between 0.5 and 1.0. Luginbühl reported that the increase in disintegration time of tablets consisting of Starch 1500[®] as disintegrant sets in above a mass fraction of 0.7 [110]. There are two possible explanations for this observation: Firstly, the increase in disintegration time is a result of the increase in the cohesive energy (see tensile strength). Secondly, the highly viscous structure, due to the swelling of the disintegrant, hampers the penetration of the water and thus delays the disintegration.

iii) Avicel PH102[®]: Avicel PH102[®] also shows an increase in disintegration time at higher mass fractions similar to Vivastar[®] and Starch 1500[®]. But unlike the three other disintegrants, Avicel PH102[®] is not very effective at low concentrations resulting in a u-shaped curve.

As the disintegration time for tablets consisting only of proquazone is very high (about 11 hours), it is well conceivable that there is also a minimal required concentration existing for UICEL, Vivastar[®] and Starch 1500[®]. This threshold must lie between 0 and 5% (w/w), because it could not have been detected within the range of the used amounts. Thus, the critical concentration is so small that the substance is supposed to form a penetrating cluster *via* pores, which are already preexisting in the tablet or/and formed during disintegration.

The dissolution profiles of proquazone in tablets consisting of proquazone in combination with various disintegrants in different mass fractions are depicted in figure 41 and figure 42. Obviously the drug release is accelerated with increasing amount of UICEL. This observation is perfectly reflected by the $t_{50\%}$ -values listed in table 30. The $t_{50\%}$ -value is defined as the time until 50% of the available drug is dissolved. The comparison between the different disintegrants shows clear differences in the efficiency of drug release. The disintegrants can be ranked in the following order:

Vivastar[®] > UICEL = Starch 1500[®] \gg Avicel PH102[®].

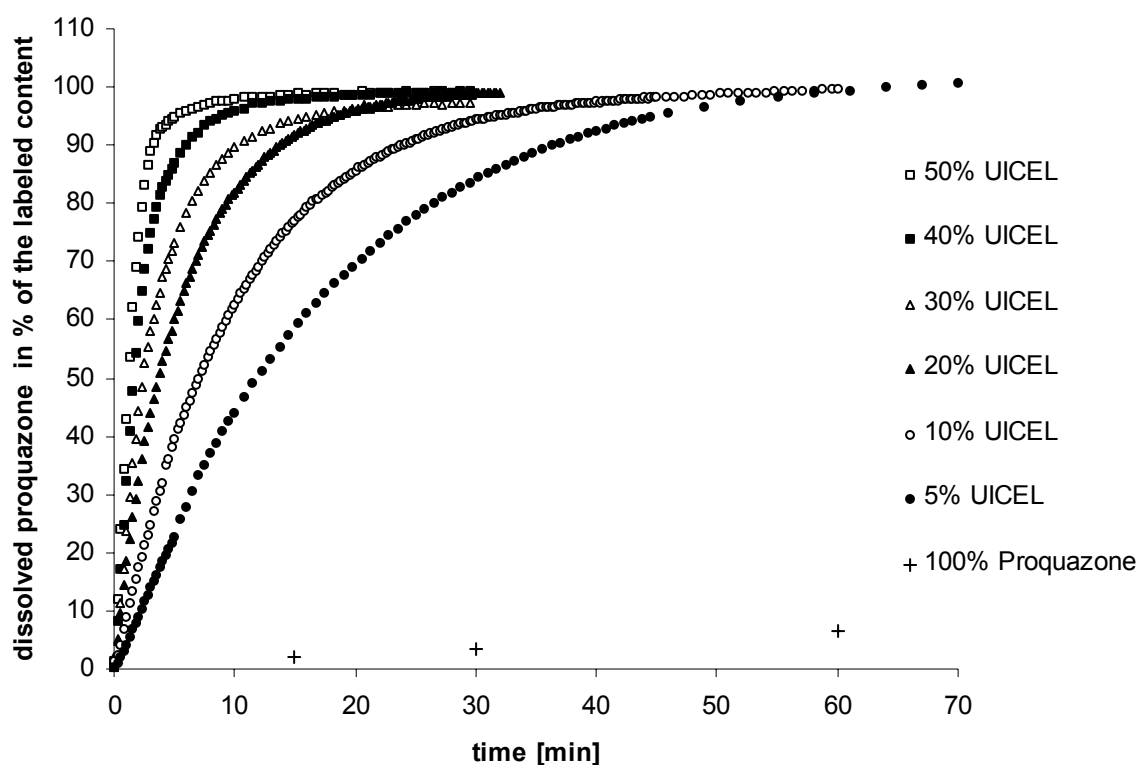


Figure 41: Dissolution of proquazone in tablets consisting of proquazone and UICEL in different mass fractions.

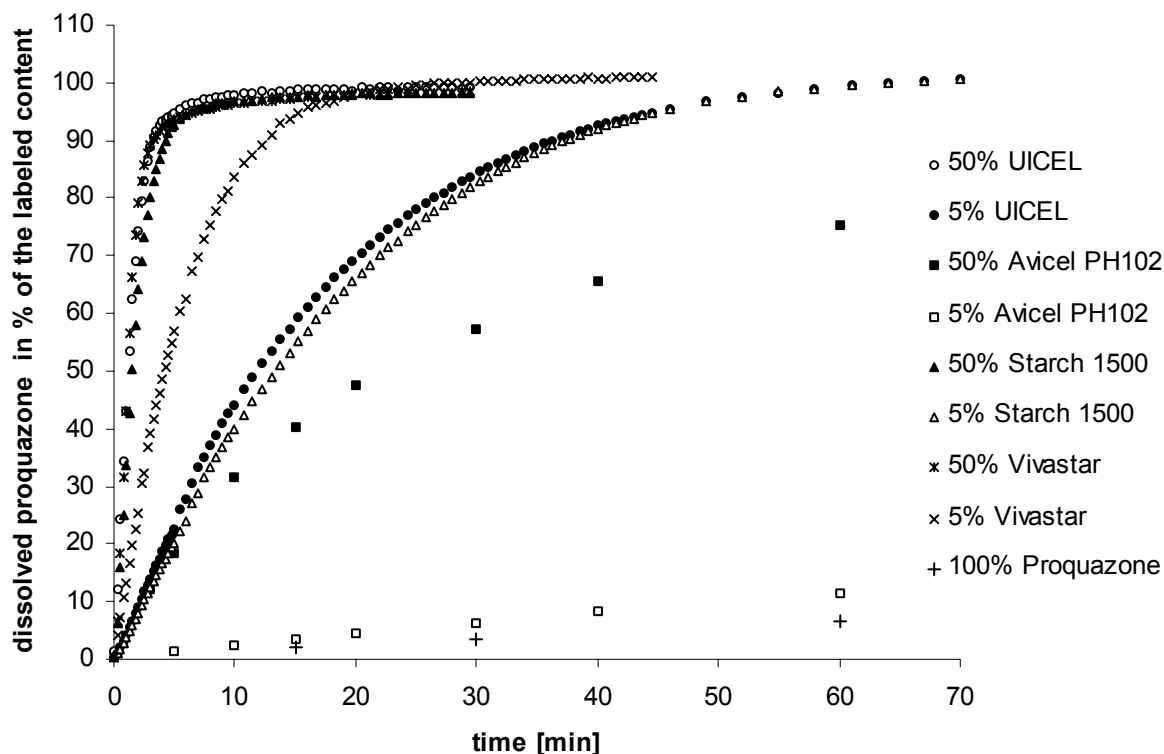


Figure 42: Dissolution of proquazone in tablets consisting of proquazone and different disintegrants in the ratios 50:50 and 95:5.

Drug release involves the disintegration of the tablet and the dissolution of the active ingredient. Both processes take place simultaneously at least until disintegration is completed. There are several methods for describing the dissolution of disintegrating tablets. From a mathematical point of view, some of them are very complicated and not suitable for the “daily use” [185, 186]. The mostly used equation is made up of two exponential functions [187]. The deviation of this equation is based on the assumption that the rate of the dissolving material is proportional to the weight of undissolved particles. The equation used in this context (equation (38)) is derived from Fick’s first law and some considerations about the surface area during drug release (see Appendix D). Even though the equation consists also of two exponential functions, the physical meaning and interpretation of the involved parameters are quite different compared to the above-mentioned two exponential equation of EI-Yazigi. Unfortunately the fitting could not be performed for Avicel PH102[®] because of an insufficient number of data points. The results for the other disintegrants are listed in table 31.

Table 31: Fitting parameters according to equation (38) for the dissolution of proquazone from tablets consisting of proquazone and disintegrant (with the Standard Error of the Mean (SEM); (n=4)).

disintegrant	A_{v0} [m ² /cm ³]	k_1 [min ⁻¹]	k_2 [min ⁻¹]	r_2	A_{max} [cm ²]	A_{vmax} [m ² /cm ³]
UICEL						
5%	2.23 (0.001)	0.0584 (0.0001)	1.76 (0.00)	1.000	75	0.0718
10%	4.58 (0.002)	0.0995 (0.0001)	3.72 (0.00)	0.999	119	0.1193
20%	9.28 (0.007)	0.1856 (0.0006)	7.61 (0.01)	0.997	197	0.2206
30%	10.46 (0.015)	0.2946 (0.0024)	8.78 (0.01)	0.996	261	0.3383
40%	11.60 (0.013)	0.4747 (0.0044)	9.58 (0.01)	0.997	352	0.5464
50%	14.17 (0.017)	0.7615 (0.0081)	11.68 (0.01)	0.996	456	0.8649
Vivastar®						
5%	9.90 (0.007)	0.1659 (0.0007)	7.89 (0.01)	0.999	217	0.2039
50%	3.29 (0.004)	0.9937 (0.0243)	2.75 (0.00)	0.996	399	0.8657
Starch 1500®						
5%	2.38 (0.002)	0.0517 (0.0002)	1.84 (0.00)	1.000	68	0.6530
50%	7.22 (0.010)	0.6357 (0.0042)	6.03 (0.00)	0.999	349	0.6852

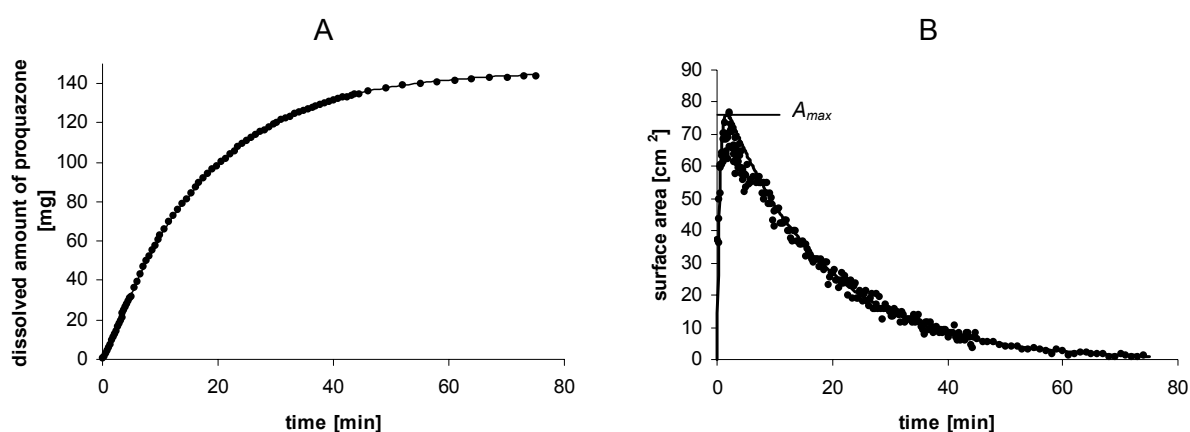


Figure 43: Illustration of the goodness of fit for the drug release of proquazone from tablets consisting of proquazone (95% (w/w)) and UICEL (5% (w/w)). A: dissolution profile fitted according to equation (38) ; B: surface area of proquazone particles versus time calculated according to equation (2) (appendix D) as a result of the dissolution rate data (figure 43 A) and fitted according to equation (3) (appendix D).

The goodness of fit for the drug release from all formulations is expressed by the excellent correlation coefficient and is also demonstrated visually in figure 43.

Discussion of the involved parameters:

i) maximum possible volume-specific surface area, A_{v0}

A_{v0} would correspond to the maximum volume-specific area if the dissolution rate k_2 could be neglected compared to the disintegration rate k_1 . Since k_2 is higher than k_1 , the actual



maximum volume-specific area A_{vmax} is smaller than the hypothetical value A_{v0} . A_{v0} can be considered as a measure for the efficacy of the disintegrant. Thus, it is conceivable that a higher amount of disintegrant causes an increase of A_{v0} . However, Vivastar[®] represents an exception. The efficacy of 50% is smaller compared to 5% of Vivastar[®]. This irregularity could originate from the fact, that Vivastar[®] forms a gel-like structure at higher concentration due to the pronounced swelling capacity.

However, it has to be kept in mind that A_{v0} is a hypothetical and notional volume-specific surface area, which will never be achieved throughout the whole disintegration process. Therefore it is not surprising that the specific surface area determined by laser diffractometer (see table 29) is smaller than A_{v0} .

ii) disintegration rate k_1 and dissolution rate k_2

For the interpretation of the parameters k_1 and k_2 it has to be kept in mind that they relate to the change of the surface area and not to the change of the weight of proquazone during drug release. However, for reasons of simplicity k_1 and k_2 are called “rate of disintegration” and “rate of dissolution”, respectively.

With the exception of the formulation containing 50% of Vivastar[®], the parameter k_2 is always higher than k_1 by a factor of about 10. Thus, the formation of new surface area due to disintegration is the rate-limiting step. This circumstance is also becoming evident by the fact, that the rate of disintegration k_1 ranks the formulations in the same order like the $t_{50\%}$ -values. In the terminal phase the surface area vanishes as fast as it appears from disintegration. This situation is analogous to the flip-flop phenomenon in pharmacokinetics where the absorption is rate limiting and determines the terminal phase. Thus, the dissolution rate k_2 can only be determined with data at the beginning of the drug release either by feathering or by nonlinear regression.

For all investigated disintegrants an increasing amount of disintegrant results in an increased disintegration rate k_1 . The physical meaning of the dissolution rate k_2 is a little bit more complicated. The dissolution rate k_2 is depending on the particle size and consequently on the volume-specific surface area. This correlation can be illustrated by plotting k_2 versus A_{v0} (figure 44) resulting in a straight line with a slope ($0.830 \text{ cm}^3/\text{min}/\text{m}^2$) that is very near the value for the term J/ρ_s ($0.810 \text{ cm}^3/\text{min}/\text{m}^2$). Thus, the dissolution rate k_2 and the decrease of surface area per time due to dissolution $-dA/dt$ can be written according to equation (52) and equation (53), respectively. The fact that the term $-dA/dt$ is depending on the volume-specific surface area A_{v0} and the flux J is reasonable. However, equation (53) is just an approximation and not strictly valid, because the volume-specific surface area is also a function of time as the particle size is decreasing, which is not taken into account.

$$k_2 = A_{v0} \cdot \frac{J}{\rho_t} = \frac{A_0}{m_0} \cdot J \tag{equation (52)}$$

$$-\frac{dA}{dt} = k_2 \cdot A = A_{v0} \cdot \frac{J}{\rho_t} \cdot A \tag{equation (53)}$$

$$m(t) = m_0 \frac{k_2 \cdot k_1}{k_1 - k_2} \left(\frac{1}{k_2} (1 - e^{-k_2 \cdot t}) - \frac{1}{k_1} (1 - e^{-k_1 \cdot t}) \right) \tag{equation (54)}$$

- where: k_2 : rate of dissolution [min^{-1}]
- k_1 : rate of disintegration [min^{-1}]
- A_{v0} : maximum possible volume-specific surface area [cm^2/cm^3]
- A : surface area of proquazone during dissolution [cm^2]
- A_0 : maximum possible surface area [cm^2]
- J : flux [$\text{mg}/\text{min}/\text{cm}^2$]
- ρ_t : true density of proquazone [g/cm^3]
- m_0 : weight of proquazone at $t = 0$ (dose strength) [g]

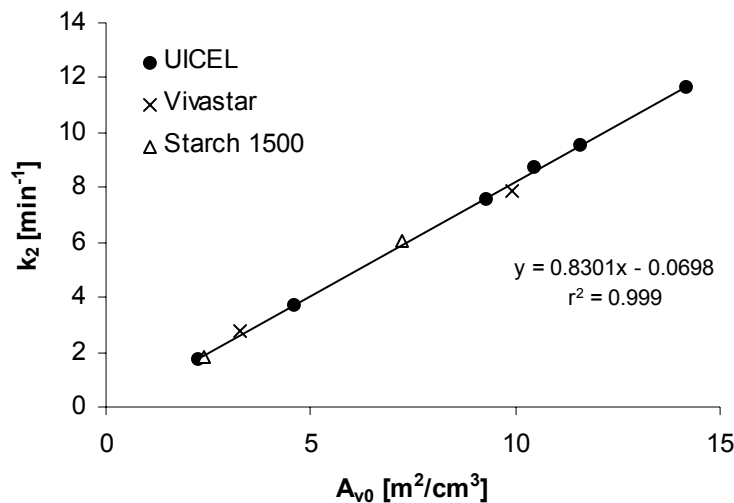


Figure 44: Correlation between the dissolution constant k_2 and the volume-specific surface area A_{v0} with a slope, which equals J/ρ_t .

The resulting equation (54) obtained by combining equation (38) and equation (52) equals the equation developed by El-Yazigi [187]. However, despite the identical mathematical expressions, the physical meaning of the involved parameter is totally different. Thus, the rate of dissolution k_2 can for instance be expressed by well-known physical parameters and the parameter A_{v0} provides a good possibility to estimate the efficacy of the disintegrant.

Nevertheless, the power and reliability of the new equation describing drug release should be evaluated by further experiments. The plausibility of the new equation could be verified by determining the surface area of proquazone with gas adsorption measurements. Thereby, a measured BET-surface area, which is close to the highest calculated parameter A_{vmax} could strongly support the new equation.



The successful application of the equation is limited by the measuring procedure: In order to determine the rate of dissolution k_2 , it is crucial that the time interval between the measurements at the beginning of the drug release is short compared to the involved dissolution process.

4.8 Stability of acetylsalicylic acid in combination with UICEL and Avicel PH102[®]

The stability of the moisture sensitive acetylsalicylic acid is intensively studied in literature. Two main approaches exist to describe the decomposition of acetylsalicylic acid. Leeson *et al.* suggested a “suspension”-model, where the acetylsalicylic acid is decomposed dissolved in a thin water layer surrounding the drug particles [188]. Another theory proposed the formation of reaction nuclei on the crystal surfaces [189]. Independent of the involved reaction mechanism, an apparent (pseudo) zero-order reaction was assumed in this study at least at the initial stage. The decomposition of acetylsalicylic acid in combination with UICEL and Avicel PH102[®] at ambient conditions (temperature: 25°C; relative humidity: 45%) is shown in figure 45. For purposes of clarity, the standard error of the mean is only depicted in one case. The corresponding degradation rate constants k_0 are listed in table 32.

Table 32: Degradation rate constants k_0 of acetylsalicylic acid in compressed and uncompressed mixtures together with UICEL and Avicel PH102[®] (with the Standard Error of the Mean (SEM); (n=4)).

amount of cellulose [% (w/w)]	$k_0 \cdot 10^3$ [mg /100 mg /day]	
	UICEL	Avicel PH102 [®]
powder		
0%		0.07 (0.03)
50%	-0.09 (0.08)	0.93 (0.47)
90%	4.42 (1.15)	31.76 (4.54)
compact		
0%		0.12 (0.03)
50%	-0.05 (0.20)	1.71 (0.33)
90%	5.53 (1.28)	28.02 (2.11)

The stability results of acetylsalicylic acid exposed to higher stresses are visualized in figure 46. As expected, elevated temperatures and higher relative humidities accelerate the degradation.

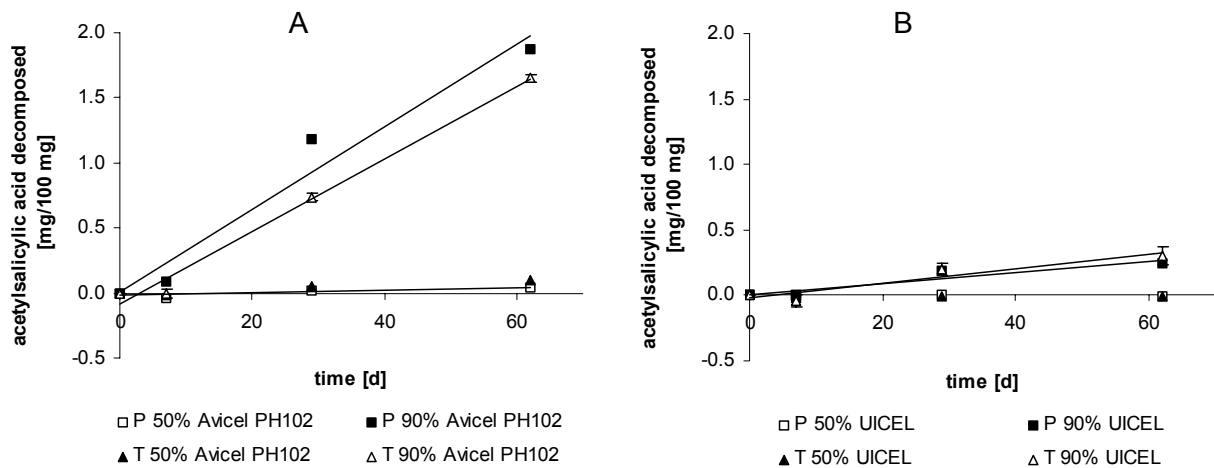


Figure 45: Decomposition of acetylsalicylic acid related to time for Avicel PH102[®] (A) and UICEL (B) (n=4).

Figure 45 and figure 46 demonstrate that the degradation of acetylsalicylic acid is depending on the amount of cellulose. With an increasing amount of UICEL and Avicel PH102[®], the decomposition of acetylsalicylic acid is also increasing. However, the degradation in the presence of UICEL is much lower compared to Avicel PH102[®]. Comparing both substances, the degradation rate constants in table 32 are significantly different ($p < 0.001$) and also the decomposition of the accelerated tests clearly show that acetylsalicylic acid is decomposed faster in the presence of Avicel PH102[®].

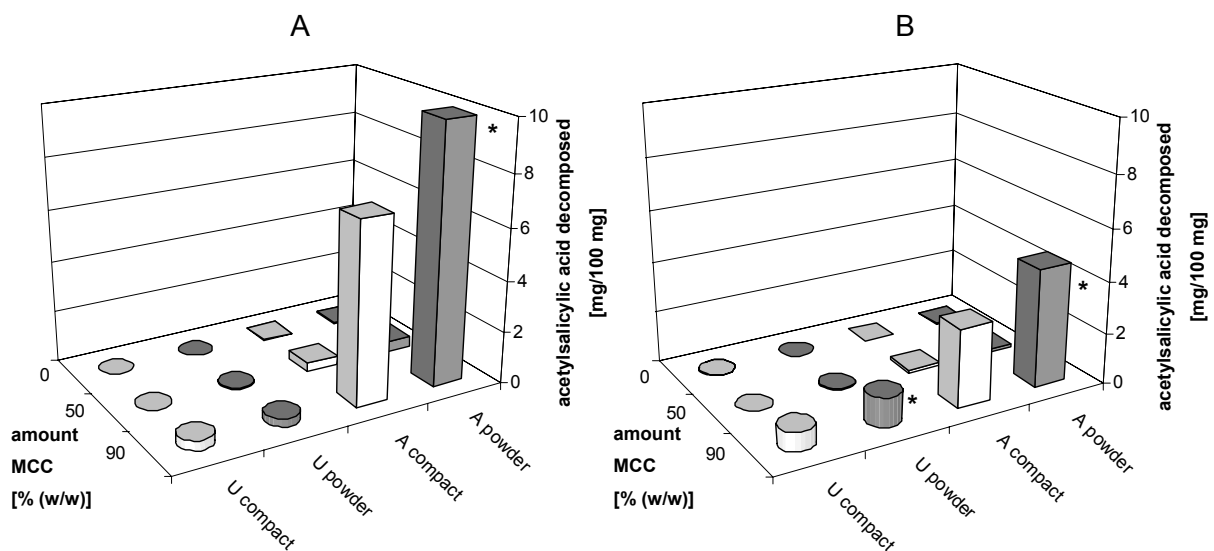


Figure 46: Decomposition of acetylsalicylic acid under stress storage conditions. A: conditions: 45% RH, 70°C, 7 day; B: conditions: 75% RH, 25°C, 62 days; legend: UICEL: rounded columns; Avicel PH102[®]: square-edged columns; powder: dark colored; compact: light colored; asterisk: significant difference between powder and compact (n=4).



Concerning the comparison between the decomposition of acetylsalicylic acid in compacts and in powders at ambient conditions, the findings agree with the conclusion found by Ahlneck *et al.*, who reported that the change in porosity has a minor or no effect on the stability of acetylsalicylic acid [190]. However, under elevated temperatures and higher relative humidities there are some cases where the differences between the degradation of acetylsalicylic acid in a powder and in a compact are significant. ($p \ll 0.001$). The powders, which show a significant higher decomposition of acetylsalicylic acid compared to the compacts, are labeled with an asterisk in figure 46.

The rate constant of the decomposition under ambient conditions as well as the one time measurements of the accelerated tests clearly demonstrate, that acetylsalicylic acid is more stable in combination with UICEL than with Avicel PH102[®]. The possible reasons for the discrepancy between both substances are manifold. The two most important arguments will be discussed in the following section:

i) The pH-value is of crucial importance for the stability in the solid state [190]. Figure 47 depicts the degradation rate constant of acetylsalicylic acid related to the pH-value. It can be inferred from the figure that the reaction is strongly catalyzed by hydrogen (pH: 0-2) and hydroxyl ions (pH: 9-13). The degradation rate is low and constant in the pH range 5-8 and has a minimum in the pH range 2-3 [191]. Scheef *et al.* found an acid strength of 3.94 for Avicel PH102[®] [192]. Since the pH-values of a suspension is supposed to run parallel to the acid strength [117, 193] and since Avicel PH102[®] is characterized by a lower pH-value for the suspension than UICEL (see table 10), the surface acidity of UICEL is assumed to be slightly higher than 3.94. In consequence, comparing with the pH-rate profile (see figure 47), UICEL should rather favor the decomposition of acetylsalicylic acid. Thus, the difference in the pH-value may not cause the difference in decomposition.

ii) The relevance of the moisture sorption of the excipient on the drug stability is controversially discussed in literature. On the one hand moisture sorption by microcrystalline cellulose is correlated to the drug stability [194, 195]. On the other hand workers found that the moisture in starch and different qualities of lactose does not impair the drug stability [196, 197]. Thus, the moisture content may not directly be responsible for the decomposition of a moisture sensitive drug. If just the water surrounding the particles is supposed to be involved in the decomposition of the drug, then the surface property could be of more importance than the moisture content, which can be considered as bulk property. Ahlneck *et al.* demonstrated that microfibrillated cellulose, showing a lower degree of crystallinity compared to microcrystalline cellulose, has a less pronounced adversely impact on the stability of acetylsalicylic acid despite its higher moisture content [198]. These findings are in perfect agreement with the results of this study. Even though UICEL is not a microfibrillated cellulose, it has a higher amorphous fraction compared to Avicel PH102[®]. Thus, due to the higher

amorphous fraction, which is also reflected by the lower dispersive free energy of UICEL compared to Avicel PH102[®] (see table 28), a lower amount of water is available for degradation of acetylsalicylic acid on the surface of the particles. But not only the surface density of the water on the particles is supposed to be different. The overall surface area of the Avicel PH102[®] particles is higher compared to UICEL (see table 25). Thus, the different influence of UICEL and Avicel PH102[®] on the degradation of acetylsalicylic acid can be explained by different surface properties combined with a different surface area of the particles [199, 200]. Since the surface area is decreasing under pressure (see figure 24), this theory provides also the explanation for the lower decomposition of acetylsalicylic acid in a compact.

However, the problem how the surface water is becoming available for the decomposition of acetylsalicylic acid is not solved. The sublimation of aspirin can most likely be excluded [201]. It is conceivable that acetylsalicylic acid molecules, which are dissolved in the water layer surrounding the drug particles, reach the water adsorbed by the cellulose particles by diffusion.

Three facts are limiting the significance of the performed stability test. Firstly, the analytical determination of salicylic acid as a measure for the degradation of acetylsalicylic acid has the drawback that the extent of decomposition may be underestimated due to sublimation of salicylic acid [201]. Secondly, it has to be kept in mind, that the experiments were conducted in an open system with an “infinite” moisture reservoir. However, the moisture will be limited at more realistic storage conditions. Thus, it is difficult to apply the results on a formulation stored in a closed vessel. The last fact that has not yet been discussed is the influence of the particle size on the degradation. The mean particle size of the used acetylsalicylic acid determined by laser diffractometry was $290.0 \pm 2.0 \mu\text{m}$. It might be expected that a higher surface area of the drug will enhance its decomposition.

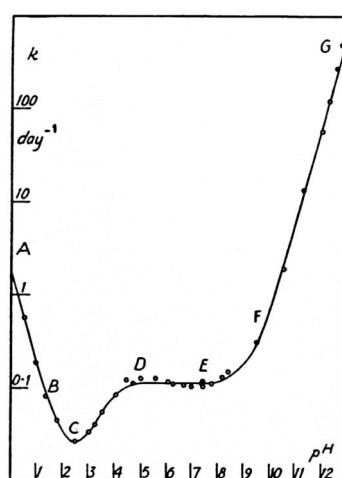


Figure 47: Degradation rate for acetylsalicylic acid as a function of pH at 17°C [191].



5 Conclusions and outlook

X-ray proved to be the method of choice for the determination of the sample identity and the degree of crystallinity. Additionally, it also provides useful information about the extent of lattice transition from cellulose I to cellulose II. X-ray measurements could demonstrate that the crystalline regions of UICEL show the cellulose II lattice whereas Avicel PH102[®] contains the cellulose I polymorph. Concerning UICEL, the formation of a pseudo-polymorphic form with ethanol, which is added during the manufacturing process, could also be excluded because a significant concentration of ethanol could not be detected. The evaluation of the x-ray diffractograms but also the measurements of the true density revealed that the degree of crystallinity is smaller for UICEL compared to Avicel PH102[®].

The fact that UICEL and Avicel PH102[®] differ not only in the polymorphic form of the crystalline parts but also in the degree of crystallinity makes it difficult to ascribe further possible secondary discrepancies between the two substances to one of these two primary differences:

i) moisture content:

Because of the uncertainty concerning the determination of an accurate absolute value for the degree of crystallinity, it is not impossible that the higher moisture content of UICEL is just a consequence of the higher fraction of the amorphous phase.

ii) surface free energy:

The highly discriminating IGC proved to be the more accurate and appropriate method to determine the surface free energy than the liquid penetration method. Thereby, UICEL showed a slightly but significantly lower surface free energy (including the dispersive as well as the polar component) compared to Avicel PH102[®]. The difference could not be unambiguously attributed to the difference in the polymorphic form, because it is well known from literature [202] that a lower crystallinity will result in a lower surface free energy.

iii) compression properties:

UICEL turned out to be less plastic compared to Avicel PH102[®]. In this case it is highly probable that the difference in the compression behavior is associated with the polymorphic form. A higher amorphous fraction and a higher moisture content would rather improve the plastic behavior. Thus, differences in the degree of crystallinity and in the moisture content may be excluded as possible causes for the worse compression properties of UICEL compared to Avicel PH102[®]. The assumption that the different polymorphic forms are the causal reason for the differences in the compression behavior may be supported by some theoretical considerations on a molecular level. During deformation the compression pressure is supposed to induce shearing stresses within the crystalline regions. As mentioned in the introduction, the molecules in the cellulose II lattice are strongly

interbonded. Thus, the parallel movement and slipping of the cellulose molecules are inhibited.

UICEL revealed to be a material of outstanding disintegration properties. The disintegration time of tablets consisting of UICEL and proquazone was even shorter as when Vivastar® (sodium starch glycolate) was used as superdisintegrant. However, swelling of the particles could be excluded as possible disintegration mechanism for UICEL. For Guyot-Hermann, the increase in particle diameter does also not seem to be sufficient to explain the disintegration mechanism of starch. He hypothesized a particle-particle repulsive force [203]. In this work a new but similar model is proposed. Figure 48 shows the assumed interrelationship of various parameters involved in the disintegration process.

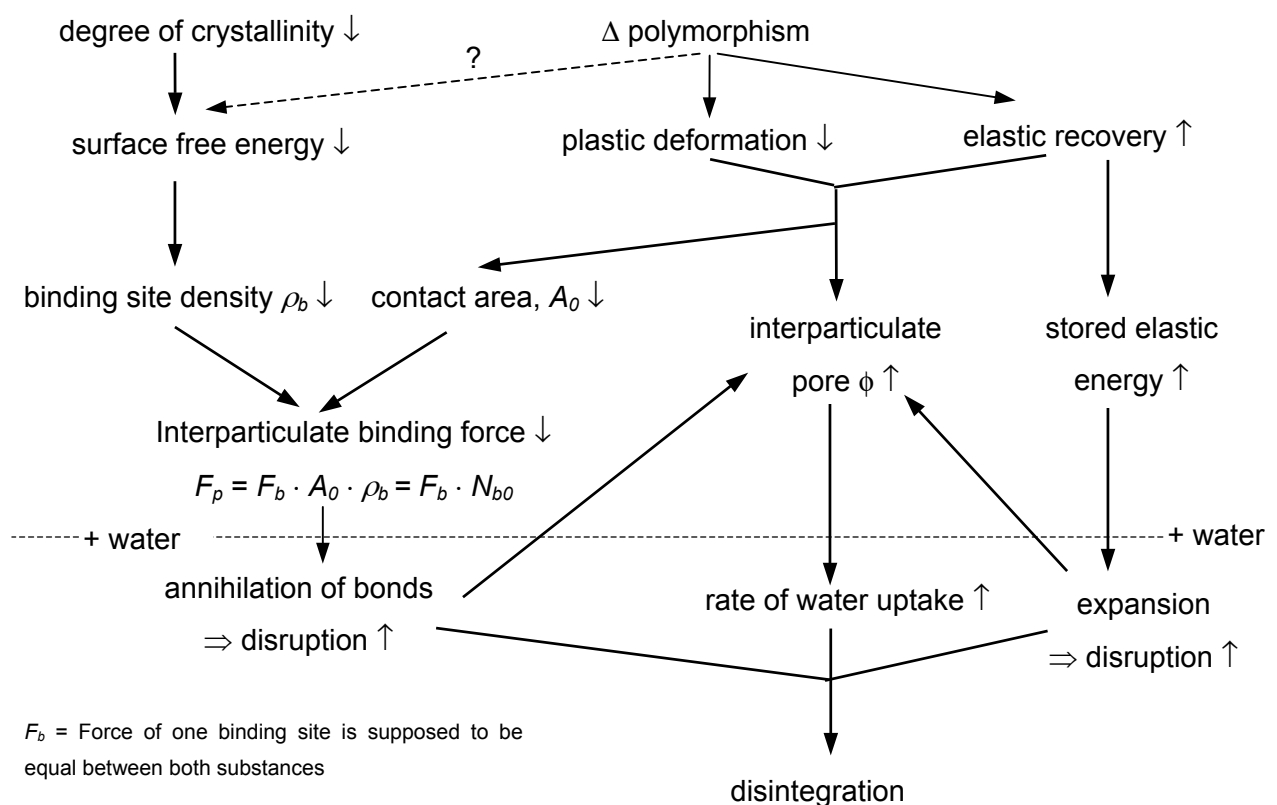


Figure 48: Proposed disintegration mechanism for UICEL. The noted tendencies (↓,↑) refer to UICEL compared to Avicel PH102®. F_p : force between two particles; F_b : force of one binding site; A_0 : bonding surface area; ρ_b : surface density of bonding sites; N_{b0} : number of bonds between two particles.

Heckel analysis and modified Heckel analysis clearly indicate that UICEL is less ductile than Avicel PH102®. It is suggested that the decreased plastic deformation and increased elastic recovery for UICEL compared to Avicel PH102® cause on the one hand a decreased bonding



area between the particles in the tablet and on the other hand a larger pore size within the tablet. The large pore size in UICEL tablets could in fact be confirmed by mercury porosimetry. Since the pore radius is raised to the 5th power in the Washburn equation, small variations of the pore size have already a great impact on the rate of water uptake.

Combining the aforementioned smaller bonding area with the proposed lower binding site density due to a reduced surface free energy of UICEL compared to Avicel PH102[®], the cohesion energy in the UICEL tablets is smaller, which is consistent with the lower radial tensile strength. In consequence, the hydrogen bonds between the particles will rapidly be annihilated as soon as the water reaches the particles in the tablet. The following disruption of the structure will result in a pore widening, which in turn will act as a positive feedback on the rate of water uptake.

Furthermore, due to the higher elastic recovery of UICEL tablets compared to Avicel PH102[®] tablets, a “compressed spring” model can be postulated. The higher elastic energy stored in UICEL tablets is released by the penetrating water. Thereby, the regeneration of the original shape contributes to the disruption of the tablet.

To sum it up, the disintegration can be considered as the result of two processes: i) the water uptake (vertical or axial movement) and ii) the separation of the particles due to elastic expansion of the compressed particles and annihilation of the interparticulate hydrogen bonds followed by penetration of water between the particles (horizontal or radial movement).

It can also be attempted to describe the two processes (water uptake and annihilation of hydrogen bonds) qualitatively by a mathematical expression. According to equation (55) the overall disintegration time t_{tot} is the sum of the time for the water uptake t_w (according to the Washburn equation) and the time for the disruption t_s of the particles (see appendix E).

$$t_{tot} = t_w + t_s = \frac{l^2}{K_1} + \frac{\sqrt{N_{b0}} - \sqrt{N_b}}{K_2} \quad \text{equation (55)}$$

where: t_w : time for water uptake

t_s : time for separation of two bonded particles

l : depth of water penetration front

N_{b0} : total amount of bonds between two particles at the beginning

N_b : number of bonds at time t_s

K_1 : constant (depending on viscosity, surface tension of the water and pore radius)

K_2 : annihilation rate constant

Equation (55) is a rough and approximate description of the processes illustrated in figure 48. It does not take into account the pore widening due to disruption, which is additionally supposed to accelerate the disintegration. However, equation (55) is suitable to interrelate

the involved parameter and can be visualized in a three-dimensional contour plot and its projection onto the xz plane (see figure 49).

The thick solid line in figure 49 describes the water uptake according to the Washburn equation, whereas the thin solid curve represents the whole disintegration process. Thus, the length of the projected contour lines (horizontal solid lines in the projected plots (B, D)) equals the time it takes for the water to penetrate between the particles by annihilation of the hydrogen bonds.

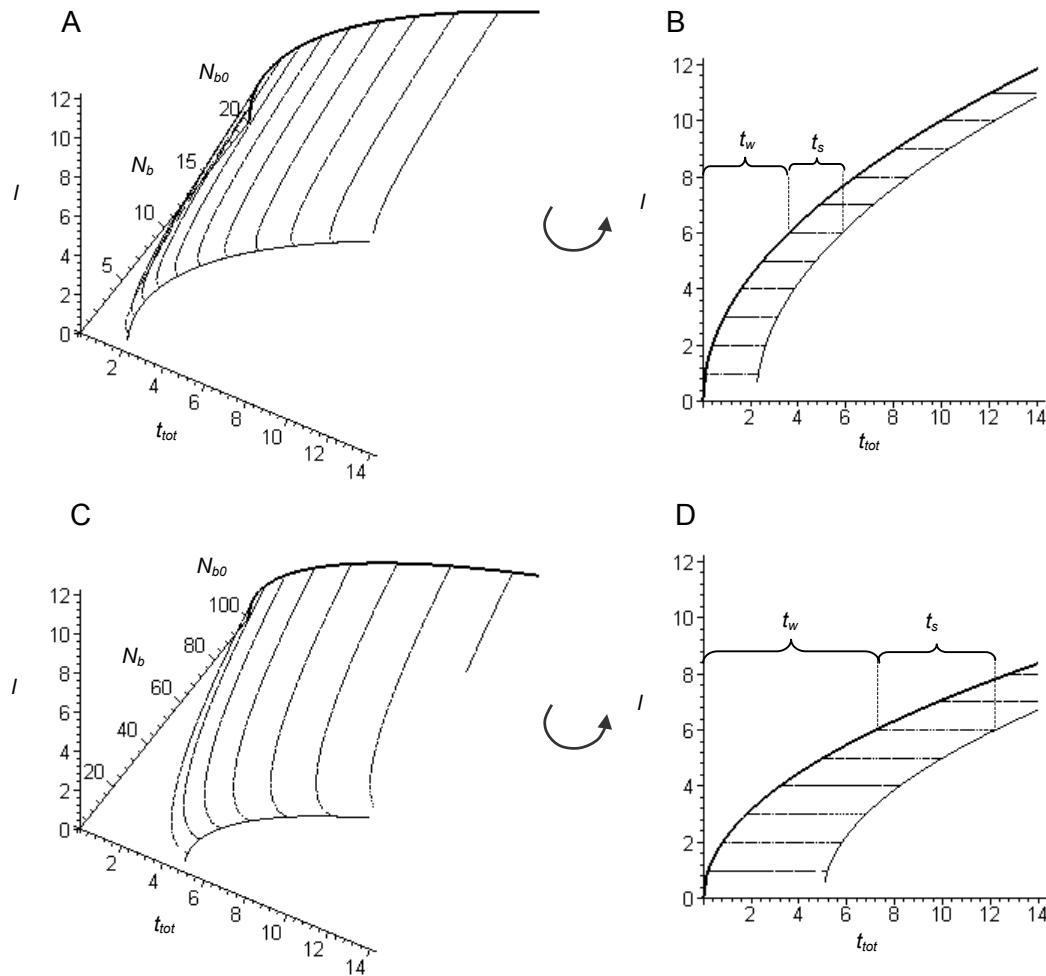


Figure 49: Visualization of the disintegration process composed of the water uptake and the particle separation. l : height of the water front within the tablet. N_b : number of bonding sites per bonding area. B, D projected views of A, C. A, B: UICEL: K_1 : 10; K_2 : 2; N_{b0} : 20; C, D: Avicel PH102[®]: K_1 : 5; K_2 : 2; N_{b0} : 100. The units are arbitrary.

The time t_w it takes till the water has moved up to a certain level l inside the tablet is shorter for UICEL compared to Avicel PH102[®]. The faster rate of water uptake is the result of the higher pore size of UICEL and is expressed by the higher value for K_1 . But also the time it takes for the separation of two particles is shorter due to the lower number N_{b0} of bonds



between to particles after compression. The nature of the hydrogen bonds may be considered to be very similar for both substances. Thus, in figure 49 the rate constant K_2 for annihilation was assumed to be equal.

Drug release study

The experiment concerning the release of proquazone from tablets of a binary mixture consisting of proquazone and a disintegrant (UICEL, Avicel PH102[®], Vivastar[®], Starch 1500[®]) showed three facts that make UICEL so attractive as disintegrant: i) In the contrary to the other excipients, UICEL is acting as a disintegrant also when adding in higher amounts (e.g. as filler). ii) UICEL shows the highest ratio of tensile strength to disintegration time. iii) Related to the drug release, UICEL is as effective as Starch 1500[®].

Furthermore, UICEL is well suited for being used as an excipient for direct compression, due to the better flowability compared to Avicel PH102[®].

A new biexponential equation did not only prove to be extremely successful in describing the release of proquazone but also provided a good means for the classification of the efficacy of disintegrants.

Stability study

Despite the higher moisture content of UICEL compared to Avicel PH102[®], the decomposition of acetylsalicylic acid was significantly smaller when combined with UICEL than with Avicel PH102[®]. At least in the case of acetylsalicylic acid, the determination of the moisture content of the used excipients is totally insufficient for the estimation of the drug stability. The surface area of the excipient and its surface properties (crystallinity, surface free energy) seem to be much more decisive.

Outlook

In the last years, there was a trend away from multi-drug towards single-drug formulations in order to avoid pharmacological interactions, to minimize side effects and to therapy more selectively. An analogous reduction of the number of involved excipients could simplify the system, eliminate physical interactions between components and help to gain a more profound knowledge of manufacturing processes. Thus, reducing the number of excipients would render the system better predictable. From this point of view, multifunctional excipients like UICEL, which can be used as binder, filler and disintegrant could be of great advantage. However, prior to the scale-up of the production of UICEL, the influence of certain factors (e.g. amount of sodium hydroxide and ethanol, duration of mercerization) on the product quality should be thoroughly investigated.

Despite the very extensive examination concerning the properties of the cellulose products, the degree of polymerization has not been taken into consideration within this study. However, Kleinebudde *et al.* [204] showed that the degree of polymerization can remarkably influence the physicochemical but also the process-oriented properties of microcrystalline and powder cellulose.

The „compressed spring“ model as disintegration mechanism could be confirmed by additional experiments, which try to correlate parameters characteristic for the elastic behavior of the material with disintegration properties. Thereby, Hiestand's indices (strain index, bonding index) could serve as useful tools [205].

In this study the extraordinary disintegration properties of UICEL used in simple systems could be demonstrated. Yet, UICEL has not been tested as disintegrant incorporated into granules. It is well conceivable that the disintegration properties of UICEL will vanish when it is combined with a binder. Acting like a glue or mortar, the binding agent will on the one hand increase the bonding area and the bonding strength and on the other hand decrease the pore size and thus interfere with the disintegration mechanism of UICEL.

The efficiency of the new equation describing drug release should be evaluated by further experiments. The plausibility of the model could be checked by relating the measured surface area (BET-surface) to the surface area calculated by the new equation.

6 References

- [1] Lowes, M.M.J., Caira, M.R., Lötter, A.P., Van der Watt, J.G. (1987) Physicochemical properties and X-ray structural studies of the trigonal polymorph of carbamazepine. *Journal of Pharmaceutical Sciences*, **76**(9), 744-752.
- [2] Azibi, M., Draguet-Brughmans, M., Bouche, R., Tinant, B., Germain, G., Declercq, J.P., Van Meerssche, M. (1983) Conformational study of two polymorphs of spiperone: possible consequences on the interpretation of pharmacological activity. *Journal of Pharmaceutical Sciences*, **72**(3), 232-235.
- [3] Goldberg, I., Becker, Y. (1987) Polymorphs of tamoxifen citrate: detailed structural characterization of the stable form. *Journal of Pharmaceutical Sciences*, **76**(3), 259-264.
- [4] Aguiar, A.J., Krc, J., Kinkel, A.W., Samyn, J.C. (1967) Effect of polymorphism on the absorption of chloramphenicol from chloramphenicol palmitate. *Journal of Pharmaceutical Sciences*, **56**(7), 847-853.
- [5] Bauer, J., Spanton, S., Henry, R., Quick, J., Dziki, W., Porter, W., Morris, J. (2001) Ritonavir: an extraordinary example of conformational polymorphism. *Pharmaceutical Research*, **18**(6), 859-866.
- [6] Morissette, S.L., Soukasene, S., Levinson, D., Cima, M.J., Almarsson, O. (2003) Elucidation of crystal form diversity of the HIV protease inhibitor ritonavir by high-throughput crystallization. *Proceedings of the National Academy of Sciences (PNAS)*, **100**(5), 2180-2184.
- [7] Specifications: test procedures and acceptance criteria for new drug substances and new drug products: chemical substances. International Conference on Harmonisation (ICH), Guideline specification Q6A, Step 4, October, 1999.
- [8] Decision Tree: Investigating the need to set acceptance criteria for polymorphism in drug substances and drug products. International Conference on Harmonisation (ICH), Guideline specification Q6A, Step 4, October, 1999.
- [9] Byrn, S., Pfeiffer, R., Ganey, M., Hoiberg, C., Poochikian, G. (1995) Pharmaceutical solids: a strategic approach to regulatory considerations. *Pharmaceutical Research*, **12**(7), 945-954.
- [10] Schwarz, T.W. (1966) Molded solid dosage forms: suppositories. In: American Pharmacy, Sprowls, J.B., Beal, H.M. (Eds), Lippincott, Philadelphia.
- [11] Guyot-Hermann, A.M., Leblanc, D., Draguet-Brughmans, M. (1985) Gamma sorbitol as a diluent in tablets. *Drug Development and Industrial Pharmacy*, **11**(2&3), 551-564.
- [12] Guyot-Hermann, A.M., Guyot, J.C. (1990) Un des éléments du cahier des charges: l'état physique des excipients. *Sciences Techniques et Pratiques Pharmaceutiques - S.T.P. Pharma*, **6**(hors série), 37-44.
- [13] Concheiro, A., Vila-Jato, J.-L., Torres, D. (1987) Problématique des excipients pour compression directe. *Sciences Techniques et Pratiques Pharmaceutiques - S.T.P. Pharma*, **3**(11), 886-894.
- [14] Giron, D. (1990) Le polymorphisme des excipients. *Sciences Techniques et Pratiques Pharmaceutiques - S.T.P. Pharma*, **6**(hors série), 87-98.
- [15] Fell, J.T., Newton, J.M. (1970) Prediction of the tensile strength of tablets. *Journal of Pharmacy and Pharmacology*, **22**(3), 247-248.
- [16] Botez, C.E., Stephens, P.W., Nunes, C., Suryanarayanan, R. (2003) Crystal structure of anhydrous δ -D-mannitol. *Powder Diffraction*, **18**(3), 214-218.
- [17] Burger, A., Henck, J.-O., Hetz, S., Rollinger, J.M., Weissnicht, A.A., Stöttner, H. (2000) Energy/temperature diagram and compression behavior of the polymorphs of D-mannitol. *Journal of Pharmaceutical Sciences*, **89**(4), 457-468.

- [18] Debord, B., Lefebvre, C., Guyot-Hermann, A.M., Hubert, J., Bouché, R., Guyot, J.C. (1987) Study of different crystalline forms of mannitol: comparative behaviour under compression. *Drug Development and Industrial Pharmacy*, **13**(9-11), 1533-1546.
- [19] Yoshinari, T., Forbes, R.T., York, P., Kawashima, Y. (2002) Moisture induced polymorphic transition of mannitol and its morphological transformation. *International Journal of Pharmaceutics*, **247**(1-2), 69-77.
- [20] Yoshinari, T., Forbes, R.T., York, P., Kawashima, Y. (2003) The improved compaction properties of mannitol after a moisture-induced polymorphic transition. *International Journal of Pharmaceutics*, **258**(1-2), 121-131.
- [21] Kryszewski, M., Wojciechowski, P., Okrasa, L., Kozanecki, M., Ulanski, J. (2002) Cellulose derivatives - organic crystals and liquid crystals - used the longest, known the least. *Polish Journal of Chemistry*, **76**(2-3), 187-200.
- [22] Klemm, D., Philipp, B., Heinze, T., Heinze, U., Wagenknecht, W. (1998) Comprehensive cellulose chemistry, Volume 1. Wiley-VCH, Weinheim.
- [23] Payen, A. (1838) Mémoire sur la composition du tissu propre des plantes et du ligneux. *Comptes rendus hebdomadaires des Séances de l'Académie des Sciences. Tome 3*, **7**, 1052-1056.
- [24] Freudenberg, K., Braun, E. (1928) Methylcellulose. *Justus Liebigs Annalen der Chemie*, **460**, 288-304.
- [25] Freudenberg, K. (1928) Nachtrag zu der Mitteilung über Methylcellulose. *Justus Liebigs Annalen der Chemie*, **461**, 130-131.
- [26] Haworth, W.N. (1928) Structure of carbohydrates. *Helvetica Chimica Acta*, **11**, 534-548.
- [27] Gralen, N. (1943) Molecular weight of native cellulose. *Nature*, **152**, 625.
- [28] Doelker, E. (1993) Comparative compaction properties of various microcrystalline cellulose types and generic products. *Drug Development and Industrial Pharmacy*, **19**(17-18), 2399-2471.
- [29] Doelker, E., Gurny, R., Schurz, J., Janosi, A., Matin, N. (1987) Degrees of crystallinity and polymerization of modified cellulose powders for direct tableting. *Powder Technology*, **52**(3), 207-213.
- [30] Schurz, J., Klapp, H. (1976) Investigations on microcrystalline and microfine cellulose powders. *Das Papier*, **30**(12), 510-513.
- [31] Hearle, J.W.S., Peters, R.H. (1963) Fibre structure. Butterworths, London.
- [32] Staudinger, H., Feuerstein, K. (1936) Über hochpolymere Verbindungen, *Justus Liebigs Annalen der Chemie*, **526**, 72-102.
- [33] Staudinger, H. (1932) Die hochmolekularen organischen Verbindungen. Springer, Berlin.
- [34] Hearle, J.W.S. (1958) A fringed fibril theory of structure in crystalline polymers. *Journal of Polymer Science*, **28**, 432-435.
- [35] Preston, R.D., Nicolai, E., Reed, R., Millard, A. (1948) An electron microscope study of cellulose in the wall of *Valonia ventricosa*. *Nature*, **162**, 665-667.
- [36] Kono, H., Numata, Y., Erata, T., Takai, M. (2004) ¹³C and ¹H resonance assignment of mercerized cellulose II by two-dimensional MAS NMR spectroscopies. *Macromolecules*, **37**(14), 5310-5316.
- [37] Atalla, R.H., VanderHart, D.L. (1984) Native cellulose: A composite of two distinct crystalline forms. *Science*, **223**(4633), 283-285.
- [38] VanderHart, D.L., Atalla, R.H. (1984) Studies of microstructure in native celluloses using solid-state ¹³C NMR. *Macromolecules*, **17**(8), 1465-1472.

- [39] Atalla, R.H., VanderHart, D.L. (1989) Studies on the structure of cellulose using Raman spectroscopy and solid state ^{13}C NMR. In: Cellulose and Wood – Chemistry and Technology, Schuerch, C. (Ed.), Wiley, New York.
- [40] Hirai, A., Tsuji, M., Horii, F. (1997) Culture conditions producing structure entities composed of Cellulose I and II in bacterial cellulose. *Cellulose*, **4**(3), 239-245.
- [41] Sisson, W.A. (1938) The existence of mercerized cellulose and its orientation in halicystis as indicated by X-ray diffraction analysis. *Science*, **87**, 350.
- [42] Fink, H.-P., Philipp, B. (1985) Models of cellulose physical structure from the viewpoint of the cellulose I→II transition. *Journal of Applied Polymer Science*, **30**(9), 3779-3790.
- [43] Dinand, E., Vignon, M., Chanzy, H., Heux, L. (2002) Mercerization of primary wall cellulose and its implication for the conversion of cellulose I→cellulose II. *Cellulose*, **9**(1), 7-18.
- [44] Kroon-Batenburg, L.M.J., Kroon, J. (1997) The crystal and molecular structures of cellulose I and cellulose II. *Glycoconjugate Journal*, **14**(5), 677-690.
- [45] O'Sullivan, A.C. (1997) Cellulose: the structure slowly unravels. *Cellulose*, **4**(3), 173-207.
- [46] Langan, P., Nishiyama, Y., Chanzy, H. (2001) X-ray structure of mercerized cellulose II at 1 Å resolution. *Biomacromolecules*, **2**(2), 410-416.
- [47] Blackwell, J., Kolpak, F.J., Gardner, K.H. (1977) Structures of native and regenerated celluloses. In: Cellulose Chemistry and Technology, Arthur, J.C. (Ed.), American Chemical Society, Washington, D.C.
- [48] Meyer, K.H., Misch, L. (1937) Positions des atomes dans le nouveau modèle spatial de la cellulose, *Helvetica Chimica Acta*, **20** 232-244.
- [49] Mark, H., Meyer, K.H. (1929) Über den Bau des kristallisierten Anteils der Cellulose. II. *Zeitschrift für Physikalische Chemie, Abteilung B*, **2**, 115-145.
- [50] Andress, K.R. (1929b) Das Röntgendiagramm der mercerisierten Cellulose. *Zeitschrift für Physikalische Chemie, Abteilung B*, **4**, 190-206.
- [51] Sarko, A., Muggli, R. (1974) Packing analysis of carbohydrates and polysaccharides. III. Valonia cellulose and cellulose II. *Macromolecules*, **7**(4), 486-494.
- [52] Gardner, K.H., Blackwell, J. (1974) The structure of native cellulose. *Biopolymer*, **13**(10), 1975-2001.
- [53] Kolpak, F.J., Blackwell, J. (1976) Determination of the structure of cellulose II. *Macromolecules*, **9**(2), 273-278.
- [54] Maurer, A., Fengel, D. (1992) Parallel orientation of the molecular chains in cellulose I and cellulose II deriving from higher plants. *Holz als Roh- und Werkstoff*, **50**(12), 493.
- [55] Kroon-Batenburg, L.M.J., Bouma, B., Kroon, J. (1996) Stability of cellulose structures studied by MD simulations. Could mercerized cellulose II be parallel? *Macromolecules*, **29**(17), 5695-5699.
- [56] Andress, K.R. (1929a) Das Röntgendiagramm der nativen Cellulose. *Zeitschrift für Physikalische Chemie, Abteilung B*, **2**, 380-394.
- [57] Battista, O.A., Coppick, S., Howsmon, J.A., Morehead, F.F., Sisson, W.A. (1956) Level-off degree of polymerization. *Industrial and Engineering Chemistry*, **48**(2), 333-335.
- [58] Battista, O.A. (1950) Hydrolysis and crystallization of cellulose. *Industrial and Engineering chemistry*, **42**(3), 502-507.
- [59] Reus-Medina, M., Lanz, M., Kumar, V., Leuenberger, H. (2004) Comparative evaluation of the powder properties and compression behaviour of a new cellulose-based direct compression excipient and Avicel PH-102. *Journal of Pharmacy and Pharmacology*, **56**(8), 951-956.

- [60] Kumar, V., Reus-Medina, M., Yang, D. (2002) Preparation, characterization, and tableting properties of a new cellulose-based pharmaceutical aid. *International Journal of Pharmaceutics*, **235**(1-2), 129-140.
- [61] Stahl, P.H. (1980) Feuchtigkeit und Trocknen in der pharmazeutischen Technologie. D. Steinkopf Verlag, Darmstadt.
- [62] Hausner, H.H. (1967) Friction conditions in a mass of metal powders. *International Journal of Powder Metallurgy*, **3**(4), 7-13.
- [63] Carr, R.L. (1965a) Evaluating flow properties of solids. *Chemical Engineering*, **72**(2), 163-168.
- [64] Carr, R.L. (1965b) Classifying flow properties of solids. *Chemical Engineering*, **72**(3), 69-72.
- [65] Ingersoll, H.G. (1946) Fine structure of viscose rayon. *Journal of Applied Physics*, **17**, 924-939.
- [66] Segal, L., Creely, J.J., Martin, A.E., Conrad, C.M. (1959) An empirical method for estimating the degree of crystallinity of native cellulose using the X-ray diffractometer. *Textile Research Journal*, **29**, 786-794.
- [67] Lee, S.B., Shin, H.S., Ryu, D.D.Y. (1982) Adsorption of cellulase on cellulose: effect of physicochemical properties of cellulose on adsorption and rate hydrolysis. *Biotechnology and Bioengineering*, **24**(10), 2137-2153.
- [68] Kilian, H.G. (1960) Kristallisieren und Schmelzen von verschiedenen Hochpolymeren nach röntgenographischen Messungen. *Kolloid-Zeitschrift*, **176**(1), 49-62.
- [69] Hermans, P.H. (1949) Physics and chemistry of cellulose fibres with particular reference to Rayon. Elsevier, New York.
- [70] Brenner, F.C., Frilette, V., Mark, H. (1948) Crystallinity of hydro-celluloses. *Journal of the American Chemical Society*, **70**, 877-878.
- [71] Hüttenrauch, R., Keiner, I. (1976) Wie kristallin sind „mikrokristalline“ Cellulose? *Pharmazie*, **31**(3), 183-187.
- [72] Nelson, M.L., O'Connor, R.T. (1964b) Relation of certain infrared bands to cellulose crystallinity and crystal lattice type. Part II. A new infrared ratio for estimation of crystallinity in cellulose I and II. *Journal of Applied Polymer Science*, **8**(3), 1325-1341.
- [73] Scherrer, P. (1918) Bestimmung der Grösse und der inneren Struktur von Kolloidteilchen mittels Röntgenstrahlen. *Nachrichten von der Königlichen Gesellschaft der Wissenschaften zu Göttingen*, 98-100.
- [74] Washburn, E.W. (1921) The dynamics of capillary flow. *The Physical Review*, **17**(3), 273-283
- [75] Michel, J. -C., Rivière, L.-M., Bellon-Fontaine, M.-N. (2001) Measurement of the wettability of organic materials in relation to water content by the capillary rise method. *European Journal of Soil Science*, **52**(3), 459-467.
- [76] Owens, D.K., Wendt, R.C. (1969) Estimation of the surface free energy of polymers. *Journal of Applied Polymer Science*, **13**(8), 1741-1747.
- [77] Young, T. (1805) An essay on the cohesion of fluids. *Philosophical Transactions of the Royal Society of London*, **95**, 65-87.
- [78] Bangham, D.H., Razouk, R.I. (1937) Adsorption and wettability of solid surfaces. *Transactions of the Faraday Society*, **33**, 1459-1463.
- [79] Girifalco, L.A., Good, R.J. (1957) A theory for the estimation of surface and interfacial energies. I. Derivation and application to interfacial tension. *Journal of Physical Chemistry*, **61**, 904-909.
- [80] Good, R.J., Girifalco, L.A. (1960) A theory for estimation of surface and interfacial energies. III. Estimation of surface energies of solids from contact angle data. *Journal of Physical Chemistry*, **64**, 561-565.

- [81] Fowkes, F.M. (1964) Attractive forces at interfaces. *Journal of Industrial and Engineering Chemistry*, **56**(12), 40-52.
- [82] Van Oss, C.J., Good, R.J., Chaudhury, M.K. (1988) Additive and nonadditive surface tension components and the interpretation of contact angles. *Langmuir*, **4**(4), 884-891.
- [83] Riddle, F.L., Fowkes F.M. (1990) Spectral shifts in acid-base chemistry. 1. Van der Waals contribution to acceptor numbers. *Journal of the American Chemical Society*, **112**(9), 3259-3264.
- [84] McClellan A.L., Harnsberger, H.F. (1967) Cross-sectional areas of molecules adsorbed on solid surfaces. *Journal of Colloid and Interface Science*, **23**(4), 577-599.
- [85] Gutmann, V. (1978) The donor-acceptor approach to molecular interactions. Plenum Press, New York.
- [86] Tshabalala, M.A. (1997) Determination of the acid-base characteristics of lignocellulosic surfaces by inverse gas chromatography. *Journal of Applied Polymer Science*, **65**(5), 1013-1020.
- [87] Schultz, J., Lavielle, L. (1989) Interfacial properties of carbon fiber-epoxy matrix composites. In: *Inverse Gas Chromatography*, Lloyd, D.R., Ward, T.C., Schrieber, H.P. (Eds), American Chemical Society, Washington.
- [88] Saint Flour, C., Papirer E. (1982) Gas-solid chromatography: a method of measuring surface free energy characteristics of short glass fibers. 2. Through retention volumes measured near zero surface coverage. *Industrial and Engineering Chemistry Product Research and Development*, **21**(2), 666-669.
- [89] Grimsey, I.M., Feeley, J.C., York, P. (2002) Analysis of the surface energy of pharmaceutical powders by inverse gas chromatography. *Journal of Pharmaceutical Sciences*, **91**(2), 571-583.
- [90] Felix, J.M. Gatenholm, P. (1993) Characterization of cellulose fibers using inverse gas chromatography. *Nordic Pulp and Paper Research Journal*, **8**(1), 200-203.
- [91] Planinsek, O., Buckton, G. (2003) Inverse gas chromatography: Considerations about appropriate use for amorphous and crystalline powders. *Journal of Pharmaceutical Sciences*, **92**(6), 1286-1294.
- [92] Bell, L.N., Labuza, T.P. (2000) Moisture sorption: practical aspects of isotherm measurement and use, second edition. American Association of Cereal Chemists, St. Paul.
- [93] Brunauer, S., Emmett, P. H.; Teller, E. (1938) Adsorption of gases in multimolecular layers. *Journal of the American Chemical Society*, **60**, 309-19.
- [94] Anderson, R.B. (1946) Modifications of the Brunauer, Emmett and Teller equation. *Journal of the American Chemical Society*, **68**, 686-691.
- [95] Guggenheim, E.A. (1966) Applications of statistical mechanics. Clarendon Press, Oxford.
- [96] De Boer, J.H. (1953) The dynamical character of adsorption, Clarendon Press, Oxford.
- [97] Visavarungroj, N., Herman, J. and Remon, J.P. (1990) Crosslinked starch as sustained release agent. *Drug Development and Industrial Pharmacy*, **16**(7), 1091-1108.
- [98] Leach, H.W., McCowen, L.D. and Schoch, T.J. (1959) Structure of the starch granule I. Swelling and solubility patterns of various starches. *Cereal Chemistry*, **36**, 534-544.
- [99] Bowen, F.E., Vadino, W.A. (1984) A simple method for differentiating sources of pregelatinized starch NF. *Drug Development and Industrial Pharmacy*, **10**(3), 505-514.
- [100] Heckel, R.W. (1961a) Density pressure relationships in powder compaction. *Transactions of the Metallurgical Society of AIME*, **221**, 671-675.
- [101] Kuentz, M., Leuenberger, H. (1999) Pressure susceptibility of polymer tablets as a critical property: a modified Heckel equation. *Journal of Pharmaceutical Science*, **88**(2), 174-179.

- [102] Hersey, J.A., Rees, J.E. (1971) Deformation of particles during briquetting. *Nature Physical Science*, **230**, 96.
- [103] Heckel, R.W. (1961b) An analysis of powder compaction phenomena. *Transactions of the Metallurgical Society of AIME*, **221**, 1001-1008.
- [104] Armstrong, N.A., Haines-Nutt, R.F. (1974) Elastic recovery and surface area changes in compacted powder systems. *Powder Technology*, **9**, 287-290.
- [105] Newton, J.M., Rowley, G.J., Fell, T., Peacock D.G. and Ridgway, K. (1971) Computer analysis of the relation between tablet strength and compaction pressure. *Journal of Pharmacy and Pharmacology*, **23**(Suppl.), 195-201.
- [106] Leuenberger, H. (1980) Zur Theorie der Pulverkompression, Habilitationsschrift, Basel.
- [107] Dees, P.J., Polderman, J. (1981) Mercury porosimetry in pharmaceutical technology. *Powder Technology*, **29**(1), 187-197.
- [108] Van Kamp H.V., Bolhuis, G.K., de Boer, A.H., Lerk, C.F., Lie-A-Huen, L. (1986) The role of water uptake on tablet disintegration. *Pharmaceutica Acta Helveticae*, **61**(1), 22-29.
- [109] Ferrari, F., Bertoni, M., Caramella, C. and Waring, M.J. (1994) Comparative evaluation of hydrocolloid dressings by means of water uptake and swelling force measurements. *International Journal of Pharmaceutics*, **112**(1), 29-36.
- [110] Luginbühl, R. (1994) Anwendung der Perkolationstheorie zur Untersuchung des Zerfallsprozesses, der Wasseraufnahme und der Wirkstofffreisetzung von binären Tablettensystemen. Dissertation, Universität Basel.
- [111] Schmid, M. (1998) Anwendung der Perkolationstheorie und der fraktalen Geometrie zur Interpretation der mechanischen und dynamischen Eigenschaften von Einkomponententabletten. Dissertation, Universität Basel.
- [112] Colombo, P., Conte, U., Caramella, C., Geddo, M., La Manna, A. (1984) Disintegrating force as a new formulation parameter. *Journal of Pharmaceutical Sciences*, **73**(5), 701-705.
- [113] Caramella, C., Ferrari, F., Conte, U., Gazzaniga, A., La Manna, A., Colombo, P. (1989) Experimental evidence of disintegration mechanisms. *Acta Pharmaceutica Technologica*, **35**(1), 30-33.
- [114] Weibull, W. (1951) A statistical distribution function of wide applicability. *Journal of Applied Mechanics*, **18**, 293-297.
- [115] Gibaldi, M., Feldman, S. (1967) Establishment of sink conditions in dissolution rate determinations. *Journal of Pharmaceutical Sciences*, **56**(10), 1238-1242.
- [116] Koch, H. (1976) Einführung in die Biopharmazie Folge VII. *Österreichische Apotheker-Zeitung*, **30**(6), 111-119.
- [117] Carstensen, J.T., Li Wan Po, A. (1992) The state of water in drug decomposition in the moist solid state: Description and modelling. *International Journal of Pharmaceutics*, **83**(1-3), 87-94.
- [118] Baehr, M., Führer, C., Puls, P. (1991) Molecular weight distribution, hemicellulose content and batch conformity of pharmaceutical cellulose powders. *European Journal of Pharmaceutics and Biopharmaceutics*, **37**(3), 136-141.
- [119] Landin, M., Martinez-Pacheco, R., Gomez-Amoza, J.L., Souto, C., Concheiro, A., Rowe, R.C. (1993) Effect of country of origin on the properties of microcrystalline cellulose. *International Journal of Pharmaceutics*, **91**(2-3), 123-131.
- [120] Krässig, H.A. (1993) Cellulose: structure, accessibility and reactivity. Gordon and Breach Science Publishers, Yverdon.
- [121] Wada, M., Sugiyama, J., Okano, T. (1995) Two crystalline phase ($I\alpha/I\beta$) system of native celluloses in relation to plant phylogenesis. *Mokuzai Gakkaishi*, **41**(2), 186-192.

- [122] Wada, M., Okano, T., Sugiyama, J. (2001) Allomorphs of native crystalline celluloses evaluated by two equatorial d-spacings. *Journal of Wood Science*, **47**(1), 124-128.
- [123] Hult, E.-L., Iversen, T., Sugiyama, J. (2003) Characterization of the supermolecular structure of cellulose in wood pulp fibres. *Cellulose*, **10**(2), 103-110.
- [124] Fink, H.-P., Fanter, D., Philipp, B. (1985) Röntgen-Weitwinkeluntersuchungen zur übermolekularen Struktur beim Cellulose-I-II-Phasenübergang. *Acta Polymerica*, **36**(1), 1-8.
- [125] Jayme, G., Knolle, H. (1964) Empirical x-ray determination of the degree of crystallinity of cellulosic materials. *Papier (Paris)*, **18**(6), 249-255.
- [126] Ruland, W. (1961) X-ray determination of crystallinity and diffuse disorder scattering. *Acta crystallographica*, **14**, 1180-1185.
- [127] Vonk, C.G. (1973) Computerization of Ruland's X-ray method for determination of the crystallinity in polymers. *Journal of Applied Crystallography*, **6**(Pt. 2), 148-152.
- [128] Chung, F.H., Scott, R.W. (1973) A new approach to the determination of crystallinity of polymers by X-ray diffraction. *Journal of Applied Crystallography*, **6**(Pt. 3), 225-230.
- [129] Nelson, M.L., O'Connor, R.T. (1964a) Relation of certain infrared bands to cellulose crystallinity and crystal lattice type. Part I. Spectra of lattice types I, II, III and of amorphous cellulose. *Journal of applied polymer science*, **8**(3), 1311-1324.
- [130] Tasker, S., Badyal, J. P. S., Backson, S.C.E., Richards, R.W. (1994) Hydroxyl accessibility in celluloses. *Polymer*, **35**(22), 4717-4721.
- [131] Wells, J.I. (1988) Pharmaceutical preformulation: the physicochemical properties of drug substances. Wiley, New York.
- [132] Callahan, J.C., Cleary, G.W., Elefant, M., Kaplan, G., Kensler, T., Nash, R.A. (1982) Equilibrium moisture content of pharmaceutical excipients. *Drug Development and Industrial Pharmacy*, **8**(3), 355-369.
- [133] Mhraryan, A., Llagostera, A.P., Karmhag, R., Stromme, M., Ek, R. (2004) Moisture sorption by cellulose powders of varying crystallinity. *International Journal of Pharmaceutics*, **269**(2), 433-442.
- [134] Parfitt, G.D., Sing, K.S.W. (1976) Characterization of Powder Surfaces. Academic Press, London.
- [135] Timmermann, E.O. (2003) Multilayer sorption parameters: BET or GAB values? *Colloids and Surfaces A: Physicochemical and Engineering Aspects*, **220**(1-3), 235-260.
- [136] Maroulis, Z.B., Tsami, E., Marinos-Kouris, D., Saravacos, G.D. (1988) Application of the GAB model to the moisture sorption isotherms for dried fruits. *Journal of Food Engineering*, **7**(1), 63-78.
- [137] Iglesias, H.A., Chirife, J. (1995) An alternative to the Guggenheim, Anderson and De Boer model for the mathematical description of moisture sorption isotherm of foods. *Food Research International*, **28**(3), 317-321.
- [138] Van den Berg, C. (1985) Development of B.E.T.-like models for sorption of water on foods, theory and relevance. In: Properties of Water in Foods in Relation to Quality Stability, Simatos, D., Multon, J.L. (Eds), Nijhoff, Dordrecht.
- [139] Sing, K.S.W., Everett, D.H., Haul, R.A.W., Moscou, L., Pierotti, R.A., Rouquerol, J., Siemieniowska, T. (1985) Reporting physisorption data for gas/solid systems with special reference to the determination of surface area and porosity (Recommendations 1984). *Pure and Applied Chemistry*, **57**(4), 603-619.
- [140] Khan, F., Pilpel, N. (1986) The effect of particle size and moisture on the tensile strength of microcrystalline cellulose powder. *Powder Technology*, **48**(2), 145-150.
- [141] Zografi, G., Kontny, M.J. (1986) The interactions of water with cellulose- and starch-derived pharmaceutical excipients. *Pharmaceutical Research*, **3**(4), 187-194.

- [142] Zografi, G., Kontny, M.J., Yang, A.Y.S., Brenner, G.S. (1984) Surface area and water vapor sorption of microcrystalline cellulose. *International Journal of Pharmaceutics*, **18**(1-2), 99-116.
- [143] Marshall, K., Sixsmith, D. (1974-1975) Some physical characteristics of microcrystalline cellulose 1. Powders for pharmaceutical use. *Drug Development Communications*, **1**(1), 51-71.
- [144] Ardizzone, S., Dioguardi, F.S., Mussini, T., Mussini, P.R., Rondinini, S., Vercelli, B., Vertova, A. (1999) Microcrystalline cellulose powders: structure, surface features and water sorption capability. *Cellulose*, **6**(1), 57-69.
- [145] Krycer, I., Pope, D.G., Hersey, J.A. (1982) An evaluation of the techniques employed to investigate powder compaction behaviour. *International Journal of Pharmaceutics*, **12**(2-3), 113-134.
- [146] Picker, K.M. (2001) Time dependence of elastic recovery for characterization of tableting materials. *Pharmaceutical Development and Technology*, **6**(1), 61-70.
- [147] Celik, M. (1992) Overview of compaction data analysis techniques. *Drug Development and Industrial Pharmacy*, **18**(6-7), 767-810.
- [148] Doelker, E. (1994) Assessment of powder compaction. In: Powder Technology and Pharmaceutical Processes, Chulia, D., Deleuil, M., Pourcelot, Y. (Eds), Elsevier, Amsterdam.
- [149] Sun, C., Grant, D.J.W. (2001) Influence of elastic deformation of particles on Heckel analysis. *Pharmaceutical Development and Technology*, **6**(2), 193-200.
- [150] Celik, M., Marshall, K. (1989) Use of a compaction simulator system in tableting research. *Drug Development and Industrial Pharmacy*, **15**(5), 759-800.
- [151] Geoffroy, J.M., Carstensen, J.T. (1991) Effects of measurement methods on the properties of materials. *Powder Technology*, **68**, 91-96.
- [152] Khan, F., Pilpel, N., Ingham, S. (1988) The effect of moisture on the density, compaction and tensile strength of microcrystalline cellulose. *Powder Technology*, **54**(3), 161-164.
- [153] Suzuki, T., Nakagami, H. (1999) Effect of crystallinity of microcrystalline cellulose on the compactibility and dissolution of tablets. *European Journal of Pharmaceutics and Biopharmaceutics*, **47**(3), 225-230.
- [154] Fell, J.T., Newton, J.M. (1971) Effect of particle size and speed of compaction on density changes in tablets of crystalline and spray-dried lactose. *Journal of Pharmaceutical Sciences*, **60**(12), 1866-1869.
- [155] Leu, R.U. (1993) Anwendung der Theorie der Perkolation auf die Pulverkompensation: Ein neues Modell zur Beschreibung der Härte, der Bruchfestigkeit und der Elastizität von Tabletten. Dissertation, Universität Basel.
- [156] Nyström, C., Karehill, P.-G. (1996) The importance of intermolecular bonding forces and the concept of bonding surface area. In: Pharmaceutical Powder Compaction Technology, Alderborn, G., Nyström, C. (Eds), Marcel Dekker, New York.
- [157] Duberg, M., Nyström, C. (1986) Studies on direct compression of tablets XVII. Porosity-pressure curves for the characterization of volume reduction mechanisms in powder compression. *Powder Technology*, **46**(1), 67-75.
- [158] Alderborn, G., Duberg, M., Nyström, C. (1985) Studies on direct compression of tablets X. Measurement of tablet surface area by permeametry. *Powder Technology*, **41**(1), 49-56.
- [159] Erdős, S., Bezegh, A. (1977) Studies on the mechanism of disintegration. *Die Pharmazeutische Industrie*, **39**(11), 1130-1135.
- [160] Ferrari, F., Rossi, S., Bertoni, M., Caramella, C., Geddo, M. (1991) Modelling of water penetration into fast disintegrating tablets. *S.T.P. Pharma Sciences*, **1**(2), 137-144.
- [161] Guyot-Hermann, A.M. (1992) Tablet disintegration and disintegrating agents. *S.T.P. Pharma Sciences*, **2**(6), 445-462.

- [162] Lerk, C.F., Bolhuis, G.K., de Boer, A.H. (1979) Effect of microcrystalline cellulose on liquid penetration in and disintegration of directly compressed tablets. *Journal of Pharmaceutical Sciences*, **68**(2), 205-211.
- [163] Westermarck, S., Juppo, A.M., Kervinen, L., Yliruusi, J. (1999) Microcrystalline cellulose and its microstructure in pharmaceutical processing. *European Journal of Pharmaceutics and Biopharmaceutics*, **48**(3), 199-206.
- [164] O'Brien, S.B.G.M. (1993) Some surface tension and contact angle problems in industry. In: Contact angle, wettability and adhesion: Festschrift in honor of Professor Robert J. Good, Mittal, K.L. (Ed.), VSP, Utrecht.
- [165] Parsons, G.E., Buckton, G., Chatham, S.M. (1993) Comparison of measured wetting behaviour of materials with identical surface energies, presented as particles and plates. *Journal of Adhesion Science and Technology*, **7**(2), 95-104.
- [166] Chibowski, E., Holysz, L. (1997) On the use of Washburn's equation for contact angle determination. *Journal of Adhesion Science and Technology*, **11**(10), 1289-1301.
- [167] Buckton, G. (1995) Interfacial phenomena in drug delivery and targeting. Harwood Academic Publishers, Chur.
- [168] Buckton, G., Newton, J.M. (1986) Assessment of the wettability of powders by use of compressed powder discs. *Powder Technology*, **46**(2-3), 201-208.
- [169] Marmur, A. (1993) Contact angle equilibrium: the intrinsic contact angle. In: Contact angle, wettability and adhesion: Festschrift in honor of Professor Robert J. Good, Mittal, K.L. (Ed.), VSP, Utrecht.
- [170] Parsons, G.E., Buckton, G., Chatham, S.M. (1992) The extent of the errors associated with contact angles obtained using liquid penetration experiments. *International Journal of Pharmaceutics*, **82**(1-2), 145-150.
- [171] Letelier, M.F., Leutheusser, H.J., Rosas, Z. (1979) Refined mathematical analysis of the capillary penetration problem. *Journal of Colloid and Interface Science*, **72**(3), 465-470.
- [172] Kiesvaara, J., Yliruusi, J. (1991) The effect of compression pressure and compression time on the surface free energy of tablets. *Acta Pharmaceutica Nordica*, **3**(3), 171-177.
- [173] Papirer, E., Brendle, E., Balard, H., Vergelati, C. (2000) Inverse gas chromatography investigation of the surface properties of cellulose. *Journal of Adhesion Science and Technology*, **14**(3), 321-337.
- [174] Planinsek, O., Pisek, R., Trojak, A., Srcic, S. (2000) The utilization of surface free-energy parameters for the selection of a suitable binder in fluidized bed granulation. *International Journal of Pharmaceutics*, **207**(1-2), 77-88.
- [175] Grimsey, I.M., Sunkersett, M., Osborn, J.C., York, P., Rowe, R.C. (1999) Interpretation of the differences in the surface energetics of two optical forms of mannitol by inverse gas chromatography and molecular modelling. *International Journal of Pharmaceutics*, **191**(1), 43-50.
- [176] Czeremuskin, G., Mukhopadhyay, P., Sapiha, S. (1997) Elution behavior of chemically different probes on the evaluation of surface properties of cellulose by inverse gas chromatography. *Journal of Colloid and Interface Science*, **194**(1), 127-137.
- [177] Ticehurst, M.D., Rowe, R.C., York, P. (1994) Determination of the surface properties of two batches of salbutamol sulphate by inverse gas chromatography. *International Journal of Pharmaceutics*, **111**(3), 241-249.
- [178] Belgacem, M.N., Blayo, A., Gandini, A. (1996) Surface characterization of polysaccharides, lignins, printing ink pigments, and ink fillers by inverse gas chromatography. *Journal of Colloid and Interface Science*, **182**(2), 431-436.
- [179] Ticehurst, M.D., York, P., Rowe, R.C., Dwivedi, S.K. (1996) Characterization of the surface properties of α -lactose monohydrate with inverse gas chromatography, used to detect batch variation. *International Journal of Pharmaceutics*, **141**(1,2), 93-99.

- [180] Amidon, G.L., Lennernäs, H., Shah, V.P., Crison, J.R. (1995) A theoretical basis for a biopharmaceutical drug classification: the correlation of *in vitro* drug product dissolution and *in vivo* bioavailability. *Pharmaceutical Research*, **12**(3), 413-420.
- [181] Clissold, S.P., Beresford, B. (1987) Proquazone. A review of its pharmacodynamic and pharmacokinetic properties, and therapeutic efficacy in rheumatic diseases and pain states. *Drugs*, **33**(5), 478-502.
- [182] Yu, L.X., Carlin, A.S., Amidon, G.L., Hussain, A.S. (2004) Feasibility studies of utilizing disk intrinsic dissolution rate to classify drugs. *International Journal of Pharmaceutics*, **270**(1-2), 221-227.
- [183] Hugentobler, A. (1993) Untersuchung zur Bindemittelauswahl bei verschiedenen Wirkstoffkompositionen. Dissertation, Universität Basel.
- [184] Von Orelli, J., Leuenberger, H. (2004) Search for technological reasons to develop a capsule or a tablet formulation with respect to wettability and dissolution. *International Journal of Pharmaceutics*, **287**(1-2), 135-145.
- [185] Nelson, K.G., Wang, L.Y. (1977) Determination of time course of tablet disintegration I: numerical method. *Journal of Pharmaceutical Sciences*, **66**(12), 1758-1761.
- [186] Nelson, K.G., Wang, L.Y. (1978) Determination of time course of tablet disintegration II: method using continuous functions. *Journal of Pharmaceutical Sciences*, **67**(1), 86-89.
- [187] El-Yazigi, A. (1981) Disintegration-dissolution analysis of percent dissolved-time data. *Journal of Pharmaceutical Sciences*, **70**(5), 535-537.
- [188] Leeson, L.J., Mattocks, A.M. (1958) Decomposition of aspirin in the solid state. *Journal of the American Pharmaceutical Association*, **47**(5), 329-333.
- [189] Hasegawa, J., Hanano, M., Awazu, S. (1975) Decomposition of acetylsalicylic acid and its derivatives in solid state. *Chemical and Pharmaceutical Bulletin*, **23**(1), 86-97.
- [190] Ahlneck, C., Lundgren, P. (1985) Methods for the evaluation of solid state stability and compatibility between drug and excipient. *Acta Pharmaceutica Suecica*, **22**(6), 305-314.
- [191] Edwards, L.J. (1950) The hydrolysis of aspirin. *Transactions of the Faraday Society*, **46**, 723-735.
- [192] Scheef, C.-A., Oelkrug, D., Schmidt, P.C. (1998) Surface acidity of solid pharmaceutical excipients III. Excipients for solid dosage forms. *European Journal of Pharmaceutics and Biopharmaceutics*, **46**(2), 209-213.
- [193] Glombitza, B.W., Oelkrug, D., Schmidt, P.C. (1994) Surface acidity of solid pharmaceutical excipients I. Determination of the surface acidity. *European Journal of Pharmaceutics and Biopharmaceutics*, **40**(5), 289-293.
- [194] Carstensen, J.T., Osadca, M., Rubin, S.H. (1969) Degradation mechanism for water-soluble drugs in solid dosage forms. *Journal of Pharmaceutical Sciences*, **58**(5) 549-553.
- [195] Lee, L., Dekay, H.G., Banker, G.S. (1965) Effect of water vapor pressure on moisture sorption and the stability of aspirin and ascorbic acid in tablet matrices. *Journal of Pharmaceutical sciences*, **54**(8), 1153-1158.
- [196] Manudhane, K.S., Contractor, A.M. Kim, H.Y., Shangraw, R.F. (1969) Tableting properties of a directly compressible starch. *Journal of Pharmaceutical Sciences*, **58**(5), 616-620.
- [197] Du, J., Hoag, S.W. (2001) The influence of excipients on the stability of the moisture sensitive drugs aspirin and niacinamide: comparison of tablets containing lactose monohydrate with tablets containing anhydrous lactose. *Pharmaceutical Development and Technology*, **6**(2), 159-166.
- [198] Ahlneck, C., Alderborn, G. (1988) Solid state stability of acetylsalicylic acid in binary mixtures with microcrystalline and microfine cellulose. *Acta Pharmaceutica Suecica*, **25**(1), 41-52

-
- [199] Mhraryan, A. (2005) Engineering of native cellulose structure for pharmaceutical applications. Thesis, University at Uppsala.
- [200] Landin, M., Pérez-Marcos, B., Casalderrey, M., Martinez-Pacheco, R., Gomez-Amoza, J.L., Souto, C., Concheiro, A., Rowe, R.C. (1994) Chemical stability of acetylsalicylic acid in tablets prepared with different commercial brands of dicalcium phosphate dihydrate. *International Journal of Pharmaceutics*, **107**(3), 247-249.
- [201] Gore, A.Y., Naik, K.B., Kildsig, D.O., Peck, G.E., Smolen, V.F., Banker, G.S. (1968) Significance of salicylic acid sublimation in stability testing of aspirin-containing solids. *Journal of Pharmaceutical Sciences*, **57**(11), 1850-1854.
- [202] Van Krevelen, D.W. (1990) Properties of Polymers. Elsevier, Amsterdam.
- [203] Guyot-Hermann, A.M., Ringard, J. (1981) Disintegration mechanism of tablets containing starches. Hypothesis about the particle-particle repulsive force. *Drug Development and Industrial Pharmacy*, **7**(2), 155-177.
- [204] Kleinebudde, P., Jumaa, M., Saleh, F.E. (2000) Influence of degree of polymerization on behavior of cellulose during homogenization and extrusion/spheronization. *The AAPS Journal*, **2**(3), article 21, 1-10.
- [205] Hiestand, H.E.N., Smith, D.P. (1984) Indices of tableting performance. *Powder Technology*, **38**, 145-159.

B. From art to science

**Physicochemical concepts and percolation theory
applied in powder technology**

1 Summary

In the last recent years, FDA's Process Analytical Technology (PAT) initiative has pushed forward the idea of improving the quality of the pharmaceutical products (six sigma goal) by a deeper understanding of the processes involved during manufacturing. Using the concept of analogies and the percolation theory this study illustrates by the means of three case studies how the steep path could look like, which leads to a more scientific based understanding of powder technology.

The search for the best mathematical model to describe the compression behavior of disordered particulate systems has a very long history. A new approach derived within this study is based on the observation, that gaseous as well as particulate systems are compressible. Thus, the well known Van der Waals equation, developed in physical chemistry for the description of the state of real gases, was adapted and applied for the compression of powder systems. A considerable number of substances with different physicochemical properties were compressed using the universal testing instrument Zwick® 1478. The acquired "in die" data were fitted according to the new adapted Van der Waals and to the classical Heckel equation for comparative reasons. The goodness of fit of the new equation tended to be better compared to the Heckel equation. Furthermore, the adapted Van der Waals equation turned out to be appropriate for brittle and ductile materials over the whole compression pressure range. However, just one parameter could unambiguously be assigned to a physical property of the used substances. Namely, parameter B_v represents the true volume. Even though an exact physical meaning could not be found for parameter A_v and C_v , they seem to correlate with the mean yield pressure of the substances. Thus, these two parameters could be used to distinguish between brittle and plastic materials.

The flowability of a powder plays a decisive role in many processes during manufacturing of solid dosage forms (e.g. blending, tableting etc.). The cumulative flow rate (discharged mass versus time) of particulate materials out of a hopper is a linear function. In the contrary to fluids, the flow of a powder is completely unaffected by the height of filling. Thus, the flow of powders cannot be described analogous to the flow of liquids. As the movement of particles in a powder shows some similarities compared to the movement of molecules in a diffusion process, Fick's first law is considered as the basis of the new approach within this study. The concentration in Fick's first law was replaced by the bulk density. An "active orifice area" was introduced, which accounts for the fact that the particles prevent themselves from flowing below a critical orifice area. In order to verify this approach, the discharged mass of spherical shaped particulate materials (MCC pellets, sugar pellets, glass ballotini) of various sizes was measured during its flow out of a hopper (half center angle of 17°). Introducing "sink

conditions”, the new equation proved to be successful in describing the linear flow behavior of particulate material. If the material specific relationship between the involved parameters and the particle size are known, it is possible to predict the flow behavior according to the new equation. It seems to be very promising to extend the developed concept on other processes like blending.

The third part of the study deals with the dilution capacity, which equals the maximum possible mass fraction of a non-compactable substance B, which can be incorporated into a well compactable substance A to produce tablets of adequate strength. This critical fraction is achieved if percolation of substance A is only attained at zero porosity. Thus, the new equation for the calculation of the dilution capacity is based on the percolation threshold of substance A concerning the radial tensile strength.

Two binary mixtures consisting of substance A/substance B (Avicel PH101[®]/acetaminophen and Ethocel[®]/acetaminophen) were chosen at different ratios to verify experimentally the new equation. The values for the dilution capacities of the two excipients (Avicel PH101[®]: 70.0%; Ethocel[®]: 63.7%) according to the new equation turned out to be in good agreement ($\pm 5\%$) with the results according to method of Minchom *et al.*, which has the drawback to be very time consuming. Because no substance can be considered as completely non-compactable, it is possible to produce tablets with a measurable strength above the calculated dilution capacity. Since the new equation assumes that only the well compactable substance A contributes to the strength of a tablet, the resulting value for the dilution capacity is very rigorous but may be considered as a true property of the excipient and independent of the system. As a rough approximation, the dilution capacity can also be estimated by the difference $1 - \rho_{rtapped}$ ($\rho_{rtapped}$: relative tapped density).

As a conclusion, the “translation” of existing laws in physical chemistry into the field of pharmaceutical technology is a very promising concept with a lot of potential although the considered equations need some modifications and cannot be performed one-to-one. The already well-established concept of percolation theory proved to be very successful to calculate the dilution capacity and provides therefore an excellent tool for the formulation of poorly compactable substances.

2 Introduction

Pharmaceutical powder technology is still mainly considered more as an art than a science. Not least because of the Process Analytical Technology (PAT) initiative of the FDA (Food and Drug Administration), the transformation from an art to a science will be accelerated in the next few years.

The main problem, which thereby has to be overcome, consists not only in the fact that a formulation is a very complex system, which is influenced by many parameters, but also in the large number of poorly understood processes involved in manufacturing. Thus, the still traditional „trial and error“ experiments in the development of a new formulation often result in a non-robust product. “Right first time” is therefore the ultimate goal, which is also in the interest of the pharmaceutical industry, as it can save a lot of money.

Ranging from the use of Artificial Neuronal Networks (ANN), percolation theory and laws of physical pharmacy, many concepts are at our disposal to push forward the vision of a more science based pharmaceutical powder technology. Within this context the attention will be focused on the percolation theory and the concept of analogies, which proved to be very successful in other scientific fields (e.g. the Bateman equation, which nowadays is of utmost importance in pharmacokinetics, was originally developed to describe the radioactive decay of daughter nuclei [1]). If it is possible to relate a system back to another system, which is already well known, then the new system can be figured out much more easily.

2.1 Aims of the study

The introduction of the direct-compression process and high-speed rotary tablet presses has totally changed the tablet manufacturing. Both developments have increased the demands on the functionality of excipients considering flow and compression properties. Therefore, the aim of the study is to get a deeper insight into these processes by drawing parallels to existing concepts in physical chemistry.

Dilution capacity is a property of utmost importance for excipients used in direct compression. Thus, in this study an equation should be derived, which is able to predict or at least estimate the maximum proportion of a poorly compactable substance, which can be incorporated into the excipient.

3 Theory

3.1 Powder – the 4th state of matter

For a long time we are used to divide the matter in our environment into the three traditional states of matter: solids, liquids and gases. However, the classification of powders or granules to one of the three states is not that easy or even impossible. Thus, the question is certainly allowed whether the powders can be considered as 4th state of matter [2]. Comparing powders with the three states of matters, similarities can be found for all of them: i) solid: powders can be deformed reversibly or irreversibly. ii) liquid: powders are able to flow. iii) gas: powders are to some extent compressible. The problem of classification can also be illustrated by considering the situation depicted in figure 1, where air or a gas is blowing through a powder bed in an upward direction. With increasing gas rate the solid powder bed starts to get fluidized (B). This state is characterized by properties, which are very comparable to those of liquids. At even higher gas rates the powder will continue to expand and will finally become gas-like (D).

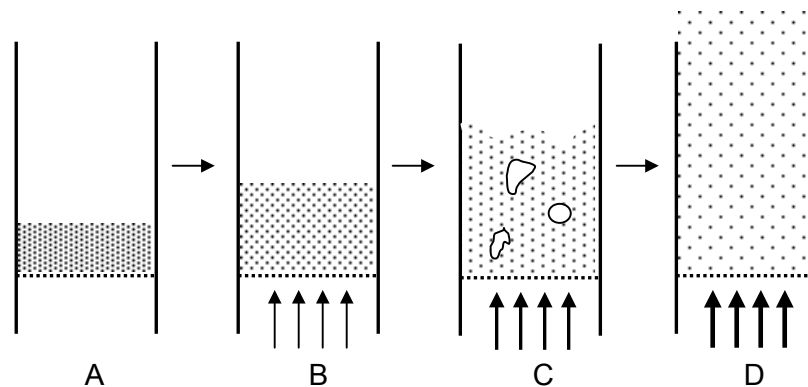


Figure 1: Behavior of a solid bed with increasing gas rate. A: solid bed; B: fluid bed; C: bubbles announce the “phase transition” fluid-gaseous; D: “gaseous” bed.

It is quite tempting to compare a powder particle with a molecule in a liquid or gas. However, the analogy is limited. Due to the higher masses for powder particles compared to molecules the thermal energy kT (k : Boltzmann’s constant; T : absolute temperature) is totally unimportant and the number of involved particles is usually much lower. The mean square velocity of molecules is directly proportional to the temperature. The average distance between two molecules and the overall volume of the system (consisting of molecules) are therefore closely related to the temperature. Furthermore, temperature and pressure define the phase transition. However in the case of a powder particle, the potential energy mgd (energy when a particle of mass m is raised by its own diameter d . g : 9.81 m/s^2 ; d : $500 \text{ }\mu\text{m}$;

density ρ : 2000 kg/m³) is $1.6 \cdot 10^{11}$ times kT (T : 298 K). Thus, a random movement (analogous to the classic Brownian motion in liquids) of powder particles can be excluded unless perturbed by external disturbances. From this point of view the airflow, which is blowing through the powder bed in figure 1 can be considered to imitate the effect of the temperature. Thus, granular systems, which are externally driven (e.g. fluidized by vibration) can be characterized by an effective “granular temperature” [3, 4].

It is certainly interesting to find out how far the properties of a powder system can be explained by concepts of physical chemistry, which were developed on a molecular level.

3.2 Compression

The compression of powder is a popular practice, which is used for manufacturing metal products, ceramic products and last but not least tablets. Concerning the compression of particulate material, two terms have to be distinguished. i) The compressibility is the ability of the material to undergo a reduction in volume. ii) The compactibility is defined as the ability of the material to produce tablets with sufficient strength under the effect of densification [5, 6]. In the context of this study, the attention is directed to the compressibility. The compression can be described qualitatively by dividing the process into four stages according to Train [7].

stage I: Overcoming the friction forces, the apparent volume of the particulate material is reduced by interparticulate slippage. The result of stage I is a very dense packing.

stage II: This stage is characterized by the formation of columns, vaults, bridges within the material. These structures can already withstand the imposed load up to a certain degree.

stage III: Increasing the pressure, the particles start to deform. After a reversible elastic deformation, the material is deformed irreversibly either by brittle fracture, plastic flow or both. Due to the increase in bonding surface area, the transition of the system “solid in gaseous” to the system “gaseous in solid” takes place.

stage IV: In the last stage a very strong structure is formed. The behavior of this compact under pressure is determined by the properties of the solid material.

However, it has to be noticed, that the mentioned transitions from one stage to the other are fluent. Furthermore, it is also conceivable that particles in various zones within the compact can be in different stages of compression at the same time.

There is an enormous number of parameters, which can affect powder compression. Particle size [8, 9, 10], compaction speed [9, 11], relative humidity [12], dimension of the tablet, particle shape [13], roughness of the particle surface and even the molecular structure can influence the compression and the properties of the resulting compacts.

Considerable research effort has been directed towards the development of mathematical models to describe the powder compression process. Celik gives a comprehensive overview of the proposed compression equations [14]. Each compression equation relates the state of compression (rel. density, porosity, volume, etc.) to the applied pressure. The most used models are the Heckel equation (see equation (1)) [15, 16], its modification (see equation (2)) [17], the equation according to Kawakita (see equation (3)) [18] and the equation derived by Cooper and Eaton [19]. Despite a considerable number of equations none of them proved to be satisfactory to describe universally the powder compression. The problem to find an adequate description originates from the numerous involved parameters mentioned above and the fact that the mechanical behavior of particulate bodies can not be explained by laws valid for continuum solid bodies. From this point of view it is certainly worth looking for parallels to other “particulate” and compressible systems. Gases, as described in the introduction, do not only comply with these properties, but they do also have the great advantage that many established equations are available for characterizing their state. The ideal gas law, based on the laws of Boyle-Mariotte and Gay-Lussac, is in turn the basis of further, more elaborate equations like the Van der Waals equation of state [20], Berthelots equation [21] or Dieterici equation [22]. It is certainly no coincidence that several equations empirically found for the compression of powders exhibit some similarities to one of these equations [18, 23].

$$\text{Heckel:} \quad \ln\left(\frac{1}{1-\rho_r}\right) = K \cdot \sigma + A \quad \text{equation (1)}$$

$$\text{modified Heckel:} \quad \sigma = \frac{1}{C} \left[\rho_{rc} - \rho_r - (1-\rho_{rc}) \ln\left(\frac{1-\rho_r}{1-\rho_{rc}}\right) \right] \quad \text{equation (2)}$$

$$\text{Kawakita:} \quad C_k = \frac{V_0 - V}{V_0} = \frac{ab\sigma}{1+b\sigma} \quad \text{with} \quad a = \frac{V_0 - V_\infty}{V_0} \quad \text{equation (3)}$$

where: ρ_r : relative density ($\rho_r = 1 - \varepsilon$ with ε : porosity) of the tablet

σ : compression pressure [MPa]

K, C, b : constants [MPa⁻¹]

A, a : constants

ρ_{rc} : relative critical density

V_0 : initial apparent volume [cm³]

V_∞ : apparent volume after infinite pressure [cm³]

V : apparent volume under applied pressure [cm³]

C_k : degree of volume reduction

The new compression equation is derived from the Van der Waals equation (see equation (4)), which is one of the most used equations to predict the behavior of real gases. Van der Waal modified the ideal gas law in two important ways. Firstly, he introduced a term to

account for the attractive forces between gas molecules (an^2/V^2) and secondly he inserted a term to account for the volume of the gas molecules (nb). According to the Van der Waals equation, the pressure can also be written as the sum of a repulsive and attractive term (see equation (5)).

$$\left(p + \frac{an^2}{V^2}\right)(V - nb) = nRT \quad \text{equation (4)}$$

$$p = \frac{nRT}{V - nb} - \frac{an^2}{V^2} = p_{rep} + p_{attr} \quad \text{equation (5)}$$

where: p : pressure [Pa]

V : volume [m^3]

n : number of moles [mol]

b : material constant, measure for the molecular volume; accounts for incompressibility [m^3/mol]

a : material constant, accounts for attraction [$m^6 \cdot Pa/mol^2$]

R : universal gas constant: 8.3145 J/(mol·K)

T : absolute temperature [K]

p_{rep} : repulsive term [Pa]

p_{attr} : attractive term [Pa]

Concerning the compression of powders, Van der Waals equation of state was adapted as follows:

Since the thermal energy is supposed to play a minor role, the term nRT is substituted by the constant C_v . The terms nb and an^2 are also replaced by the parameter B_v and A_v , respectively.

Furthermore volume V in equation (5) corresponds to the apparent volume V_a , which can be expressed as the ratio of the true volume V_t (of the substance) to the relative density ρ_r . The resulting equation (6) represents the Van der Waals equation adapted for powder compression.

$$\sigma = \frac{C_v}{\underbrace{V_a - B_v}_{p_{rep}}} - \frac{A_v}{\underbrace{V_a^2}_{p_{attr}}} = \frac{C_v}{V_t \left(\frac{1}{\rho_r} - \frac{B_v}{V_t} \right)} - \frac{A_v}{V_t^2} \cdot \rho_r^2 \quad \text{equation (6)}$$

where: σ : compression pressure [MPa]

V_a : apparent volume of the compact ($V_a = V_t/\rho_r$) [cm^3]

ρ_r : relative density

V_t : true volume of the substance [cm^3]

($V_t = m/\rho_t$ with m : weight of the substance; ρ_t : true density)

C_v, A_v, B_v : "Van der Waals" coefficients. $C_v = nRT$ [$cm^3 \cdot MPa$]; $A_v = an^2$ [$cm^6 \cdot MPa$]; $B_v = nb$ [cm^3]

term p_{rep} and p_{attr} : repulsive and attractive part of the Van der Waals equation

3.3 Flow

The flowability of a powder is defined as the ability of the powder to flow in a desired manner in a specific piece of equipment [24]. The flow of a powder plays a very important role in powder technology. It is involved in several processes like blending, powder transfer, tableting, encapsulation etc. On the one hand the flow behavior of a powder can decisively affect the quality of the product (e.g. content uniformity). On the other hand it can be a limiting factor in terms of the production rate (e.g. compression speed).

Powder flow is influenced by a big variety of factors including particle size, particle shape, particle density, moisture content, consolidation pressure and even time of storage. Information about the powder flow can be obtained by different methods: angle of repose [25], shear cell measurement [26], bulk density measurements (Hausner ratio, Carr's index) [27, 28, 29], determination of the critical orifice diameter and the determination of the flow rate of the powder discharged out of a hopper. The last method is used within this study. It has the advantage that it is a dynamic and direct measurement, which provides the possibility to quantify the uniformity of flow when the discharged mass is registered in dependency of time.

Until now, no universal mathematical model is existing, which could predict the powder flow behavior in every situation. Despite the common ability to flow, there are some arguments against the identical mathematical description for the flow of liquids and particulate materials. As described above, the lack of random movement results in the tendency of powders to form static configuration known as arching. Additionally, due to the friction of the particles along the wall of the container, the pressure at the bottom of the container is independent of the height of filling. Thus, the tempting analogy to the flow of liquids was abandoned and displaced by another concept, which proved very successful in physical chemistry on a molecular level. During the flow of a powder out of a hopper the particles move from a region with a high to one with a low package density. We could therefore assume a similarity to the diffusion process, which can be described by Fick's first law (equation (7)). In the field of blending we can observe a similar process, where mixing is achieved by changing positions between particles. The blenders that take advantage of this principle are therefore also called diffusion blenders (e.g. Turbula[®]).

$$\frac{dm}{dt} = \frac{D \cdot A \cdot dc}{dh} \approx \frac{D \cdot A \cdot (c_1 - c_2)}{\Delta h} \quad \text{equation (7)}$$

where: dm/dt : transported mass per time

A : area

D : diffusion coefficient

$(c_1 - c_2)/\Delta h$: gradient of the concentration

In order to derive the new equation based on Fick's first law, we refer to an experiment, which consists of the measurement of the discharge of particulate material out of a conical shaped hopper characterized by an orifice area A and a specific half center angle α (angle measured from vertical) (see figure 2).

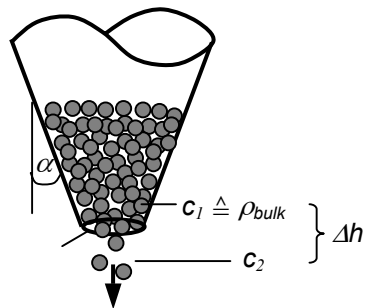


Figure 2: Flow of particles out of a hopper (A : area of the orifice; α : half center angle; c_1 : concentration in the hopper; c_2 : concentration out of the hopper)

Considering some modifications, Fick's first law (equation (7)) can be applied to the flow of particulate material:

- i) The bulk density ρ_{bulk} in the hopper experiment is assumed to be the analogous term to the concentration c_1 in Fick's first law. Additionally, we suppose that the density out of the hopper is negligible in comparison to the bulk density ρ_{bulk} ("sink conditions").
- ii) Because Δh is hard to determine D and Δh are summarized to a new constant Π^* (mass permeability coefficient) analogous to the permeability coefficient P in physical chemistry. Π^* has the dimension of volume flux or of linear velocity.
- iii) For each powder material, a critical area A_{crit} of the outlet orifice can be defined. The flow of the particulate material is impossible for orifice areas smaller than A_{crit} . Thus, the orifice area A has to be replaced by the "active area", which equals the orifice area A corrected by the critical area A_{crit} .

Taking into account these assumptions, we can suppose equation (8) for the flow of a particulate material out of a hopper.

$$\frac{dm}{dt} = \Pi^* \cdot \rho_{bulk} \cdot (A - A_{crit}) \quad \text{equation (8)}$$

where: dm/dt : discharged mass per time, flow rate [g/s]
 Π^* : ($= D/\Delta h$) mass permeability coefficient [cm/s]
 ρ_{bulk} : bulk density of the particulate material [g/cm³]
 A : area of the orifice [cm²]
 A_{crit} : critical area of the orifice [cm²]

The flow of liquids is governed mainly by the hydrostatic pressure and the internal friction (viscosity). In this study two equations were derived (see appendix F) to describe the flow profile of liquids. Equation (9) just takes into account the hydrostatic pressure, whereas equation (10) takes both influencing factors into consideration. However, the differential equation (10) can only be solved numerically.

$$\text{model I: } m_d = m_0 - \left[m_0^{5/6} - \frac{5}{6} A_2 \rho^{5/6} \sqrt{2g} \cdot \left(\frac{3}{\tan^2 \alpha \cdot \pi} \right)^{1/6} \cdot t \right]^{6/5} \quad \text{equation (9)}$$

$$\text{model II: } \left(-\frac{dm}{dt \cdot \rho} \right)^2 \cdot \left(\frac{1}{A_2^2} - \frac{1}{A^2} \right) + \left(-\frac{dm}{dt \cdot \rho} \right) \cdot \frac{2R}{\rho} - 2gh = 0 \quad \text{equation (10)}$$

where: m_d : discharged mass of liquid [kg]
 m : mass of liquid in the hopper [kg]
 m_0 : mass of liquid at time $t = 0$ [kg]
 A_2 : area of the orifice [m²]
 ρ : density of the liquid [kg/m³]
 g : gravity acceleration: 9.81 m/s²
 α : half center angle
 t : time [s]
 A : area of the liquid level at time t [m²]
 h : height of the liquid level at time t [m]
 R : resistance (see appendix F) [Pa·s/m³]

3.4 Percolation theory

Percolation theory is used to describe the behavior of disordered systems. Flory (1941) [30] and Stockmayer (1943) [31] were the first who introduced this concept to characterize gelation. However, the terminology of the percolation process is based on the work of Broadbent and Hammersley (1957) [32].

In order to apply the percolation theory to a disordered system, two conditions have to be fulfilled. Firstly, it must be possible to subdivide the disordered system into subunits, which are arranged in a geometrical order. Secondly, each subunit must be assigned to a property A or B with a probability p_A or p_B ($p_B = 1 - p_A$), respectively. Since these conditions are not very restricting and since disordered systems are very widespread in nature, percolation theory turned out to be a very fruitful tool, which has been applied in order to explain different phenomena such as the process of polymerization [30, 31], fire propagation in forests [33], electrical conductivity [34, 35], distribution of an underground oil reservoir [36], epidemic spreading [37] etc.. Leuenberger introduced the percolation theory in the pharmaceutical field [38].

The next section gives a short overview of some important aspects, which are discussed in more detail in the textbook by Stauffer and Aharony [33].

The aforementioned geometrical order is determined by lattices, which can be one (1D), two (2D) and three dimensional (3D). The lattice sites may be arranged in different geometrical patterns, e.g. square lattice (2D), honeycomb lattice (2D), cubic lattice (3D) etc. The lattice sites can either be occupied with the probability p_A or be unoccupied with the counter probability ($p_B = 1 - p_A$) depending whether the corresponding subunit exhibit the property A or B.

A group of connected (directly neighboring) sites, which are occupied, is called cluster. If the probability p_A is small, then there are a lot of small clusters. With an increasing probability p_A the number of clusters is decreasing, whereas the size of the clusters is increasing. At the critical probability p_c (percolation threshold) an “infinite” cluster is formed penetrating the whole lattice in all directions (see figure 3).

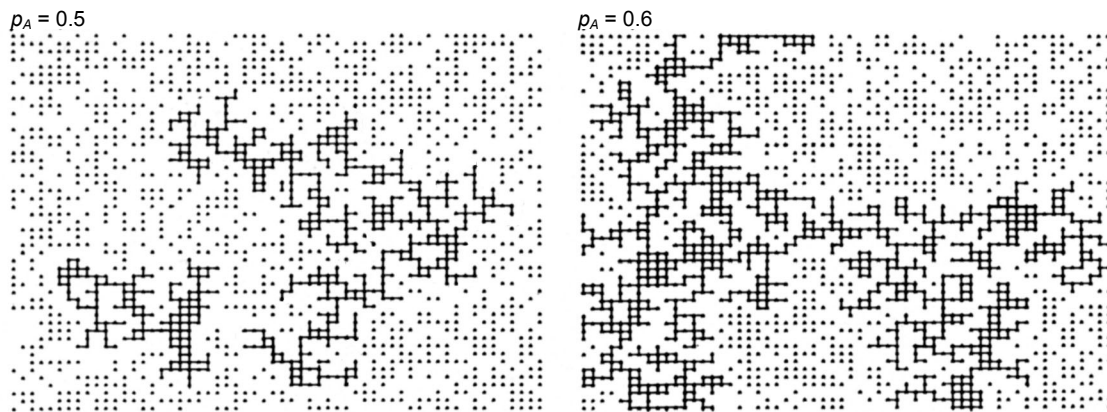


Figure 3: Square lattice (site percolation) with an occupation probability below (left side) and above (right side) the percolation threshold p_c ($p_c = 0.593$). Above the critical probability an “infinite” cluster percolates the system.

Apart from the so far discussed site percolation, other types of percolation are known such as bond, site-bond, directed and continuum percolation. The percolation threshold p_c is depending on the type of percolation, type and dimension of the lattice. Close to the percolation threshold, the behavior of the system is expected to change very abruptly. Thus, near the percolation threshold, properties of the system obey the scaling law (fundamental power law), which is presented in equation (11) in a general form. Unlike the percolation threshold p_c , the exponent q in equation (11) depends just on the dimensionality of the system (universal critical exponent).

$$X = S^* (p - p_c)^q \quad \text{equation (11)}$$

where: X : system property

S^* : scaling factor

p : occupation probability (corresponds to p_A in the section before)

p_c : percolation threshold

q : critical exponent

Percolation theory was used successfully to describe various tablet properties. The application of the percolation theory in powder technology is reviewed in an excellent paper by Leuenberger [39].

Powder systems, compacted or not, consist of particles and void space. Thus, underlying a lattice, the occupied sites correspond to material whereas the unoccupied sites correspond to void space (pores). Applying the percolation theory in powder technology, the probability p of the occupied sites is usually replaced by the analogous relative density ρ_r .

In this study the percolation theory is used to describe the tensile strength, which was already intensively investigated by Kuentz and Leuenberger [40, 41]. Based on the percolation theory, they proposed a power law (see equation (12)), which proved superior compared to the well-known equation of Ryshkewitch and Duckworth [42]. The experimentally found exponent T_f (3.2) was just slightly higher than the theoretical value (2.7) derived independently by Kuentz *et al.* [41] and Guyon [43]. Within this study, the theoretical value was used for two reasons: Firstly, the experimental determination of the critical exponent is fraught with the problem of a “flip-flop” effect [41], *i.e.* the fitting of the data according to the power law is not very straightforward. Secondly, a smaller critical exponent will lead to a higher critical relative density. Thus, the resulting dilution capacity will surely not be overestimated.

$$\sigma_{t(A)} = S (\rho_{r(A)} - \rho_{rc(A)})^{T_f} \quad \text{equation (12)}$$

where: $\sigma_{t(A)}$: radial tensile strength of a compact consisting of component A

S : scaling factor

T_f : critical exponent, used theoretical value: 2.7.

$\rho_{r(A)}$: relative density of component A

$\rho_{rc(A)}$: critical relative density (percolation threshold) of component A

The critical relative density $\rho_{rc(A)}$ corresponds to the solid fraction of component A with the maximum porosity $\varepsilon_{c(A)}$, which still keeps together the particles to form a percolating network leading to a compact with minimal strength ($\sigma_t \geq 0$). Thus, the void space, which is determined by the maximum porosity $\varepsilon_{c(A)}$, could be filled with a poorly compactable substance while maintaining the minimal strength (see dilution capacity on page 120).

If a poorly compactable substance B like acetaminophen or ascorbic acid is considered not to contribute to the tensile strength (treated like pores) when compressed in a binary mixture

with a well compactable excipient A, then equation (13) can be suggested, which is derived from equation (12) (see appendix G).

$$\sigma_{t(AB)} = S_2 (\rho_{r(AB)} - \rho_{rc^*(AB)})^{T_f} \quad \text{equation (13)}$$

where: $\sigma_{t(AB)}$: radial tensile strength of a compact consisting of components A and B

S_2 : scaling factor ($S_2 \neq S$)

T_f : critical exponent (fraction exponent): theoretical value: 2.7.

$\rho_{r(AB)}$: solid fraction (relative density of the binary mixture)

$\rho_{rc^*(AB)}$: solid fraction when component A starts to percolate

3.5 Dilution capacity

It is well conceivable that direct compression will become a subject of growing interest in the near future not only because of its advantages compared to wet granulation (see table 1) but also stimulated by FDA's PAT initiative. It is much easier to model a few than a lot of processes, as it is the case in wet granulation. However, wet granulation is still a very popular technique because poor compactibility and poor flow properties exhibited by many drug substances can easily be overcome by the formation of granules. Apart from flow and compactibility problems, direct compression has the drawback that the maximum drug load is generally limited to 30%. Thus, an excipient for direct compression should also exhibit a high dilution potential (dilution capacity), which is defined according to Wells and Langridge as the proportion of a non or poorly compactable drug B, which can be incorporated into a well compactable substance A to produce "satisfactory tablets" [44]. The term "satisfactory tablets" can be related to various properties such as the friability or tensile strength.

Table 1: Advantages and disadvantages of direct compression.

advantages	disadvantages
<ul style="list-style-type: none"> • suited for drugs sensitive to heat or moisture • requires few unit operations => shorter processing time, energy-efficient • favors faster dissolution rate 	<ul style="list-style-type: none"> • not suited for poorly flowing substances • not suited for poorly compactable drugs • drug content is limited to approximately 30% • segregation problems

Kuentz and Leuenberger [40] were the first authors who proposed an equation for the calculation of the dilution capacity. However, in this study a slightly different equation (equation (14)) is used, which is derived in appendix H. It has to be pointed out that this equation is just strictly valid if the effect of substance B on the tensile strength can be neglected. Thus, only the matrix formed by substance A determines the strength of the tablets.

$$X_{c(B)} = 1 - \frac{\rho_{t(A)}}{\rho_{t(B)}} \cdot \frac{1}{\left(\frac{\rho_{t(A)}}{\rho_{t(B)}} + \frac{1}{\rho_{rc(A)}} - 1 \right)} \quad \text{equation (14)}$$

where: $X_{c(B)}$: dilution capacity

$\rho_{t(A)}$: true density of component A [g/cm³]

$\rho_{t(B)}$: true density of component B [g/cm³]

$\rho_{rc(A)}$: critical relative density of component A

If the true densities of substance A and B are similar, then the dilution capacity $X_{c(B)}$ equals approximately the difference $1 - \rho_{rc(A)}$.

Minchom and Armstrong [45] developed a method for the experimental determination of the dilution capacity. This approach is also applied within this study to verify the plausibility of the new theoretical equation.

4 Materials and methods

The substances used for the different studies are listed in table 2. Various substances were involved in the compression study, in order to verify the range of validity for the new approach. The flow measurements were performed using two liquids of different viscosities (water and glycerol) and three spherical shaped particulate materials (glass ballotini, Cellets[®], Sugar spheres[®]) in different sizes. The dilution capacity was investigated using two binary systems consisting of a well compactable (Avicel PH101[®] or Ethocel[®]) and a poorly compactable substance (acetaminophen).

Table 2: Overview of the used substances.

substance/product	trade name	distributor	study
Acetylsalicylic acid		Hänseler, Switzerland	compression
Calcium carbonate		Hänseler, Switzerland	compression
Caffeine pulvis anhydrous		Sandoz, Switzerland	compression
Lactose anhydrous NF DT ¹⁾	Lactose Sheffield	Quest International, USA	compression
MCC ²⁾	MCC 102G	Pharmatrans, Switzerland	compression
Sodium chloride		Hänseler, Switzerland	compression
Acetaminophen		Siegfried, Switzerland	compression
Sea sand		Riedel de Haën, Germany	compression
Pregelatinized Starch	Starch 1500 [®]	Colorcon, USA	compression
MCC ²⁾ Pellets	Cellets [®] (700, 500, 350, 200)	Pharmatrans, Switzerland	flow
Glass ballotini (0.8 , 0.5 , 0.3 mm)			flow
Sugar pellets	Sugar spheres [®] (850, 710, 600, 500, 250)	Pharmatrans, Switzerland	flow
Glycerol 98%		Hänseler, Switzerland	flow
Water			flow
MCC ²⁾	Avicel PH101 [®]	FMC, USA	dilution capacity
Ethylcellulose	Ethocel [®]	Fluka, Switzerland	dilution capacity
Acetaminophen		Sandoz, Switzerland	dilution capacity

¹⁾ NF: National Formulary; DT: Direct Tableting

²⁾ MCC: Microcrystalline cellulose

4.1 Storage

Prior to processing or testing, the powders were stored over a saturated solution of K₂CO₃ (corresponding to a relative humidity of 45±10%) [46].

4.2 Characterization of the substances

The true density ρ_t of the substances was measured with a Beckman® Air Comparison Pycnometer Model 930 (Beckman Instruments, Fullerton, USA).

The determination of the bulk density ρ_{bulk} and tapped density ρ_{tapped} was performed according to the USP 24-NF 19 using 100.0 g of each substance. The test procedure is also described in detail on page 14. Equation (15) and equation (16) were used to calculate the relative bulk density ρ_{rbulk} and the relative tapped density $\rho_{rtapped}$, respectively.

$$\rho_{rbulk} = \frac{\rho_{bulk}}{\rho_t} \quad \text{equation (15)}$$

$$\rho_{rtapped} = \frac{\rho_{tapped}}{\rho_t} \quad \text{equation (16)}$$

where: ρ_{rbulk} : relative bulk density
 $\rho_{rtapped}$: relative tapped density
 ρ_{bulk} : bulk density [g/cm³]
 ρ_{tapped} : tapped density [g/cm³]
 ρ_t : true density [g/cm³]

The particle size of the materials was determined using a laser scattering based particle sizer (MasterSizer X Long Bed, Malvern Instruments, Worcestershire, UK) equipped with a sample preparation unit (MSX64 - Manual Dry Powder Feeder, Malvern Instruments, Worcestershire, UK) for dry measurements. If the particle size was expected to be higher than 600 μm then the 1000 mm otherwise the 300 mm range lens was used.

4.3 Compression study

Using the Zwick® 1478 Universal Testing Instrument (Zwick® GmbH, Ulm, Germany), the materials were compressed with a speed of 5 mm/min to a maximum force of 60 kN. The round cross section area of the used flat punch had a diameter of 11 mm. The amount of material was selected so that the height of the tablets at maximum pressure was about the same for all used substances (see table 3).

Table 3: Overview of the used amounts of the involved substances.

substance	sample weight [g]	substance	sample weight [g]
Acetaminophen	0.400	MCC	0.440
Caffeine pulvis anhydrous	0.420	Sodium chloride	0.620
Cellets® 350	0.440	Sea sand	0.650
Lactose anhydrous	0.450	Starch 1500®	0.460

The investigation of the compression behavior of the substances was performed by fitting “in die” data according to the Heckel equation (equation (1)) and the adapted Van der Waals equation (equation (6)). The fitting procedure was accomplished with Systat for Windows Version 10.0 (SPSS Incorporation, Chicago, USA) using linear regression analysis for the Heckel equation and non-linear regression analysis for the modified Van der Waals equation. The height h of the tablet during compression was monitored by the Zwick® 1478 Universal Testing Instrument (Zwick® GmbH, Ulm, Germany). The relative density ρ_r and the true volume V_t , used for the fitting, were calculated according to equation (17) and equation (18), respectively.

$$\rho_r = \frac{\rho_a}{\rho_t} = \frac{m}{\rho_t \cdot V_a} = \frac{m}{\rho_t \cdot h \cdot r^2 \cdot \pi} \quad \text{equation (17)}$$

where: ρ_a : apparent density [g/cm³]
 ρ_t : true density [g/cm³]
 m : weight of the tablet [g]
 V_a : apparent volume of the tablet [cm³]
 h : height of the tablet [cm]
 r : radius of the cross section area of the tablet [cm]

$$V_t = \frac{m}{\rho_t} \quad \text{equation (18)}$$

where: V_t : true volume [cm³]
 m : weight of the compressed material [g]
 ρ_t : true density [g/cm³]

The parameters K and A of equation (1) and A_v , B_v and C_v of equation (6) were used to characterize the compression behavior of the materials. The mean yield pressure σ_y was defined as the reciprocal of the Heckel parameter K [47].

4.4 Flow study

The flow measurements were performed according to the experimental setup depicted in figure 4. The weight of the material (particulate or fluid) discharged out of the hopper (half center angle α : 17°; material: acrylic glass) was recorded by a balance, which transmitted the data to a connected computer. The measurements were performed using orifices of different diameters (5 mm, 7 mm, 9 mm). The measured flow profiles of the particulate material (Cellets®, Sugar spheres® and glass ballotini) were analyzed according to equation (8). The flow of the examined liquids was investigated according to equation (9) and equation (10).

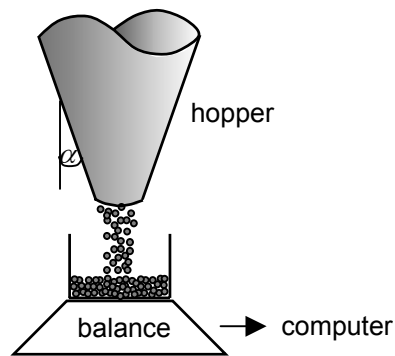


Figure 4: Experimental setup for the flow measurements of particulate materials and fluids.

4.5 Dilution capacity study

The binary mixtures were prepared by blending the substances for 7 minutes using a tumbler (diffusion) mixer (Turbula T2A, W.A. Bachofen AG, Basel, Switzerland). The used ratios of the two substances are listed in table 4.

Table 4: Composition of the mixtures used for the dilution capacity study. Avicel PH101[®] and Ethocel[®] were used as well compactable substance A, acetaminophen as poorly compactable substance B.

ingredient	composition [% (w/w)]									
acetaminophen	0	10	20	30	40	50	60	70	80	90
excipient	100	90	80	70	60	50	40	30	20	10
Avicel PH101 [®]	✓	✓	✓	✓	✓	✓	✓	✓	✓	
Ethocel [®]	✓	✓	✓	✓	✓	✓	✓	✓	✓	✓

400 ± 1 mg, round (11 mm diameter), flat tablets were prepared using the Zwick[®] 1478 Universal Testing Instrument (Zwick[®] GmbH, Ulm, Germany). The compression speed was set to 10 mm/min. Prior to each compression cycle, the punches and the die wall were lubricated with magnesium stearate. The tablets were compressed at different pressure levels ranging from 5.26 to 52.61 MPa for mixtures containing Avicel PH102[®] and from 1.05 to 52.61 MPa for mixtures containing Ethocel[®].

The crushing force F was determined using the Zwick[®] 1478 Universal Testing Instrument (Zwick[®] GmbH, Ulm, Germany). The preforce was 0.3 N and the testing speed was 10 mm/min. The radial tensile strength was calculated according to equation (19) [48].

$$\sigma_{t(AB)} = \frac{2F}{\pi \cdot D \cdot h} \quad \text{equation (19)}$$

where: $\sigma_{t(AB)}$: radial tensile strength of tablet consisting of substances A and B [MPa]

F : crushing force [N]

D : diameter of the tablet [mm]

h : height of the tablet (thickness) [mm]

The radial tensile strength was analyzed according to equation (13), which is based on the concept of percolation theory [40] (appendix G). After setting the tensile strength to the inverse power of the exponent T_f (equation (20)), the data were linearly fitted using Systat for Windows Version 10.0 (SPSS Incorporation, Chicago, USA). The resulting slope a and intercept b were used to calculate the solid fraction $\rho_{rc^*(AB)}$ (solid fraction when component A starts to percolate). Based on theoretical considerations [41], a value of 2.7 was assumed for the critical exponent T_f .

$$\sigma_{t(AB)}^{1/T_f} = S_2^{1/T_f} \cdot \rho_{r(AB)} - S_2^{1/T_f} \cdot \rho_{rc^*(AB)} = a \cdot \rho_{r(AB)} - b \quad \text{equation (20)}$$

where: $\sigma_{t(AB)}$: radial tensile strength of compact consisting of components A and B

S_2 : scaling factor

T_f : critical exponent (fraction exponent): theoretical value: 2.7.

$\rho_{r(AB)}$: solid fraction (relative density of the binary mixture)

$\rho_{rc^*(AB)}$: solid fraction when component A starts to percolate (= b/a)

Determination of the dilution capacity, $X_{c(B)}$

For all mixtures, the radial tensile strength of the tablets was plotted versus the compression pressure. Applying the trapezium method, the area under the curve (AUC) was determined in order to calculate the area ratio, which is defined as the AUC (of each mixture) normalized by the AUC of 100% excipient. The area ratio (formerly known as work potential [45]) related to the amount of excipient was then linearly fitted in the range of 50-100% excipient (see figure 5). The experimentally determined dilution capacity $X_{c(B)}$ was obtained by the extrapolation of regression line back to an area ratio = 0 (intercept of x-axis).

The theoretical dilution capacity was calculated according to equation (14), which is derived in appendix H.

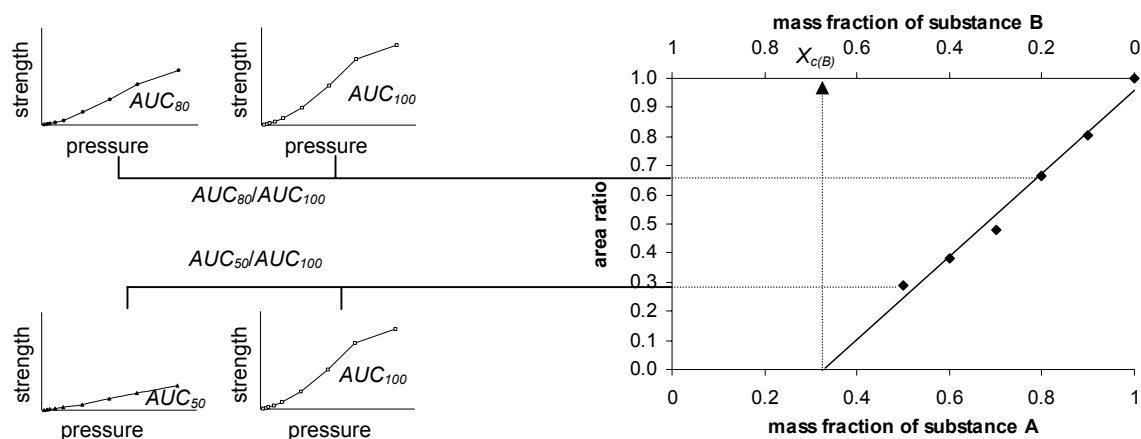


Figure 5: Visualization of the experimental determination of the dilution capacity $X_{c(B)}$.

5 Results and Discussion

5.1 Compression study

Data for the mean particle size, the true density ρ_t and the bulk density ρ_{bulk} are tabulated in table 5 for the used substances.

Table 5: Characterization of the used substances (with the Standard Error of the Mean (SEM)).

substance	mean particle size (n=5) [μm]	true density, ρ_t (n=6) [g/cm^3]	bulk density, ρ_{bulk} (n=3) [g/cm^3]
Acetaminophen	231.4 (12.1)	1.30 (0.007)	0.485 (0.008)
Caffeine pulvis anhydrous	172.3 (34.2)	1.46 (0.022)	0.265 (0.007)
Cellets [®] 350	405.8 (2.1)	1.56 (0.013)	0.782 (0.001)
Lactose anhydrous NF DT ¹⁾	216.4 (12.0)	1.56 (0.000)	0.553 (0.005)
MCC ²⁾	115.1 (1.3)	1.54 (0.003)	0.378 (0.005)
Sodium chloride	482.5 (7.1)	2.16 (0.004)	1.313 (0.004)
Sea sand	263.7 (3.3)	2.65 (0.006)	1.389 (0.016)
Starch 1500 [®]	170.1 (10.9)	1.47 (0.004)	0.633 (0.007)

¹⁾ NF: National Formulary; DT: Direct Tableting

²⁾ MCC: Microcrystalline cellulose

Table 6: “In die” Heckel parameters for the compression of several substances in the compression pressure range of 10-80 MPa (with the Standard Error of the Mean (SEM); (n=5)).

substance	K [$10^{-3} \cdot \text{MPa}^{-1}$]	A	r^2	mean yield pressure, σ_y [MPa]
Acetaminophen	13.6 (0.8)	1.501 (0.029)	0.985	73.5 (4.4)
Caffeine pulvis anhydrous	11.0 (0.2)	0.975 (0.005)	0.985	90.9 (1.3)
Cellets [®] 350	17.5 (0.1)	0.667 (0.002)	0.999	57.1 (0.5)
Lactose anhydrous NF DT ¹⁾	8.9 (0.0)	0.942 (0.003)	0.981	112.4 (0.9)
MCC ²⁾	18.4 (0.3)	0.588 (0.003)	0.997	54.3 (1.0)
Sodium chloride	15.4 (0.2)	0.888 (0.002)	1.000	64.9 (1.0)
Sea sand	5.9 (0.0)	0.757 (0.003)	0.997	169.5 (2.3)
Starch 1500 [®]	20.4 (0.5)	0.856 (0.006)	0.998	49.0 (1.1)

¹⁾ NF: National Formulary; DT: Direct Tableting

²⁾ MCC: Microcrystalline cellulose

The compression profile, which was generated during the compression (“in die”), was analyzed according to the Heckel equation and the adapted Van der Waals equation. The fitting parameters according to the Heckel equation are listed in table 6. Because the Heckel equation can just be used to describe the compression process in the linear section of the Heckel plot (see figure 6) *i.e.* after the rearrangement and fragmentation of the particles, the analysis was performed in the compression pressure range of 10-80 MPa. However, except for the sea sand, the goodness of fit is worse for brittle substances (acetaminophen, caffeine,

lactose) compared to ductile materials (Cellets[®] 350, MCC, sodium chloride, Starch 1500[®]). Since the curved region in the Heckel plot is more pronounced for brittle substances, it is possible, that the selected pressure range (10-80 MPa) still includes a part of the initial curve, resulting in a worse correlation coefficient (see figure 6). The Heckel constant K and the derived mean yield pressure σ_y can be used in order to quantify the ductile behavior of the materials. A high K value, equivalent to a low mean yield pressure σ_y , is characteristic for a material with good plastic deformation properties. Concerning the plastic flow behavior, the substances can therefore be ranked in the following descending order:

Starch 1500[®] > MCC > Cellets[®] 350 > sodium chloride > acetaminophen > caffeine > lactose > sea sand

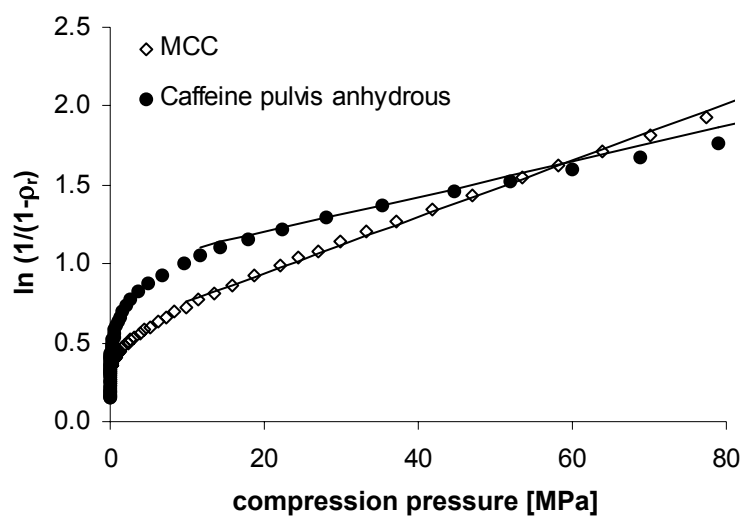


Figure 6: Typical Heckel plots for MCC (plastic material) and Caffeine pulvis anhydrous (brittle material) with the corresponding linear fits in the pressure range of 10-80 MPa.

The compression profiles (“in die”) for all eight substances are depicted in figure 7 combined with the fitting curves according to the modified Van der Waals equation. The corresponding fitting values are listed in table 7.

The correlation coefficients for the fitting of the compression data according to the adapted Van der Waals equation are for all substances in the same order of magnitude or even better compared to those resulting from the evaluation according to the Heckel equation. The new equation has the great advantage, that its use is not restricted to a certain pressure range. The new model is able to describe the whole compression process, including the initial stage characterized by particle rearrangement and fragmentation. Thus, the range of validity is much broader compared to the Heckel equation.

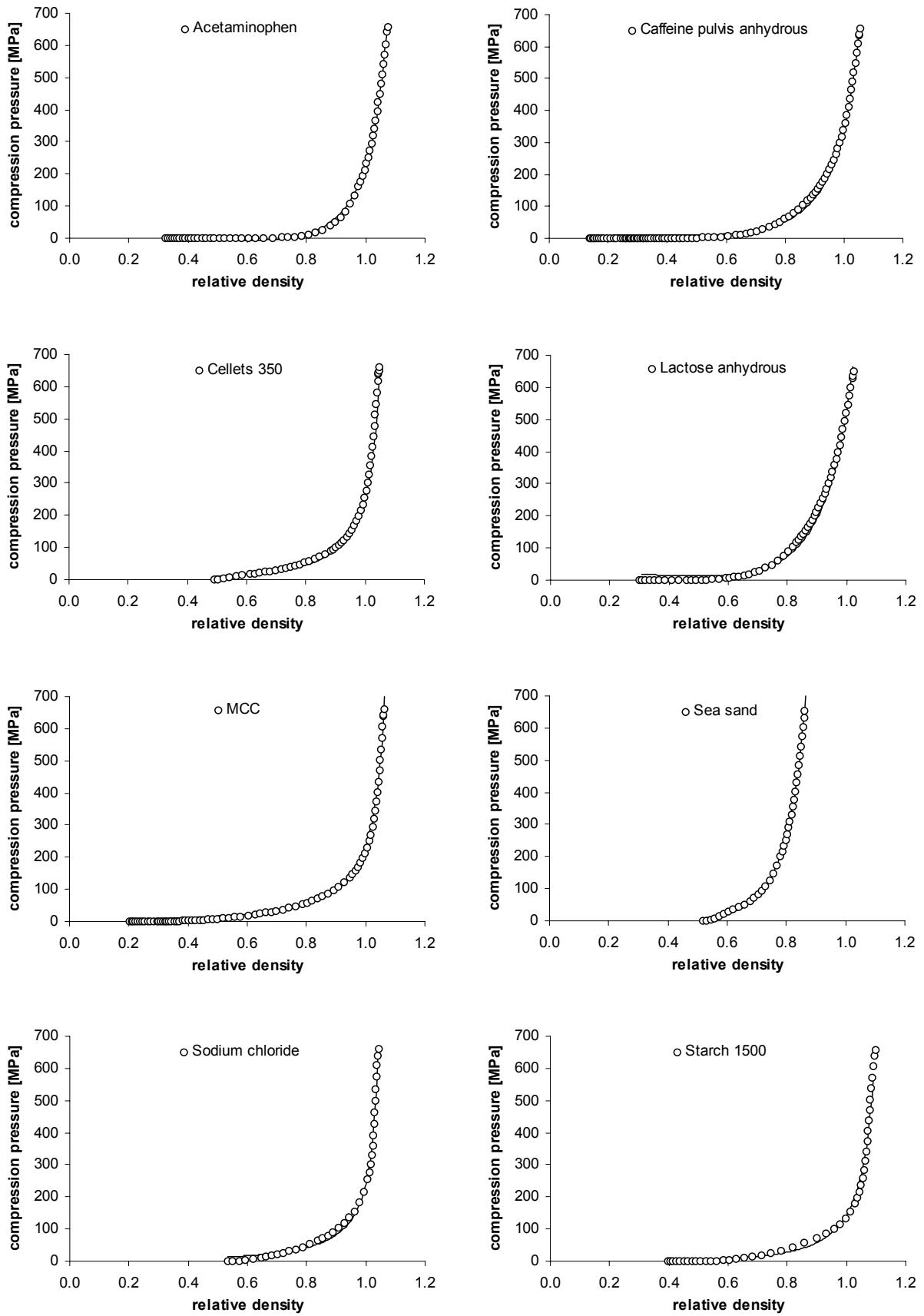


Figure 7: Compression profiles for all eight substances. The solid lines represent the model according to the adapted Van der Waals equation.

Table 7: Fitting parameters according to the adapted Van der Waals equation (equation (6)) for several substances based on “in die” data over the whole compression pressure range (with the Standard Error of the Mean (SEM); (n=5)).

substance	B_v [cm ³]	C_v [cm ³ MPa]	A_v [cm ⁶ MPa]	r^2	V_t [cm ³]
Acetaminophen	0.267 (0.001)	19.4 (0.3)	22.5 (0.3)	0.998	0.308
Caffeine pulvis anhydrous	0.251 (0.001)	20.0 (0.4)	17.2 (0.1)	0.992	0.288
Cellets [®] 350	0.258 (0.000)	7.4 (0.4)	4.0 (0.1)	0.997	0.282
Lactose anhydrous NF DT ¹⁾	0.246 (0.001)	39.9 (0.8)	35.7 (0.2)	0.990	0.288
MCC ²⁾	0.259 (0.001)	6.7 (0.2)	2.8 (0.1)	0.996	0.286
Sodium chloride	0.268 (0.001)	5.7 (0.3)	2.5 (0.4)	0.996	0.287
Sea sand	0.257 (0.000)	27.2 (0.4)	26.5 (0.4)	0.999	0.245
Starch 1500 [®]	0.276 (0.000)	7.8 (0.1)	6.2 (0.2)	0.993	0.313

Table 7 shows that the values for B_v and the true volume V_t of the compressed particles ($V_t = m/\rho_t$) just slightly differ. In analogy to the term nb in the Van der Waals equation of state (equation (4)), B_v can be considered to equal the volume at infinite pressure and to correspond to the true volume of all particles. The observed difference between the two values (B_v and V_t) can be explained by the fact that the evaluation is based on “in die” data. The ratio of the true volume to the value for B_v is expected to be much closer to unity for the fitting of “out of die” data.

Compared to B_v , the physical meaning of C_v is not that obvious and can therefore not be revealed so easily. Parmentier related the constant C in his hyperbola equation (analogous to C_v in the adapted Van der Waals equation) to the yield property of the material [49]. Indeed, plotting the values for C_v against the mean yield pressure σ_y obtained by the Heckel analysis clearly confirms the relationship between both values (figure 8). Small mean yield pressures, which are characteristic for ductile substances, correspond to small values for C_v and brittle substances show high values for both the mean yield pressure and the C_v values. Thus, by means of C_v a distinction can be drawn between brittle and plastic materials.

The term $\frac{A_v}{V_t^2} \rho_r^2$ can be called inner or intrinsic pressure, which could be related to the attractive forces or the cohesiveness of the powder. The whole term corresponds to the term $1/b$ in the equation of Kawakita (equation (3)), who suggested that $1/b$ is proportional to a material specific yield value [50]. In fact, a relation to the mean yield pressure can also be demonstrated for A_v (see figure 8).

However, the diagrams of C_v and A_v versus the mean yield pressure show very similar patterns, indicating that a correlation between both coefficients is very probable. This assumption can be supported by the Van der Waals equation: both coefficients include the factor n . Unfortunately, the physical meaning of n is unclear. The suggestion that n is a measure for the total number of compressed molecules can *a priori* be excluded, since not all

molecules are involved in the particle-particle interactions. The possibility, that n reflects the number of particles, is also rather improbable. In this case, the values for A_v and C_v would be expected to be higher for microcrystalline cellulose than for Cellets® 350. However, it is also possible, that n expresses the number of (possible) contact points, which also depends on the relative density.

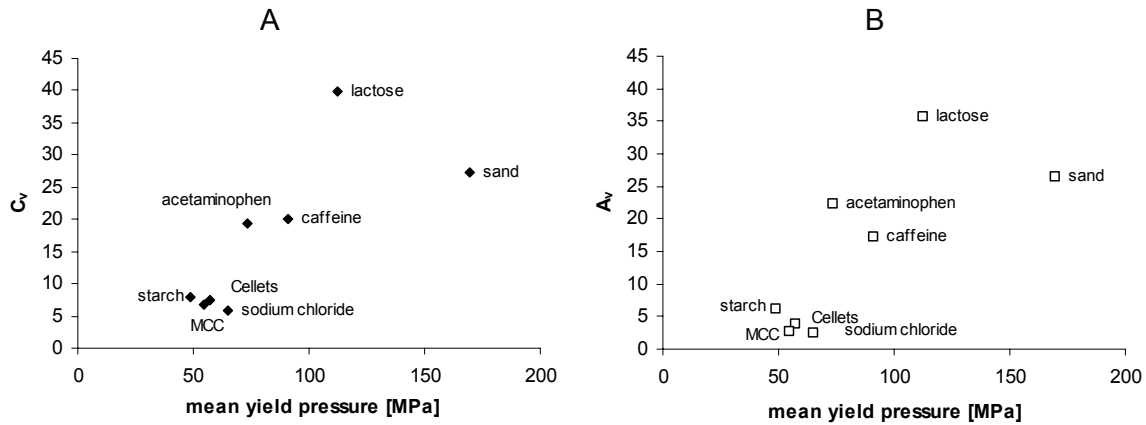


Figure 8: Correlation between the “Van der Waals” coefficients and the mean yield pressure σ_y . A: C_v against σ_y ; B: A_v against σ_y .

There is another approach how the correlation of the two constants A_v and C_v can be explained. Supposing no compression pressure, the relative density in equation (6) represents the relative bulk density ρ_{r0} . Thus, for C_v we can write equation (21).

$$C_v = \frac{A_v}{V_t} \cdot \rho_{r0}^2 \cdot \left(\frac{1}{\rho_{r0}} - \frac{B_v}{V_t} \right) \quad \text{equation (21)}$$

Replacing C_v in equation (6) by the term in equation (21) and assuming furthermore that B_v equals V_t , we get equation (22).

$$\left(\sigma + \underbrace{\frac{A_v}{V_t^2} \cdot \rho_r^2}_{p_{attr}} \right) \left(\frac{1}{\rho_r} - \frac{B_v}{V_t} \right) = \underbrace{\frac{A_v}{V_t^2} \cdot \rho_{r0}^2}_{p_{attr0}} \left(\frac{1}{\rho_{r0}} - \frac{B_v}{V_t} \right) \quad \text{equation (22)}$$

Equation (22) is very similar to the rewritten equation of Kawakita (equation (23)), which is derived from the original equation of Kawakita (equation (3)) by introducing the relative density ρ_r .

$$\left(\sigma + \frac{1}{b} \right) \left(\frac{1}{\rho_r} - \frac{V_\infty}{V_t} \right) = \frac{1}{b} \left(\frac{1}{\rho_{r0}} - \frac{V_\infty}{V_t} \right) \quad \text{equation (23)}$$

Assuming that V_∞ equals B_v , the only significant difference between equation (22) and equation (23) is the fact, that p_{attr} depends on the relative density, whereas $1/b$ is constant throughout the whole compression process. If p_{attr} really reflects the cohesive property of the material, it is plausible that the value for p_{attr} is depending on the relative density.

When using equation (22) or equation (23), it has to be kept in mind that the bulk density in the die can differ from the bulk density determined according to the USP 24-NF 19. The discrepancy between the two bulk densities can be explained by the different volumes involved and by the completely different filling procedures.

5.2 Flow study

The values for the bulk density and the mean particle size used to evaluate the flow of the particulate materials out of the hopper are summarized in table 8.

Table 8: Bulk density and mean particle size of the particulate material (with the Standard Error of the Mean (SEM)).

material	bulk density, ρ_{bulk} (n=6) [g/ml]	mean particle size, $d_{particle}$ (n=6) [μm]
Cellets [®]		
700	0.916 (0.001)	849.7 (7.9)
500	0.882 (0.001)	621.9 (1.6)
350	0.884 (0.002)	405.8 (2.1)
200	0.879 (0.003)	294.5 (3.5)
Sugar spheres [®]		
850	0.939 (0.003)	974.9 (2.2)
710	0.911 (0.004)	837.5 (0.8)
600	0.929 (0.005)	726.8 (2.9)
500	0.898 (0.003)	571.4 (1.9)
250	0.877 (0.004)	327.4 (1.3)
glass ballotini		
0.8	1.727 (0.004)	690.6 (7.4)
0.5	1.695 (0.004)	531.2 (3.1)
0.3	1.678 (0.003)	331.1 (1.4)

Typical flow diagrams of particulate materials and a liquid are depicted in figure 9. Concerning the liquid, the flow profile is flattening by and by. This non-linear relationship of the discharged mass (not constant flow rate) can be explained by the effect of the hydrostatic pressure, which is diminishing as the height of the liquid level is decreasing. These considerations can be confirmed by the model I according to equation (9), which just takes into account the hydrostatic pressure (see figure 10). The slopes of the corresponding curves are also decreasing in dependency of the time. However, the predicted values according to model I are too high for both water and especially glycerin. Considering additionally the viscosity of the liquids, the model II (equation (10)) is able to predict extremely well the real flow behavior (see figure 10).

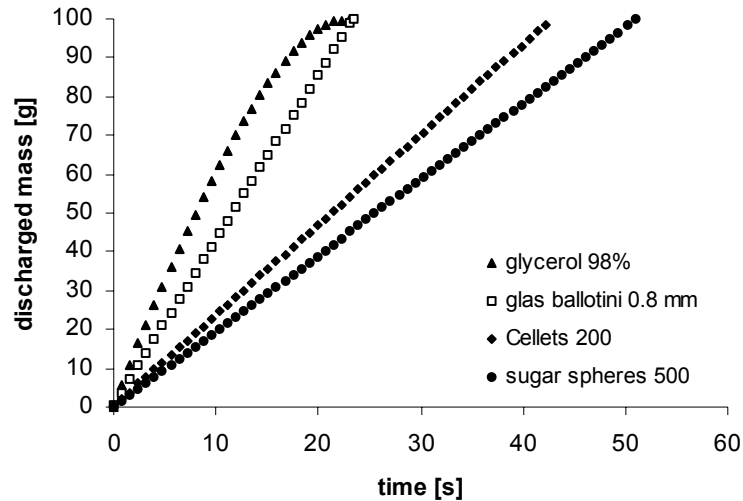


Figure 9: Flow profiles of different materials out of a hopper with an orifice diameter of 5 mm.

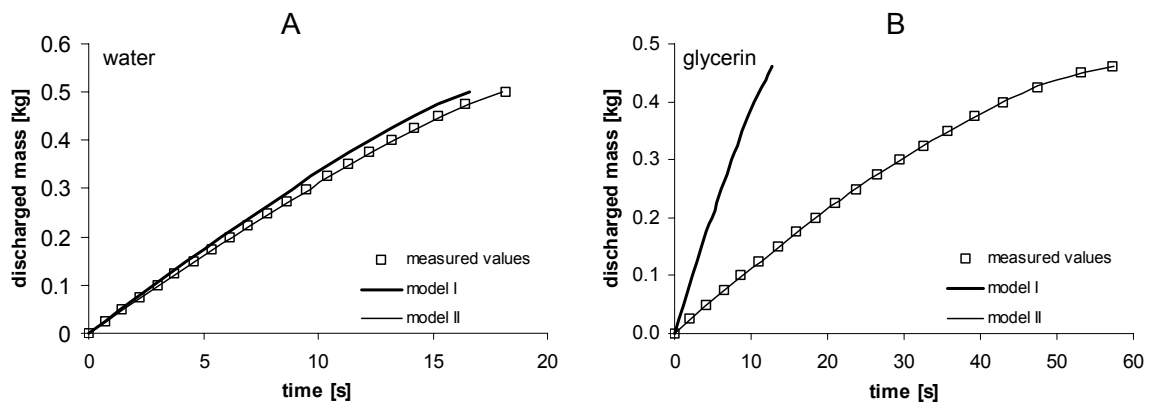


Figure 10: Flow profiles of two liquids out of a hopper with an orifice diameter of 5 mm and two predictive curves according to model I (equation (9)) and model II (equation (10)). A: water: ρ : 1000 kg/m³; m_0 : 0.50 kg, η : 0.001 Ns/m²; B: glycerin 98%: ρ : 1261 kg/m³; m_0 : 0.46 kg, η : 1.08 Ns/m².

Concerning particulate material, the flow rate is constant and reflects the use of a “sand-clock”. Even though some authors reported that the flow rate is not linearly related to the orifice area [51], the postulated linear relationship could be confirmed within this study at least in the investigated range of orifice areas (see figure 11). The extrapolation of the linear regression back to a flow rate of zero gives the critical orifice area A_{crit} . The values of the critical areas A_{crit} and the corresponding critical diameters d_{crit} are listed in the table 9. The smaller the particles are, the smaller is the critical area A_{crit} . Figure 12 shows that the critical diameter correlates linearly with the particle diameter irrespective of the material. The ratio q of the critical diameter d_{crit} to the particle diameter $d_{particle}$ shows that small particles are more

efficiently immobilized by the surrounding particles than bigger one. Small particles are supposed to build easily bridges within the bulk that hinder the material to flow freely.

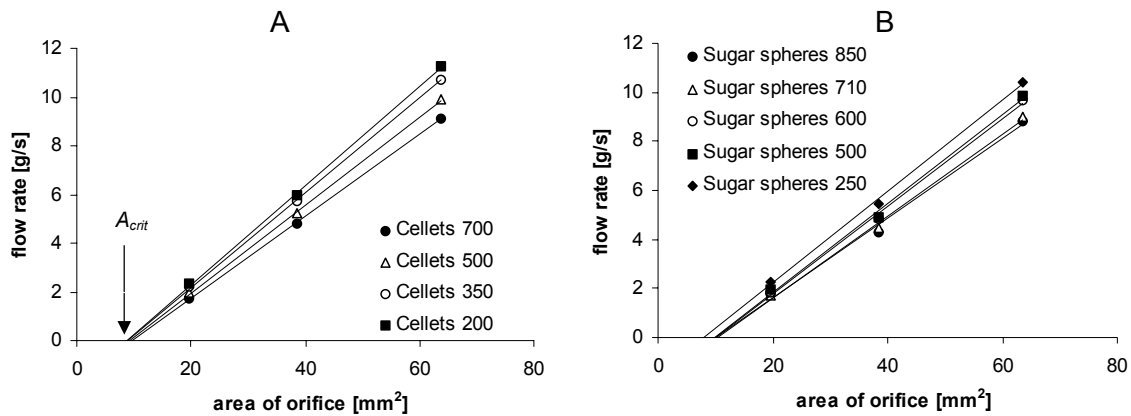


Figure 11: Determination of the critical area A_{crit} by means of linear correlation of the flow rate and the area of the used orifice. A: Cellets®; B: Sugar spheres®.

Table 9: Values for critical areas, the corresponding critical diameter and the ratio q of the critical diameter to the particle diameter.

material	critical area A_{crit} [mm²]	critical diameter d_{crit} [mm]	$q = d_{crit}/d_{particle}$
Glass ballotini 0.8 mm	9.571	3.49	5.05
Glass ballotini 0.5 mm	9.465	3.47	6.54
Glass ballotini 0.3 mm	8.608	3.31	10.00
Cellets® 700	9.477	3.47	4.09
Cellets® 500	9.214	3.43	5.51
Cellets® 350	8.675	3.32	8.19
Cellets® 200	8.586	3.31	11.25
Sugar spheres® 850	10.183	3.60	3.69
Sugar spheres® 710	10.283	3.62	4.32
Sugar spheres® 600	10.025	3.57	4.92
Sugar spheres® 500	9.766	3.53	6.17
Sugar spheres® 250	8.067	3.20	9.79

Dividing the measured flow rate through the corrected area of the orifice and the bulk density ρ_{bulk} , the mass permeability coefficient Π^* can be calculated according to equation (8). From a mathematical point of view, the mass permeability coefficient equals the mean velocity of the particles passing through the orifice. The relationship between the mass permeability coefficient and the particle diameter is depicted for all used materials in figure 13. Since no tendency could be seen relating the orifice area to the mass permeability coefficient, the values represent an average of the values obtained for all three orifices. Considering figure 13, it is evident that the mass permeability coefficient Π^* is depending on the material. Π^* of glass ballotini is higher compared to the Cellets® and Sugar spheres®, within the same range of particle size. Glass ballotini can flow faster than the Cellets® and Sugar spheres®

particles. The reason could lie in different surface properties and in consequence in different friction properties. For all three kinds of particles (glass ballotini, Cellets[®] and Sugar spheres[®]) Π^* is higher for small particles. Even though we saw that small particles can build more efficiently bridges, it seems that they can flow faster once they were moving compared to bigger particles.

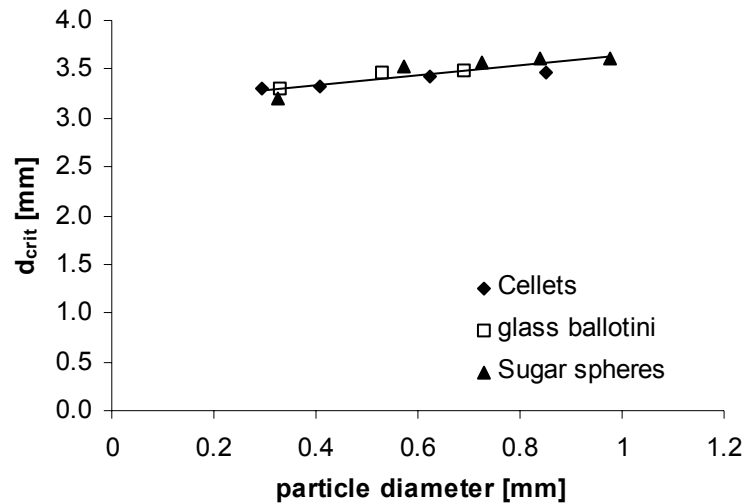


Figure 12: Visualization of the linear correlation of the critical diameter d_{crit} and the measured particle diameter $d_{particle}$.

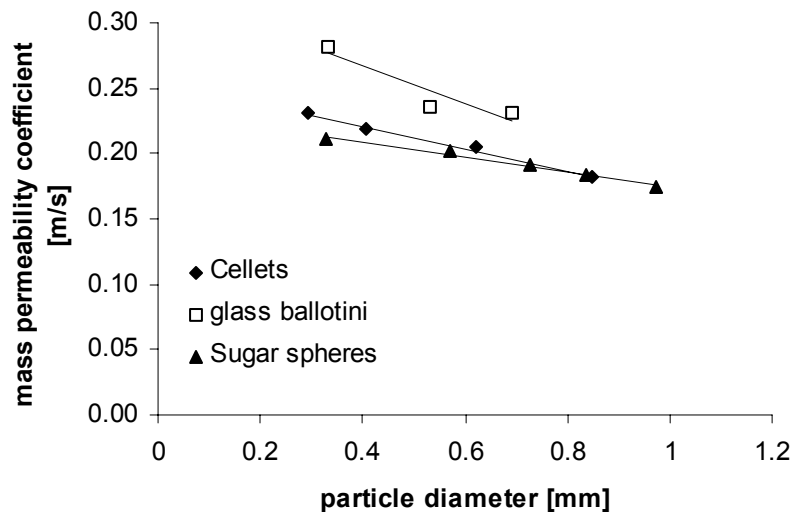


Figure 13: Relationship between the mass permeability coefficient and the particle diameter for Cellets[®], glass ballotini and Sugar spheres[®].

5.3 Dilution capacity study

The characterization of the involved components concerning their densities is summarized in table 10.

Table 10: Overview of the densities for the involved substances. (with the Standard Error of the Mean (SEM)).

density	Avicel PH101®	Ethocel®	Acetaminophen
true density, ρ_t [g/cm ³] (n=8)	1.555 (0.003)	1.255 (0.001)	1.291 (0.001)
bulk density, ρ_{bulk} [g/cm ³] (n=6)	0.293 (0.001)	0.443 (0.001)	0.251 (0.002)
rel. bulk density, ρ_{rbulk}	0.189 (0.001)	0.353 (0.001)	0.194 (0.002)
tapped density, ρ_{tapped} [g/cm ³] (n=6)	0.395 (0.001)	0.513 (0.001)	0.421 (0.003)
rel. tapped density, $\rho_{rtapped}$	0.254 (0.001)	0.409 (0.001)	0.326 (0.003)

Figure 14 clearly demonstrates for several mixtures that equation (20), which is based on the percolation theory is well suited to explain the radial tensile strength of tablets consisting of a binary mixture of a well (substance A) and a poorly compactable substance (substance B). However, the goodness of fit is decreasing as the amount of poorly compactable substance is increasing (see table 11). Possible explanations are manifold: i) Kuentz pointed out that the regression coefficient depends on the slope. ii) It is also conceivable that acetaminophen cannot be considered as completely non-compactable as supposed in the derivation of equation (20).

Table 11: Results of the linear fit according to equation (20).

Amount of excipient	Avicel PH101®		Ethocel®	
	$\rho_{rc}^{*(AB)}$	r^2	$\rho_{rc}^{*(AB)}$	r^2
100	0.263	0.998	0.370	0.998
90	0.291	0.996	0.387	0.999
80	0.318	0.996	0.401	0.998
70	0.354	0.993	0.405	0.996
60	0.391	0.992	0.419	0.993
50	0.424	0.981	0.430	0.994
40	0.467	0.986	0.446	0.986
30	0.502	0.985	0.464	0.983
20	0.525	0.983	0.502	0.981
10	n.d.	n.d.	0.499	0.967

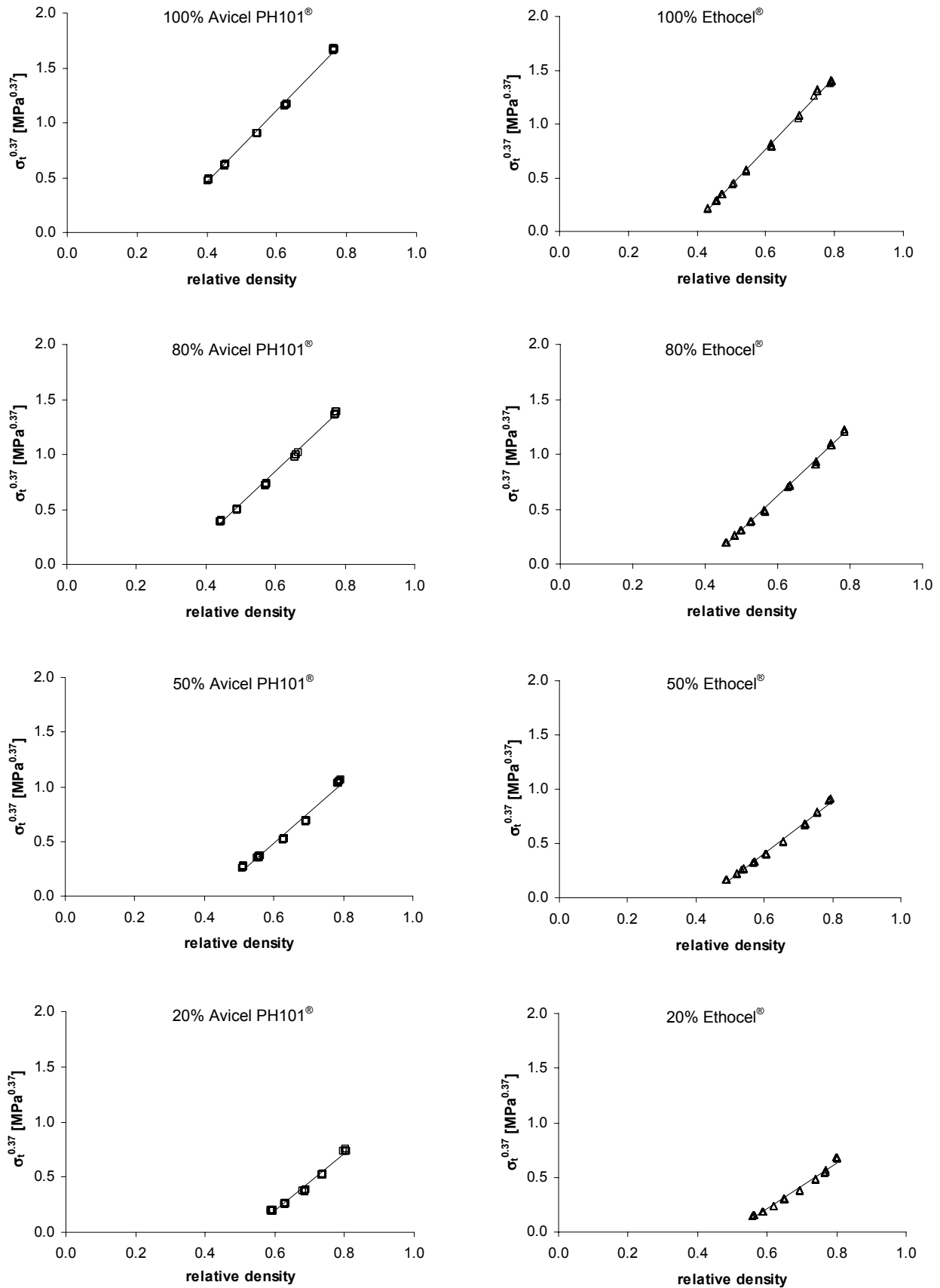


Figure 14: Tensile strength $\sigma_t^{0.37}$ versus the relative density of tablets consisting of excipient and acetaminophen in different ratios. Excipient: Avicel PH101[®] (on the left side) and excipient: Ethocel[®] (on the right side). The fit is performed according to equation (20).

The solid fraction $\rho_{rc^*(AB)}$, which represents the solid fraction where the excipient (substance A) starts to percolate is plotted in figure 15 versus the mass fractions of the two components. One curve is based on theoretical considerations (see equation (24) derived in appendix H), the other curve is based on the results of the fitting of the experimental data according to equation (20). Both curves converge at lower amounts of the poorly compactable substance B and rise at higher amounts of acetaminophen. This observation can be explained by the fact, that the amount of excipient, which ensures the mechanical strength, is reduced with higher amounts of drug. However, the upswing of the “theoretical curve” is much more pronounced compared to the “experimental” curve, which can nearly be considered as linear. The divergence can be explained by the assumption that acetaminophen also contributes to the strength of the tablet at higher mass fractions. Therefore, acetaminophen is not completely non-compactable as presumed for the derivation of the “theoretical” curve. This conclusion can be supported by the fact, that $\rho_{rc^*(AB)}$ is always smaller than unity according to the “experimental” curve. Consequently, for all possible compositions there is always a solid fraction, which guarantees at least a minimum strength of the tablet. The “theoretical” curve however predicts a maximum possible amount of the poorly compactable substance, which is achieved when the “critical” solid fraction $\rho_{rc^*(AB)}$ equals unity at infinite pressure. This proportion also referred to as dilution capacity $X_{c(B)}$ is indicated in figure 15. The “theoretical” curve is a marginal or extreme case, independent of the drug and its properties and thus more rigorous than the “experimental” curve. The area above the curve represents the solid fractions, which ensure the formation of a compact at the corresponding mass fraction of the component. Thus, the curve and the resulting area are an excellent tool to estimate the solid fraction, which is necessary to get a tablet of a minimum strength at a given drug load.

$$\rho_{rc^*(AB)} = \rho_{rc(A)} \left(1 + \frac{1 - X_{(A)}}{X_{(A)}} \cdot \frac{\rho_{t(A)}}{\rho_{t(B)}} \right) \quad \text{equation (24)}$$

where: $\rho_{rc^*(AB)}$: solid fraction when component A starts to percolate
 $\rho_{rc(A)}$: critical relative density of component A
 $\rho_{t(A)}$, $\rho_{t(B)}$: true density of component A and component B, respectively
 $X_{(A)}$: mass fraction of component A

The divergence between the “experimental” and the “theoretical” curve is more pronounced for Ethocel[®] compared to Avicel PH101[®]. The slope of the “experimental” curve is much smaller in the case of Ethocel[®]. It could be suggested that the coincidence of both curves is getting better as the difference between both substances (substance A and substance B) concerning the compactibility is increasing. This assumption could be supported by the fact that the radial tensile strength of Avicel PH101[®] is much higher compared to Ethocel[®] (see figure 14 and figure 16). Thus, the effect of acetaminophen can be neglected in a broader range in the case of Avicel PH101[®].

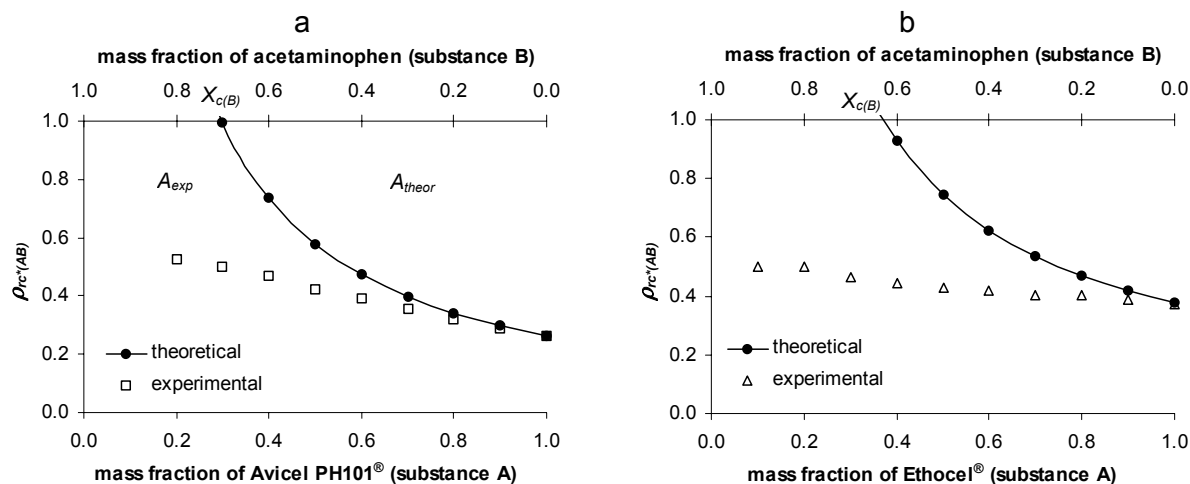


Figure 15: Theoretical and experimental “critical” solid fraction $\rho_{rc^*(AB)}$ as a function of the mass fraction of the excipient. a: excipient: Avicel PH101®; b: excipient: Ethocel®.

The calculated values of the critical relative densities (see table 11) for the two monosubstances (100% Avicel PH101® and 100% Ethocel®) are very close to those of the relative tapped densities (see table 10). These findings are in agreement with the results of Kuentz and Leuenberger [40]. The lower percolation threshold for pure Avicel PH101® compared to Ethocel® results in a higher dilution capacity for Avicel PH101® according to equation (14). The determination of the dilution capacity for Avicel PH101® and Ethocel® according to Minchom *et al.* is illustrated in figure 16. The corresponding values listed in table 12 are very similar compared with those calculated according to the new equation. Also using acetaminophen as poorly compactable substance, Habib *et al.* [52] determined the dilution capacity of Avicel PH101® based on the concept of Minchom *et al.*. They found a dilution capacity of 65%, which is very close to the value calculated within this study (64.6%). However, considering figure 16, the drawback of Minchom’s procedure becomes quite obvious. There is no clear linear range visible (see correlation coefficient in figure 16), thus the selection of the data for the linear fit is problematic. On the one hand, the extrapolation should not be performed from afar, *i.e.* the area ratios of lower mass fractions of the excipient should be preferred for the linear regression. On the other hand the influence of the poorly compactable substance is increasing at lower mass fractions of the excipient. Thus, the resulting dilution capacity is no longer reflecting a pure property of substance A. In this study, the linear regression was performed in the range of 50-100% (w/w) of excipient, knowing that the result is affected by the property of acetaminophen.

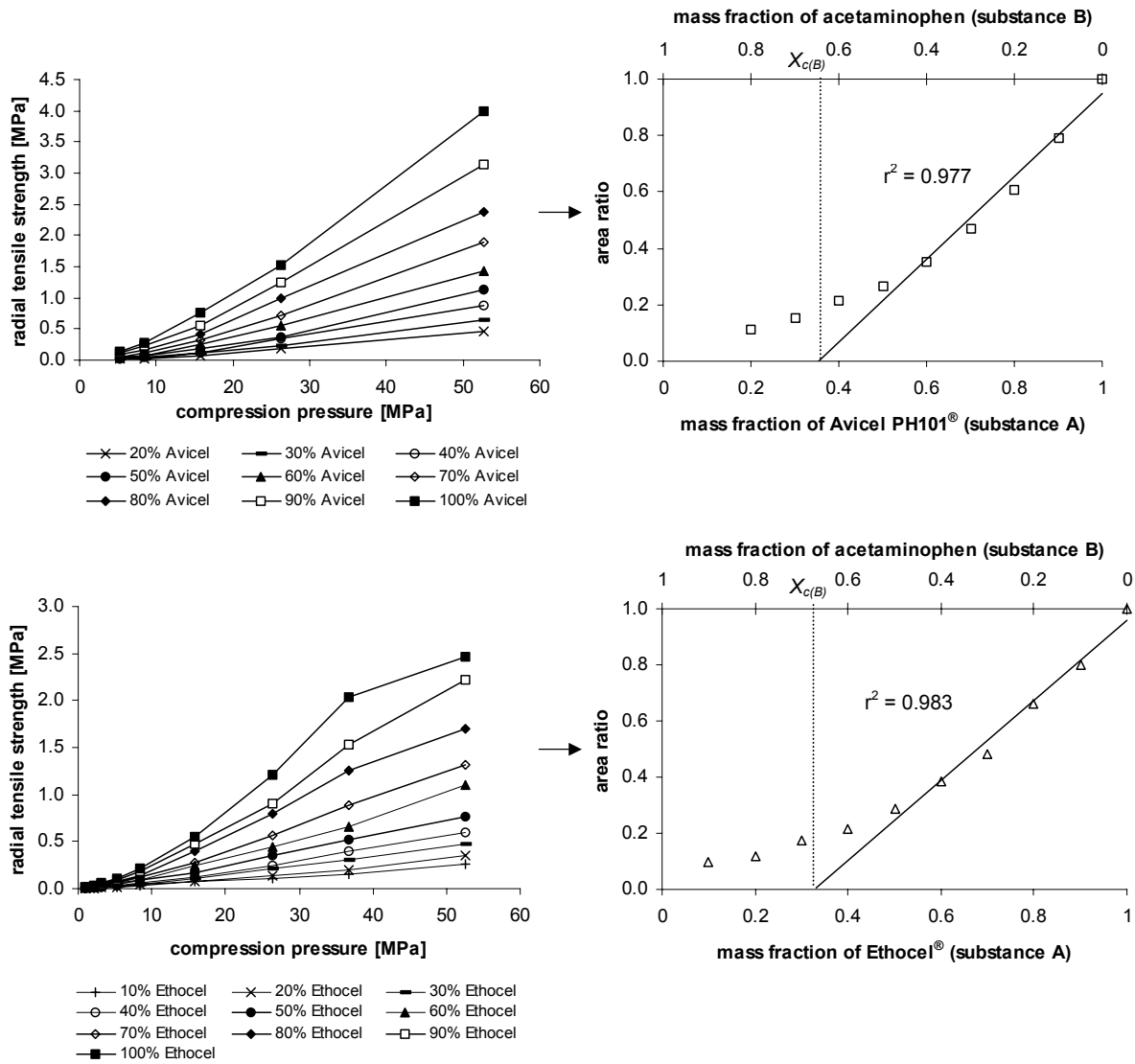


Figure 16: Visualization of the determination of the dilution capacity for Avicel PH101® and Ethocel® according to Minchom [45] (please notice the different scaling of the y-axis in the tensile strength diagrams).

Table 12: Dilution capacity of Avicel PH101® and Ethocel®.

excipient	Dilution capacity, $X_{c(B)}$ [%]	
	according to the equation (14)	according to Minchom <i>et al.</i> [45]
Avicel PH101®	70.0	64.6
Ethocel®	63.7	67.3

6 Conclusions and outlook

The concept of analogies turned out to be very fruitful to describe processes like the compression and the flow.

The equation derived from the Van der Waals equation of state revealed to be extremely well suited to describe the compression behavior of several particulate materials. Unlike the Heckel equation, the adapted Van der Waals equation is valid over the whole compression pressure range for both, brittle and plastic substances.

The present study was performed by means of “in die” data. In further studies, the derived equation should also be used to analyze data, obtained by “out of die” measurements. Thereby, the assumption could be confirmed that the parameter B_v equals the true volume V_t of the compressed material. The two other parameters A_v and C_v could not yet be assigned exactly to a physical property of the compressed substances. However, both parameters seem to correlate with the mean yield pressure, obtained by the Heckel analysis.

It has to be pointed out, that there are some important differences between gases and particles. Apart from the fact, that the temperature has a totally different impact on the two systems (see also page 111), it is important to notice, that the particle collisions are in general inelastic whereas the collisions in a gas are supposed to be elastic.

Considering these discrepancies between both systems and the fact that the Van der Waals equation is also just an approximation for describing the state of gases, it is well-conceivable that further modifications have to be performed to adapt the equation in order to describe the behavior of particulate material. According to the modified Van der Waals equation, the “inner pressure” p_{attr} is proportional to the square of the relative density. Although it is plausible that p_{attr} is depending on the relative density, further approaches could assume that p_{attr} and the relative density are just related in a linear manner.

Concerning the flow study, the equation derived from Fick’s first law proved to be very successful at least for the investigated spherical particles. If the correlation of the critical diameter d_{crit} with the particle diameter $d_{particle}$ and the correlation of the mass permeability coefficient Π^* with the particle diameter $d_{particle}$ are known, it should be possible to predict the flow of the particles according to this equation knowing the bulk density and the particle diameter.

It would be extremely interesting to look for a relationship between the mass permeability coefficient Π^* and cohesion and adhesion properties of the used material. These friction properties could be accessible by shear cell experiments.

The use of flow regulating agents such as colloidal silicon dioxide could provide further information for the meaning of the mass permeability coefficient. In the case of Sugar

spheres[®], first experiments showed that the mass permeability coefficient is extremely sensitive to powder residue due to abrasion.

In our experiments we just dealt with the flowability of spherically shaped particles. The flow of irregularly shaped particles like granules should therefore also be investigated. Furthermore, the shape (half center angle) and the material of the hopper has not yet been taken into account.

Under the theoretical assumption that only the well compactable substance A contributes to the strength of the tablet when combined with a completely non-compactable substance B, equation (24) can be used to calculate the minimal solid fraction $\rho_{rc^*(AB)}$, which is necessary to get tablets of minimal strength ($\sigma_t \geq 0$) at a given mass fraction $X_{(A)}$ of substance A.

$$\rho_{rc^*(AB)} = \rho_{rc(A)} \left(1 + \frac{1 - X_{(A)}}{X_{(A)}} \cdot \frac{\rho_{t(A)}}{\rho_{t(B)}} \right) \quad \text{equation (24)}$$

where: $\rho_{rc^*(AB)}$: solid fraction when component A starts to percolate
 $\rho_{rc(A)}$: critical relative density of component A
 $\rho_{t(A)}$, $\rho_{t(B)}$: true density of component A and component B, respectively
 $X_{(A)}$: mass fraction of component A

However, in reality every compacted substance exhibits at least a small mechanical strength. Thus, equation (24) can be considered to be very rigorous. In consequence, using equation (24) for the development of a new formulation, scientists will always be on the safe side.

$$X_{c(B)} = 1 - \frac{\rho_{t(A)}}{\rho_{t(B)}} \cdot \frac{1}{\left(\frac{\rho_{t(A)}}{\rho_{t(B)}} + \frac{1}{\rho_{rc(A)}} - 1 \right)} \quad \text{equation (14)}$$

where: $X_{c(B)}$: dilution capacity
 $\rho_{t(A)}$: true density of component A [g/cm³]
 $\rho_{t(B)}$: true density of component B [g/cm³]
 $\rho_{rc(A)}$: critical relative density of component A

The values for the dilution capacity calculated according to the new equation (equation (14)) were very close to the values determined according to the method of Minchom [45]. However, the technique of Minchom is hampered by the problem of selecting a linear region for the fitting procedure. The new method is free of such arbitrary elements and is less time consuming, since only the critical relative density $\rho_{rc(A)}$ of component A has to be determined. Furthermore, the dilution capacity according to the new equation is not affected by the property of the poorly compactable substance and can therefore be considered to reflect an inherent property of the excipient. Because $\rho_{rc(A)}$ is usually very close to the relative tapped density $\rho_{rtapped}$, the following rule of thumb may be postulated as a first approximation: The

value for the dilution capacity can be supposed to be around the difference $1 - \rho_{rtapped}$. However, this rough estimation is only valid if the true densities of both substances are very similar (compare with the results of Ethocel®).

It has to be kept in mind that the dilution capacity according to the new equation assures just a minimal strength ($\sigma_t \geq 0$), which is not *a priori* consistent with the original definition according to Wells *et al.* [44] who associated the dilution capacity with “satisfactory” properties of the tablets. Therefore, in the case of a practical application, it has to be verified if really 100% of the maximum possible dilution capacity can be utilized. This could be possible, since the poorly compactable substance always contributes to some extent to the strength of the compact. However, in terms of a robust formulation, it is proposed not to exceed 90% of the possible dilution capacity.

In future studies, the validity and relevance of the new equations have to be verified examining further substances used for direct compression (e.g. UICEL).

7 References

- [1] Bateman, H. (1910) The solution of a system of differential equations occurring in the theory of radioactive transformations. *Proceedings of the Cambridge Philosophical society*, **XV**, part V, 423-427.
- [2] Leuenberger, H., Lanz, M. (2002) Powder – the fourth state of matter? *Pharm Tech Japan*, **18**(7), 995-1001.
- [3] D'Anna, G., Mayor, P., Barrat, A., Loreto, V., Nori, F. (2003) Observing brownian motion in vibration-fluidized granular matter. *Nature*, **424**(6951), 909-912.
- [4] Jaeger, H.M., Nagel, S.R., Behringer, R.P. (1996) Granular solids, liquids, and gases. *Reviews of Modern Physics*, **68**(4), 1259-1273.
- [5] Alderborn, G., Nyström, C. (1996) Nomenclature. In: *Pharmaceutical Powder Compaction Technology*, Alderborn, G., Nyström, C. (Eds), Marcel Dekker, New York.
- [6] Jetzer, W., Leuenberger, H., Sucker, H. (1983) The compressibility and compactibility of pharmaceutical powders. *Pharmaceutical Technology*, **7**(4), 33-39.
- [7] Train, D. (1956) An investigation into the compaction of powders. *Journal of Pharmacy and Pharmacology*, **8**(10), 745-761.
- [8] Fell, J.T., Newton, J.M. (1971) Effect of particle size and speed of compaction on density changes in tablets of crystalline and spray-dried lactose. *Journal of Pharmaceutical Sciences*, **60**(12), 1866-1869.
- [9] Roberts, R.J., Rowe, R.C. (1986) The effect of the relationship between punch velocity and particle size on the compaction behaviour of materials with varying deformation mechanisms. *Journal of Pharmacy and Pharmacology*, **38**(8), 567-571.
- [10] Duberg, M., Nyström, C. (1982) Studies on direct compression of tablets. *Acta Pharmaceutica Suecica*, **19**(6), 421-436.
- [11] Roberts, R.J., Rowe, R.C. (1985) The effect of punch velocity on the compaction of a variety of materials. *Journal of Pharmacy and Pharmacology*, **37**(6), 377-384.
- [12] Nokhodchi, A. (2005) An overview of the effect of moisture on compaction and compression. *Pharmaceutical Technology*, **29**(1) 46-66.
- [13] Alderborn, G. (1996) Particle dimensions. In: *Pharmaceutical Powder Compaction Technology*, Alderborn, G., Nyström, C. (Eds), Marcel Dekker, New York.
- [14] Celik, M. (1992) Overview of compaction data analysis techniques. *Drug Development and Industrial Pharmacy*, **18**(6,7), 767-810.
- [15] Heckel, R.W. (1961a) Density pressure relationships in powder compaction. *Transactions of the Metallurgical Society of AIME*, **221**, 671-675.
- [16] Heckel, R.W. (1961b) An analysis of powder compaction phenomena. *Transactions of the Metallurgical Society of AIME*, **221**, 1001-1008.
- [17] Kuentz, M., Leuenberger, H. (1999) Pressure susceptibility of polymer tablets as a critical property: a modified Heckel equation. *Journal of Pharmaceutical Science*, **88**(2), 174-179.
- [18] Kawakita, K., Lüdde, K.-H. (1970/71) Some considerations on powder compression equations. *Powder Technology*, **4**, 61-68.
- [19] Cooper, A.R., Eaton, L.E. (1962) Compaction behavior of several ceramic powders. *Journal of the American Ceramic Society*, **45**(3), 97-101.

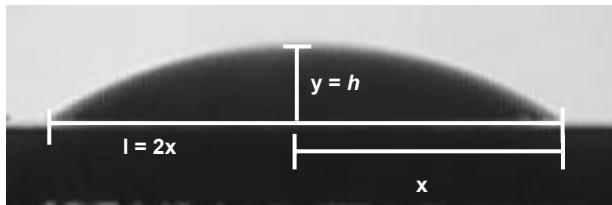
- [20] Van der Waals, J.D. (1873) On the continuity of the gaseous and liquid states. Thesis, University at Leiden.
- [21] Berthelot, M.D. (1907) Sur les thermomètres à gaz et sur la réduction de leurs indications à l'échelle absolue des températures. *Travaux et Mémoires du bureau international des poids et mesures*, Tome XIII, 1-113.
- [22] Dieterici, C. (1899) Über den kritischen Zustand. *Annalen der Physik und Chemie*. Neue Folge, **69**, 685-705.
- [23] Führer, C. (1965) Über den Druckverlauf bei der Tablettierung. *Deutsche Apotheker-Zeitung*, **105**(34), 1150-1153.
- [24] Prescott, J.K., Barnum, R.A. (2000) On powder flowability. *Pharmaceutical Technology*, **24**(10), 60-84.
- [25] Train, D. (1958) Some aspects of the property of angle of repose of powders. *Journal of Pharmacy and Pharmacology*, **10**(Suppl.), 127T-135T.
- [26] Schwedes, J. (1996) Measurement of flow properties of bulk solids. *Powder Technology*, **88**, 285-290.
- [27] Carr, R.L. (1965a) Evaluating flow properties of solids. *Chemical Engineering*, **72**(2), 163-168.
- [28] Carr, R.L. (1965b) Classifying flow properties of solids. *Chemical Engineering*, **72**(3), 69-72.
- [29] Hausner, H.H. (1967) Friction conditions in a mass of metal powders. *International Journal of Powder Metallurgy*, **3**(4), 7-13.
- [30] Flory, P.J. (1941) Molecular size distribution in three dimensional gelation I-III. *Journal of the American Chemical Society*, **63**(11), 3083-3090, 3091-3096, 3096-3100.
- [31] Stockmayer, W. H. (1943) Theory of molecular size distribution and gel formation in branched-chain polymers. *Journal of Chemical Physics*, **11**(2) 45-55.
- [32] Broadbent, S.R., Hammersley, J.M. (1957) Percolation processes. I. Crystals and mazes. *Proceedings of the Cambridge Philosophical Society, Mathematical and physical sciences*, **53**, 629-641.
- [33] Stauffer, D., Aharony, A. (1994) Introduction to percolation theory, revised second edition. Taylor and Francis, London.
- [34] Ottavi, H., Clerc, J., Giraud, G., Roussenoq, J., Guyon, E., Mitescu, C.D. (1978) Electrical conductivity of a mixture of conducting and insulating spheres: an application of some percolation concepts. *Journal of Physics C: Solid State Physics*, **11**(7), 1311-1328.
- [35] Kirkpatrick, S. (1973) Percolation and Conduction. *Reviews of Modern Physics*, **45**(4), 574-588.
- [36] Sahimi, M. (1994) Applications of percolation theory. Taylor and Francis, London.
- [37] Dammer, S.M., Hinrichsen, H. (2003) Epidemic spreading with immunization and mutations. *Physical Review E*, **68**, 016114 1-8.
- [38] Leuenberger, H., Rohera, B.D., Haas, C. (1987) Percolation theory – a novel approach to solid dosage form design. *International Journal of Pharmaceutics*, **38**(1-3), 109-115.
- [39] Leuenberger, H. (1999) The application of percolation theory in powder technology. *Advanced Powder Technology*, **10**(4), 323-352.
- [40] Kuentz, M., Leuenberger, H. (2000) A new theoretical approach to tablet strength of a binary mixture consisting of a well and a poorly compactable substance. *European Journal of Pharmaceutics and Biopharmaceutics*, **49**(2), 151-159.

-
- [41] Kuentz, M., Leuenberger, H., Kolb, M. (1999) Fracture in disordered media and tensile strength of microcrystalline cellulose tablets at low relative densities. *International Journal of Pharmaceutics*, **182**(2), 243-255.
- [42] Ryshkewitch, E. (1953) Compression strength of porous sintered alumina and zirconia. *Journal of the American Ceramic Society*, **36**(2), 65-68.
- [43] Guyon, E., Roux, S., Bergmann, D.J. (1987) Critical behaviour of electric failure thresholds in percolation. *Journal de Physique*, **48**(6), 903-904.
- [44] Wells, J.I., Langridge, J.R. (1981) Dicalcium phosphate dihydrate – microcrystalline cellulose systems in direct compression tableting. *International Journal of Pharmaceutical Technology and Product Manufacture*, **2**(2), 1-8.
- [45] Minchom, C.M., Armstrong, N.A. (1987) A proposed technique for expressing the capacity of directly compressible tablet diluents. *British Pharmaceutical Conference*, 69P.
- [46] Stahl, P.H. (1980) Feuchtigkeit und Trocknen in der pharmazeutischen Technologie. D. Steinkopf Verlag, Darmstadt.
- [47] Hersey, J.A., Rees, J.E. (1971) Deformation of particles during briquetting. *Nature Physical Science*, **230**, 96.
- [48] Newton, J.M., Rowley, G.J., Fell, T., Peacock D.G. and Ridgway, K. (1971) Computer analysis of the relation between tablet strength and compaction pressure. *Journal of Pharmacy and Pharmacology*, **23**(Suppl.), 195-201.
- [49] Parmentier, W. (1978) Untersuchungen zur Interpretation von Kraft-Weg-Diagrammen. *Pharmazeutische Industrie*, **40**(8), 860-865.
- [50] Lüdde, K.-H., Kawakita, K. (1966) Die Pulverkompression. *Die Pharmazie*, **21**(7), 393-403.
- [51] Schwedes, J. (1970) Fliessverhalten von Schüttgütern in Bunkern. Verlag Chemie, Weinheim.
- [52] Habib, Y., Augsburger, L., Reier, G., Wheatley, T., Shangraw, R. (1996) Dilution Potential: A new perspective. *Pharmaceutical Development and Technology*, **1**(2), 205-212.

Appendix

Appendix A (contact angle: height and length method)

(Assumption: projected drop is a segment of a circle and contact angle $\theta < 90^\circ$)

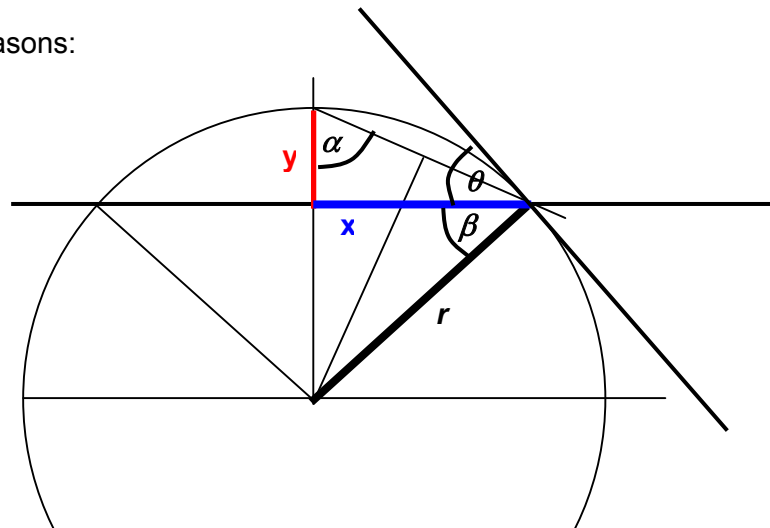


It follows for trigonometric reasons:

$$(1) \cos \alpha = \frac{y}{\sqrt{x^2 + y^2}}$$

$$(2) \beta = \alpha - \left(\frac{\pi}{2} - \alpha\right) = 2\alpha - \frac{\pi}{2}$$

$$(3) \alpha = \arctan \frac{x}{y}$$



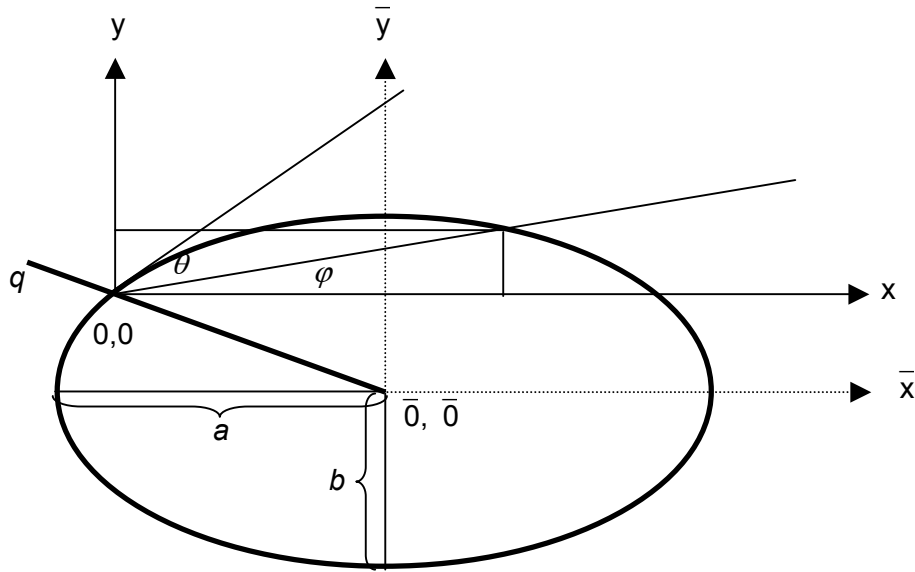
$$r = \frac{\sqrt{x^2 + y^2}}{2} \cdot \overset{(1)}{\frac{1}{\cos \alpha}} = \frac{\sqrt{x^2 + y^2}}{2} \cdot \frac{\sqrt{x^2 + y^2}}{y} = \frac{x^2 + y^2}{2 \cdot y} \quad (4)$$

$$\theta = \frac{\pi}{2} - \overset{(2)}{\beta} = \frac{\pi}{2} - \left(2\alpha - \frac{\pi}{2}\right) = \pi - 2\alpha = \pi - 2 \cdot \overset{(3)}{\arctan \frac{x}{y}} \quad (5)$$

With a drop length $l = 2x$ and drop height $h = y$ the contact angle becomes:

$$\theta = \pi - 2 \cdot \arctan \frac{l}{2h} \quad (6)$$

Appendix B (contact angle: ellipse fitting method)



$$\text{Ellipse equation: } \frac{\bar{x}^{-2}}{a^2} + \frac{\bar{y}^{-2}}{b^2} = 1 \quad (1)$$

$$\text{with } c = \frac{b}{a} \quad (2)$$

$$\text{follows: } \bar{x}^{-2} c^2 + \bar{y}^{-2} = b^2 \quad (3)$$

The coordinates of the point of intersection of the ellipse and a line $q: \bar{y} = m \cdot \bar{x}$ are:

$$\bar{x} = \frac{b}{\sqrt{c^2 + m^2}}, \bar{y} = \frac{mb}{\sqrt{c^2 + m^2}} \quad (4)$$

Coordinate transformation: $\bar{0}, \bar{0} \Rightarrow 0, 0$

The origin of the new coordinate system equals the calculated point of intersection:

$$x = \bar{x} + \frac{b}{\sqrt{c^2 + m^2}}, y = \bar{y} - \frac{mb}{\sqrt{c^2 + m^2}} \quad (5)$$

Substitution of \bar{x} and \bar{y} from equation (5) in equation (3) results in the ellipse equation of the new coordinate system:

$$\left(x - \frac{b}{\sqrt{c^2 + m^2}}\right)^2 c^2 + \left(y + \frac{mb}{\sqrt{c^2 + m^2}}\right)^2 = b^2 \quad (6)$$

$$\text{or: } y = \sqrt{b^2 - c^2 \left(x - \frac{b}{\sqrt{c^2 + m^2}}\right)^2} - \frac{mb}{\sqrt{c^2 + m^2}} \quad (7)$$

$$\text{for the angle } \varphi \text{ we can write: } \tan \varphi = \frac{y}{x} = \frac{\sqrt{b^2 - c^2 \left(x - \frac{b}{\sqrt{c^2 + m^2}} \right)^2} - \frac{mb}{\sqrt{c^2 + m^2}}}{x} \quad (8)$$

The contact angle θ results when x approaches 0. For the calculation of this limit value we use the law of Bernoulli-de l'Hospital (equation (9)):

$$\lim_{x \rightarrow 0} \frac{f(x)}{g(x)} = \lim_{x \rightarrow 0} \frac{f'(x)}{g'(x)} \quad (9)$$

it follows:

$$\begin{aligned} \lim_{x \rightarrow 0} \frac{\sqrt{b^2 - c^2 \left(x - \frac{b}{\sqrt{c^2 + m^2}} \right)^2} - \frac{mb}{\sqrt{c^2 + m^2}}}{x} &= \lim_{x \rightarrow 0} \frac{1}{2} \cdot \frac{-2c^2 \left(x - \frac{b}{\sqrt{c^2 + m^2}} \right)}{\sqrt{b^2 - c^2 \left(x - \frac{b}{\sqrt{c^2 + m^2}} \right)^2}} = \\ &= \frac{\frac{c^2 b}{\sqrt{c^2 + m^2}}}{\sqrt{b^2 - \frac{c^2 b^2}{c^2 + m^2}}} = \frac{\frac{c^2 b}{\sqrt{c^2 + m^2}}}{\sqrt{\frac{b^2 c^2 + b^2 m^2 - b^2 c^2}{c^2 + m^2}}} = \frac{c^2 b}{bm} = \frac{c^2}{m} \end{aligned}$$

$$\text{To summarize: } \tan \theta = \frac{c^2}{m} \quad (10)$$

The coordinates of the drop are fitted with equation (7). The resulting parameters b , c and m are then used to calculate the contact angle θ according to equation (10).

If the ellipse is approaching a circle (ratio c of the ellipse axis equals 1) then $\tan \theta$ becomes m^{-1} .

Appendix C (Washburn equation)

The Washburn equation can be derived from Poiseuille's law (equation (1)) and the capillary pressure Δp (equation (2)).

$$\frac{dV}{dt} = \frac{\pi \cdot \Delta p}{8\eta \cdot l} \cdot r^4 \quad (1)$$

where: V : adsorbed volume of the liquid
 η : viscosity of the liquid
 l : length of the column of liquid after time t
 r : radius of the capillary

$$\Delta p = \frac{2\gamma \cdot \cos \theta}{r} \quad (2)$$

where: γ : surface tension of the liquid
 θ : contact angle

For the volume V of a capillary we can write:

$$V = l \cdot r^2 \cdot \pi \quad (3)$$

Putting the equations (2) and (3) in equation (1) gives us the differential equation (4).

$$\frac{dV}{dt} = \frac{\pi \cdot r^2 \cdot \pi}{8\eta \cdot V} \cdot r^4 \cdot \frac{2\gamma \cdot \cos \theta}{r} = \frac{\pi^2 \cdot r^5 \cdot \gamma \cdot \cos \theta}{4\eta \cdot V} \quad (4)$$

Integrating equation (4) we find the following expression for the volume:

$$V^2 = \frac{\pi^2 \cdot r^5 \cdot \gamma \cdot \cos \theta}{2\eta} \cdot t + l \quad (5)$$

The integration constant l has to be 0 because the volume at the time $t = 0$ equals 0.

In a rough approximation the porous body can be considered as a bundle of n capillaries ($V_n = V \cdot n$). Furthermore we can introduce the expression for the weight m : $m = \rho \cdot V_n$, where ρ is the density of the liquid. So we get equation (6).

$$m^2 = \frac{\pi^2 \cdot r^5 \cdot \gamma \cdot \cos \theta}{2\eta} \cdot t \cdot n^2 \cdot \rho^2 \quad (6)$$

$$\text{or: } m^2 = \frac{c \cdot \gamma \cdot \cos \theta}{\eta} \cdot t \cdot \rho^2 \quad \text{with} \quad c = \frac{\pi^2 \cdot r^5}{2} \cdot n^2$$

Appendix D (equation for drug release)

Fick's first law (1) represents the basis of the new semi-heuristic equation.

$$J = \frac{dm}{dt \cdot A} = D \cdot \frac{(c_s - c)}{\Delta h} \approx D \cdot \frac{c_s}{\Delta h} \quad (1)$$

where: J : flux [mg/min/cm²]

m : amount of drug, which is dissolved [mg]

t : time [min]

A : surface area [cm²]

D : diffusion constant (diffusion coefficient, diffusivity) for the drug that is diffusing in the medium [cm²/min]

$(c_s - c)/\Delta h$: concentration gradient [mg/cm⁴]

c_s : solubility [mg/cm³]

c : concentration of drug in the medium at time t [mg/cm³]

Assuring perfectly sink conditions and keeping the stirring speed unchanged, the flux J may be assumed to be constant. It can be acquired from the intrinsic dissolution measurement or from an equivalent method where the surface area is known.

In order to describe the dissolution rate, equation (1) can be rewritten (2).

$$\frac{dm}{dt} = J \cdot A(t) \quad (2)$$

Considering a tablet containing a disintegrant, the surface area A will be a function of the disintegration and dissolution. The disintegration leads to an increase, whereas the dissolution causes a decrease of the surface area. Looking at the plot of the surface area versus time for a tablet consisting of 95% of proquazone and 5% of UICEL as disintegrant (figure 1), the profile reminds of the Bateman equation, which is used in pharmacokinetics to describe the concentration of a drug in the plasma by considering absorption and elimination to be first order processes.

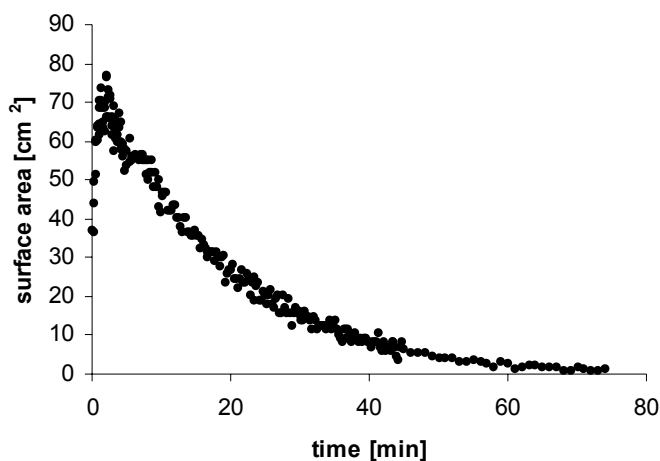


Figure 1: Surface area during the release of proquazone from a tablet containing 5% of UICEL as disintegrant.

Thus, equation (3) is proposed to describe the surface area in function of time by analogy to the Bateman equation.

$$A = A_0 \frac{k_1}{k_1 - k_2} (e^{-k_2 t} - e^{-k_1 t}) \quad (3)$$

where: A : surface area [cm^2]

A_0 : maximum possible surface area [cm^2]

k_1 : rate of area increase due to disintegration ("disintegration rate") [min^{-1}]

k_2 : rate of area decrease due to dissolution ("dissolution rate") [min^{-1}]

t : time [min]

The following differential equation system can be considered as origin of equation (3).

$$\frac{dA}{dt} = k_1 \cdot A_p - k_2 \cdot A \quad (4)$$

$$\frac{dA_p}{dt} = -k_1 \cdot A_p \quad (5)$$

where: A_p : inherent surface area (of proquazone particles) which can be accessed by disintegration ($A_{p0} = A_0$)

Integrating the combination of equation (2) and equation (3) gives us equation (6).

$$m(t) = J \cdot A_0 \frac{k_1}{k_1 - k_2} \left(-\frac{1}{k_2} e^{-k_2 t} + \frac{1}{k_1} e^{-k_1 t} \right) + I \quad (6)$$

The integration constant I can be obtained by using $m(0) = 0$ as boundary condition (7).

$$I = J \cdot A_0 \frac{k_1}{k_1 - k_2} \left(\frac{1}{k_2} - \frac{1}{k_1} \right) \quad (7)$$

Combining equation (6) with equation (7) we get the final result for the amount of drug m , which is dissolved at time t (8).

$$m(t) = J \cdot A_0 \frac{k_1}{k_1 - k_2} \left(\frac{1}{k_2} (1 - e^{-k_2 t}) - \frac{1}{k_1} (1 - e^{-k_1 t}) \right) \quad (8)$$

Appendix E (disintegration time)

The disintegration may be considered to be made up of two distinct processes: water uptake and the rupture of the hydrogen bonds between the particles.

1) Water uptake

The water uptake can be described by the Washburn equation (equation (1)):

$$l^2 = \frac{r \cdot \gamma \cdot \cos \theta}{2\eta} \cdot t_w = t_w \cdot K_1 \quad \text{or: } t_w = \frac{l^2}{K_1} \quad (1)$$

where: l : length of the column of liquid after time t_w
 r : radius of the capillary
 γ : surface tension of the liquid
 θ : contact angle
 η : viscosity of the liquid
 t_w : time
 K_1 : constant

Since the water can penetrate during disintegration from the upper and lower surface area into the tablet, the tablet is totally saturated due to capillarity when the water reaches half the height of the tablet $h_0/2$. Thus, according to equation (1) we can write for the corresponding time t_{wd} equation (2).

$$t_{wd} = \frac{h_0^2}{4 \cdot K_1} \quad (2)$$

where: h_0 : height of the tablet

2) Annihilation of the bonds

Figure 1 depicts two particles, which are brought in contact during compression. The circle area with the radius r represents the bonding area.

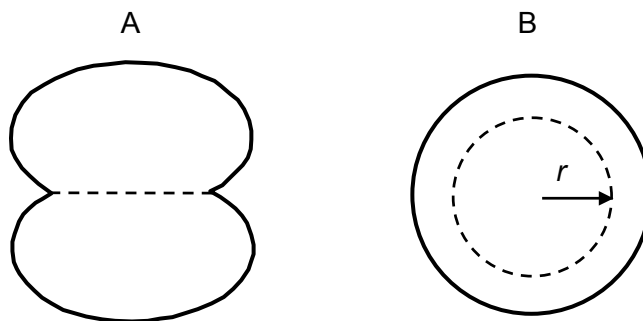


Figure 1: Two compressed particles. A: side view; B: top view; r is the radius of the bonding area.

The bonds that are accessible for annihilation are located on the perimeter of the bonding area. Thus, equation (3) is proposed for the decrease of number of bonds dN_b/dt_s .

$$\frac{dN_b}{dt_s} = -k \cdot \frac{2\pi \cdot r}{\sqrt{A_b}} \quad (3)$$

where: N_b : number of bonds

k : annihilation rate constant

r : radius of the bonding area

A_b : area of one bonding-site; $\sqrt{A_b}$: distance between two bonds

The total number of bonds N_b is given by equation (4).

$$N_b = \frac{r^2 \cdot \pi}{A_b} \quad (4)$$

Combining equation (3) with equation (4) gives the differential equation (5).

$$\frac{dN_b}{\sqrt{N_b}} = -2k \cdot \sqrt{\pi} \cdot dt_s \quad (5)$$

The final equation (6) results by the integration of equation (5), taking into account the boundary condition: $N_b(t_s=0) = N_{b0}$.

$$\sqrt{N_{b0}} - \sqrt{N_b} = k \cdot \sqrt{\pi} \cdot t_s \quad \text{or: } t_s = \frac{\sqrt{N_{b0}} - \sqrt{N_b}}{k \cdot \sqrt{\pi}} = \frac{\sqrt{N_{b0}} - \sqrt{N_b}}{K_2} \quad (6)$$

$$\text{with: } N_{b0} = \frac{r_0^2 \cdot \pi}{A_b} = r_0^2 \cdot \pi \cdot \rho_b$$

where: r_0 : radius of the bonding area at time $t = 0$

ρ_b : area density of bonds

$$K_2 = k \cdot \sqrt{\pi}$$

The two particles are separated at time t_{sd} when the number N_b equals 0. Therefore, we can write equation (7) for the time t_{sd} .

$$t_{sd} = \frac{\sqrt{r_0^2 \cdot \pi \cdot \rho_b}}{K_2} \quad (7)$$

3) Combination of the two processes

The total time t_{tot} for both processes can be considered as sum of the times for each single process (equation (8)).

$$t_{tot} = t_w + t_s = \frac{l^2}{K_1} + \frac{\sqrt{N_{b0}} - \sqrt{N_b}}{K_2} \quad (8)$$

If we assume that the disintegration is completed as soon as the particles in the centre of the tablet are disintegrated then the overall disintegration time t_{totd} is given by equation (9). This condition for the determination of the disintegration may be regarded as very rigorous, since particles of a diameter of 2 mm already pass through the screen of the disintegration apparatus and meet therefore the requirements for disintegration a long time before they are disintegrated into the primary particles.

$$t_{totd} = t_{wd} + t_{sd} = \frac{h_0^2}{4 \cdot K_1} + \frac{\sqrt{N_{b0}}}{K_2} \quad (9)$$

where: t_{totd} : disintegration time

t_{wd} : time till all pores within a tablet are filled with water

t_{sd} : time till two particles are totally separated

h_0 : height of the tablet

N_{b0} : total amount of bonds between two particles at the beginning

K_1 : constant (see equation (1))

K_2 : annihilation rate constant

Appendix F (flow of a liquid out of a hopper)

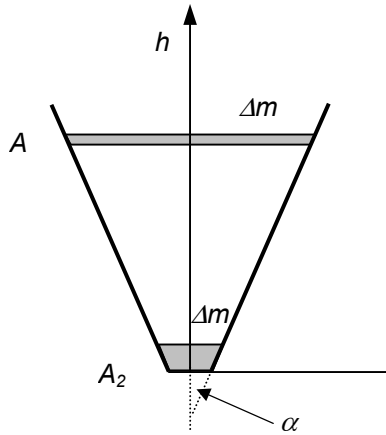


Figure 1: hopper

The outflow Q is defined as:

$$Q = -\frac{dV}{dt} \quad (1)$$

where: V : is the volume of liquid in the hopper
 t : time

For reasons of mass conservation, the following equations must hold true.

$$Q = A_2 \cdot v_2 \quad (2)$$

$$Q = A \cdot v \quad (3)$$

where: A : surface area of the
 A_2 : Area of the orifice
 v : velocity of the liquid on the liquid surface
 v_2 : velocity of the liquid at the orifice

Some trigonometric considerations lead to the two following relationship:

$$h \approx \left(\frac{3V}{\tan^2 \alpha \cdot \pi} \right)^{1/3} \quad (4)$$

$$A \approx h^2 \tan^2 \alpha \cdot \pi \quad (5)$$

1) approach neglecting effect of viscosity

Considering the principle of energy conservation, we can write for a thin layer with the mass Δm (see figure 1):

$$\Delta mgh + \frac{\Delta m}{2} v^2 = \frac{\Delta m}{2} v_2^2 \quad (6)$$

Assuming $A_2 \ll A$ and combining equation (6) with equation (2) and (3) gives:

$$2gh = Q^2 \left(\frac{1}{A_2^2} - \frac{1}{A^2} \right) = Q^2 \left(\frac{A^2 - A_2^2}{A^2 A_2^2} \right) \approx Q^2 \frac{1}{A_2^2} \quad (7)$$

Taking into account the definition of the outflow Q (equation (2)) and replacing h with the term in equation (4) result in:

$$\left(2g \left(\frac{3V}{\tan^2 \alpha \cdot \pi} \right)^{1/3} \right)^{1/2} = -\frac{dV}{dt} \cdot \frac{1}{A_2} \quad (8)$$

This differential equation can be solved:

$$V = \left[V_0^{5/6} - \frac{5}{6} A_2 \sqrt{2g} \cdot \left(\frac{3}{\tan^2 \alpha \cdot \pi} \right)^{1/6} \cdot t \right]^{6/5} \quad (9)$$

Since V is the volume of the liquid in the hopper, the discharged mass m_d can be expressed with the following equation:

$$m_d = m_0 - \left[m_0^{5/6} - \frac{5}{6} A_2 \rho^{5/6} \sqrt{2g} \cdot \left(\frac{3}{\tan^2 \alpha \cdot \pi} \right)^{1/6} \cdot t \right]^{6/5} \quad (10)$$

2) approach including effect of viscosity

Considering a real flow with inherent friction, we can rewrite equation (6) in the following way.

$$\Delta mgh + \frac{\Delta m}{2} v^2 = \frac{\Delta m}{2} v_2^2 + \Delta p \Delta V \quad (11)$$

Introducing the density ρ of the liquid, we obtain:

$$2gh + v^2 = v_2^2 + \Delta p \frac{2}{\rho} \quad (12)$$

The drop of pressure Δp can be expressed by the resistance R and the outflow Q .

$$\Delta p = R \cdot Q \quad (13)$$

According to the law of Hagen-Poiseuille the resistance R in a tube is given by:

$$R = \frac{8\eta \cdot l}{\pi \cdot r^4} \quad (14)$$

where: η : viscosity of the liquid

l : length of the tube

r : radius of the tube

As a first approximation we can write for the resistance R in a conical shaped hopper:

$$\frac{1}{R} = \frac{1}{R_1} + \frac{1}{R_2} + \dots + \frac{1}{R_n} = \frac{\pi}{8\eta} \left(\frac{r_1^4 + r_2^4 + \dots + r_n^4}{\Delta h} \right) \quad (15)$$

The radius r can be expressed by the height h :

$$r = h \cdot \tan \alpha + r_{or} \quad (16)$$

where: α : half center angle

r_{or} : radius of the orifice

Equation (15) can be rewritten as integral. Together with equation (16) the following expression results for the resistance R .

$$R = \frac{8\eta}{\pi} \cdot \lim_{n \rightarrow \infty} \frac{\Delta h}{r_1^4 + r_2^4 + \dots + r_n^4} = \frac{8\eta}{\pi} \cdot \int_0^{h_0} \frac{1}{(h \cdot \tan \alpha + r_{or})^4} \cdot dh = \frac{8\eta}{3\pi \cdot \tan \alpha} \cdot \left(\frac{1}{r_{or}^3} - \frac{1}{(h \cdot \tan \alpha + r_{or})^3} \right) \quad (17)$$

Combining equation (12) with equation (1), (2), (3) and (13) we get the following differential equation, which can just be solved numerically:

$$\left(-\frac{dm}{dt \cdot \rho} \right)^2 \cdot \left(\frac{1}{A_2^2} - \frac{1}{A^2} \right) + \left(-\frac{dm}{dt \cdot \rho} \right) \cdot \frac{2R}{\rho} - 2gh = 0$$

$$\text{with: } R = \frac{8\eta}{3\pi \cdot \tan \alpha} \cdot \left(\frac{1}{r_{or}^3} - \frac{1}{(h \cdot \tan \alpha + r_{or})^3} \right); \quad A \approx h^2 \tan^2 \alpha \cdot \pi; \quad h \approx \left(\frac{3m}{\tan^2 \alpha \cdot \pi \cdot \rho} \right)^{\frac{1}{3}}$$

Appendix G (power law for a binary mixture of a well and poorly compactable substance)

If a tablet consists of a binary mixture of two components A and B then the relative densities of both substances are given by equation (1)

$$\rho_{r(A)} = \frac{V_{t(A)}}{V_a} = \frac{m_{(A)}}{V_a \rho_{t(A)}} \quad \text{and} \quad \rho_{r(B)} = \frac{V_{t(B)}}{V_a} = \frac{m_{(B)}}{V_a \rho_{t(B)}} \quad (1)$$

where: $\rho_{r(X)}$: relative density of component X
 $V_{t(X)}$: true volume of component X
 V_a : apparent volume of the compact
 $m_{(X)}$: mass of the component X
 $\rho_{t(X)}$: true density of component X

For the solid fraction (relative density of the binary mixture of A and B) we can write equation (2).

$$\rho_{r(AB)} = \frac{V_{t(A)} + V_{t(B)}}{V_a} = \rho_{r(A)} + \rho_{r(B)} = \rho_{r(A)} \left(1 + \frac{\rho_{r(B)}}{\rho_{r(A)}} \right) = \rho_{r(A)} \left(1 + \underbrace{\frac{m_{(B)} \cdot \rho_{t(A)}}{m_{(A)} \cdot \rho_{t(B)}}}_{const} \right) \quad (2)$$

The term in the parenthesis is constant throughout the whole compression process, thus also for the special case where component A starts to percolate ($\rho_{r(A)} = \rho_{rc(A)}$). For the corresponding solid fraction we can write $\rho_{r(AB)} = \rho_{rc^*(AB)}$. Thus we can write equation (3).

$$\rho_{rc^*(AB)} = \rho_{rc(A)} \cdot const \quad (3)$$

However, it has to be kept in mind that $\rho_{rc^*(AB)}$ is not identical with the critical relative density of the mixture. $\rho_{rc^*(AB)}$ is just the solid fraction when component A starts to percolate.

Assuming that just substance A is responsible for the strength of the tablet, we can consider the tensile strength $\sigma_{t(AB)}$ of the binary mixture to be identical with the tensile strength $\sigma_{t(A)}$ of the component A ($\sigma_{t(AB)} = \sigma_{t(A)}$).

If we suppose that the tensile strength of compacts consisting of the substance A can be described by equation (4) then we can further write equation (5) on condition mentioned above.

$$\sigma_{t(A)} = S(\rho_{r(A)} - \rho_{rc(A)})^{T_f} \quad (4)$$

where: $\sigma_{t(A)}$: radial tensile strength of compact consisting of component A

S: scaling factor

T_f : critical exponent (fraction exponent): theoretical value: 2.7.

$\rho_{r(A)}$: relative density of component A

$\rho_{rc(A)}$: critical relative density (percolation threshold)

$$\sigma_{t(AB)} = S(\rho_{r(AB)} - \rho_{rc(AB)})^{T_f} \quad (5)$$

Combining equation (5) with equation (2) and equation (3) we get finally equation (6).

$$\sigma_{t(AB)} = S \left(\frac{\rho_{r(AB)}}{\text{const}} - \frac{\rho_{rc^*(AB)}}{\text{const}} \right)^{T_f} = S_2 \cdot (\rho_{r(AB)} - \rho_{rc^*(AB)})^{T_f} \quad (6)$$

Appendix H (dilution capacity)

Equation (1) (derived in appendix G) is the starting equation for the theoretical calculation of the dilution capacity.

$$\rho_{r(AB)} = \rho_{r(A)} \left(1 + \frac{m_{(B)} \cdot \rho_{t(A)}}{m_{(A)} \cdot \rho_{t(B)}} \right) \quad (1)$$

The ratio of $m_{(B)}$ to $m_{(A)}$ can be replaced by the mass fraction, which is defined according to equation (2).

$$X_{(A)} = \frac{m_{(A)}}{m_{tot}}; \quad X_{(B)} = \frac{m_{(B)}}{m_{tot}} = \frac{m_{tot} - m_{(A)}}{m_{tot}} = 1 - X_{(A)} \quad (2)$$

Combining equation (1) with equation (2) we get:

$$\rho_{r(AB)} = \rho_{r(A)} \left(1 + \frac{1 - X_{(A)}}{X_{(A)}} \cdot \frac{\rho_{t(A)}}{\rho_{t(B)}} \right) \quad (3)$$

This equation also holds for the case where the relative density $\rho_{r(A)}$ equals the critical relative density $\rho_{rc(A)}$. The corresponding solid fraction is referred to as $\rho_{rc^*(AB)}$ (see also appendix G). We can write:

$$\rho_{rc^*(AB)} = \rho_{rc(A)} \left(1 + \frac{1 - X_{(A)}}{X_{(A)}} \cdot \frac{\rho_{t(A)}}{\rho_{t(B)}} \right) \quad \text{or} \quad \rho_{rc^*(AB)} = \rho_{rc(A)} \left(1 + \frac{X_{(B)}}{1 - X_{(B)}} \cdot \frac{\rho_{t(A)}}{\rho_{t(B)}} \right) \quad (4)$$

The maximum possible proportion $X_{c(B)}$ of the poorly compactable substance B (= dilution capacity) is achieved when the solid fraction equals unity *i.e.* when the tablet is compressed at infinite pressure. Thus, we can write for $X_{c(A)}$ and the dilution capacity $X_{c(B)}$:

$$X_{c(A)} = \frac{\rho_{t(A)}}{\rho_{t(B)}} \cdot \frac{1}{\left(\frac{\rho_{t(A)}}{\rho_{t(B)}} + \frac{1}{\rho_{rc(A)}} - 1 \right)} \quad \text{or} \quad X_{c(B)} = 1 - \frac{\rho_{t(A)}}{\rho_{t(B)}} \cdot \frac{1}{\left(\frac{\rho_{t(A)}}{\rho_{t(B)}} + \frac{1}{\rho_{rc(A)}} - 1 \right)} \quad (5)$$

Curriculum vitae

Name	Michael Lanz
Date of Birth	1 st October 1974
Place of Origin	Rohrbach (BE)

Education

2001-2005	PhD study under the supervision of Prof. Dr. H. Leuenberger at the Institute of Pharmaceutical Technology (University of Basel) Assistant in practical courses in solid dosage forms
Nov. 2000	Swiss federal diploma in pharmacy
1994-2000	Studies in pharmacy at the University of Bern, Zurich and Basel
1989-1994	High school at Gymnasium Bern Neufeld

Publications

- Leuenberger, H., Lanz, M. (2005) Pharmaceutical powder technology – from art to science: the challenge of the FDA's Process Analytical Technology initiative. *Advanced Powder Technol.*, **16**(1), 3-25.
- Reus-Medina, M., Lanz, M., Kumar, V., Leuenberger, H. (2004) Comparative evaluation of the powder properties and compression behaviour of a new cellulose-based direct compression excipient and Avicel PH102®. *J. Pharm. Pharmacol.*, **56**(8), 951-956.
- Leuenberger, H., Lanz, M. (2002) Powder – the fourth state of matter? *Pharm Tech Japan*, **18**(7), 995-1001.

During my studies I attended lectures and presentations given by:

Aebi, U., Altorfer, H., Berger-Büter K., Bruppacher, R., Caraballo, I., Drewe, J., Folkers, G., Giron, D., Güntert, T., Hädener, A., Haefeli, W., Heide, L., Herrling, P., Honegger, U., Hostettmann, K., Hussain, A., Imanidis, G., Krähenbühl, S., Lehr, C.-M., Leuenberger, H., Lüdin, E., Meier, C., Meier-Abt, P., Melchiorre, C., Merkle, H.P., Mühlebach, S., Müller, H., Rudolph, U., Rüegg, M., Saito, F., Scapozza, L., Schaffner, W., Scholer, A., Seelig, A., Sticher, O., Zimmermann, J.